

UNIVERSITY COLLEGE LONDON
UCL

PHD THESIS

Hippocampal Spatial Representation: Integrating Environmental and Self-motion Signals

Author:

Yi LU

Supervisor:

Dr. Neil BURGESS

Dr. Francesca CACUCCI

Thesis submitted to UCL for consideration for the degree of Doctor in
Philosophy

Declare

I, Yi Lu, confirm that the work presented in this thesis is my own. Where information has been derived from other sources, I confirm that this has been indicated in the thesis.

Experiment 1 in Chapter 3 was reported in the paper by Chen, G.*, King, J. A.*, Lu, Y.*, Cacucci, F., & Burgess, N. (2018). Spatial cell firing during virtual navigation of open arenas by head-restrained mice. *Elife*, 7, e34789.

Experiment 2 in Chapter 4 was reported in the paper by Chen, G.*, Lu, Y.*, King, J. A., Cacucci, F., & Burgess, N. (2019). Differential influences of environment and self-motion on place and grid cell firing. *Nature communications*, 10(1), 630.

I contributed in data collection, data analysis and manuscript writing in both papers.

Yi Lu

Dedication

First I would like to thank my primary supervisor Professor Neil Burgess for giving me the opportunity to join this PhD program in Cognitive Neuroscience at University College London, and China Scholarship Council for providing me with generous funding. And many thanks to both of my supervisors Professor Francesca Cacucci and Professor Neil Burgess, for always being patient and supportive, and for giving me adequate training and freedom to explore my research interests.

I also want to thank Dr. Guifen Chen for instructing me on how to conduct animal experiments, and Professor Tom Wills for discussion and suggestion on data analysis in the dark trial experiment. Thanks to Dr. Fabio Rodrigues, Dr. Laurenz Mussieq and Dr. Josh Bassett, who have been my role model and inspiration in struggling time. Big cheers to all the Cacucci Lab members: Alice O’Leary, Tara O’Driscoll, Isabella Varsavsky and Megan Powell and the Burgess lab members: Daniel Bush and Changming Yu. It is a great pleasure to work with you all.

My final gratitude goes to my parents, who encouraged and helped me through many frustrating and self-doubting moments in my PhD years, like they always did. Love you dearly and forever.

Abstract

Electrophysiological recording in freely-moving rodents has established that place cells fire when the animal occupies a specific location and grid cells fire when at several locations, arranged on a regular triangular grid. Experiments and theories suggest that place cells and grid cells 1) receive inputs reflecting both environmental and self-motion information, and 2) are functionally connected to each other. Yet it remains elusive how the environmental and self-motion inputs dictate either place cell or grid cell firing. In a series of experiments I address this question by manipulating the inputs independently while simultaneously recording place and grid cells activity.

Firstly, I introduce our visual 2-d virtual reality system, in which mice run on an air-supported Styrofoam ball with their head held but allowed to rotate in the horizontal plan. The virtual arena is projected on surrounding screens and on the floor at a viewpoint that shifts with rotation of the ball. With sufficient training, mice can navigate freely in the virtual environment and successfully retrieve rewards from an unmarked location. Electrophysiological data confirms that place, grid and head-direction cells show characteristic spatial tuning in VR.

In a second experiment, the gain factor that maps mice's running speed to visual translation of the virtual environment is manipulated. Results show that place cell firings are more driven by vision while grid cells incorporate self-motion inputs better.

The last experiment had mice navigate in darkness. Without visual input co-recorded place cells and grid cells both suffer disruption in spatial tuning, albeit tuning is better preserved near to environmental boundaries.

These results demonstrated that environmental and self-motion signals contribute to place and grid cells' spatial representation of different significance, and constrain models with presumptions about how the place cells and grid cells integrate inputs and interact with each other.

Impact statement

I presented here our powerful 2-d virtual reality (VR) system which offers advantages over traditional navigation research paradigms by enabling manipulations that are impossible in the real-world, i.e. allowing visual projection of an environment that need not directly reflect a physical reality or the animals' movements. Such decoupling of self-motion and external inputs enable us to separate innate network property from sensory driven representation, and potentially help us understand processes that are sensory dependent and those that generate across sensory modalities. Providing head stability of the animal, Our VR setup allows neural recordings such as two-photon microscopy to be conducted during awake navigation, hugely expanding our research territory into large-scale network organisation and intracellular subthreshold neural process that underline the hippocampal spatial representation.

Hippocampus is of no less resemblance of the CPU in our brain than of the GPS in the brain. It is suggested by many that hippocampus is involved in the more fundamental aspects of information process, such that the knowledge we gained from studying neural mechanisms of its spatial representation could potentially enlighten us on a broad spectrum of cognitive functions. Last but not the least, Hippocampal pathology is also closely linked to severe neurodegenerative diseases such as Alzheimer's dementia. Finer definition of what cognitive process is and what is not hippocampal dependent

could help develop test batteries that detects and predicts hippocampal pathology at an early stage to help clinical diagnosis and prognosis of diseases, and potentially improve life quality of many.

Contents

List of Figures	12
List of Tables	16
1 Introduction	17
1.1 What does the hippocampal formation do?	17
1.1.1 Hippocampal formation and memory	19
1.1.2 Hippocampal formation and spatial coding	21
1.2 The anatomical and physiological properties of the hippocampal formation	24
1.2.1 Hippocampal CA1	26
1.2.2 Entorhinal cortex	32
1.2.3 Intrinsic connections in the hippocampal formation	41
1.2.4 Extrinsic connections	44
1.3 Spatial representation based on environmental cues and self-motion tracking	50

1.3.1	Environmental cues	51
1.3.2	Path integration	56
1.4	Rationale for experiments in this thesis	65
2	General Methods	66
2.1	Animals	66
2.2	Surgery	67
2.3	Behavioural paradigm	68
2.3.1	VR method	68
2.4	Data collection	76
2.4.1	Histology	78
2.4.2	Firing rate map construction and spatial cell classification . . .	79
3	Spatial cell firing during virtual navigation of open arenas by head-restrained mice	82
3.1	Introduction	82
3.2	Materials and methods	84
3.2.1	Animals	84
3.2.2	Recording procedure	85
3.2.3	Behavioral analysis	87
3.2.4	Statistical analysis	87

3.3	Results	92
3.3.1	Navigation in VR	92
3.3.2	Electrophysiology	96
3.4	Discussion	115
4	Differential influences of environment and self-motion on place and grid cell firing	120
4.1	Introduction	120
4.2	Methods	123
4.2.1	Animal	123
4.2.2	Manipulating the gain of visual motion vs physical motion . . .	123
4.2.3	Data analysis	125
4.2.4	Statistical analysis	130
4.3	Results	136
4.3.1	Place cells under gain manipulation	136
4.3.2	Grid cells under gain manipulation	145
4.4	Discussion	156
5	Absence of Visual Input Affects Place and Grid Cell Activity	159
5.1	Introduction	159
5.2	Methods	161

5.2.1	Animals	161
5.2.2	Behavioural training	161
5.2.3	Data analysis	162
5.3	Results	163
5.3.1	Navigation in the dark	163
5.3.2	Electrophysiology	165
5.4	Discussion	177
5.4.1	Speed distribution in darkness	177
5.4.2	Spatial cell properties in the dark	177
5.4.3	Boundary effects in the dark	178
6	General discussion	180
6.1	Difference between place cells and grid cells in combining external and self-motion inputs	180
6.2	Possible causes of discrepancy between place cells and grid cells	182
6.2.1	Velocity versus static cues	182
6.2.2	Distal versus proximal cues	184
6.2.3	Novel versus familiar environments	186
6.3	Future direction	187
	Bibliography	189

List of Figures

1.1	Horizontal section through the rat hippocampus	25
1.2	Illustration of cell morphology in hippocampus CA1	27
1.3	Neurons in superficial and deep layer of entorhinal cortex	35
1.4	Intrinsic connections in hippocampus	42
1.5	Pattern and strength of cortical connectivity of the rat hippocampal formation	46
1.6	The major anatomic pathways through which the vestibular signals reach the hippocampus and the entorhinal cortex	49
2.1	Virtual reality setup	69
2.2	Virtual environments and example trajectory maps in the four training phases	75
2.3	Top view of the 60x60cm (left) and 80x80cm (right) recording boxes . .	77
2.4	Histology and implant traces in CA1 and MEC.	78
3.1	Behavior in VR compare to R	92

3.2	Running direction distribution	94
3.3	Performance on the ‘fading beacon’ task	95
3.4	Spatial cell classification	97
3.5	Place cell firing in real and virtual environments	98
3.6	Spatial cell firing properties in 60x60cm and 90x90cm virtual environments	100
3.7	Directional information of place cell firing (bits/spike) as a function of the distance from the nearest wall	101
3.8	Comparison between VR and R trials in square and cylindrical environments in additional data from 4 mice	102
3.9	Grid cell firing in real and virtual environments	104
3.10	Trial order and trial length effects on comparing cell firing properties in real and virtual environments in additional data from 4 mice	106
3.11	Head direction cell firing in real and virtual environments	107
3.12	Eleven directional cells recorded in dMEC	108
3.13	Effect of rotating the virtual environment on spatial firing patterns . .	110
3.14	Spatial information of place cells that did not follow the 180°-rotation of VR environment	112
3.15	Effect of running speed on theta frequency and firing rates in real and virtual environments	113
3.16	Spatial cell field size was modulated by running speed in a similar way in real and virtual environments	114

3.17	Theta phase precession	114
4.1	Spatial cell classification	126
4.2	Comparison of grid firing patterns with hexagonal virtual floor tiling pattern	126
4.3	Proportion of ‘remapped’ place cells	128
4.4	Simultaneously recorded place and grid cells in mouse #987	134
4.5	Simultaneously recorded place and grid cells in mouse #1061	135
4.6	Place and grid cell firing properties in VR baseline and gain manipulated trials	137
4.7	Place cell firing patterns under visual gain increase	138
4.8	Place cell firing patterns under visual gain decrease	140
4.9	Place cells and grid cells with compact non-remapping firing patterns .	142
4.10	Distribution of motor influence (MI) score per animal	144
4.11	Distribution of MI score for population vector per animal	144
4.12	Grid cell firing patterns under visual gain increase	145
4.13	Grid cell firing patterns under visual gain decrease	148
4.14	Direction dependent offsets of grid patterns	150
4.15	Analysis of individual firing fields and distance to the nearest boundary	153
4.16	MI score for spatial cells in MEC	154
4.17	Speed modulation of LFP theta frequency and speed cell firing rates . .	155

5.1	Running speed and occupancy in boundary and centre region	164
5.2	Spatial cell classification	166
5.3	Comparison of grid cell firing patterns between dark and light trials . .	167
5.4	Comparison of place cell firing patterns between dark and light trials .	170
5.5	Comparison of head direction cell firing patterns between dark and light trials	172
5.6	Cumulative density function of spatial tuning reduction in place cells and grid cells from the light to dark trials	173
5.7	Place cell field size and stability are modulated by its distance towards the nearest wall	174
5.8	Place cell and grid cell firing in the boundary and centre region	176

List of Tables

2.1	Number of animals resused across multiple experiments	67
3.1	Trial information	86
3.2	Statistical test results	88
4.1	Trial information	124
4.2	Statistical test results	131

Chapter 1

Introduction

1.1 What does the hippocampal formation do?

The hippocampus and parahippocampal regions are among the most studied brain areas both in their basic biological structures and cognitive functions. The rather clear laminar organization and largely unidirectional signal pathway discovered in the hippocampus provide an opportunity for close scrutiny of how the specific physiological structure give rise to function.

It has been long established that the hippocampal formation is crucial for memory function and spatial navigation. Pathological degradation of hippocampal formation has been linked to neurodegenerative dementias such as Alzheimer's Disease (Hyman et al., 1984; van Hoesen et al., 1991). Cognitive assessment of patients with hippocampal lesions and animal studies consistently reported correspondence between hippocampal integrity and memory function (Scoville & Milner, 1957; Parkinson et al., 1988; Vargha-Khadem et al., 1997). On the other hand, the gradual revelation that the hippocampal formation contains an elaborate system of 'space' representation

(O’Keefe et al., 1971; Taube et al., 1990a; Hafting et al., 2005) and might support abstract learning of representational structure (Tolman, 1948; Eichenbaum & Cohen, 2014; Constantinescu et al., 2016) has boosted recent interest in the study of hippocampal function. The hippocampus has also been linked to other functions such as emotion (Papez, 1937), attention control (Kaada et al., 1953) and novelty detection (Vinogradova, 1995).

Over the past decades of research, a consensus was yet to be reached regarding the principal role of hippocampal representation. However, in both memory and navigation literature, a functional dissociation has been proposed between the hippocampus and parahippocampal regions. Specifically, hippocampal damage was related to episodic or contextual memory deficits while lesions in parahippocampal regions were linked to semantic/non-contextual memory (Vargha-Khadem et al., 1997). Similarly in rodents, spatial coding in the hippocampus proper (e.g. the spatial tuning of place cells) is more context-dependent, while medial entorhinal cortex seems to have established a context-invariant metric representation (O’Keefe et al., 1971; Hafting et al., 2005). Yet, why this dichotomy exists and how the two systems interact have not been entirely elucidated, neither do we know about how they are supported by different inputs such as the environmental cues and self-motion cues. My research focuses on the comparison between place cells in the hippocampal CA1 and grid cells in the medial entorhinal cortex (MEC) and how their representations reflect the influence of environmental cues as well as the self-motion signal.

In this introduction, I will begin with a brief review of the evidence that links hippocampal formation to memory function and spatial coding, as well as how they might be related. Then, following accumulated rodent focused neuroscience studies, I will describe the anatomical structures of the hippocampal formation, concentrating

on the cytoarchitecture and functional properties of cells in hippocampal CA1 and MEC emphasizing on their spatial representations. Following this, I will adopt the perspective of interpreting hippocampal formation as a spatial coding system and highlight how external environmental cues and self-motion cues could contribute to its neural representations (for a review also see Evans et al. (2016)). Finally, I will provide an overview of three experiments that I conducted either in collaboration with my colleagues or independently, which attempt to shed light on how different types of information converges in the hippocampal formation and to understand how different spatial representation arise and interact.

1.1.1 Hippocampal formation and memory

Patients with bilateral medial temporal lobe resections including hippocampal formation suffered from severe recent (largely anterograde) memory loss (Scoville & Milner, 1957; Corkin, 2002). These patients have difficulty recalling facts and events following the operation as well as from months or years before the surgery. In contrast, they can remember the details of their early life events. Cognitive tests also confirm their grave memory deficits compared to normal intelligence scores, and their memory performance is worse if interrupted between learning and retrieval (Scoville & Milner, 1957). Standard consolidation theory suggests that hippocampus might play an important role for systems consolidation, which refers to the gradual transferring of the hippocampal-dependent memory trace (‘engrams’) to stable long-term storage in neocortical areas (McClelland et al., 1995; Dudai, 2004). Such anterograde amnesia and temporally-graded retrograded amnesia (TGRA) were consistently reported in clinical studies (Kapur & Brooks, 1999; Manns et al., 2003), however, more controversially reported in animal research. Many studies found that both recent and remote memories

were impaired for rats with hippocampal lesions performing the Morris water maze task (Bolhuis et al., 1994; Mumby et al., 1999; Sutherland et al., 2001; Clark et al., 2005; Ocampo et al., 2017). In a context fear conditioning task, both TGRA (Kim & Fanselow, 1992; Maren et al., 1997; Anagnostaras et al., 1999; Winocur et al., 2009) and null results (Lehmann et al., 2007; Sutherland et al., 2008; Sparks et al., 2011; Broadbent & Clark, 2013) were reported in hippocampal lesioned rats.

The hippocampal formation related memory deficit is also content specific, as well as being sensitive to the time at which the memory is acquired. Patients reported that they were unable to retain new declarative memory, which indicated by the explicit recall of events and facts but not perceptual-motor learning (Brooks & Baddeley, 1976) or rule-based skill learning (Cohen & Squire, 1980). Some also reported that in patients with more restricted damage to the hippocampal area, only context-dependent episodic memory but not semantic memory which are facts or knowledge that are context-insensitive was affected (Vargha-Khadem et al., 1997; Tulving & Markowitsch, 1998; Aggleton, 2000; Spiers et al., 2001). In animal studies, it is shown that hippocampal lesion damaged spatial memory (Parkinson et al., 1988; Murray et al., 1989; Angeli et al., 1993; Gaffan, 1998), associative memory (Murray & Mishkin, 1985; Murray et al., 1993), working memory (Olton et al., 1979), temporal memory (Rawlins, 1985) and novel object recognition (Cohen & Stackman, 2015). Bilateral ablations of the hippocampal formation in monkeys compromised their task performance in learning object-place associations but not in object recognition (Parkinson et al., 1988) nor in learning visual-visual paired associations or cross-modal tactile-visual associations (Murray & Mishkin, 1985).

Such dissociation of hippocampal related amnesia affecting different memory components leads to the theory proposing the hippocampus as the primary hub for

forming associations and organizational structures in memory (reviewed by Eichenbaum (2017)). It is worth noting that both in human and animal memory studies, spatial memory deficits are consistently reported to accompany hippocampal lesion, leading to the suggestion that the hippocampal formation could be important for spatial representation.

1.1.2 Hippocampal formation and spatial coding

Hippocampal formation supports spatial coding

It was first discovered in rats that the hippocampal CA1 principal neurons increase their firing rates when the animal ran into specific locations in an open-field environment, they were thus named place cells (O’Keefe et al., 1971; O’Keefe, 1976). Later more spatially tuned hippocampal neurons such as head direction cells, grid cells, boundary vector cells/border cells were discovered in the hippocampal formation (Taube et al., 1990a; Hafting et al., 2005; Lever et al., 2009; Solstad et al., 2008). In studies that the hippocampus was partially or entirely lesioned by surgical or pharmacological methods, animal performance decayed in various spatially demanding tasks. Tasks that require allocentric spatial learning such as the Morris water maze and delayed matching-to-place (Morris et al., 1982, 1986, 1990; Steele & Morris, 1999), as well as those involving spatial working memory such as non-matching-to-place (Olton et al., 1978; Rawlins & Olton, 1982) were most sensitive to the disruption of the hippocampal function. Spatial associative tasks such as contextual fear conditioning (Selden et al., 1991; Kim & Fanselow, 1992), object-in-place (Parkinson et al., 1988; Kesner, 1993) and object-trace-place learning (Hunsaker et al., 2006) are also hippocampal-dependent.

How does spatial coding benefit memory formation and general cognitive representation?

What is spatial representation? What do we need it for and what makes it different from the primary sensory features that our brain is tuned to? Let us consider spatial representation from three different perspectives.

The most obvious purpose is localization. Instincts demand us to know where the sources of security (food sources, breeding locations, etc.) and dangers are located. Location in the world provides a good stable reference in which to represent items and events for later retrieval (e.g. spatial memory). This stability is derived from two processes. One is from the high-level abstraction of spatially and temporally varying multimodal sensory inputs. Locations can be recognized even after substantial changes in superficial appearance as well as after a long time. For example, food-caching birds can store food in several locations and later retrieve them (Roth & Pravosudov, 2009). Hippocampal volume and number of hippocampal neurons were found to increase with environmental harshness and spatial memory demand in these species (Roth & Pravosudov, 2009). The other derives from allocentric, meaning locations are defined relative to the external environment other than to the proprioceptive experience of the observer. A world-centred locational representation could potentially register across multimodal sensory inputs which are represented in different egocentric frames and facilitate sensory integration. Its robustness to moment-to-moment changes in subjects' current states (e.g. body gesture and heading direction) could also support better long-term encoding and retrieval. Supported by behavioural evidence, experienced honeybees are able to home from all directions around the hive at a speed comparable to their counterparts trained on an equally long fixed-route (Menzel et al., 2000). Understanding how allocentric spatial representation is achieved will help us understand

how information is organized and stored in long-term memory.

The second perspective of spatial representations is translation. Under a common reference frame, relationships between locations can be represented as vectors that can be integrated. Darwin (1873) was the first to describe that diverse species with a fixed home base are often capable of integration of inertial signals, which he called 'dead reckoning' (or 'path integration'), the ability to keep track of displacement from a home base. Central place foragers like ants and bees use path integration as their predominant system of navigation (Collett & Collett, 2000). A vector-based path integration system is complementary and facilitates landmark-based navigation (Cheng et al., 2007). For example, when familiar landmarks were rotated from its regular place, desert ants followed them for a short while, then switched to a direct path towards the home base, suggesting that they kept track of the home vector and switched to a path integration controlled navigation strategy when landmarks became unreliable (Wehner, 2003). Other than path integration, vectors from stored memory could be summed with the current path vector, or with another memorized vector, to generate novel vector relationships between otherwise unconnected locations (Collett & Collett, 2000; Landau et al., 1984). This flexible and sometimes offline vector-based learning is one of the most potent arguments for the presence of a general map structure for spatial representation, also known as the 'cognitive map' theory (Tolman, 1948).

Interestingly, theories of 'cognitive map' and 'path integration' that describe the organisation of allocentric location and vector-like integration processes were proposed long before the neural evidence. And since the discovery of place cells and grid cells, they appear to be fulfilling the purposes (further discussed in Section 1.3).

Last but not the least, it is important to acknowledge the tight coupling between locomotion, location and sensory changes. Translation between locations are the

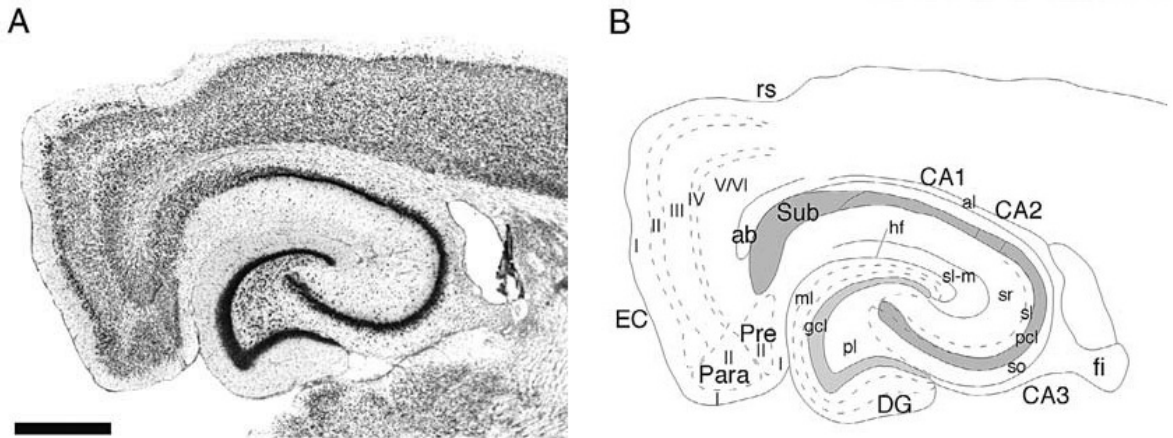
1.2. THE ANATOMICAL AND PHYSIOLOGICAL PROPERTIES OF THE HIPPOCAMPAL FORMATION

direct result of locomotion and in turn, cause sensory perception to change. In the hippocampus self-motion and sensory inputs intermingle and interact to define locations. Animals adopt movement-based sensory registration strategy to anchor their home location. Researchers observed that desert ants took learning walks upon leaving their nest foraging for food, they circled the nest in bigger and bigger radius while pausing from time to time and aligning themselves to face the exact direction of the nest. Based on this observation it was hypothesized that those behaviours allowed multiple 'snapshots' of the nest area to be taken and labelled with distances and orientations according to path integration inputs, ultimately supporting retrieval of nest location (Müller & Wehner, 2010). The advantage of direct registration between environmental inputs and locomotion(velocity) signal, instead of error correction at the level of spatial representation, is that by calibrating the self-motion signal, sensory cues project influence to a larger spatial and temporal extent (presumably because of the relatively stable locomotion inputs). It is not yet known whether any general environmental regularity (e.g. dominant frequency of natural visual scene) can help transfer the registration over a large territory to continually support accurate velocity representation. Nevertheless, exploring the possibility could help us understand the mechanism of long-distance natural navigation.

1.2 The anatomical and physiological properties of the hippocampal formation

Having laid out the behavioural problem, we are now adopting a bottom-up strategy to understand how neurons and brain regions are organized and connected, as well as the implications of such anatomical structure on current theories and models of

hippocampal function. I will be using the following language and classifications to discuss the aforementioned questions. Unless specified otherwise, the neuroanatomy discussed below pertains to the rat brain. The nomenclature used here follows the logic used by Lavenex and Amaral in ‘The Hippocampus Book’ (Chapter 3, Andersen et al. (2007)): 1) Hippocampal formation is defined as the functional brain system that includes hippocampus (CA1, CA2 and CA3), dentate gyrus, subiculum, presubiculum, parasubiculum and entorhinal cortex (See Figure 1.1); 2) each position within the hippocampal formation is defined by three axes - the longitudinal axis that extends from the rostradorsal portion to the caudoventral portion of the brain (septotemporal axis), the transverse axis that is orthogonal to the longitudinal axis and the superficial-to-deep axis that runs perpendicular to the layers of each hippocampal region, with layers closest to the pial surface being labelled as superficial and those closer to the ventricles as deep. Hippocampal anatomy is marked by its clear laminar organization, convergent multi-modal afferent connections and highly divergent and interconnected intrinsic projections. The description will be specifically focused on hippocampal region CA1 (where place cells are recorded) and entorhinal cortex (where grid cells can be found).



1.2. THE ANATOMICAL AND PHYSIOLOGICAL PROPERTIES OF THE HIPPOCAMPAL FORMATION

Figure 1.1: **Horizontal section through the rat hippocampus.** Nissl-stained section (A), and section outlined and marked with regions and layers (B). Bar in A = 500 μm and applies to both panels (Source: Adapted from Andersen et al. (2007)).

1.2.1 Hippocampal CA1

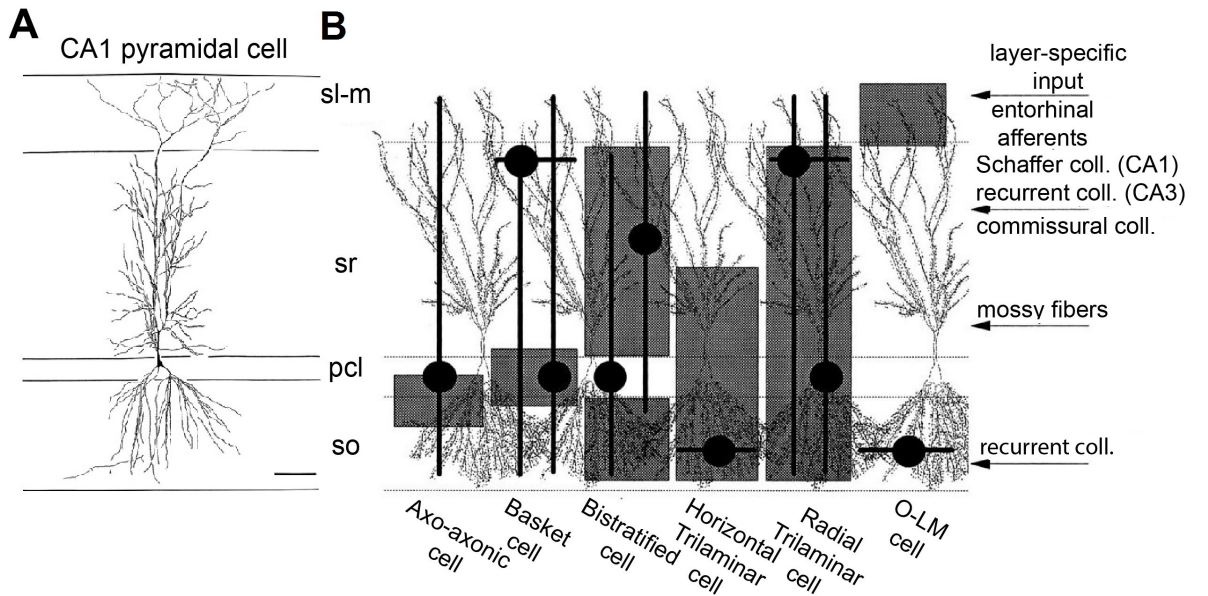
CA1 neuron cytoarchitecture and physiological properties

The hippocampus consists of subfields CA1, CA2 and CA3. Their sub-division is justified by multiple criteria including afferent and efferent projections, neural morphology and neurochemical markers. Connections within the hippocampal formation are largely unidirectional (Andersen et al., 1971). CA1 is the last stop in the information flow and also the output hub in the hippocampus proper.

The principal neuron type in CA1 is the pyramidal cell (Ramon y Cajal, 1911; Lorente De N , 1934; Ishizuka et al., 1995). Pyramidal cells typically present a triangular cell body, a basal dendritic tree and a main apical dendritic tree (see Figure 1.2). Pyramidal cells in CA1, in comparison to those in CA2/CA3, have smaller cell bodies and are more densely packed into a thin layer named pyramidal cell layer (pcl). Their basal dendrites extend deeply towards the alveus occupying a layer called stratum oriens (so), whilst their apical dendrites extend superficially towards the hippocampal fissure passing through two layers, stratum radiatum (sr, proximal apical) and stratum lacunosum-moleculare (sl-m, distal apical). The orientation of these dendritic trees is remarkably homogeneous across the whole area making CA1 suitable for generating large-scale field potentials.

The primary apical dendrites of pyramidal cells branch obliquely into stratum radiatum and continue to branch after they enter the stratum lacunosum-moleculare forming an

apical tuft. One of the major excitatory projections to CA1, the perforant pathway originating in layer III of the entorhinal cortex, innervates the apical tufts in stratum lacunosum-moleculare (Hjorth-Simonsen & Jeune, 1972). Measuring passive membrane conductance revealed that CA1 dendrites impose strong filtering and attenuation on synaptic potentials between its site of origin and site of integration (Pyapali et al., 1998), advising that distal dendritic inputs such as ones from the perforant pathway were likely ineffective at the levels of the soma or axon output. Mechanisms such as the membrane resistance decrease with increased distance from the soma, and dendritic spikes being initiated by voltage-gated ion channels, were found to compensate. Most interestingly, it was shown that dendritically generated Na^+ and Ca^+ spikes are sufficient in inducing long-term potentiation (LTP) (Golding et al., 2002), and are facilitated when combined with modest activation of the Schaffer collateral synapses (projections from CA3) in upper apical dendrites (Jarsky et al., 2005). Together these dendritic properties portrait pyramidal cells in CA1 as compartmental processors in which input integration happens when temporal and amplitude criteria are met.



1.2. THE ANATOMICAL AND PHYSIOLOGICAL PROPERTIES OF THE HIPPOCAMPAL FORMATION

Figure 1.2: **Illustration of cell morphology in hippocampus CA1.** Camera lucida drawing of a CA1 pyramidal neuron (A) and classification of interneurons (B). Bar = $100\mu\text{m}$. (Source: Adapted from Andersen et al. (2007)).

Interneurons constitute only a small proportion of cells in hippocampus ($\sim 10\%$), however they represent one of the most diverse cell populations (see Figure 1.2). Unlike pyramidal cells, their cell bodies are scattered in all hippocampal layers. Interneurons form short-range but divergent projections to either pyramidal cells or other interneurons and release the inhibitory neurotransmitter GABA on their targets. Despite their diversity, many identified interneuron types are very specific in their targeting. For example, basket cells and O-LM cells selectively innervate the vicinity of the soma and distal apical dendrites of pyramidal cells, respectively. They generate enormous axonal plexuses that have more than 10,000 synaptic varicosities and are estimated to innervate 1000+ postsynaptic pyramidal cells. Others interneurons prefer to target neurons with specific neurochemical properties, for example, the interneuron selective CR-positive cells innervate the CCK-containing cells but not the PV-containing cells (Gulyás et al., 1996).

There are also major differences between hippocampal interneurons and pyramidal cells. Interneurons have more depolarized membrane potential, distinctive topology and distribution of voltage-gated ion channels (Fraser & MacVicar, 1991; Martina & Jonas, 1997). As a result, spikes initiated in dendrites of interneurons propagate rapidly to the soma with high fidelity. Their fast kinetics in action potential generation places them in a privileged position to pace network synchronization, indeed most interneurons are phase-locked to oscillatory field potentials (Colom & Bland, 1987). One study demonstrated that a large population of mutually connected fast-spiking basket cells generates gamma oscillations, via shunting inhibition, even when faced with highly

heterogeneous tonic excitatory input (Vida et al., 2006).

Functional properties of the hippocampal CA1

In CA1 cells can be broadly divided into principal neurons (pyramidal cells) and interneurons as previously mentioned. Their firing properties also distinguish between each other, I.e. the majority of pyramidal cells are complex spike cells which have on average lower firing rate (<10 Hz) and tend to fire spikes in short bursts of 2 – 7 spikes with 1.5 - 6 msec interspike intervals (Ranck, 1973). Those cells when active mostly show significant spatial tuning by firing only in a restricted region (the ‘place field’) in an environment, which is the reason they are named place cells (O’Keefe et al., 1971; O’Keefe, 1976; O’Keefe & Nadel, 1978). Interneurons distinguish from pyramidal cells by firing at a regular interspike interval and a higher rate (Ranck, 1973), although some interneurons also have bursty spiking pattern and fire at a lower rate (Csicsvari et al., 1999). For interneurons, many have a weaker but detectable spatial correlate with more sensitive measures (Frank et al., 2001), while others attribute their role to network oscillation (Ranck, 1973; Csicsvari et al., 1999) and speed modulation (McNaughton et al., 1983). Both cell types displayed speed modulation by increasing their firing rate as a function of animals’ running speed (McNaughton et al., 1983).

Prominent network oscillations at 5-10 Hz (‘theta’) and 40-100 Hz (‘gamma’) were found in local field potential (LFP) recorded during paradoxical sleep and wakefulness all over the rodents’ hippocampal formation including CA1 (Vanderwolf, 1969; Bragin et al., 1995). And both pyramidal neurons and interneurons tend to fire in phase, mostly preferred firing at the negative phase of the LFP theta oscillation (Ranck, 1973; Csicsvari et al., 1999). On top of that, place cells fire at a progressively earlier phase of LFP theta when animals traverse their place fields (‘phase precession’, O’Keefe &

1.2. THE ANATOMICAL AND PHYSIOLOGICAL PROPERTIES OF THE HIPPOCAMPAL FORMATION

Recce (1993)). Evidence suggests that place cells seem to have a broad spectrum of behavioural correlates including allocentric location which I am going to elaborate below.

Place cells

Place cells were first described in the hippocampal CA1 field but later recorded in all subregions of the hippocampal formation (O'Keefe et al., 1971; O'Keefe, 1976). From the observation that the firing patterns of those place cells did not respond to any single sensory cues nor distinguishable motional or motivational factors, it was insightfully proposed that those are units constructing a spatial framework as in the cognitive map theory, meaning with different cells firing at different locations the population firing fields 'map' all the locations within an environment (O'Keefe et al., 1971; O'Keefe, 1976). Ever since place cells have become a milestone of the blooming field of navigational research and thus one of our main subjects in the following experiments.

Evidence supporting the 'cognitive map' theory includes that in an open-field environment many place cells formed omnidirectional compact fields that tiled the whole environment (O'Keefe & Nadel, 1978; Muller et al., 1987; Wilson & McNaughton, 1993). Those place fields were often shown to be stable across repeated exposures to the same environment but drastically 'remap' (changing firing rate or firing fields location) across environments with different configurations and situated in different rooms (Muller & Kubie, 1987; Thompson & Best, 1990; Bostock et al., 1991; Quirk et al., 1992). It was likely that cell activities were organised with underlying attractor states representations for different environments (Hopfield, 1982; Zhang, 1996; Samsonovich & McNaughton, 1997; Wills et al., 2005). Finally, reconstructions of position from place cell activity

confirmed that with less than 100 cells the computed positions were highly accurate, with only $\sim 5\text{cm}$ of deviation from the actual positions (Wilson & McNaughton, 1993; Zhang et al., 1998). Place cells were later recorded in other species such as bats and human (Ulanovsky & Moss, 2007; Ekstrom et al., 2005).

Contradictory to the holistic view of place cell ensemble representation, it seems that place cells are rather loosely organized such that individuals respond to different subsets of cues (O’Keefe & Burgess, 1996; Gothard et al., 1996b,a; Shapiro et al., 1997; Tanila et al., 1997; Skaggs & McNaughton, 1998; Chen et al., 2013). There is, however, the consistent ensemble activity pattern of place cells to carry sequential/trajectory information. For example, place cells often fire differently depending on their start or end locations (Gothard et al., 1996b,a). Retrospective and prospective coding were found in place cells firing when rats navigate in a plus maze (Ferbinteanu & Shapiro, 2003). Most convincing evidence is the discovery of ‘replay’, a phenomenon that is robustly detected during the quiescent or sleeping period after active exploration when place cells spontaneously reactivated sequentially according to their place fields contingency during awake navigation but temporally compressed (Wilson & McNaughton, 1994; Louie & Wilson, 2001; Lee & Wilson, 2002; Foster & Wilson, 2006). Moreover, accumulating evidence suggested that place cell activity also carries non-spatial information. Relevant to the sequential replay is the encoding of elapsed time in place cells that can be dissociated from spatial coding (Pastalkova et al., 2008; MacDonald et al., 2011, 2013; Kraus et al., 2013).

Place cells also change their firing according to non-spatial features such as expectancy of rewards and memory demand (Hölscher et al., 2003; Dupret et al., 2010). Basic sensory features such as auditory and olfactory cues are also found to be represented by place cells (Wood et al., 1999; Aronov et al., 2017). The activity of place cells is found

1.2. THE ANATOMICAL AND PHYSIOLOGICAL PROPERTIES OF THE HIPPOCAMPAL FORMATION

to encode both object location and object identity when they are encountered in an enclosure (Manns & Eichenbaum, 2009; Deshmukh & Knierim, 2013). Taken together, place cells seem to be representing events-in-context information, i.e. episodic memory, that evolves sensory features bounded to spatial, temporal and even conceptual context.

The rich representation linked to place cells leads to the questioning of whether allocentric spatial representation characterizes the function of CA1 pyramidal cells the best (Eichenbaum et al., 1999; Buzsáki & Moser, 2013). Nevertheless, when spatial location is the most prominent regularity in a task such as when the animal free-forages in an open-field enclosure, place cells and a whole battery of hippocampal spatial cells reliably keep track of the animal’s allocentric location and provide the basis for vital navigation tasks. Their representation correlates well with animals’ navigational behaviour (Lenck-Santini et al., 2001) and disruption of place cell representation impede the memory of goal location (Dupret et al., 2010).

1.2.2 Entorhinal cortex

Entorhinal cortex neuron cytoarchitecture and physiological properties

The entorhinal cortex is the major gateway between the hippocampus and the cortex. It is widely accepted that there are two subfields of the entorhinal cortex, namely lateral entorhinal cortex (LEC) and medial entorhinal cortex (MEC), according to their distinctive cytoarchitecture and connectivity patterns (Blackstad, 1956; Shipley, 1975; Brodmann, 1909; van Groen et al., 2003; Canto et al., 2008). They are also considered to be participating in different cognitive functions. Mainly MEC is thought to mostly involved in spatial representation, while lateral entorhinal cortex plays a bigger role in non-spatial representation (Fyhn et al., 2004; Hargreaves et al., 2005). I will focus on

a description of the anatomical organization of the MEC.

The laminar structure of entorhinal cortex is less clear-cut compared to that of CA1. The currently recognized six-layered division defines layer II, III, V and VI as cellular layers while layer I and IV are sparse in cell bodies. Layer II is populated with stellate cells and pyramidal cells. They both project to dentate gyrus and CA3. Layer III is occupied by a more heterogeneous group of neurons such as pyramidal cells (the majority cell population), stellate cells, fusiform cells and multipolar cells. They send projections via perforant and alvear pathways to CA1 and subiculum. Layer V contains three main classes of neurons: pyramidal cells, small spherical cells and fusiform cells. The majority of these cells send axons to the white matter in a column-like organisation, as well as recurrent collaterals to entorhinal cortex superficial layers. Layer V is also the termination of projection from CA1 and subiculum (reviewed by Canto et al. (2008)).

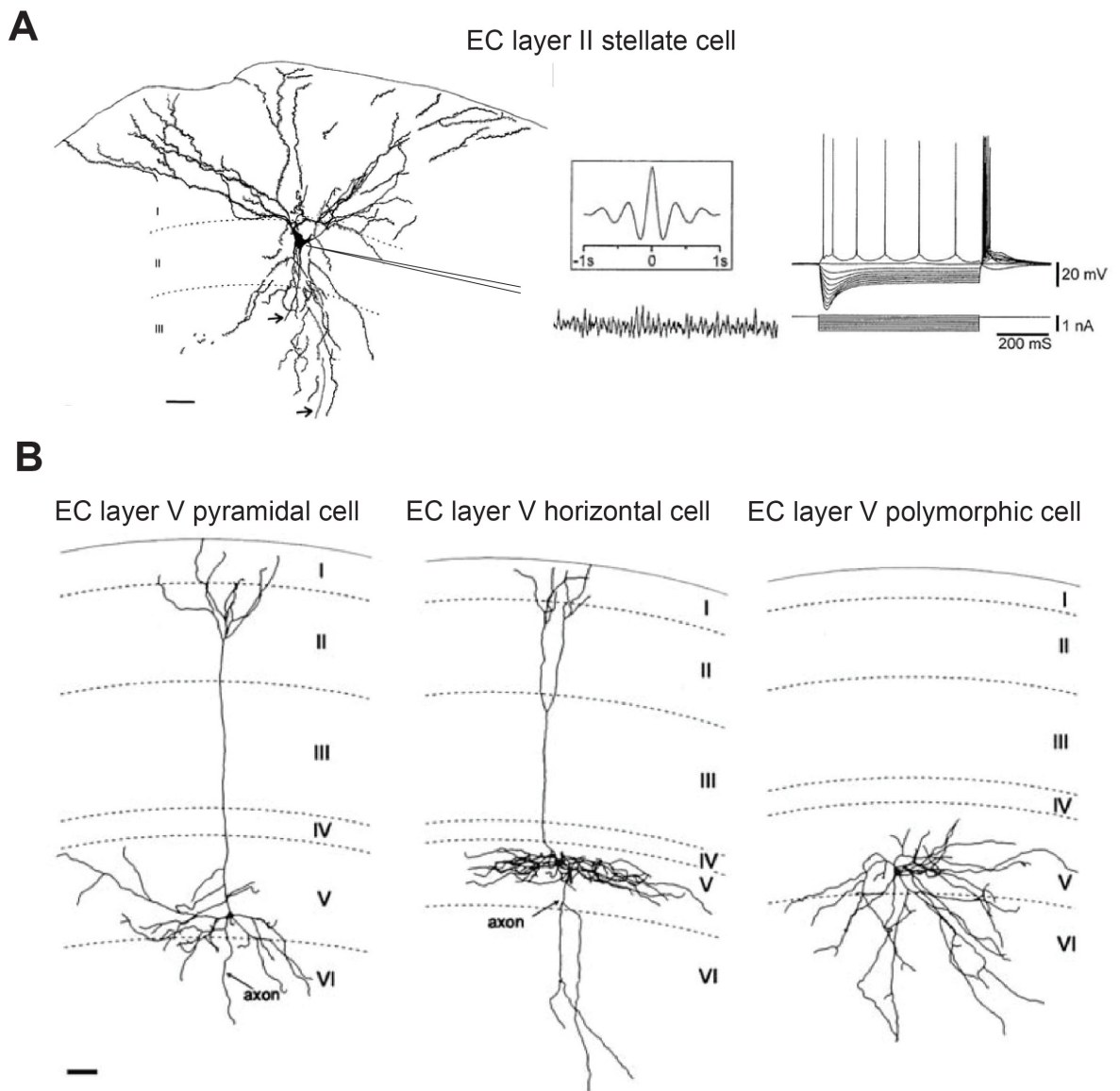
Stellate cells and pyramidal cells are major principal cell types in the entorhinal cortex. Stellate cells are most abundant in MEC layer II where they radiate dendrites out to layer I-III and send collaterals to the dentate gyrus and CA3 (see Figure 1.3A). Stellate cells are characterised by their resonance and temporal integration properties that are shaped by different voltage-gated ion channels. Specifically, the membrane-potential oscillation of stellate cells changes from high frequencies in the dorsal part of MEC to low frequencies in the ventral part (Giocomo et al., 2007). Studies have shown that the knockout of hyperpolarization-activated cyclic nucleotide-gated 1 subunit (HCN1) slows down membrane resonance, along with other temporal-integrative properties, in layer II cells (Garden et al., 2008) and changes the grid scale (Giocomo et al., 2011).

Pyramidal cells are found in both superficial and deeper layers of MEC. Superficial pyramidal cells do not share the aforementioned resonance membrane properties of stellate cells such as the subthreshold membrane oscillation. In contrast, deeper

1.2. THE ANATOMICAL AND PHYSIOLOGICAL PROPERTIES OF THE HIPPOCAMPAL FORMATION

layer pyramidal cells do exhibit theta oscillation in subthreshold membrane potential, although these appear to be independent of I_h current (Dickson et al., 2000). Perhaps the most intriguing property of layer V pyramidal cells is their ability to integrate neural activity over a long period. In the presence of the muscarinic AChR agonist carbachol, pyramidal cells in layer V/VI show sustained action potential firing after current injection paused and progressive increase in firing rate with repetitive current injection over several minutes (Egorov et al., 2002). This striking property suggests they may play an important role in working and long-term memory (Egorov et al., 2002).

Like in the hippocampus, GABAergic interneurons are also abundant and diversely populate all strata of the entorhinal cortex, especially the superficial layers. Together with the excitatory cells they constitute fine-tuned neural circuits and give rise to various forms of computation.



1.2. THE ANATOMICAL AND PHYSIOLOGICAL PROPERTIES OF THE HIPPOCAMPAL FORMATION

Figure 1.3: **Neurons in superficial and deep layer of entorhinal cortex.** (A) Camera lucida drawing of a stellate cell(left). Membrane potential oscillation of the stellate cell held at membrane potential positive to -55 mV (middle bottom). Autocorrelogram of the membrane potential (middle top) showing rhythmicity. In the right panel is the voltage response of a stellate cell to step current injection. Notice here the obvious 'sag' after current onset, and the rebound spiking after the termination of current injection. (B) Camera lucida drawing of principal cells and interneurons in entorhinal cortex layer V. Bar = 100 μ m. (Source: Adapted from Andersen et al. (2007))

MEC neuron functional properties

MEC hosts a variety of neuronal types each has distinct behavioural correlated but forms indispensable pieces to our spatial coding system. In the superficial layer (layer II and III, hippocampal efferent) and deeper layers (layer V, hippocampal afferent layer) reside different cell populations which stress the importance of understanding the entorhinal-hippocampal circuit integratively.

Grid cells

Both stellate cells and pyramidal cells in MEC can be grid cells and they are recorded in all principle cell layers. In contrast to place cells which mostly have one single place field, a grid cell have multiple firing fields that are arranged in a regular triangular array (Fyhn et al., 2004; Hafting et al., 2005). There are three important parameters in describing a grid pattern: scale, orientation and phase. The scale represents the distance between two neighbouring fields, orientation refers to the smallest angle between the three symmetric axes of the grid to the horizontal line, and phase depicts the distance

of shift between grid patterns that have similar scale and orientation. The degree of ‘gridness’ (gridness score) was tested by calculating the difference of correlation between the autocorrelogram of the cell’s spatial rate map and rotated autocorrelogram at the expected peaks (60° and 120°) and the expected troughs (30° , 90° and 120°). The amazing regularity of grid cell firing field organization and that it evenly spanned across the environment indicate that grid cell could be the solution for a metric representation which cognitive map theory had been looking for (O’Keefe & Nadel, 1978; McNaughton et al., 1996; McNaughton et al., 2006).

The anatomical and functional organisation of grid cells also fit the prediction of such a metric system that updates location through tracked movement speed and direction (McNaughton et al., 1996; McNaughton et al., 2006). Grid cells seem to cluster in modules along the dorsoventral axis of MEC so that cells within a module are anatomically closer and functionally more similar. Namely, grid cells from the same module tend to have similar grid scale and orientation, while across different modules from dorsal-most to a ventral-most portion of MEC, grid cells show discrete stepwise increased scale ($30\text{cm} - 2\text{m}$) and less coherent orientation (Hafting et al., 2005; Barry et al., 2007; Stensola et al., 2012). Interestingly, place cell field sizes were found continually expanding along the dorsoventral axis of CA1 (Jung et al., 1994; Maurer et al., 2005; Kjelstrup et al., 2008), suggesting some functional connection in between. Models and simulations proposed that by operating like a modulo system with different bases the grid cell population are capable of representing vectors between locations over a range much bigger than the biggest grid scale recorded (Fiete et al., 2008; Bush et al., 2015).

Like place cells, grid cells are also shown to replay following place cell replay sequence (Ólafsdóttir et al., 2016). Contradicting to the simplified view of grid cells being the

1.2. THE ANATOMICAL AND PHYSIOLOGICAL PROPERTIES OF THE HIPPOCAMPAL FORMATION

perfect allocentric map for space, local grid regularity was shown to be distorted by the presence of boundary and reward (Stensola et al., 2015; Krupic et al., 2018; Boccara et al., 2019). Grid firing pattern was shown on non-spatial features such as auditory and conceptual space (Aronov et al., 2017; Constantinescu et al., 2016). However, our current definition of grid cells strictly requires regular field-to-field distances and angles which were solely adopted from navigation studies. It is difficult to construct a conceptually comparable measure to test whether the grid-like pattern exists in other non-spatial features.

Head direction cells, speed cells and conjunctive cells

Head direction cells are cells that fire whenever an animal is facing a particular allocentric direction. They are first recorded in the subicular complex (Taube et al., 1990a,b), and later discovered widely distributed in subcortical and cortical limbic areas (Sharp et al., 2001; Taube, 2007). In MEC layer III and V, where the projection from presubiculum ends head direction cells are also recorded (Sargolini et al., 2006). The head direction signal is an essential contribution to self-localization as well as to path integration. The head direction system is by far the most compelling evidence that a path-integrating continuous attractor network mechanism exists in nature. Functionally, co-recorded head direction cells fire in a high concordance, the angular distance between pairs of head direction cells always remained constant even when their allocentric tuning has shifted or destabilized (Taube et al., 1990a,b; Taube & Burton, 1995; Muir et al., 2009; Yoder & Taube, 2009). Anatomically, in the *Drosophila melanogaster* ellipsoid body, activity of compass neurons track the animal’s heading direction through a bump of activity in a ring-shaped structure shifted by self-motion and visual landmarks inputs (Seelig & Jayaraman, 2015; Kim et al., 2017).

Interestingly, cells with conjunctive representation for both spatial grid patterns and head direction tuning coexist with head direction cells in layer III, V and VI of MEC. And together with head direction cells and grid cells, their firing rate increase as a function of animals' running speed (Sargolini et al., 2006). According to the continuous attractor network model, the conjunctive representation of grid firing pattern and running speed and head direction could serve as 'shifter cell' that drive the grid cell network activity to track displacement via self-motion signals (McNaughton et al., 2006). Moreover, dedicated speed coding MEC neurons (Kropff et al., 2015), as well as the speed-modulated local field potential theta frequency (Jeewajee et al., 2008) further provided plentiful of movement-based signals to support velocity-based localization in MEC.

Border cells

In MEC there is a group of neurons that fire when animals in close contact with one or more environmental borders (Solstad et al., 2008). In the boundary vector cell (BVC) model it was proposed that boundary vector cells serve as the anchor to place fields by providing direction and distance measures relative to nearby boundaries (O'Keefe & Burgess, 1996; Hartley et al., 2000; Barry et al., 2006). For grid cells, it was found that after encountering borders, grid fields accuracy increased in the perpendicular direction to the border while remained unchanged parallel to the border, coincident with that border cell firing rates are sharply tuned in the orthogonal direction to the wall and had low specificity along the direction of the wall (Solstad et al., 2008). It was further established that boundary representation is highly environment invariant, and when they do change between different environments their activity is in line with co-recorded grid cells and head direction cells (Solstad et al., 2008). Taken together, it was strongly

1.2. THE ANATOMICAL AND PHYSIOLOGICAL PROPERTIES OF THE HIPPOCAMPAL FORMATION

suggested that border cells, head direction cells and grid cells cooperate to establish a stable allocentric metric representation in MEC.

Other functional cell types

Cells that fired in a certain direction and distance towards multiple objects were also discovered in MEC (object vector cells, Høydal et al. (2019)). Compare to the classical spatial cells types that code location in the framework of enclosed environments, object vector cells have more flexible and less geometrically defined spatial representation. As moveable objects also constitute an important part of our natural experience, how they are integrated into our spatial representation calls for future investigation.

Interactions between hippocampal-entorhinal spatial cells

The interaction between different spatial cells is dynamic yet somewhat hierarchical. Developmental studies In rats have shown that within the hippocampal-entorhinal system, the head direction cells are among the first to display adult-like tuning properties as early as age P14 (14 days postnatal) when they just started to navigate (Wills et al., 2010; Langston et al., 2010; Bjerknes et al., 2015). Place cells catch up later (from P16) to show spatial selectivity but continue to develop in spatial information and fields stability, which peaked after the regular firing pattern of grid cells emerge around P20 (Wills et al., 2010; Langston et al., 2010; Muessig et al., 2015).

Lesion studies probing the head direction system converged on the conclusion that the generation of head direction signal and their attractor network organization happened subcortically. Disrupting cortical inputs generally caused none to mild effect on head direction signal in subcortical regions, while the other way around abolished proper

head directional signal in the downstream (Blair et al., 1998; Calton et al., 2003; Bassett et al., 2007; Taube, 2007; Sharp & Koester, 2008; Muir et al., 2009; Yoder & Taube, 2009; Clark & Taube, 2011; Yoder et al., 2011; Clark & Taube, 2012). Except for the integrity of postsubiculum played an important role in integrating the landmark control into head directional tuning as well as in orienting other spatial cells (Goodridge & Taube, 1997; Yoder & Taube, 2009).

Grid cell ensemble firing contingency, as predicted from their attractor network organization, maintain robust while their regular hexagonal firing pattern being susceptible to disruption in lack of stable inputs from head direction cells and place cells (Bonnevie et al., 2013; Winter et al., 2015). Place cells, on the other hand, consistent with the fact they respond to diverse environmental and idiothetic cues, maintain but with degraded selectivity of spatial firing with disrupted inputs from either head direction cells or grid cells (Calton et al., 2003; Brun et al., 2008a; Koenig et al., 2011; Brandon et al., 2014).

1.2.3 Intrinsic connections in the hippocampal formation

The majority of intrinsic connections in the hippocampal formation are unidirectional (See Figure 1.4). Principal cells in the superficial layers of the entorhinal cortex send projections to the dentate gyrus, CA3, CA1 and subiculum via the perforant Alvear pathways. Specifically, layer II and layer III of MEC and LEC each project to topographically different parts of hippocampal areas (for review, see Witter (1993)).

1.2. THE ANATOMICAL AND PHYSIOLOGICAL PROPERTIES OF THE HIPPOCAMPAL FORMATION

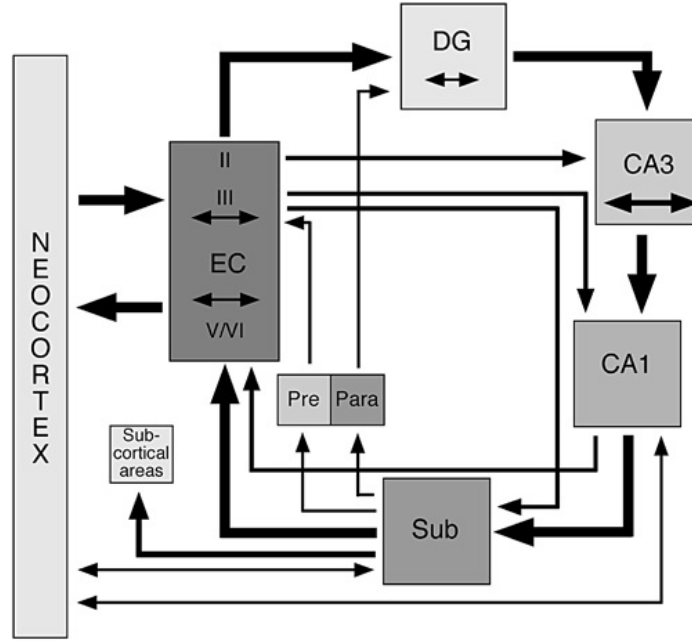


Figure 1.4: **Intrinsic connections in hippocampus.** (Source: Adapted from Andersen et al. (2007)).

Axons from entorhinal layer II terminate in the molecular layer of the dentate gyrus and stratum lacunosum-molecular layer of CA3. Fibres from entorhinal layer III innervate stratum lacunosum-moleculare of CA1 and the superficial portion of the molecular layer of the subiculum. In the dentate gyrus, projections from LEC terminate in the superficial portion of the molecular layer while projections from MEC terminate in the deeper portion of the molecular layer. LEC and MEC projections to proximal and distal (according to the proximity to dentate gyrus in transverse axis) parts of CA3, distal and proximal portions of CA1, and proximal and distal portions of the subiculum, respectively (Steward & Scoville, 1976; Steward, 1976; Witter et al., 1989).

Granule cells in the dentate gyrus then exclusively project to CA3 through mossy fibres which terminate in a narrow zone just above the pyramidal cell layer of CA3. CA3 then sends axon collaterals to CA1 (Schaffer collaterals), CA2 and CA3 (recurrent collaterals) in stratum radiatum and stratum oriens. The Schaffer collaterals projection

is also topographically organized. Proximal CA3 neurons tend to project more to CA1 at more septal levels than their locations while distal CA3 neurons more to temporal levels of CA1. Within the same septotemporal level, proximal CA3 innervates the distal portion of CA1 and distal CA3 innervates the proximal portion of CA1 (Ramon y Cajal, 1911; Blackstad et al., 1970; Tamamaki et al., 1987; Naber et al., 2001).

As described above, CA3 and entorhinal cortex are the two major intrinsic inputs to CA1 within the hippocampal formation. The fact that CA3 also receives input from entorhinal cortex makes connections between CA1 and entorhinal cortex both monosynaptic and disynaptic (mediated through the Schaffer collaterals). By comparing the topographic organization of these intrinsic projections we can see that both the monosynaptic and the disynaptic innervation originate and terminate in the same EC/CA1 areas. Combined with the sophisticated input integration properties in CA1 neural circuits, and information cascade emerges in CA1.

CA1 projects to subiculum in its pyramidal layer and deep part of the molecular layer (Tamamaki et al., 1987). Both of them in turn project back to the deep layers of EC (Köhler, 1985; Van Groen & Wyss, 1990). Interestingly, such return projections are again topographically organized and mirror the EC efferent projections. Specifically, distal CA1 and proximal subiculum project to the lateral entorhinal cortex, while proximal CA1 and distal subiculum project to the medial entorhinal cortex. Finally, EC deeper layers send axons that descend into the angular bundle and project information out of the hippocampal formation, to cortical and subcortical regions, as well as associative collaterals that ascend into the superficial layers to innervate superficial EC neurons (Hamam et al., 2000, 2002; Kerr et al., 2007; Canto & Witter, 2012a,b; Witter et al., 2017). Thus the closed-loop pathway within the hippocampal formation is completed. Such closed-loop projection and highly associative and

1.2. THE ANATOMICAL AND PHYSIOLOGICAL PROPERTIES OF THE HIPPOCAMPAL FORMATION

divergent connections within the hippocampal formation suggest that representations in different regions of hippocampus are associative and reciprocally informative.

1.2.4 Extrinsic connections

The hippocampal formation is connected to a broad set of brain regions, including the neocortex, amygdaloid complex, forebrain nuclei (medial septum and diagonal band of Broca), thalamus and hypothalamus, and brain stem (medial tegmentum) (Mosko et al., 1973; Herkenham, 1978; Wyss & Groen, 1992). Through these projections, sensory input (visual, auditory, olfactory and tactile etc.) and self-motion input are all converging on the hippocampus. There the spatial representation emerges. Albeit each of the connections bears its significance, I am going to emphasize neocortical, septal and vestibular projections for their critical roles in providing hippocampal formation with sensory and self-motion inputs.

Neocortical connections with the hippocampal formation

Entorhinal cortex is the hub that connects cortex and hippocampus together. Most of the cortical input to hippocampus proper passes through the entorhinal cortex. Immediately adjacent to entorhinal cortex lie the perirhinal and postrhinal cortices, both of which are polysensory convergence areas that receive input from a variety of unimodal and polymodal sensory cortices (Burwell, 2001). MEC receives its predominant input from the postrhinal cortex while LEC receives its major inputs from the perirhinal cortex. Perirhinal cortex also directly projects to distal CA1 in stratum lacunosum-moleculare and proximal subiculum in its molecular layer. Their axons co-localize with axons from LEC. Similarly, postrhinal cortex innervates the

proximal CA1 and distal subiculum, overlapping with medial entorhinal cortex inputs. To sum up, projections from perihinal and postrhinal cortices to hippocampal formation follows the topographic organization established in hippocampal intrinsic connections and forms a continuum (Burwell, 2001).

A quantitative analysis revealed that MEC and LEC receive similar amounts of input from piriform (MEC 31%, LEC 34%), temporal (MEC 21%, LEC 26%) and frontal cortices (MEC 10%, LEC 11%). However, LEC receives more projections from insular cortex (MEC 6%, LEC 21%), while MEC receives more input from cingulate (MEC 11%, LEC 3%), occipital (MEC 12%, LEC 2%) and parietal cortices (MEC 9%, LEC 3%) (see Figure 1.5; Burwell & Amaral (1998)). It is noticeable that more visual information enters the hippocampus through MEC than LEC, potentially contributing to hippocampal spatial representation.

1.2. THE ANATOMICAL AND PHYSIOLOGICAL PROPERTIES OF THE HIPPOCAMPAL FORMATION

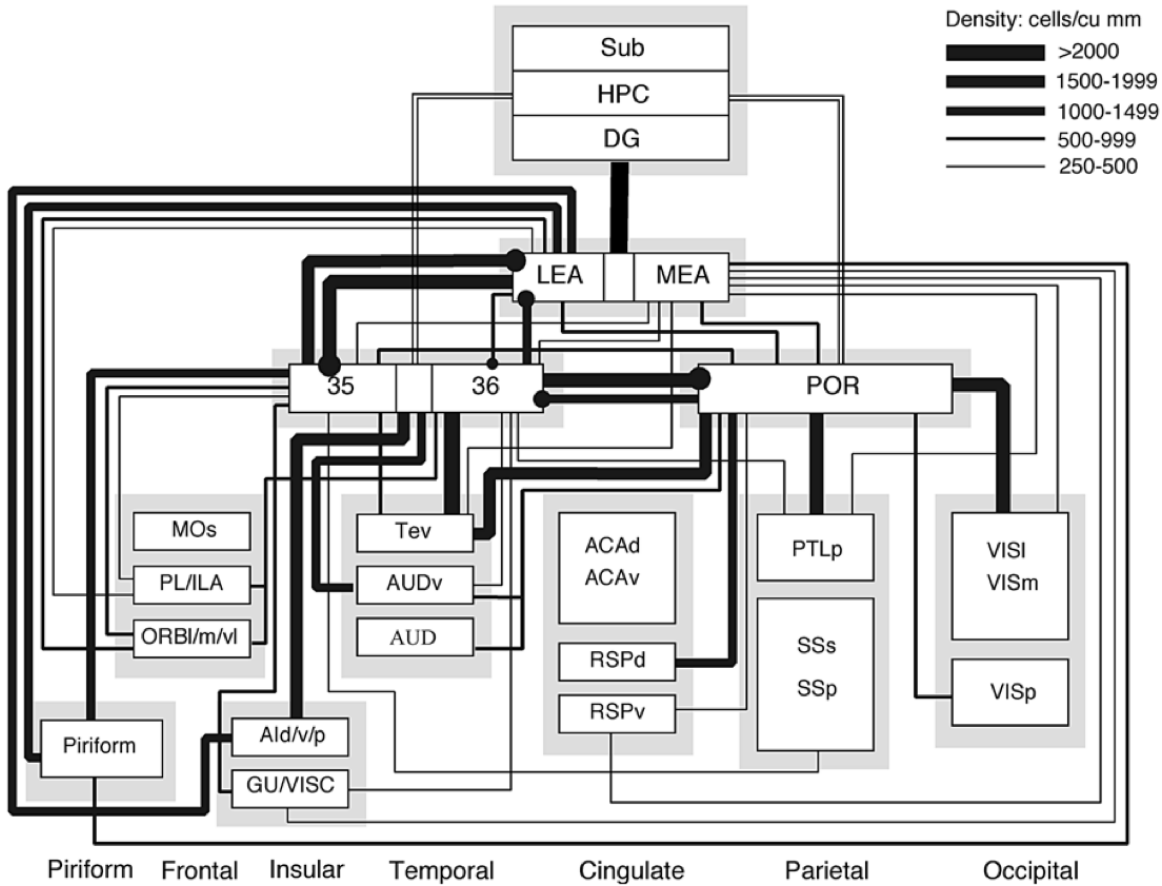


Figure 1.5: **Pattern and strength of cortical connectivity of the rat hippocampal formation.** The thickness of the solid lines represents relative strength of the connections based on the densities of retrogradely labeled neurons. Open lines represent reported connections for which no comparable quantitative data are available. ACAd and ACAc, dorsal and ventral anterior cingulate cortex; Ald/v/p, dorsal, ventral, and posterior agranular insular cortices; AUD, primary auditory cortex; MOs, secondary motor area; ORBl/m/vl, orbitofrontal cortex, lateral, medial and ventral lateral; PL/ILA, prelimbic and infralimbic area of ventromedial prefrontal cortex; PTLp, posterior parietal cortex; RSPd and RSPv, retrosplenial cortex, dorsal and ventral; SSs and SSs, primary and supplementary somatosensory areas; Tev, ventral temporal area; VISC, visceral granular insular cortex; VISl and VISm, lateral and medial visual association cortex; VISp, primary visual cortex. (Source: Adapted from Andersen et al. (2007), who also adapted from Burwell & Amaral (1998)).

Septo-hippocampal projections

A prominent EEG slow oscillation (theta band oscillation, 4-12 Hz) was recorded everywhere in the rats' hippocampal formation except for CA2 (Elazar & Adey, 1967; Mitchell & Ranck, 1980; Alonso & García-Austt, 1987a,b). Two components of the local field potential (LFP) theta oscillation were distinguished experimentally (Vanderwolf, 1969). One increase frequency and amplitude during locomotion, the other appears related to the arousal and attentional state of the animal in the absence of translational movement (Kramis et al., 1975). It is clear now that none of these field theta components are independently generated within the hippocampal formation, because Lesion or inactivation of the medial septal nucleus and the diagonal band of Broca (MSDB) completely abolishes the EEG theta oscillation in the hippocampus (Lawson & Bland, 1993). EC lesions eliminate the former component but not the latter, which was further abolished by administration of atropine (Kramis et al., 1975).

There are several proposed functions for the hippocampal theta oscillations, which include network synchronization, spike phase timing and scheduling LTP/LTD induction. Directly link to spatial representation is the function of spike phase timing. It is found that interneurons recorded in hippocampus often fire at fixed phases relative to the LFP theta oscillation (Ranck, 1973). Other than increasing their firing rate in response to location, place cells and grid cells are also shown to fire at progressively earlier phases relative to LFP theta oscillation when the animal traverses their firing fields, an effect known as 'phase precession' (O'Keefe & Recce, 1993; Hafting et al., 2008). Interestingly, the phase of spiking is better explained by distance that the animal traveled through the place field other than time or distance according to environmental cues (Huxter et al., 2003).

In order to account for phase coding of distance, the oscillatory interference model

1.2. THE ANATOMICAL AND PHYSIOLOGICAL PROPERTIES OF THE HIPPOCAMPAL FORMATION

was proposed, suggesting that there exists a slightly higher-frequency oscillator (intracellularly) whose frequency increases with running speed. As a result, the 'beating' interference of the two oscillators (theta and the intracellular oscillator) would give rise to phase precession (O'Keefe & Recce, 1993; Burgess et al., 2007; Burgess, 2008). Theoretically, the oscillatory interference model could also explain grid cells' periodic firing patterns. Thus it is important to understand the generation of both field theta oscillation and intrinsic theta oscillation, as well as the mechanism of their velocity controlled frequency. 'Theta cells' recorded in the hippocampus, medial septum and anterior thalamus show firing properties resembling the velocity controlled oscillators proposed in the oscillatory interference model (Welday et al., 2011). Recent study shows that the locomotion related theta component appears to be initiated by a group of glutamatergic neurons (VGluT2⁺) in MSDB, which are also responsible for locomotion initiation (Fuhrmann et al., 2015). Taken together, the septohippocampal system is critical for generating theta oscillation and velocity signals.

Vestibular system interactions with the hippocampal formation

Following up on the previous section, speed signal is important for spatial coding (especially for path integration). In mammals, there are often five sources of speed information: visual (optical flow), vestibular (angular and linear acceleration), proprioceptive (feedback information from muscles, tendons, and joints), efferent copy of locomotor commands and inertial signals from extr vestibular gravity receptors (Mittelstaedt & Mittelstaedt, 1982; Mittelstaedt, 1999). By far the vestibular system is the most studied source of self-motion input largely because of its critical role in head directional tuning (Taube, 2007). There are four major pathways through which the vestibular nucleus projects to the hippocampal formation (see Figure1.6).

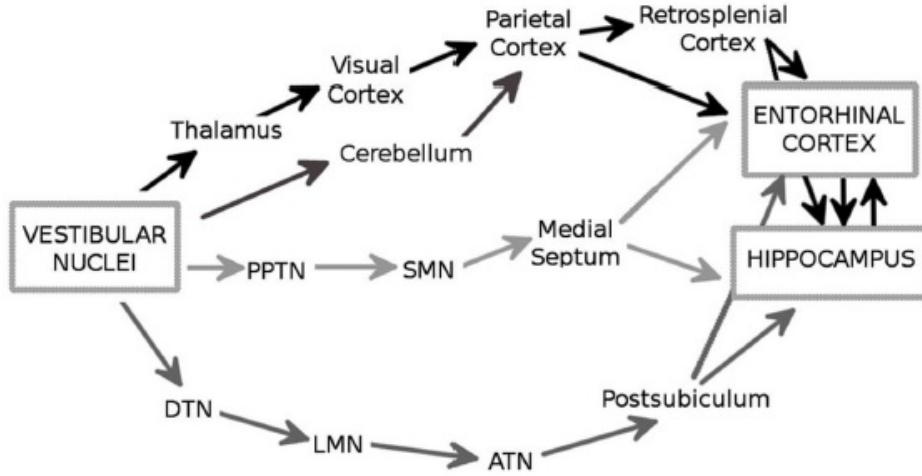


Figure 1.6: **The major anatomic pathways through which the vestibular signals reach the hippocampus and the entorhinal cortex.** PPTN: pedunculo pontine nucleus; SMN: supramammillary nucleus; DTN: dorsal tegmental nucleus; LMN: lateral mammillary nucleus; ATN: anterodorsal thalamic nucleus (Source: Adapted from Jacob et al. (2014)).

The vestibular apparatus detects both angular and linear accelerations of the head, then pass the acceleration reading to the central vestibular nuclei and transform them into velocity signals. Take the computation of angular velocity as an example, as this demonstrates well how self-motion and visual inputs interact to generate an accurate and stable sense of head rotation. When an animal rotates its head, the semicircular canals in the inner ear pick up the directional angular acceleration signals, causing downstream neurons to fire. This firing, as well as angular optic flow input, triggers both eyes of the animal to rotate to the opposite direction, helping the animal to maintain stable visual fixation (vestibulo-ocular reflex). Many cells in the mouse vestibular nucleus respond to both head rotation and eye position (eye sensitive neurons). Their sensitivity to head rotation is generally higher than those of cells that only respond to head rotation (vestibular only neurons; Beraneck & Cullen (2007)). Especially during low frequency angular motion, when the eye position tuning component is regressed out,

the total head sensitivity of eye sensitive neurons decreased significantly and became non-distinguishable from the vestibular only cells (Beraneck & Cullen, 2007). Thus visual input amplifies angular velocity coding and compensates for when acceleration is small and the vestibular response alone fails to catch up with head rotation. Although less understood, the vestibular coding of linear acceleration via otolithic input is shown to benefit path integration in the dark (Yoder et al., 2015).

1.3 Spatial representation based on environmental cues and self-motion tracking

There are different strategies one can use to adopt locational information. One is to learn the configuration of different sensory cues in the environment. Salient cues that been examined carefully in studies include environmental boundaries, distal visual landmarks, local olfactory or tactile cues and so on. Another important strategy is to update location through accumulating self-motion which is often referred to as 'path integration'. In some recent views, path integration comes to have broader connotations, for example, even including contributions to landmark perception (Savelli & Knierim, 2019). But for simplicity and better resonance with our experimental interests to examine the effects of dissociation of (virtual) external environmental visual information from self-motion information, I restrict the definition of path integration in the current thesis to the updating of self-location derived from self-motion information such as proprioception, motor efference copy and vestibular inputs.

1.3.1 Environmental cues

Behavioral experiments

There is no doubt that animals use various sensory cues to self-locate. For example, insects adopt several sensory localization strategies which include using sun and skylight to orient, store view-dependent 'snapshots' of home location and follow landmark anchored routes (Wehner, 2003). When multiple sensory cues are available, which often come with different reliability (error distribution), humans often combine them in nearly optimal fashion to estimate spatial parameters (Deneve & Pouget, 2004). A Bayesian framework was proposed to predict the integration of different sensory cues, meaning that the combination of different sources are obtained as the weighed sum proportional to the inverse of their distribution variance (Deneve & Pouget, 2004). The more stable and accurate the sensory information is, the higher weight they have. Studies showed that humans combine visual and auditory cues (Deneve et al., 2001), visual and haptic cues (Ernst & Banks, 2002) almost exactly following the optimal Bayesian rule.

Also, in order to combine multimodal inputs it is important to solve the issue of registration between different reference frames. For example, visual cues are represented in retina-centre reference frame, and auditory cues are perceived in a head-centred reference frame. However it seems the cross-modal combination of sensory cues are implemented in a common spatial frame for that the posture change that causes reference frame of different modalities to change (e.g. change of eye position) do not affect the combined distribution (Deneve & Pouget, 2004). Interestingly, similar principles are discovered in electrophysiological recordings in behaving animal.

Electrophysiological recordings in behaving animal

Place fields recorded in a familiar environment can be very stable across days (Muller et al., 1987; Thompson & Best, 1990), although changes in firing patterns also develop over longer period (Lever et al., 2002; Ziv et al., 2013). When perceived environmental changes are salient enough, place cells change their firing field locations drastically, and active cells drop in and out as if a new map is generated ('global remap', Muller & Kubie (1987); Leutgeb et al. (2005)). Minor environmental changes lead to changes in place cell firing rates without disturbing their spatial selectivity ('rate remap', Muller & Kubie (1987); Leutgeb et al. (2005)). Efforts made to 'disrupt' established firing fields suggested that several factors contribute to place cells' tuning to specific locations.

Visual cues are among the first that were tested, when distal visual cues are rotated they often dominate the orientational anchoring of place cells, head direction cells and grid cells causing them to rotate together in accordance (O'Keefe & Nadel, 1978; Muller & Kubie, 1987; Taube et al., 1990b; Hafting et al., 2005). Removing subset of cues and scale the size of cue cards have minimum effect on the majority of place cell and head direction cell firing (O'Keefe & Nadel, 1978; Muller & Kubie, 1987; Taube et al., 1990b). Unlike the concordant response reported above, conflict cue control experiments find that when local cues (local visual and tactile patterns) are rotated as well as distal cues but to the opposite direction ('double rotation'), some place cells follow the distal cues, some follow local cues and some stop firing or form new fields whose locations can not be predicted by the rotation of either cues (Shapiro et al., 1997; Knierim, 2002). In their results, Knierim (2002) also find when the discrepancy between distal and local cues is small (45°), more place cells rotate by an angle as if a compromise between the two sets of cues was taken. Similarly in another study when two cue cards (one is white, another is black) on the inside of environmental walls are rotated so that the

angular distance between them are either decreased or increased by 45° , place cells show combined influence from both cue cards (Fenton et al., 2000).

Getting rid of visual cues yields mixed effects on place cells, often depending on the animals' preceding experience (attribute to path integration, details in Section 1.4.2; Quirk, Gregory et al. (1990); Markus et al. (1994)). For grid cells, when rats free-forage in a familiar open field in darkness, it is reported that many of them remain their spatial firing regularity despite minor decrease in firing stability (Hafting et al., 2005). On the other hand, without visual input mice navigate in the dark fail to form regular periodic grid firing patterns (Chen et al., 2016; Perez-Escobar et al., 2016). One explanation to such different results is the non-visual environmental cues are handled differently (e.g., whether or not the environment floor was wiped). As crepuscular creatures, rodents exploit non-visual local cues, such as olfactory and tactile cues, to support localization. Blind rats have place cells that display normal place fields (Save et al., 1998). In the absence of visual input, Olfactory cues stabilize place cells (Save et al., 2000). Even spatially organized constellation of olfactory cues can be learnt so that their rotation controls place cell population to rotate accordingly, and their spatial shuffling cause place cells to 'remap' (Zhang & Manahan-Vaughan, 2015).

Environmental configuration also affects place cell firing. Place cell and grid cell firing patterns are mostly omnidirectional in a 2D open field (Muller et al., 1987) but their place fields expand in size and become more directional when environmental configuration constrain the animal to relatively stereotyped trajectories, such as 1-d linear track (Gothard et al., 1996a; Brun et al., 2008b; Navratilova et al., 2012), circular track (Battaglia et al., 2004), zigzagged tracks (Derdikman et al., 2009) and multi-armed mazes (McNaughton et al., 1983; Thompson & Best, 1989). When animals are transferred from a square shaped open field to a circular shaped one, place

1.3. SPATIAL REPRESENTATION BASED ON ENVIRONMENTAL CUES AND SELF-MOTION TRACKING

cells often 'remap' (Muller & Kubie, 1987; Wills et al., 2005), and the divergence of spatial population vector representation increases with experience between the two environments (Lever & Burgess, 2012). When an environment is scaled, i.e. with walls stretched or compressed in a square environment, place cell field sizes and grid cell scales changed accordingly (O'Keefe & Burgess, 1996; Gothard et al., 1996a; Barry et al., 2007; Diba & Buzsáki, 2008), and this change seems to be reduced if the animals spend enough time familiarizing the scaled environment (O'Keefe & Burgess, 1996; Barry et al., 2007). It is worth noting that in all the environmental manipulations, unlike the heterogeneous responses observed in place cells, grid cells from the the same modules changed coherently and the phase offset among them remained fixed (Stensola et al., 2012). Simultaneous recording of place cells and grid cells found that global remapping in place cells is often accompanied by phase shift or rotation in grid cells while rate remapping is not (Fyhn et al., 2007).

Last but not the least, as stated in the behavioral studies, when considering multimodal sensory integration an important issue is how to register different reference frames. Sensory inputs are by nature egocentric and centred in their receptor organs. For example, visual receptive fields are retinotopic, in order to transform them from an eye-centered coordinate to a head-centered coordinate, neurons in posterior parietal cortex (PPC) show visual sensitivity that can be described by the product of retinal receptive field profile and a function of eye position ('gain field', Andersen et al. (1985)). Many neurons in PPC show gain field tuning for visual and auditory stimulus thus potentially support flexible coordinate transformations (Xing & Andersen, 2000).

Models of sensory integration

In summary, there are several important aspects to sensory integration. First, rigid changes of environmental cues (such that no cues move relative to the others) and removal of subset of cues do not affect the cell-to-cell spatial firing relationships, as if a stable map structure exists for the whole place cell population. Second, when the cues are changed relative to each other, and discrepancy between different cues are small, weighted sum of cues are taken. Last, the influence vector of cues, representing both direction and strength of influence, often have a spatial distribution (Fenton et al., 2000). It recognized that models that adopt error distributions (e.g. Gaussian distribution) and degrade cue influence with increased distance perform well in accounting experimental data.

One of the most successful example is the boundary vector model (BVC) model (O'Keefe & Burgess, 1996; Hartley et al., 2000). The BVC model predicts that place fields are determined as a thresholded sum of a set of boundary vector cells input whose tuning is a Gaussian distribution peaked at a specific distance to a specific environment boundary. By showing prediction of place cell field change when the walls of square box are compress and/or stretched, the model's prediction closely matches the experimental observation of place field changes (O'Keefe & Burgess, 1996; Barry et al., 2006; Hartley et al., 2000). The predicted boundary vector cells were discovered in the subiculum (Lever et al., 2009). The BVC model provides substantial explanation as to the environmental anchoring/resetting process of hippocampal spatial responses and supports the general sensory summation model.

1.3.2 Path integration

Path integration as a navigation process was first proposed by Darwin: he observed that diverse species displaying a fixed home base are often capable of integration of inertial signals, a capability he called 'dead reckoning' (Darwin, 1873). Many species (birds, insects and mammals etc.) take a tortuous outbound path in search for food and return home via a direct path once the food is located. It is proposed that animals keep track of their movement from a reference point ('home') and continuously update their current location without relying on external cues, such process was named 'path integration' (Mittelstaedt & Mittelstaedt, 1980). In its original definition, path integration means to keep a linear and angular tracking of the subject's home location ('home vector'). Now it is broadly used to describe a mechanism of transforming movement into position information. Here I restrict the definition of path integration to the updating of self-location derived from self-motion information such as proprioception, motor efference copy and vestibular inputs. Path integration is important for animals because in natural environments external landmarks are often too sparse or take too much time to sample for effective navigation. In this section, I will summarise what we know about path integration at the behavioural, cognitive and computational levels.

Can animals path integrate?

There have been lots of behavioral studies trying to determine animals' skills at path integration and what factors may affect it. The difficult task of estimating the role of path integration experimentally is to make sure that the observed effects are not mediated by the presence of external sensory cues. There are two major ways that experimenters achieve this. The first one is to manipulate external cues so that their effects are either minimal or in conflict with self-motion cues. The second way is

to manipulate self-motion input directly and estimate the corresponding change in behaviour.

A classical behavioral paradigm is the 'two-leg route' task in which the animals followed an outbound path that comprised two direct paths joined by an angle, and then returned to the starting position. Studies on ants (Muller & Wehner, 1988), hamsters (Séguinot et al., 1993) and humans (Loomis et al., 1993) show that despite small errors, all these animals were able to find direct paths towards the starting location. Notice that in the experiments, ants were allowed to use the sun and skylight compass, while hamsters and humans were deprived of visual, auditory, olfactory and tactile spatial references. Observations also suggested that errors tend to increase with bigger turns in between the two legs and longer traveling distance. Interestingly, errors were not randomly distributed, instead they systematically shifted towards the direction of outbound path (Muller & Wehner, 1988). It was proposed that animal may use rather simple incremental approximation instead of a rigorous Euclidean vector summation algorithm to integrate movements step by step (Muller & Wehner, 1988).

An animal's ability to maintain a 'home vector' representation independently from landmarks was nicely demonstrated by dislocating the desert ants at their feeding location. The experimenter captured the ants after they set out from the home base and found food. Before starting their inbound journey, the ants were manually carried to a distant novel location and released (to ensure there is no prominent sensory beacon for homing). Ants' homing trajectory were immediately recorded and shown to be following the route as if they were to return home from the old feeding location (Wehner & Wehner, 1986).

Another experimental paradigm is the food hoarding experiment, where golden hamster have to leave their nest box on the periphery of a circular platform, search for a food

1.3. SPATIAL REPRESENTATION BASED ON ENVIRONMENTAL CUES AND SELF-MOTION TRACKING

source placed somewhere in the center of the arena, and return back directly to the nest box. Golden hamsters are capable of following the right direction even when visual, auditory, olfactory and tactile cues are eliminated (Etienne et al., 1986). The error between the animals' estimated home location and the real location, and in particular the angular error, increases with the amount of rotation the animal makes (Etienne et al., 1988).

When the golden hamsters are provided with conflicting information between the external cues (distal visual landmarks and local olfactory cues) and their path integration input, their behaviour reflect both sources of information. When the conflict is small (90° degree deviation) visual cues, if familiar, dominates over path integration inputs, while, if the difference is large (180° deviation), and self-motion input was uninterrupted, animals typically follow a route based on path integration, albeit some are disoriented (Etienne et al., 1990). Time also plays a role in determining the influence of distal visual cues. If familiar visual cues are presented during the food hoarding stage of the task, when the animals are in the center of the environment, they drive animal' homing direction to a closer match to themselves than when the visual cues are available during the outbound journey (Etienne et al., 1990).

In order to manipulate the self-motion input directly, researchers changed the leg length of desert ants, and found that they overestimate their travel distance when their leg lengths are shortened and underestimate travel length when leg lengths are elongated, suggesting that ants use a stride integtator to track their linear displacement (Wittlinger et al., 2007). A study compared bees foraging at higher altitude with those foraging at ground level found that the higher altitude route led to underestimation of distance, leading to the suggestion that bees use retinal image motion perceived from the ground to estimate the distance flown (Esch & Burns, 1996).

Summing up, animals can utilize many self-motion cues to keep track their angular and linear displacement from a reference point - a vector representation. Such tracking depending on introspective cues alone are prone to accumulative errors when travel distance and duration increase. External sensory cues are required to correct for errors in path integrator. When path integrator and landmark inputs are not matched, their integration depends on the amount of discrepancy between them (Etienne et al., 1990; Cheng et al., 2007).

Do hippocampal spatial cells perform path integration?

Several studies found that place cells, head direction cells and grid cells were able to maintain their normal spatial tuning (in some cases degraded) when visual input was eliminated (Quirk, Gregory et al., 1990; Markus et al., 1994; Save et al., 1998; Goodridge et al., 1998; Gothard et al., 1996a; Hafting et al., 2005), suggesting the spatial representation may be sustained via path integration. Besides, place cell firing fields were more stable between light-on and light-off conditions if rats were allowed uninterrupted exploration when the light was turned off (Quirk, Gregory et al. (1990)). Allowing rats to travel between the otherwise divided compartmental environments also induced a more coherent global representation in grid cells across compartments (Carpenter et al., 2015; Wernle et al., 2018).

However, recent studies found that grid cells recorded in mice lost their firing fields' regularity when no reliable visual cues were available (Chen et al., 2016; Perez-Escobar et al., 2016), even though pre-exposure in the light condition with uninterrupted navigation before and after switching off the light helped stabilize their firing patterns for a few minutes, before they deteriorate rapidly in the dark (Chen et al., 2016). These mixed results could be coming from experimental methods (e.g. whether olfactory

1.3. SPATIAL REPRESENTATION BASED ON ENVIRONMENTAL CUES AND SELF-MOTION TRACKING

cues were cleaned between trials, or the degree of darkness, animals' familiarity with environments, and so on), or reflecting some innate between-species difference in how visual cues and self-motion cues support localization.

Further efforts were made to establish that place cells were truly able to track distance, independently of environmental cues, with self-motion inputs. The influence of local environmental cues and time coding aspects of place cells were carefully isolated, examined and excluded. Place cells were recorded on a linear track where at one end is a movable box that was randomly dislocated when the rats left and a fixed reward location at the other end. Rats were encouraged to shuttle from end to end. Place fields close to the movable box fired at fixed distances to it at varying positions on the track in both light and dark conditions (Gothard et al., 2001). On the other hand, rats driving a car, or stationary but with rotated visual cues on a circular track, had diffuse place fields, suggesting the importance of vestibular input (Terrazas et al., 2005). Last, by recording from preweaning rats at an age before grid cells were functionally developed in the same linear track with varied starting locations, it was shown that place cells, without the influence of grid cells, can encode distance from self-motion inputs (Bjerknes et al., 2018).

Another important question is whether the hippocampal spatial representation is necessary for the animal to do path integration. Using genetic manipulation techniques, researchers specifically targeted and shut down the cell function of neuron populations and revealed that disrupting spatial tuning in MEC grid cells compromised both angular and linear path integration when mice were tested in L-maze task in a swimming pool, and the level of disruption in grid cells firing (assessed by spatial information and gridness score) was positively correlated with task deficit (Gil et al., 2018). Inactivation of MEC stellate cells also rendered mice incapable of estimating distance on a running

wheel and recognizing object locations in the dark (Tennant et al., 2018).

The development of virtual reality techniques allows researchers to dissociate environmental cues and animals' self-motion cues dissect their contributions separately (Chen et al., 2013; Saleem et al., 2013; Seelig & Jayaraman, 2015; Tennant et al., 2018). Changing the gain factor that mapped animals self-motion to visual projection resulted in the joint influence of visual and self-motion cues on place cells' firing fields (Chen et al., 2013). In *Drosophila melanogaster* ellipsoid body where the neural activity bump shifts and tracks its head direction relative to the visual scene, changing the angular visual-motion gain lead the activity bump to follow the visual angular velocity mainly (Seelig & Jayaraman, 2013). Here it needs to be considered that head-fixation limits vestibular input thus reduced the significance of self-motion cues. As shown in Aghajani et al. (2015), place cells' spatial selectivity was impaired in a 2-d environment without vestibular input. Recordings from speed modulated V1 neurons show best speed correlates to a weighted combination of visual and locomotion speed when their relative gain was changed (Saleem et al., 2013). Meanwhile, a close relationship between hippocampal place cells and V1 neurons activity was repeatedly found, so it is reasonable to assume optic flow may play a role in speed coding in the hippocampus.

In their proposed models, Raudies & Hasselmo (2015) stressed the importance of external cues (e.g. landmarks, optic flow, etc.) on path integration by pointing out the overlooked difference between head direction signal versus movement direction signal that prevailed in the hippocampal system. Using the latter to update self-motion velocity would result in errors in the path integration. The fact that the directional system is aligned in the head-centre frame makes it suitable for integrating many sensory derived motion signal (e.g. optic flow, whisker tracking, etc.). It was also suggested that topographic organization in the visual cortex, such as ventral versus dorsal visual

1.3. SPATIAL REPRESENTATION BASED ON ENVIRONMENTAL CUES AND SELF-MOTION TRACKING

pathway and dorsal versus ventral visual field sensitivity, could explain the observed gradient in grid spacing along the dorsoventral axis of MEC (Stensola et al., 2012) and how different grid modules respond to environment stretch differently (Barry et al., 2007; Raudies & Hasselmo, 2015).

Computational models that could be implemented by the hippocampal formation for path integration

Continuous attractor neural network (CANN) model

Researchers notice that head direction cells (Taube et al., 1990a; Mizumori & Williams, 1993; Chen et al., 1994; Sargolini et al., 2006; Taube, 2007) always rotate similarly together either in response to cue rotation (Knierim et al., 1995) or spontaneous drifting (Mizumori & Williams, 1993). The cell-to-cell angular phase offset hold constant among the head direction cell population across different environments. Similar coherent properties are found in co-recorded grid cells (Hafting et al., 2005; Stensola et al., 2012). Grid cells from the same module respond to environmental manipulations similarly (Fyhn et al., 2007; Stensola et al., 2012). Even when the spatial patterns of grid cell firing are disrupted, the co-firing relationship between cell pairs are preserved (Yoon et al., 2013; Chen et al., 2016; Perez-Escobar et al., 2016). Such robust functional connectivity suggests a continuous attractor network organisation in head direction cells and grid cells, given the local velocity-driven excitatory input, the CANN could reliably track accumulative displacement.

A ring attractor network model is proposed to account for how the consistent directional coding is realized in the head direction system (Skaggs et al., 1995). It was proposed that head direction cells are mutually connected with strongest excitatory connection

between cells that had similar preferred tuning direction. A ring structure is adopted so that a bump of activity would emerge and be smoothly shifted around when local asymmetrical input are imposed. It is proposed that this 'shift' cells are controlled by both self-motion cues and external cues (Sharp et al., 1996; Stackman & Taube, 1998; Bassett & Taube, 2001; Sharp et al., 2001).

In the search of a translational path integrator, researchers adopted the ring attractor network structure of a rotational integrator and extended it into a 2D network (McNaughton et al., 2006; Burak & Fiete, 2009). In the proposed CANN model grid cells with the same scales and orientations are organized in a 2D neural sheet so that cells with similar phase have the strongest mutual inhibition. A local inhibition and broad-field excitation connection allow periodic patterns to generate. Velocity sensitive shift cells then drive the activity bump to move. Conjunctive cells that have similar spatial grid tuning but also respond to running direction and speed were discovered in the deeper layers of the medial entorhinal cortex (Sargolini et al., 2006). However, there is no direction evidence yet that grid cell firing patterns perform path integration as proposed by CANN models.

Oscillatory inteference (OI) model

As discussed in Section1.2.1, Speed modulated EEG theta oscillation are recorded in hippocampal formation and 'phase precession' is discovered in place cells and grid cells. Such speed and distance coding shown in frequency and phase raise the possibility that distance tracking can be accomplished by the interference pattern of velocity driven oscillators, proposed by Oscillatory interference model (Burgess et al., 2007; Burgess, 2008; Bush & Burgess, 2014). Based on the solid observation that place cell firing modulation in theta band was higher than the field theta oscillation, it was proposed

1.3. SPATIAL REPRESENTATION BASED ON ENVIRONMENTAL CUES AND SELF-MOTION TRACKING

that 1) there exists 'velocity controlled oscillators' (VCO) whose frequency increase from a baseline as a function of animals' running speed in preferred direction; 2) their phase relative to baseline oscillation tracks displacement in that direction; 3) inputs from several VCOs with different directional preferences converge to track displacement in different direction. In such model, periodic firings emerge naturally in the interference pattern envelop such that grid cell periodicity could be accounted by converged VCOs with preferred directions different by multiples of 60° .

Supporting the OI model, many theta cells recorded in hippocampus, anterior thalamic nuclei and medial septum indeed show increased direction and speed modulated burst frequency (Welday et al., 2011). The oscillatory interference model predicted periodic spatial firing pattern such as the periodicity observed in grid cells (Hafting et al., 2005). The step-wise increase in grid scales are accompanied by the decrease of membrane oscillatory frequency in dorsoventral axis of medial entorhinal cortex (Brun et al., 2008b; Stensola et al., 2012; Giocomo et al., 2011). Evidences against OI model argue that, in its original form, OI model is built on stable theta oscillation while grid patterns are also recorded in bats whose hippocampal local field potential does not show any regular oscillatory activity (Yartsev et al., 2011). However, it was discovered later that hippocampal phase coding are robust even without regular field oscillation (Eliav et al., 2018). Another doubt is that periodic patterns are generate in single cell level instead of from network connection in OI model, making it at odds with many network properties discovered in grid cell population. Modifications to accommodate recurrent network connections show improved stability in grid patterns suggesting that the two mechanisms may act as complimentary to each other (Bush & Burgess, 2014).

1.4 Rationale for experiments in this thesis

Both sensory information and self-motion information are thought to determine spatial firing patterns of place and grid cells. However it has not been shown how these two types of information combine to drive place and grid cells' firing, and in what proportion. Often changes in self-motion are accompanied by changes in environmental sensory information, but this can be avoided in virtual reality. In the first two experiments we developed and used a novel virtual reality system in mice, to be able to independently manipulate self-motion and visual motion. The work I presented in these two chapters is a result from highly collaborative effort, which I have participated from an early stage of behavioral pilot until published recently. My contribution to the two experiments emphasis on conducting training and experiments to collect data, supporting formal data analysis and results visualization, and revision during peer review. In the final experiment we looked at the effect of removing visual inputs on hippocampal spatial representations. The work in this chapter is conducted by me independently.

Chapter 2

General Methods

2.1 Animals

Subjects (in total twenty-four male C57Bl/6 mice) were aged 11-14 weeks and weighed 25-30 grams at the time of surgery. Mice were housed under 12:12 inverted light-dark cycle, with lights on at 10 am. All work was carried out under the Animals (Scientific Procedures) Act 1986 and according to Home Office and institutional guidelines.

In total, we recorded from twenty-four mice, among which ten mice were surgically implanted by my colleague Dr. Guifen Chen and fourteen were implanted by me. Twelve mice were trained in the virtual reality system (for experiment 1 & 2), nine of them were trained and recorded by me. See Table 2.1 for details about the exact number of animals reused across experiments. In general, there is large subjects overlap between experiment 1 & 2 but much less between experiments 1/2 and experiment 3. Sessions in experiment 1 were always recorded before the gain manipulation sessions in experiment 2.

Table 2.1: Number of animals resused across multiple experiments

Animal number	Experiment 1	Experiment 2	Experiment 3
Experiment 1	11	8	2
Experiment 2	7	9	2
Experiment 3	2	2	15

Note: numbers in the diagonal cells show the subject counts in each experiment, and those in the other cells show the number of mice that had been recorded in both the experiments indicated by row label and column label.

2.2 Surgery

Mice were group-housed (2-4 mice housed in one cage) until surgery, after which they were single-housed to prevent wound infection and damage to implants from group interactions. During surgery, mice were initially anaesthetized with 3% isoflurane (Abbott; Maidenhead, UK) in O₂. Throughout the surgery, the concentration of isoflurane was lowered to 1.5 - 2.5%. Analgesia was given pre-operatively with 0.1 mg/20 g Carprofen and post-operatively with 0.1 mg/20 g Metacam for three consecutive days. Custom-made microdrives (AXONA, UK) loaded with 17 μ m platinum-iridium tetrodes were implanted and affixed to the skulls using dental cement (Kemdent Simplex Rapid), providing buffer amplification. Two mice were implanted with 8 tetrodes in CA1 (ML: 1.8 mm, AP: 2.1 mm posterior to bregma), three mice with 8 tetrodes in dorsomedial entorhinal cortex (dMEC, ML: 3.1 \sim 3.4 mm, AP: 0.2 \sim 0.3 mm anterior to the transverse sinus, angled 4 degrees posteriorly), and nineteen mice with 4 tetrodes in both sites.

For mice used in virtual reality experiments, a circular head-plate made of plastic (Stratasys Endur photopolymer) is chronically attached to the skull, with a central opening allowing the implant of tetrodes for electrophysiological recording (see Figure

2.1). After surgery, mice were relocated to a heated chamber and returned to their home cage after awakening. One week of recovery in the home cage was allowed before any behavioural training and cell screening began, until when they had ad libitum access of water and food. Their body weights were monitored and recorded weekly before the surgery and daily after surgery. After the training began, mice were maintained at 90% (> 85%) of their free-feeding body weight through food restriction.

2.3 Behavioural paradigm

We conducted three experiments which can be broadly divided into two paradigms. One is to have the mice navigate in our two-dimensional virtual reality (VR) environment and try to manipulate the visual environmental feedback independently from the animals' physical movement. The other one is to deprive mice navigating in a real environment of the visual input, by turning off the light sources in the lab and track animals' movements via infrared LEDs. During these experiences, we recorded neural spatial coding in the hippocampal CA1 and MEC to see how they are affected by environmental and self-motion inputs. Before training, mice were handled carefully 10-30 mins each day for 2-3 days after recovery from electrode implantation.

2.3.1 VR method

The virtual reality system described below was built by Professor Neil Burgess and Professor John King, Dr. Guifen Chen developed the training protocol and I helped test the setup and trained and recorded mice for the VR experiments.

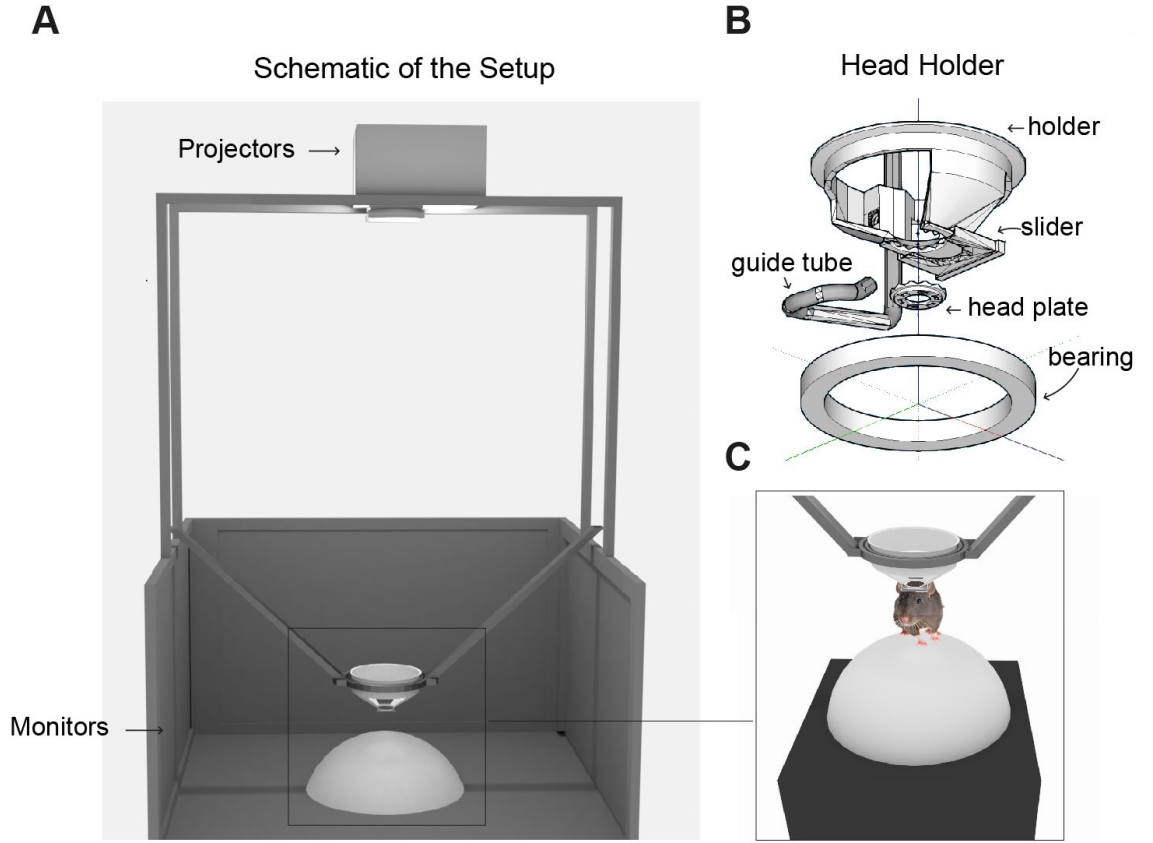


Figure 2.1: **Virtual reality setup.** (A) Schematic of the VR setup. (B) A rotating head-holder. (C) A mouse attached to the head-holder.

Virtual reality setup

The surgically attached head-plate on mice makes a self-centring joint with a holder mounted in a bearing (Kaydon reali-slim bearing KA020XP0) and is clipped into place by a slider. The bearing is held over the centre of an air-supported Styrofoam ball. Four LCD screens placed vertically around the ball and two projectors onto a horizontal floor provide the projection of a virtual environment. The ball is prevented from yaw rotation to give the mouse traction to turn its head while preventing any rotation of the ball about its vertical axis, following Aronov & Tank (2014) (See Figure 2.1).

The virtual environment runs on a Dell Precision T7500 workstation PC running Windows7 64-bit on a Xeon X5647 2.93GHz CPU, displayed using a combination of four Acer B236HL LCD monitors mounted vertically in a square array plus two LCD projectors (native resolution 480 x 320, 150 lumens) mounted above to project floor texture. The head-holder is at the centre of the square and 60mm from the bottom edge of the screens and 9500mm below the projectors. The LCD panels are 514mm x 293mm, plus bezels of 15mm all around. These six video feeds are fed by an Asus AMD Radeon 6900 graphics card and combined into a single virtual display of size 5760 x 2160px using AMD Radeon Eyefinity software. The VR is programmed using Unity3d v5.0.2f1 which allows virtual cameras to draw on specific regions of the virtual display, with projection matrices adjusted (see Kooima, 2008. <http://csc.lsu.edu/~kooima/articles/genperspective/index.html>) to the physical dimensions and distances of the screens and to offset the vanishing point from the centre. For example, a virtual camera facing the X-positive direction renders its output to a portion of the virtual display which is known to correspond to the screen area of the physical monitor facing the X-negative direction.

Translation in the virtual space is controlled by two optical mice (Logitech G700s gaming mouse) mounted with orthogonal orientations at the front and side of a 200mm diameter hollow polystyrene sphere, which floats under positive air pressure in a hemispherical well. The optical mice drive X and Y inputs respectively by dint of their offset orientations, and the gain can be controlled within the Unity software. Gain is adjusted such that real-world rotations of the sphere are calibrated so that movement on the ball couples with realistic visual translation in the VR projected to the animal. Mouse pointer acceleration is disabled at the operating system level to ensure movement of the sphere is detected in a linear fashion independent of running speed. An effort was made to minimize the effect of real-world visual cues by isolating

the VR setup with light-shutting black curtains. The mouse can freely rotate in the horizontal plane, which does not affect the VR display (but brings different screens into view). Rotation is detected and recorded for later analysis using an Axona dacqUSB tracker which records the position of two LEDs mounted at 25mm offset to left and right of the head stage amplifier. Rotation is sampled at 50Hz by detection of the LED locations using an overhead video camera, while the virtual location is sampled and logged at 50Hz.

Behaviour is motivated by the delivery of milk rewards (SMA, Wysoy) controlled by a Labjack U3HD USB Data Acquisition device. A digital-to-analogue channel applies 5V DC to a control circuit driving a 12V Cole-Parmer 1/16" solenoid pinch valve, which is opened for 100ms for each reward, allowing for the formation of a single drop of milk (5uL) under gravity feed at the end of a 1/32" bore tube held within licking distance of the animal's mouth. Control of the Labjack and reward locations in the VR is via UDP network packets between the VR PC and a second experimenter PC, to which the Labjack is connected by USB. Software written in Python 2.7 using the Labjack, tk (graphics) and twisted (networking) libraries provides a plan-view graphical interface in which the location of the animal and reward cues in the virtual environment can be easily monitored and reward locations manipulated with mouse clicks (See Figure 2.1).

Training protocol

Behavioural training in VR started while tetrodes were approaching target brain areas. Among the twelve mice that had been recorded in our VR experiments, I have trained and collected data from nine of them. Each training trial lasted 20 - 40 minutes depending on the training phases (training in the VR linear tracks often lasted 30 minutes, while training in the square VR environments lasted 40 minutes per trial) and

animals' behaviour (e.g. if they were not motivated to run then trials ended earlier). In general, animals were trained for one to two trials per day with an inter-trial interval of at least half an hour. Behavioural training involved four phases which were described below (see Figure 2.2).

1) Linear track - Narrow

Firstly, mice experienced an infinitely long 10cm-wide virtual linear track with 5 μ L milk drops delivered as rewards (lateral movement of the mice was not registered in this phase). The wall was patterned and reward locations were indicated by virtual beacons (high striped cylinders with a black circular base, see 2.2A), which were evenly placed along the track (see Figure 2.2C). When the mouse contacted the area of the base, milk was released and the beacon disappeared (mice were teleported back to the start location with the beacon reappearing in the reward location, this quick change of environment frames do not change the appearance of the virtual environment because of its periodicity and gave a sense of an infinite long track). The aim of this training phase was to habituate the mice to being head-restrained, train them to run confidently on the air-cushioned ball and to form the association between running into beacons and receiving milk rewards. Once an animal ran straightly forward and continuously received rewards in roughly every 10 seconds, it was recognised to pass the training phase. It took three days, on average, for mice to achieve the criterion and move to the next training phases.

2) Linear Track - Wide

During the second training phase, mice experienced a similar virtual linear track (see Figure 2.2B), which was wider and longer in reward-to-reward distance than the narrow linear track. In the wide track, reward beacons were evenly spaced along the long axis of the track, as before, but placed pseudo-randomly in one of three pre-defined positions

on the lateral axis (middle, left or right). This training aimed to further strengthen the association between rewards and visual beacons and to train animals to navigate towards rewarded locations via appropriate bodily rotations on top of the ball. The training was considered completed when animal learned to properly align their path towards the reward cue and got rewards at an interval of ~ 10 seconds. The second training phase also took three days, on average.

3) Square – Random Foraging

During the third training phase mice were introduced into a virtual square arena placed in the middle of a larger virtual room. Distinct visual patterns were placed both on one side of the arena wall and one side of the wall in the large room. The floor was patterned with hexagonal tiles and there was one balloon floating above the arena (see Figure 2.2E-F). The virtual arena had a size of 60x60cm or 90x90cm for different mice. Reward beacons had a base of the diameter that equalled to 10% of the arena width. Mice were trained on a ‘random foraging’ task, during which visible beacons were placed in the square box at random locations. At the early stage of training, multiple rewards were positioned proximal to the animal in order to encourage them to run. Following training, the rewards were reduced to one at a time and located at computer-generated random locations that tile the environment evenly. Animals graduate from the training when they showed smooth linear and angular movement, consistently turned away when reaching the virtual walls of the arena and were continuously receiving rewards at ~ 10 secs interval in 90x90cm square arena and ~ 7 secs interval in 60x60cm arena. It normally took 2 - 7 days in this training phase.

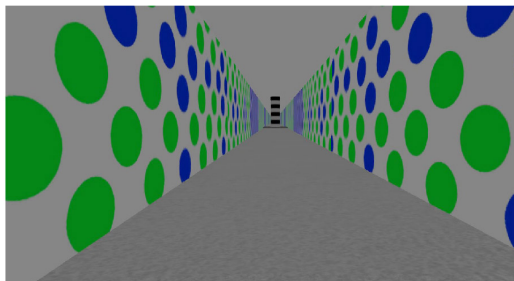
4) Square – Fading Beacon

The last training phase was the ‘fading beacon’ task. The arena used in this task was the same as random foraging task, however, the reward positions were different. During this

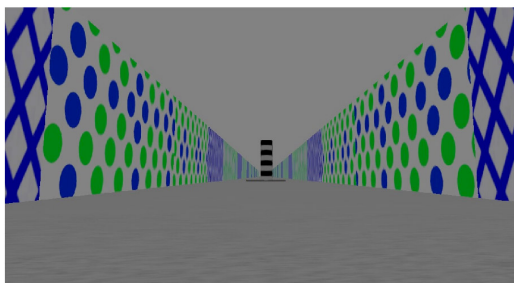
2.3. BEHAVIOURAL PARADIGM

task, every fourth beacon occurred in a fixed location and was rewarded by two drops of milk at contact (the three intervening beacons being randomly placed within the square enclosure and was rewarded by one drop of milk, beacons are presented one at a time like at the end of random foraging phase; see Figure 2.2G-H). At the beginning of this training phase the ‘fixed location beacon’ slowly faded from view over 10 contacts with decreasing opacity. The beacon would remain invisible as long as mice could find it, but would become visible again if mice could not locate it after roughly 2 min of active searching. Once mice showed consistent navigation towards the fading fixed beacon, they were moved to the ‘faded beacon’ phase of the task where the ‘fixed location beacon’ was invisible from the start of the trial and remained invisible throughout the trial. This trial phase, therefore, requires mice to navigate to an unmarked virtual location from different starting points (random locations where the 3rd visible beacon was placed). As such, the ‘fading beacon’ task serves as a continuous version of a Morris Water Maze task (Morris et al., 1982), combining reference memory for an unmarked location with a foraging task designed to optimise environmental coverage for the assessment of spatial firing patterns. The training was completed when animals were able to navigate to the unmarked reward location consistently throughout the trial and were hitting rewards at ~ 10 secs interval in 90x90cm square arena and ~ 7 secs interval in 60x60cm arena. This training phase often took 3 - 7 days which varied across animals.

A VR Linear Track - Narrow

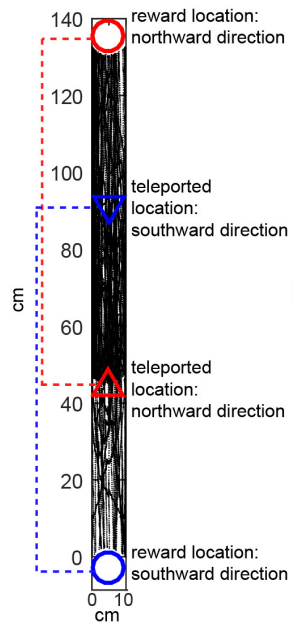


B VR Linear Track - Wide



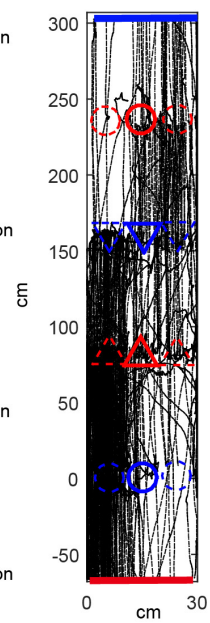
C

Running Trajectories

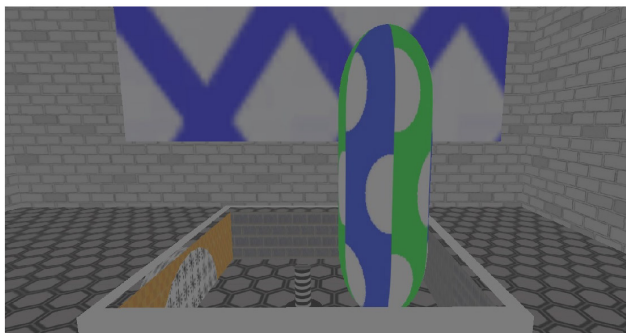


D

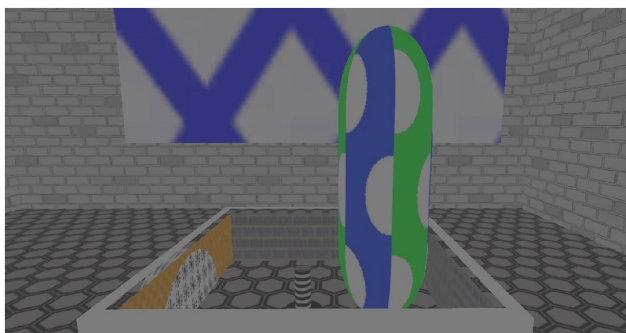
Running Trajectories



E Square - Fading Beacon Task

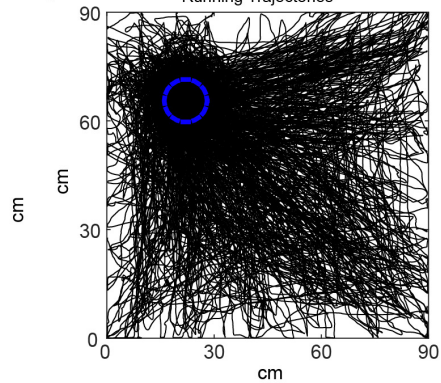


G Square- Random Foraging Task



F

Running Trajectories



H

Running Trajectories

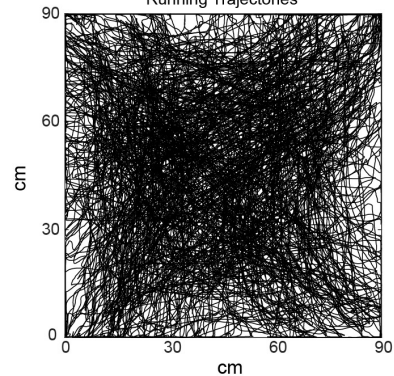


Figure 2.2: **Virtual environments and example trajectory maps in the four training phases.** (A, B, E & G) A view of the virtual narrow linear track (A), wide linear track (B), fading beacon environment (E) and random foraging environment (F). The fading beacon arena and random foraging arena are visually similar but different in reward arrangement. (C, D, F & H) Trajectory maps in a typical narrow linear track trial (C), a wide linear track trial (D), a fading beacon trial (F) and a random foraging trial (H). Note the different trajectory patterns in (F) and (H). Triangles mark the start positions, and circles the reward positions. Red and blue label positions in the northward runs and the southward runs, respectively.

2.4 Data collection

Mice were put in a real-world square box to screen for the place cells and grid cells everyday (~ 20 min per day) either right after habituation or after VR training was accomplished. Boxes were either a 60x60cm square box sat on a black Trespa 'Toplab' surface (Trespa International B.V., Weert, Netherlands) or an 80x80 cm square box on a black prism vinyl flooring (used only in the dark experiment when recordings were also done in an 80x80 cm square box). Screening boxes were placed in the middle of an enclosure surrounded by a circular set of black curtains. A white cue-card (A0, 84x119cm), illuminated by a 40W lamp was positioned higher up attached to the curtain to provide the only intentional distal cue. The recording boxes were visually patterned asymmetrically (see Figure 2.3). Mice were encouraged to freely forage in the recording box for milk droplets (SMA Wysoy infant 0-3 month) while neural activity was recorded using a the DACQ data acquisition system (AXONA Ltd., UK). Tetrodes were lowered by no more than 62.5um each day until stable recordings of well-isolated place cells or grid cells in the pyramidal layer of CA1 or MEC were obtained on a majority of

tetrodes.

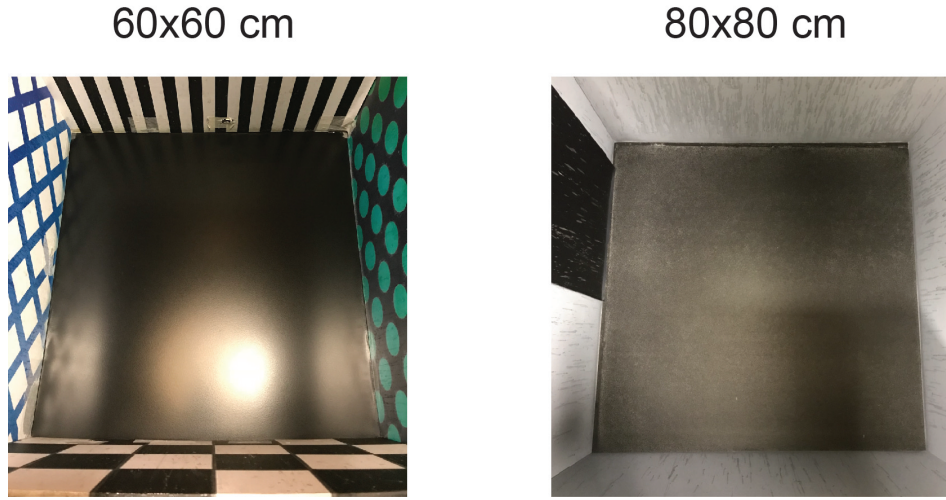


Figure 2.3: **Top view of the 60x60cm (left) and 80x80cm (right) recording boxes.**

Signals were amplified (10-20 K) and band-pass filtered (300-7 kHz) and whenever a signal exceeded a set certain tetrode specific threshold (typically about 65-75% of the maximum signal amplitude on a given channel/tetrode) it was recorded. Each tetrode channel was monitored at 48 kHz and individual action potentials/signals were stored as 50 points across a 200 μ s pre- and 800 μ s post-threshold time period. Whenever a signal exceeded the threshold on any tetrode channel the signal was recorded on all tetrode channels.

The hippocampal EEG was recorded by band-pass filtering the signal between 0.1-500 Hz and a 50 Hz notch filter at a sample rate of 250 Hz. EEG signals were typically amplified 8-15K. EEG was recorded in both CA1 and MEC tetrodes. The position and head orientation data was recorded via a camera positioned above the middle of the environment using two different size LEDs attached to the head of the animal at a fixed distance (5cm) and a fixed orientation relative to the animal's head. This allowed tracking of position as well as heading direction. Positions were sampled continuously

at 50Hz.

2.4.1 Histology

After experiments ended, all the implanted mice were killed with an overdose of sodium pentobarbital and perfused transcardially with saline followed by formalin solution. Brains were stored in formalin at least overnight before being transferred to 30% sucrose solution for two days. Slicing was then performed coronally for the CA1 implanted hemisphere and sagittally for the dMEC implanted hemisphere into 30-um-thick sections, which were mounted and stained using a Cresyl-violet/Thionin solution with standard protocol. See Figure 2.4 for the implant trace locations.

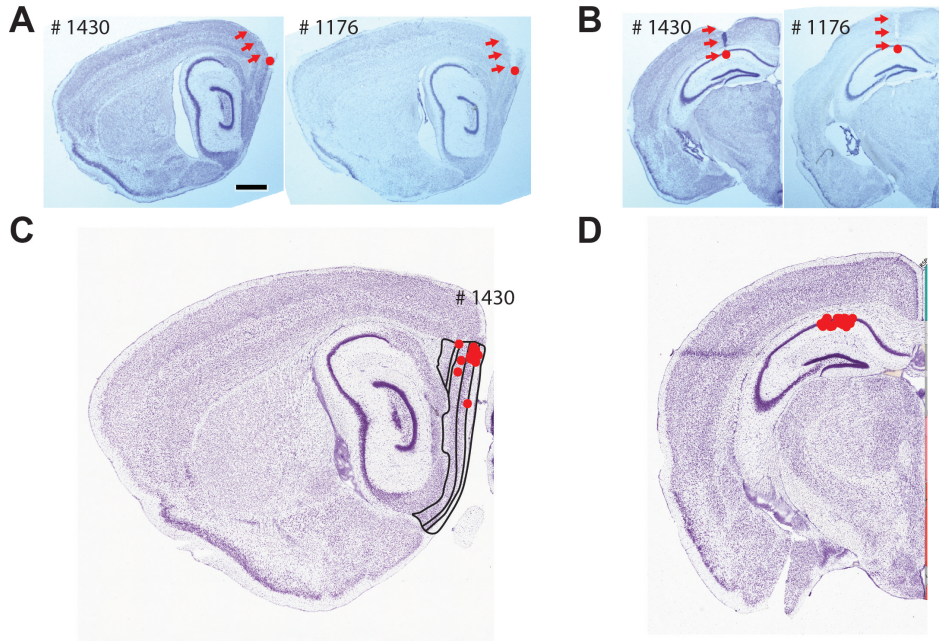


Figure 2.4: **Histology and implant traces in CA1 and MEC.** (A-B) Nissles stained sagittal slices (A) and coronal slices (B) from two double-implanted mice showing the tetrode traces in MEC and CA1. Bar = 1mm applies to all the slices in (A-B). The array of red arrows indicate the track and the red dot indicates the its termination. (C-D) All the estimated tetrodes' tip locations are marked with red dots on an example sagittal slice for MEC (C) and an coronal slice for CA1 (D). The MEC area and sublayers are outlined in (C). Note the clustering of implants at the superficial layer of dMEC and the dorsal CA1.

2.4.2 Firing rate map construction and spatial cell classification

Spike sorting was performed offline using an automated clustering algorithm (KlustaKwik, Kadir et al. (2014)) followed by a manual review and editing step using an interactive graphical tool (waveform, Daniel Manson, <http://d1manson.github.io/waveform/>). After spike sorting, firing rate maps were constructed by binning animals' positions into 1.5 x 1.5cm bins, assigning spikes to each bin, smoothing both position maps and spike maps separately using a 5x5 boxcar filter, and finally dividing the smoothed spike maps by the smoothed position maps.

Cells were classified as place cells if their spatial information in baseline trials exceeded the 99th percentile of a 1000 shuffled distribution of spatial information scores calculated from rate maps where spike times were randomly offset relative to position by at least 20 seconds. Cells were classified as grid cells if their gridness scores in baseline trials exceeded the 99th percentile of a shuffled distribution of 1000 gridness scores (Sargolini et al., 2006). Place and grid cells additionally required a peak firing rate above 2 Hz for

clarity of classification. Cells were classified as head direction cells if their directional information in baseline trials exceeded the threshold of the 99th percentile population shuffling.

Speed-modulated cells were classified from the general population of the recorded cells following McNaughton et al. (1983). Briefly, the degree of speed modulation for each cell was characterised by first defining the instantaneous firing rate of the cell as the number of spikes occurring in each position bin divided by the sampling duration (0.02 s). Then a linear correlation was computed between the running speeds and firing rates across all position samples in a trial, and the resulting r-value was taken to characterise the degree of speed modulation for the cell. To be defined as speed-modulated, the r-value for a cell had to exceed the 99th percentile of a distribution of 1000 r-values obtained from spike shuffled data.

When assessing the directional modulation of place and grid cell firing, apparent directional modulation can arise in binned firing rate data from heterogenous sampling of directions within the spatial firing field Burgess & Hitch (2005); O’Keefe & Recce (1993). Accordingly we fit a joint (‘pxd’) model of combined place and directional modulation to the data (maximising the likelihood of the data Burgess & Hitch (2005)) and perform analyses on the directional model in addition to the binned firing rate data.

Theta modulation of cell firing during the main experiment were computed using Maximum likelihood estimation of the distribution of lags, following Climer et al. (2015). Cells with theta index higher than the confidence interval of 95% were classified as theta rhythmic cells. Among that population, two-dimensional phase precession was estimated for cells that were also classified as place cells or grid cells, following Climer et al. (2015). In brief, each running trajectory passing through the defined place

field was normalized and mapped radially on an unit circle so that the proportional distance of the animal between the field edge and peak was preserved and so that the average running direction was zero (from left to right). The distance of the animal from the peak projected onto the instantaneous running direction ('Pdcd') was calculated, representing the distance the animal has travelled through the field (range -1 to 1). The theta phase of each spike was computed using the Hilbert transform of the smoothed LFP.

Chapter 3

Spatial cell firing during virtual navigation of open arenas by head-restrained mice

3.1 Introduction

Virtual reality (VR) is a powerful technique that can be used for constructing and presenting highly controlled sensory stimuli, as well as for pairing with various behavioural and neuronal recording techniques that require restrained motion of the subject thus prohibiting use in awake behaving animals (this is especially true for navigation research). First developed for insects, the rudimentary design of the early VR system has been validated and inherited ever since. It combines body-tethering an animal, a ball that rotates effortlessly on which animal can rest or walk, sensors that track movement of the animal (walk, fly, vibration etc.) and stimuli generators that present sensory inputs registered (or not) to the animal's movement (Carrel, 1972;

Dahmen, 1980; Gray et al., 2002).

VR systems were later adapted for rodents and shown adequate in engaging natural navigational behaviour (Hölscher et al., 2005; Lee et al., 2007), as well as eliciting normal spatial tuning properties in rodents' hippocampal-entorhinal circuit (Harvey et al., 2009; Dombeck et al., 2010; Domnisoru et al., 2013; Schmidt-Hieber & Hausser, 2013; Heys et al., 2014; Aronov & Tank, 2014). On the other hand, many VR studies adopt strict head fixation in the mouse to accommodate recording techniques such as intracellular recordings and two photon microscopy during awake navigation. Findings from large-scale neural network organisation to subthreshold membrane depolarization and oscillation significantly advanced our understanding of the mechanisms of hippocampal function (Harvey et al., 2009; Dombeck et al., 2010; Domnisoru et al., 2013; Schmidt-Hieber & Hausser, 2013; Heys et al., 2014; Gu et al., 2018). Virtual reality also allows the construction of any sensory 'space' in which animal could freely explore while their underline neural activity stucture being checked (Saleem et al., 2013; Constantinescu et al., 2016; Aronov et al., 2017; Ayaz et al., 2019).

Despite recent success in applying VR techniques in neuroscience research, there is a balance to be made for researchers applying the VR techniques between the degree of restriction and ecology to the animal. It was shown that when restricted of vestibular input as in the head-fixed mice, the proportion of cells in the hippocampal CA1 to display high spatial selectivity was reduced. Cells that are active, instead of responding to the allocentric location, fire in relation to the relative distance or temporal order of events. And Their activity are more modulated by animal's head direction compared to when they are allowed free foraging in the open field (Ravassard et al., 2013; Aghajan et al., 2015; Acharya et al., 2016). Head fixation also limits the sensory experience of virtual navigation to stereotypical trajectories such as following the linear track or

armed mazes which also contributes to their altered functional properties in the VR (Harvey et al., 2009; Dombeck et al., 2010; Domnisoru et al., 2013; Schmidt-Hieber & Hausser, 2013; Heys et al., 2014).

In this study we provide a solution of the state-of-art VR system that initiates the hippocampal 2D spatial representation and provides high head stability to potentially accomodate two photon microscopy. The mechanical details of our VR setup as well as our behavioral training protocol are described in Section2.3.1. Here I am focusing on animals' behavioral performance and the extracellular recording we obtained from mice hippocampal CA1 and MEC during virtual navigation. We show that mice are able to remember an unmarked reward location in our virtual environment and flexibly navigate to it from random locations. Place cell, grid cells and head direction cells are also active and displaying characteristic 2D spatial representation in the VR.

3.2 Materials and methods

3.2.1 Animals

Eleven male C57Bl/6 mice were used in this experiment. Two were implanted with eight tetrodes in the hippocampal CA1, three with eight tetrodes in the dorsomedial entorhinal cortex, and six mice received a dual implant with one microdrive in right CA1 and one in left dmEC (each microdrive carried 4 tetrodes).

3.2.2 Recording procedure

Comparison between VR and R trials

After being through all four training stages, mice were recorded in both VR and R environments for comparison. Each recording day consisted of at least one 40-min random-foraging trial in a virtual reality (VR) square environment. For seven mice the virtual environment had size 60x60 cm and for four mice 90x90 cm. After one (or more) 40-min random foraging trial(s) in the virtual square, mice were placed in a real-world square ('R', 60x60cm square, similar to the screening environment, see Figure 3.8A) for a 20-min random-foraging trial in the real-world environment. For each animal, the first days they showed well isolated spatial tuning cells in both VR and R environments were included for analysis (when multiple trials were recorded on the same day for either condition the first one were chosen). In general, even with good task behaviour in the fading beacon tasks, often further training sessions were needed for place cells and grid cells to show stable spatial tuning. Only one VR-R trial pair was included for each animal. To check the exact trial arrangement on the experimental day, and details of their pre-recording training experience are listed in Table 3.1.

To control for sequential effect between VR and R trials, we performed additional recordings from 4 mice (3 new to the experiment, one that had performed the main experiment). On one day they experienced a trial in the R square before a trial in the VR square (60x60cm) environment. On the next day, the VR trial preceded the R trial.

To further establish the difference between VR and R trials were not environment-specific, we also introduced those 4 mice to a novel cylindrical VR and cylindrical R environment which shared similar wall and floor visual patterns. Four trials were recorded on the same day in the order: VR cylinder, VR square, R cylinder

3.2. MATERIALS AND METHODS

Table 3.1: Trial information

Mouse id	Implant type ^a	Trials on the recording day	Size (cm)	Train- ing ^b (Days)	Trial dur. (mins)	Rwd. per trial	Grid cell No.	Place cell No.
449	E	VR ^c -VR-R ^d	90	13	30	404	18	0
598	C	VR ^c -VR-R ^d	90	9	30	199	0	20
864	E	VR ^c -VR-R ^d	60	9	40	394	2	0
969 ^e	CE	VR ^c (D1)-R ^d (D2)	90	20	40	377	0	14
984	C	VR ^c -VR-R ^d	90	22	40	487	0	33
986	E	VR ^c -VR-R ^d	60	11	40	593	16	0
987	CE	VR ^c -VR-R ^d	60	25	40	596	13	26
1014	CE	VR ^c -VR-R ^d	60	20	40	632	4	0
1015	CE	VR ^c -VR-R ^d	60	16	40	516	2	25
1060	CE	VR ^c -VR-R ^d	60	16	40	385	2	12
1061	CE	VR ^c -VR-R ^d	60	23	40	705	4	24

^aE: implant in left MEC; C: implant in left CA1; CE: implant in right CA1 and left MEC

^b Number of days trained in the 'fading beacon' task before recording (see Section 2.3.1)

^cVR trial included in analysis

^dR trial included in analysis

^e R trial was recorded on the next day of VR trial in mice #969

and R square. All VR trials were 40 minutes and R trials 20 minutes in length (see Figure 3.8 and Figure 3.10).

Rotation of VR environment

Additionally, 4 mice also underwent a virtual cue rotation experiment, which consisted of two 40-min random-foraging VR trial (one baseline VR trial and one rotated VR trial) and one 20 min R trial. Two mice navigating 60x60cm VR squares and two 90x90cm squares participated in this experiment. In the rotated VR trials, all cues in the virtual reality environment rotated 180 degrees compared to the baseline trial, as was the entry point mice were carried into the VR rig from. Mice were purposely

disoriented with passive rotation before introduced to each VR trial.

3.2.3 Behavioral analysis

During electrophysiological recording in the real environment (R), the mouse's position and head orientation were tracked by an overhead camera (50Hz sampling rate) using two infra-red LEDs attached to the micro-drive at a fixed angle and spacing (5 cm apart). Brief losses of LED data due to cable obstruction (typically affecting a single LED for less than 500ms) were corrected with linear interpolation between known position values. Interpolation was carried out for each LED separately. The position values for each LED were then smoothed, separately, using a 400ms boxcar filter. During electrophysiological recording in VR, head orientation was tracked as in R, the path, running speed and running direction was inferred from the VR log at 50Hz (movements of VR location being driven by the computer mice tracking the rotation of the ball, see above).

Path excess ratio was defined as the ratio between the length of the actual path that an animal takes to run from one reward location to another, and the distance between the two reward locations. All training trials in the VR square and the real (R) square environments from the 11 mice in the main experiment were included in the behavioural analyses in Figure 3.3.

3.2.4 Statistical analysis

In behavioural analyses, each animal's running speed, the directionality of path and angular velocity were tested with two-way repeated measure ANOVA (rmANOVA) on two factors each with two levels, environment (R vs VR) and experience (early-stage

3.2. MATERIALS AND METHODS

vs late-stage). For the fading beacon task only, the entire VR environment was divided into four quadrants in which one contains the location of fixed unmarked goal location (area 1). The main effect of dwell time in different quadrates was tested with one-way repeated measure ANOVA with four levels. Post hoc paired t test was calculated for comparisons between area 1 and the rest of quadrates with Bonferroni correction. In electrophysiology data analysis, tests of difference between R and VR environments in cells' spatial tuning properties were done with paired t test. In all figures * = significant at the 0.05 level, ** = significant at the 0.01 level, *** = significant at the 0.001 level. For all the statistical test results see Table 3.2.

Table 3.2: Statistical test results

Comparison	Test	Results	Fig.
Average running speed	rmANOVA:	Training: $F(1,10)=40.11$, $p<.001$	Fig.3.1C
Path vector length	VR(2) by	VR: $F(1,10)=4.82$, $p=0.053$	Fig.3.3F
Path direction change	training(2) ^a	VR: $F(1,10)=300.93$, $p<.001$	Fig.3.1I
Path direction change		Training: $F(1,10)=26.82$, $p<.001$	Fig.3.1I
Occupancy in each quadrant ^b of the arena	rmANOVA:	$F(3, 30) = 39.03$, $p<0.001$	Fig.3.3B
	quadrant(4)		
	post hoc	1vs2: $p<.001$	Fig.3.3B
	paired t test,	1vs3: $p<.001$	Fig.3.3B
	Bonferroni	1vs4: $p<.001$	Fig.3.3B
PC, spatial info.	paired t test,	$t(153)=8.90$, $p<.001$	Fig.3.5D
PC, directional info.	VR-R ^c	$t(153)=6.45$, $p<.001$	Fig.3.5E
PC, directional info. ('pxd' model)		$t(153)=7.61$, $p<.001$	Fig.3.5E
PC, field size		$t(153)=4.38$, $p<.001$	Fig.3.5F
PC, VR(60cm), spatial info.		$t(86)=7.31$, $p<.001$	Fig.3.6A

Continued on next page

CHAPTER 3. SPATIAL CELL FIRING DURING VIRTUAL NAVIGATION OF OPEN ARENAS BY HEAD-RESTRAINED MICE

Table 3.2 – continued from previous page

Comparison	Test	Results	Fig.
PC, VR(60cm), directional info.		$t(86)=-4.71, p<.001$	Fig.3.6A
PC, VR(60cm), field size		$t(86)=-3.06, p<.001$	Fig.3.6A
PC, VR(90cm), spatial info.		$t(66)=5.20, p<.001$	Fig.3.6B
PC, VR(90cm), directional info.		$t(66)=-4.52, p<.001$	Fig.3.6B
PC, VR(90cm), field size		$t(66)=-3.13, p<.01$	Fig.3.6B
GC, VR(60cm), mean firing rate		$t(42)=3.19, p<.01$	Fig.3.6C
GC, VR(60cm), grid scale		$t(42)=-11.53, p<.001$	Fig.3.6C
GC, VR(60cm), spatial info.		$t(42)=2.41, p<.05$	Fig.3.6C
GC, VR(90cm), grid scale		$t(17)=-22.72, p<.001$	Fig.3.6D
GC, VR(90cm), directional info.		$t(17)=2.62, p<.05$	Fig.3.6D
GC, VR(90cm), directional info. ('pxd' model)		$t(17)=2.76, p<.05$	Fig.3.6D
PC, spatial info.	rmANOVA:	VR:F(1,89)=25.20, $p<.001$	Fig.3.8B
	VR(2) by	interaction:F(1, 89)=34.99, $p<.001$	Fig.3.8B
PC, directional info.	configuration(2),	VR:F(1,89)=12.16, $p<.001$	Fig.3.8B
PC, field size	post hoc	VR:F(1,89)=22.11, $p<.001$	Fig.3.8B
	paired t test,	interaction:F(1,89)=4.24, $p<.05$	Fig.3.8B
GC, gridness score	Bonferroni	interaction:F(1,8)=13.35, $p<.01$	Fig.3.8C
		VR-R (configuration = square):	Fig.3.8C
		$t(8)=-2.87, p<.05$	
GC, grid scale		VR:F(1,8)=63.74, $p<.001$	Fig.3.8C
GC, grid scale	paired t test,	$t(60)=15.52, p<.001$	Fig.3.9E
GC, spatial info.	VR-R	$t(60)=4.12, p<.001$	Fig.3.9F

Continued on next page

3.2. MATERIALS AND METHODS

Table 3.2 – continued from previous page

Comparison	Test	Results	Fig.
GC, directional info.		$t(60)=2.04, p<.05$	Fig.3.9G
GC, gridness score	rmANOVA:	VR:F(1,19)=34.82, $p<.001$	Fig.3.10C
GC, grid scale	VR(2) by trial	VR:F(1,19)=74.41, $p<.001$	Fig.3.10C
GC, first 20 mins, gridness score	order(2), post hoc paired t	VR:F(1,19)=102.90, $p<.001$	Fig.3.10D
GC, first 20 mins, grid scale	test,	VR:F(1,19)=75.91, $p<.001$	Fig.3.10D
GC, first 20 mins, directional info.	Bonferroni	VR:F(1,19)=9.58, $p<.01$	Fig.3.10D
GC, first 20 mins, directional info. ('pxd' model)		VR:F(1,19)=8.18, $p=.01$	Fig.3.10D
PC, spatial info.		VR:F(1,84)=72.61, $p<.001$	Fig.3.10A
PC, directional info.		VR:F(1,84)=33.25, $p<.001$	Fig.3.10A
		interaction:F(1,84)=6.44, $p<.05$	Fig.3.10A
PC, directional info. ('pxd' model)		VR:F(1,84)=25.90, $p<.001$	Fig.3.10A
		interaction:F(1,84)=17.95, $p<.001$	Fig.3.10A
PC, field size		VR:F(1,84)=38.50, $p<.001$	Fig.3.10A
PC, first 20 mins, spatial info.		VR:F(1,84)=47.04, $p<.001$	Fig.3.10B
PC, first 20 mins, directional info.		VR:F(1,84)=44.82, $p<.001$	Fig.3.10B
		interaction:F(1,84)=3.92, $p=0.05$	Fig.3.10B
PC, first 20 mins, directional info. ('pxd' model)		VR:F(1,84)=36.50, $p<.001$	Fig.3.10B
		interaction:F(1,84)=13.01, $p<.001$	Fig.3.10B
PC, first 20 mins, field size		VR:F(1,84)=20.74, $p<.001$	Fig.3.10B
PC, cue rotation	paired t test:	$t(122)=19.44, p<.001$	Fig.3.13D
	VR-R		
PC, cue rotation		$t(17)=9.41, p<.001$	Fig.3.13E
HD, cue rotation		$t(16)=24.77, p<.001$	Fig.3.13F

Continued on next page

CHAPTER 3. SPATIAL CELL FIRING DURING VIRTUAL NAVIGATION OF OPEN ARENAS BY HEAD-RESTRAINED MICE

Table 3.2 – continued from previous page

Comparison	Test	Results	Fig.
GC, field size	rmANOVA:	VR:F(1,60)=21.28, p<.001	Fig.3.16A
	VR(2) by	speed:F(2,120)=7.06, p<.01	Fig.3.16A
PC, field size	running	VR:F(1,153)=3.50, p=0.06	Fig.3.16B
	speed(3)	speed:F(2,306)=11.13, p<.001	Fig.3.16B
GC, phase precession slope	paired t test:	t(19)=-2.55, p<.05	Fig.3.17D
GC, phase precession slope	VR-R	t(37)=-2.19, p<.05	Fig.3.17E

^arepeated measure ANOVA: factor(s)(Number of levels in each factor)

^bquadrant 1 contains the reward zone.

^cpaired t test between condition1 and condition2

3.3 Results

3.3.1 Navigation in VR

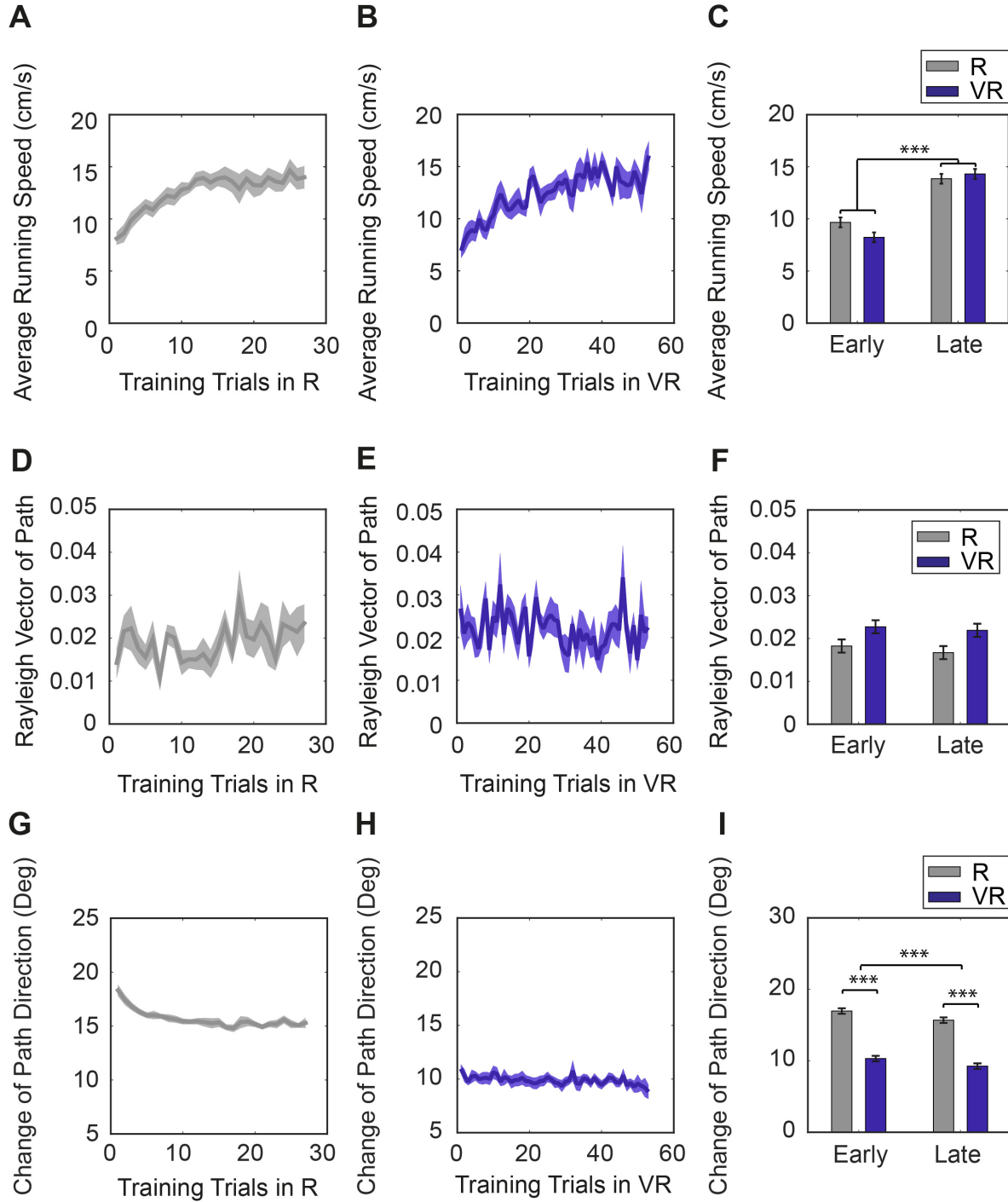


Figure 3.1: **Behavior in VR compare to R.** (A-C) Average running speeds of all trained mice ($n = 11$) across training trials in real ('R'; A) and virtual reality ('VR'; B) environments across training trials. (C) Comparisons of the average running speeds between the first 5 trials and the last 5 trials in both VR and R environments. (D-F) Average Rayleigh vector lengths of running direction across training trials in R (D) and VR (E). (F) Comparisons of the average Rayleigh vector lengths of running direction between the first 5 trials and the last 5 trials in both VR and R. Note that unimodal directionality of path was marginally higher in VR than in R and did not change significantly with experience. (G-I) Average changes of running direction (absolute angular difference in between downsampled positions) across training trials in R (G) and VR (H). (I) Comparisons of the changes of running direction between the first 5 and last 5 trials in both R and VR. Positions were sampled at 2.5Hz with 400ms boxcar smoothing in (I-N). All error bars show s.e.m.

Eleven mice were trained in the virtual reality system (see Figure 2.1 and Figure 2.2, and Materials and Methods). All training trials in the VR and the real square environments from the eleven mice were included in the behavioural analyses below. The mice displayed an initially lower running speed when first experiencing the real-world recording environment (a 60x60cm square), but reached a higher average speed after 20 or so training trials. The increase in running speed with experience was similar in the virtual environments (Figure 3.1A-C). Running speeds did not differ between the 60cm and 90cm virtual environments used for recording in seven and four of the mice respectively (12.01 ± 2.77 in 60cm VR, 14.33 ± 4.19 cm/s in 90cm VR, $p = 0.29$). Running directions in the VR environment showed a marginally greater unimodal bias compared to the real environment (R; Figure 3.1D-F). Mice displayed a greater tendency to run parallel to the four walls in VR, a tendency which reduced with experience (Figure 3.2). They also took straighter, less tortuous, paths in VR than in

3.3. RESULTS

R, as would be expected from their head-fixation (Figure 3.1G-I).

In the fading beacon task, performance steadily improved across 2-3 weeks of training (Figure 3.3D). They learned to approach the fixed reward location and could do so even after it became completely unmarked (fully faded, see Figure 3.3 and the Supplementary video of a mouse performing the task, and Materials and Methods for details of the training regime).

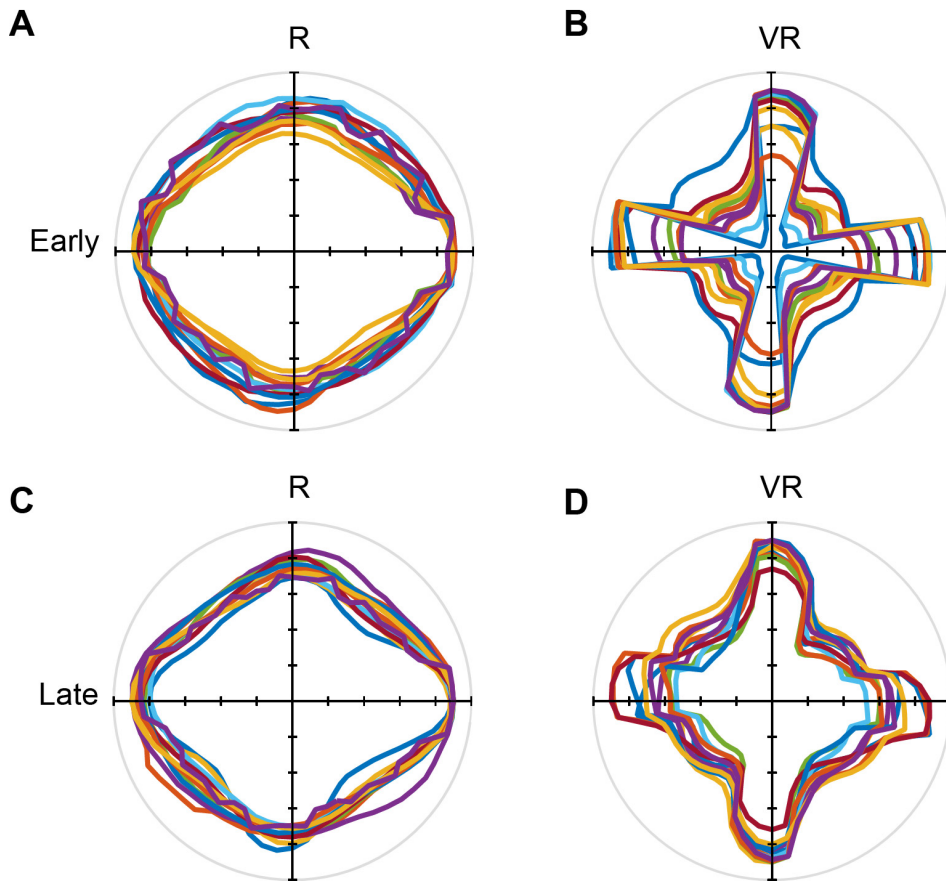


Figure 3.2: Running direction distribution. Polar plots of mice' running directions in the virtual square arena (B, D) and real-world square box (A, C) in the early (A, B) and late (C, D) training stages. Each color line indicates one animal (n=11). Path direction distribution was average over the first 5 training trials as the early stage and the last 5 training trials as the late stage.

CHAPTER 3. SPATIAL CELL FIRING DURING VIRTUAL NAVIGATION OF OPEN ARENAS BY HEAD-RESTRAINED MICE

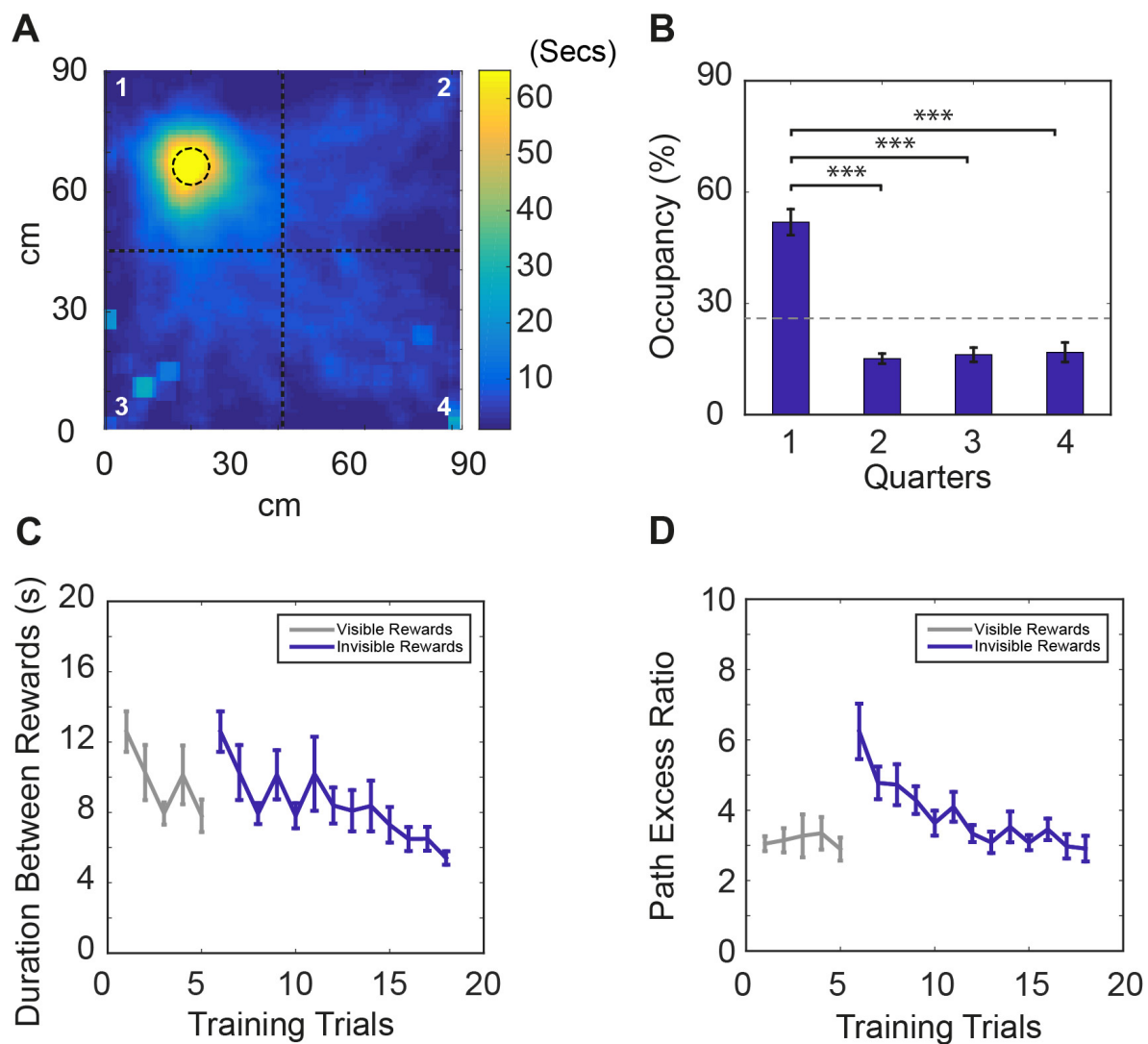


Figure 3.3: **Performance on the ‘fading beacon’ task.** (A) An example heat map showing the overall dwell time of the animal at each spatial bin to reach the fixed reward location from the last random reward location in a 40-min trial (mouse #987, trial #124). The dotted circle in quadrant #1 shows the location of the fixed reward. (B) Average time spent (as in percentage of the total trial length) in each quadrant (numbered in A). (C) Average duration of reaching the fixed reward location from the last random reward location plotted against training trials (means \pm s.e.m). (D) Average path excess ratios between the fixed reward location and the last random reward location plotted against training trials (means \pm s.e.m). Trials when the fixed reward location was visible (i.e. marked by a visual beacon) were colored gray and those when the fixed reward location was invisible were colored blue.

3.3.2 Electrophysiology

We recorded a total of 231 CA1 cells from 7 mice, 179 cells were classified as place cells in the real environment, 185 cells in the virtual environment, and 154 cells were classified as place cells in both real and virtual environments.

We recorded 141 cells in dorsomedial Entorhinal Cortex (dMEC) from 8 mice, 82 of them were classified as grid cells in the real environment, 65 of them grid cells in the virtual environment, and 61 were classified as grid cells in both real and virtual environments. Among these 141 recorded cells, 16 cells were quantified as head-direction cells (HDCs) in R, 20 cells were HDCs in VR, with 12 cells classified as HDCs in both real (‘R’) and virtual reality (‘VR’) environments. All cells were recorded while animals randomly foraged in both R and VR environments (methods for cell classification was described in Section 2.4.2. For threshold distribution see Figure 3.4).

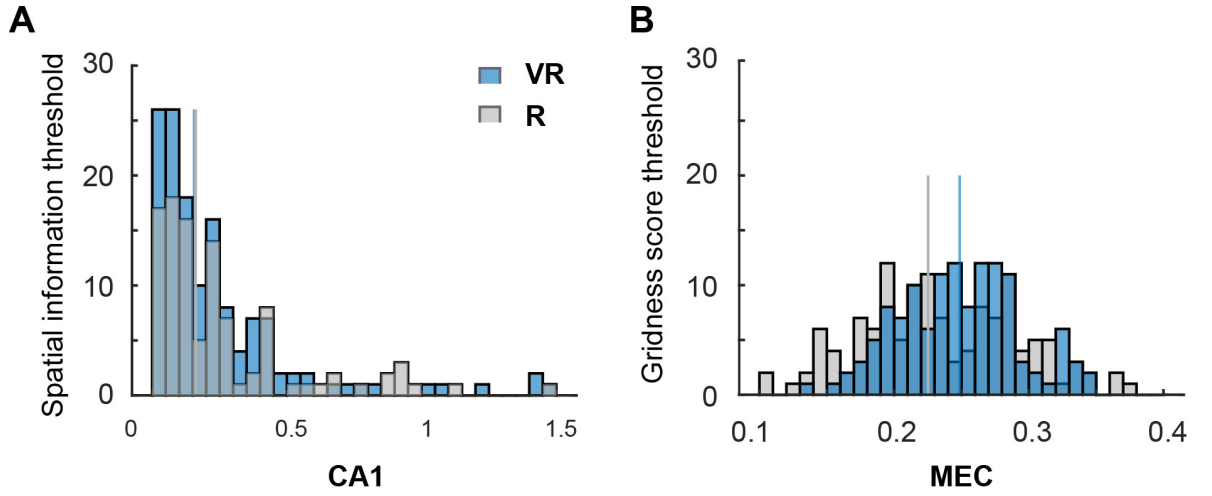
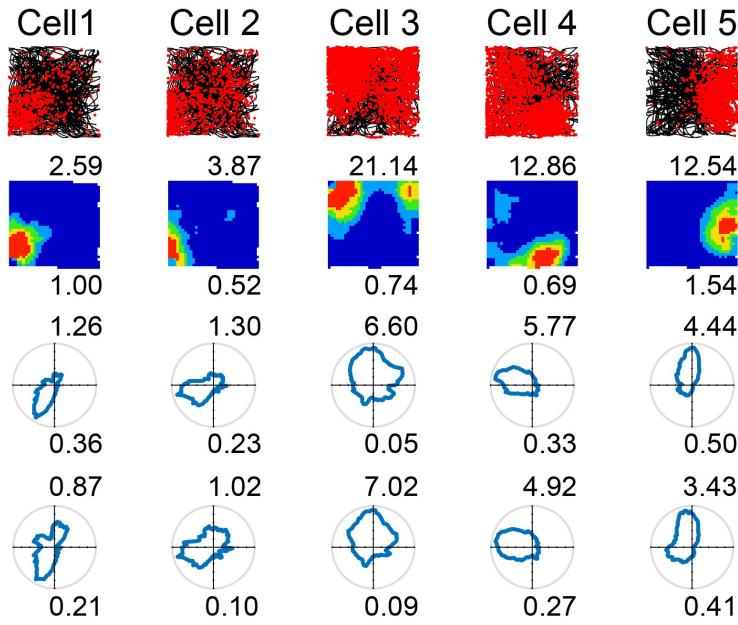


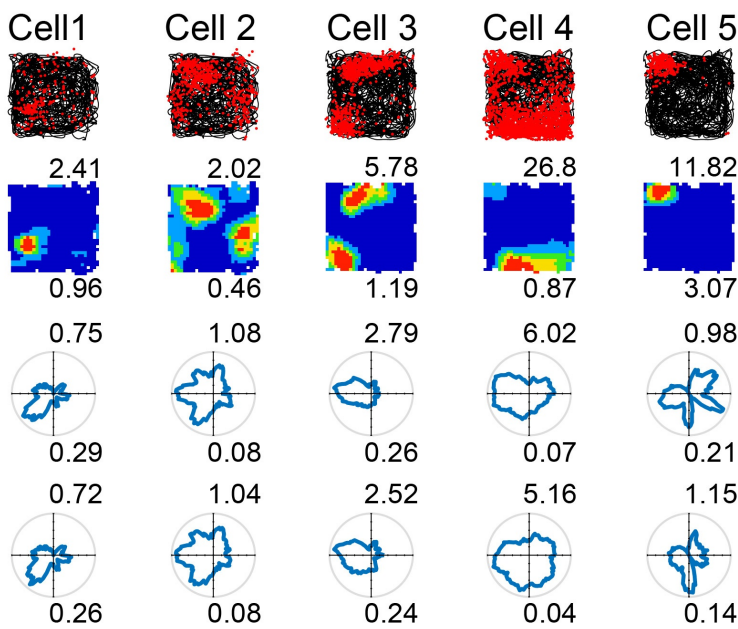
Figure 3.4: **Spatial cell classification.** Distribution of thresholds (99th percentile of the shuffled distribution in each cell) of spatial information for CA1 units (A) and gridness score for MEC units (B). Vertical line indicates the group median.

Place cells recorded from CA1 showed spatially localized firing in the virtual environment, with similar firing rates in the virtual and real square environments. Place cells had larger firing fields in VR than in R, by a factor 1.44 ($\text{field size}_{VR} / \text{field size}_R$). The spatial information content of firing fields in VR was lower than in R. In addition, the firing of place cells was more strongly directionally modulated in VR than in R. See Figure 3.5. Similar results were seen irrespective of whether recordings took place in the 60x60cm or 90x90cm VR environments (e.g., the place field expansion factor being 1.44 in 90cm VR, 1.43 in 60cm VR, $p = 0.66$, see Figure 3.6).

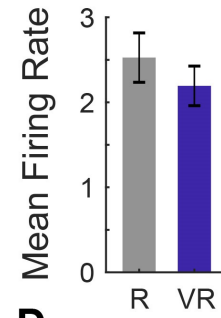
A 60x60cm virtual box



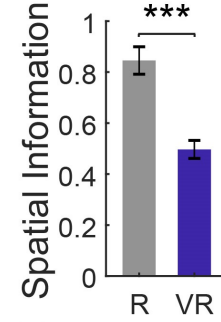
B 60x60cm real box



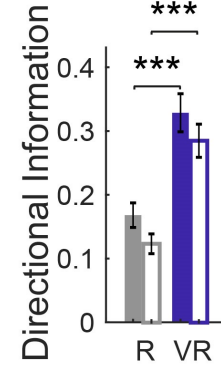
C



D



E



F

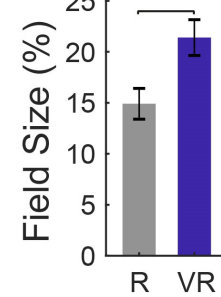


Figure 3.5: **Place cell firing in real and virtual environments.** (A-B) The same five place cells recorded in a 60x60cm virtual square (A) and in a 60x60cm real square (B, one cell per column). Top row: 40-min running trajectory (black line) with red dots showing the locations of spikes; 2nd row, firing rate maps, maximum firing rate (Hz) shown at top right, spatial information rate (bits/spike) bottom right; 3rd and 4th row: polar plots of directional firing rates (3rd row: standard binning; 4th row: after fitting a joint ‘pxd’ model to account for inhomogeneous sampling), maximum firing rate top right, directional information bottom right. (C-F) Comparison between R (grey bars) and VR (blue bars) in Mean firing rates (C), Spatial information rates (D), directional information rates (E) using standard (solid bars) and pxd binning (open bars) and Field sizes (F, bins with firing above 50% of peak firing rate, as a proportion to the size of the test environment).

3.3. RESULTS

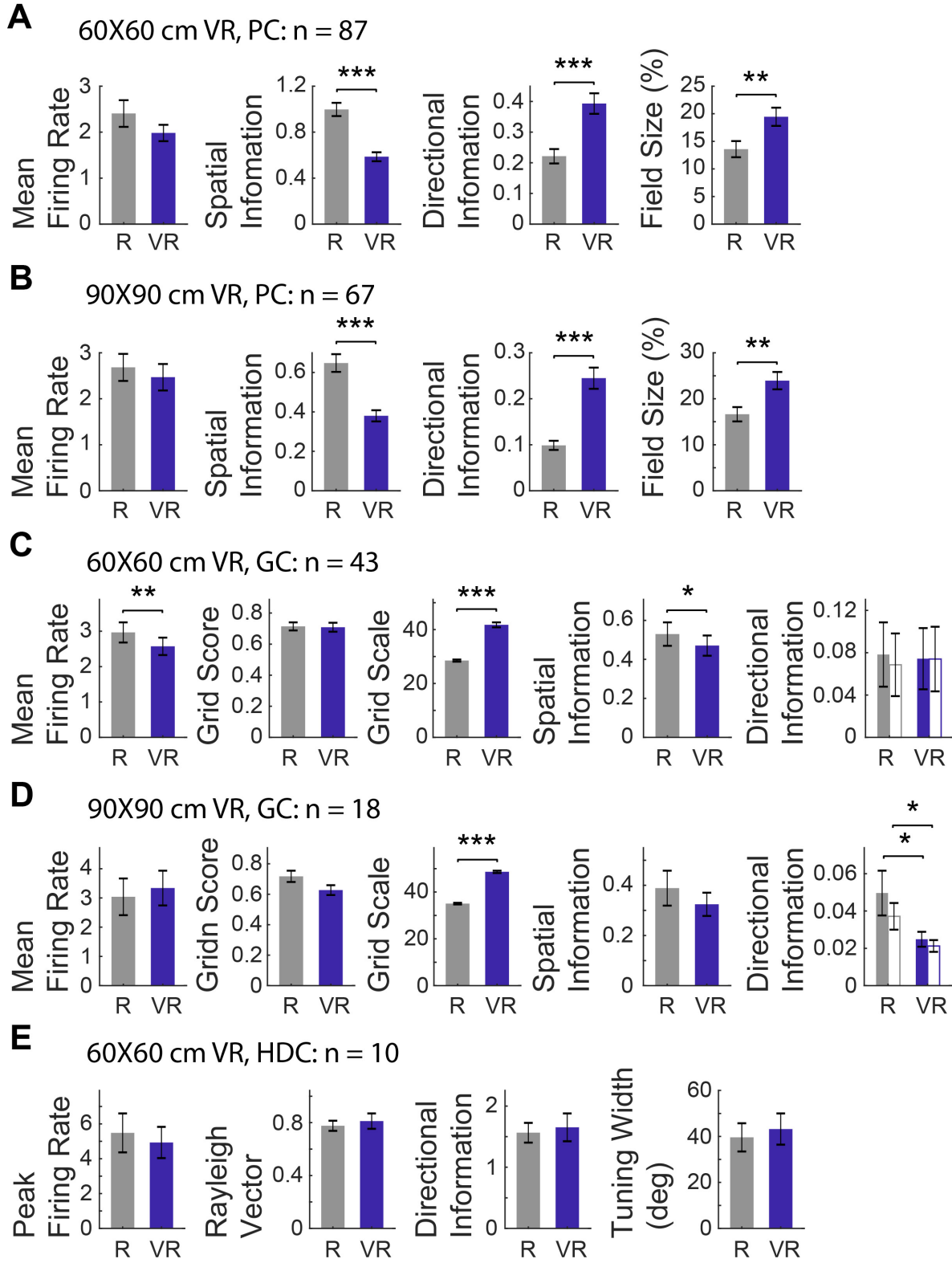


Figure 3.6: **Spatial cell firing properties in 60x60cm and 90x90cm virtual environments.** (A-B) Place cell properties in the 60x60cm VR (A) and the 90x90cm VR (B) compared to the 60x60cm R. (C-D) Grid cell properties in the 60x60cm VR (C) and the 60x60cm VR (D) compared to the 60cm R. In the plots of the directional information rates, solid bars stand for standard directional binning and open bars stand for binning with the 'pxd' model fitting. (E) Head direction cell properties in the 60cm VR and 60cm R.

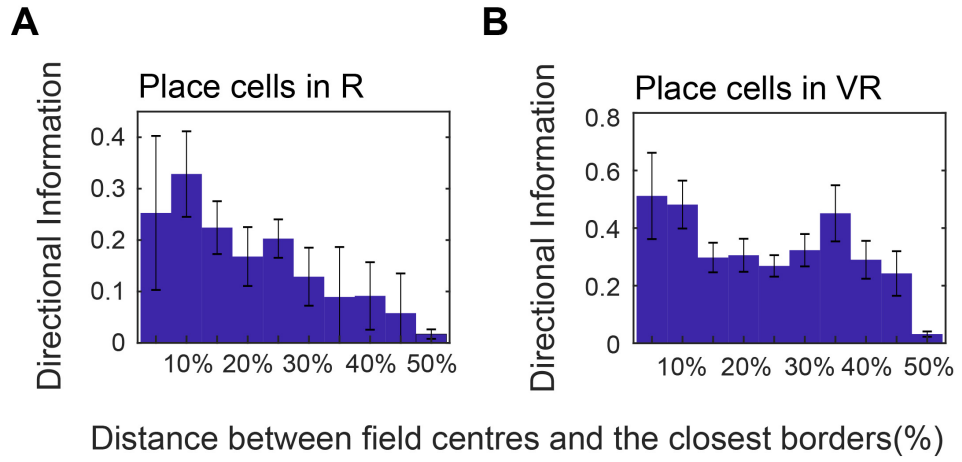


Figure 3.7: **Directional information of place cell firing (bits/spike) as a function of the distance from the nearest wall.**

One possible contribution to apparent directionality in place cell firing could be inhomogeneous sampling of direction within the (locational) firing field. This can be controlled for by explicitly estimating the parameters of a joint place and direction ('pxd') model from the firing rate distribution (Burgess & Hitch, 2005). However, using this procedure did not ameliorate the directionality in firing (see Figure 3.5). Further analyses showed that firing directionality increased near to the boundaries in both virtual and real environments (where sampling of direction is particularly inhomogeneous), but that the additional directionality in VR compared to R was apparent also away from the boundaries (See Figure 3.7). We investigated further

3.3. RESULTS

whether the increased directionality of place cell firing in VR was specific to the square VR environment, by performing additional recordings of both place and grid cells while animals foraged in (visually similar) cylindrical and square R and VR environments (in 4 mice, 3 new to the experiment, yielding a total of 90 place and 9 grid cells). The increased directionality of place cells but not grid cells in VR was present in both cylinder and square environments, supporting the generality of the result (see Figure 3.8).

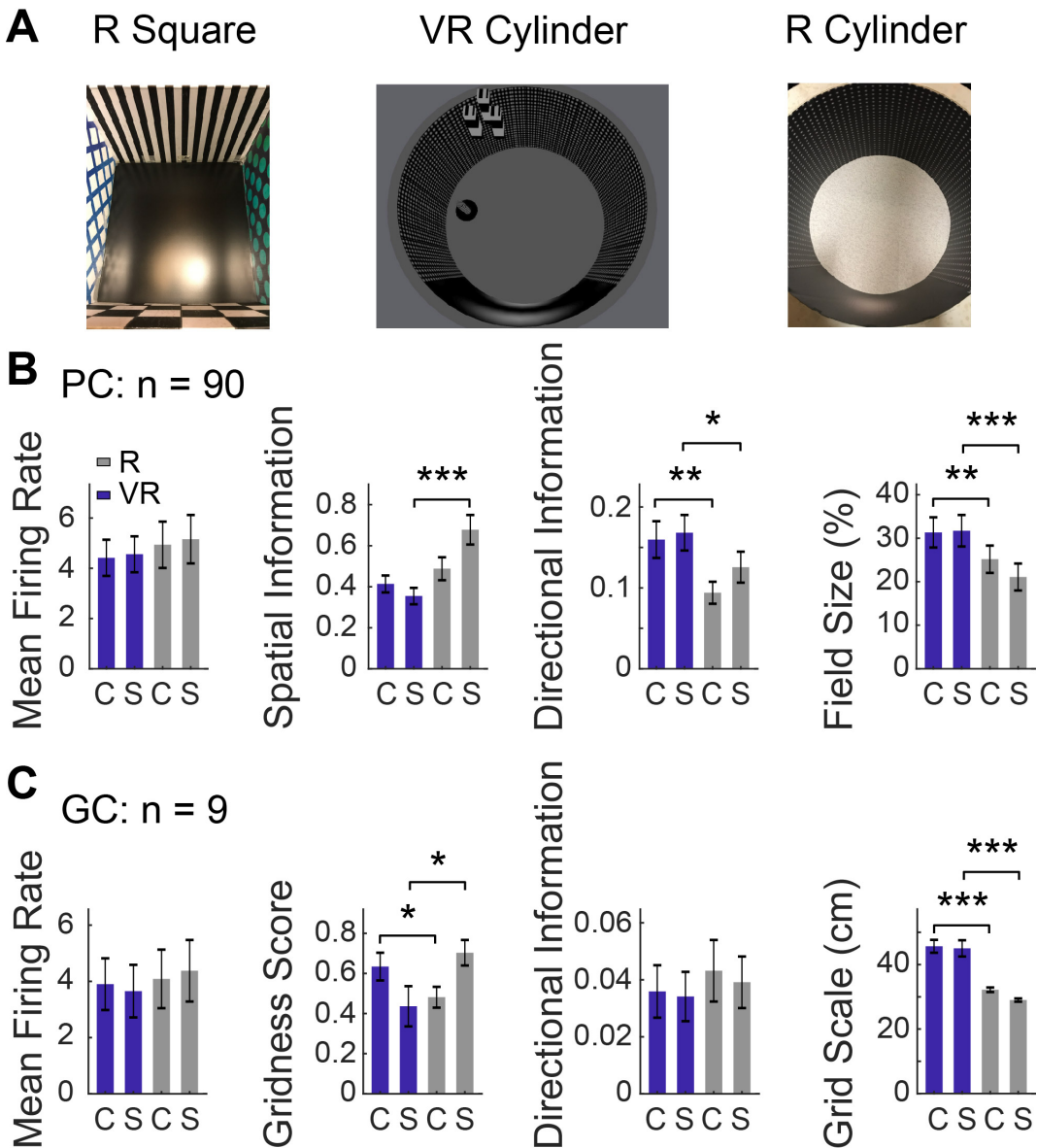


Figure 3.8: **Comparison between VR and R trials in square and cylindrical environments in additional data from 4 mice.** (A) Photos of the recording environments (see Figure 2.2 for the 'VR square' environments). (B-C) Comparison of place cell properties (B) and grid cell properties (C) between virtual and real environment as well as between cylinder (C) and square (S) enclosures.

Grid cells recorded in dmEC, showed similar grid-like firing patterns in VR as in R, with similar firing rates and 'gridness' scores. The spatial scale of the grids was larger in VR than in R, with an average increase of 1.42 ($\text{grid scale}_{VR} / \text{grid scale}_R$, $n=6$ mice). The spatial information content of grid cell firing was lower in VR than R, as with the place cells. Unlike the place cells, the grid cells showed a slight decrease in directionality from R to VR, although this appears to reflect inhomogeneous sampling of directions within firing fields, as the effect was not seen when controlling for this in a joint 'pxd' model. See Figure 3.9. Similar results were seen irrespective of whether recordings took place in the 60x60cm or 90x90cm VR environments (e.g., the grid scale expansion factor being 1.43 in 60cm, 1.36 in 90cm, $p=0.78$), although there were minor differences (the reduction in spatial information only reaching significance in the 60x60cm VR and that in directional information only reaching significance in the 90x90cm VR), see Figure 3.6. It is possible that low directional modulation of the firing of a grid cell could reflect directionally modulated firing fields with different directional tuning. Accordingly, we checked the directional information in the firing of each field, without finding any difference between R and VR (Figure 3.9H).

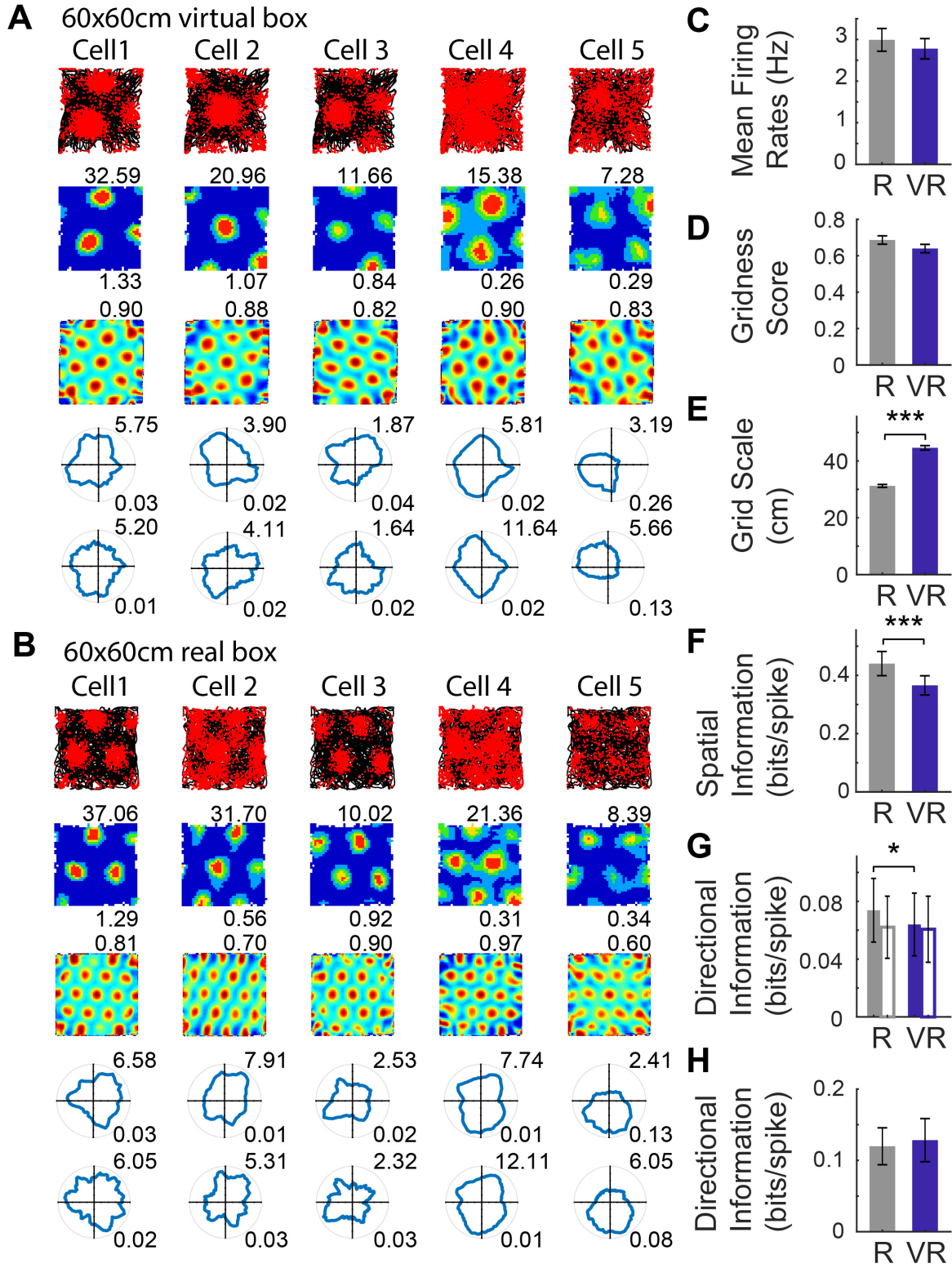
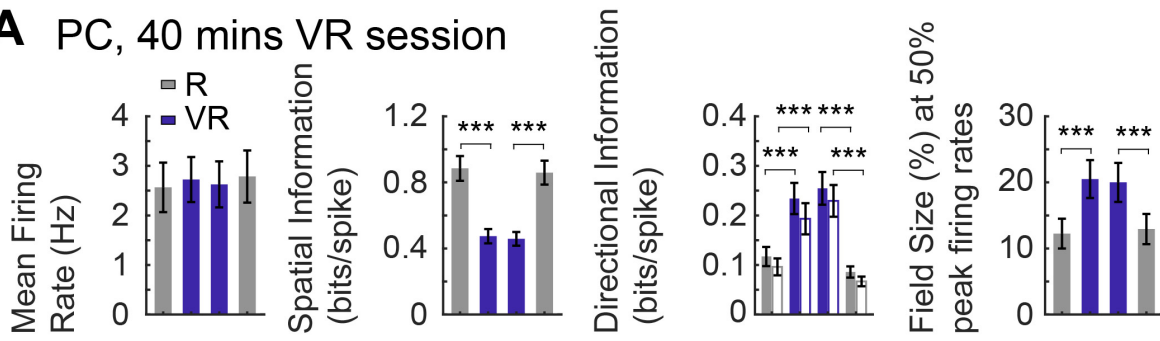


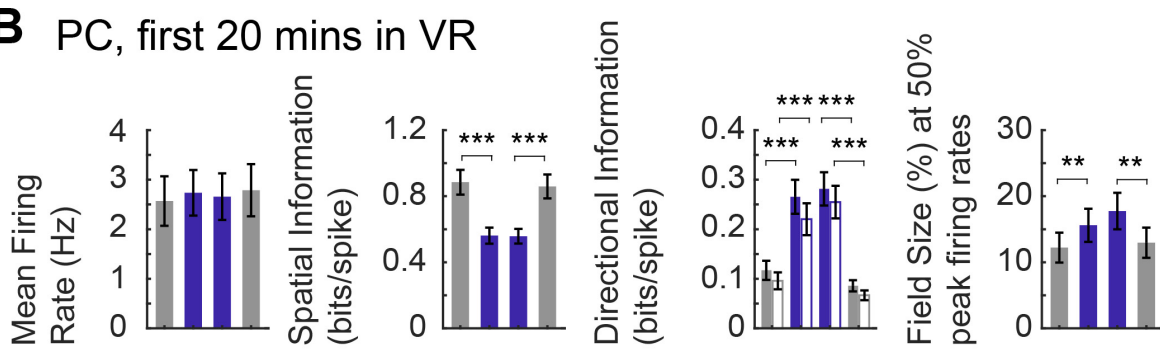
Figure 3.9: **Grid cell firing in real and virtual environments.** (A-B) The same five grid cells simultaneously recorded in a 60x60cm virtual square (A) and in a 60x60cm real square (B, one cell per column). Top row: 40-min running trajectory (black line) with red dots showing the locations of spikes; 2nd row, firing rate maps, maximum firing rate (Hz) shown top right, spatial information (bits/spike) bottom right; 3rd row: spatial autocorrelations, gridness scores top right; 4th and 5th rows: polar plots of directional firing rates (4th row: standard binning; 5th row: ‘pxd’ binning to account for inhomogeneous sampling), maximum firing rate top right, directional information bottom right. (C-H) Comparison between R (grey bars) and VR (blue bars) in mean firing rates (C), gridness scores (D), grid scales (E), spatial information (F) in bits/spike, directional information (solid bar for standard binning and open bar for ‘pxd’ binning) (G) and directional information in individual grid firing fields (H).

To check whether any differences between R and VR could reflect the trial order (VR before R), we recorded additional data from place and grid cells in R and VR on days in which R trials both preceded and followed VR trials (in 4 mice, 3 new to the experiment). We also included analysis of the first 20 mins of VR trials (matching the length of R trials), see Figure 3.10. Under these conditions, the differences in firing properties between R and VR are similar to those shown in Figures 3.5 and 3.9, again indicating generality. However, the 20 grid cells in this group did show lower gridness scores in VR than R, and 43 cells were classified as grid cells in R but only 24 as grid cells in VR. Thus grid cell firing patterns can be sensitive to the use of VR and the inherent conflict between virtual and uncontrolled cues to translation. The extra sensitivity in the second group of animals might reflect their greater age at test (mice with grid cells, main experiment: $n = 8$, age = 25.4 ± 4.3 weeks; additional experiment: $n = 3$, age = 40.1 ± 11.2 weeks; $t(9) = -3.34$, $p < .01$) but this would require further verification.

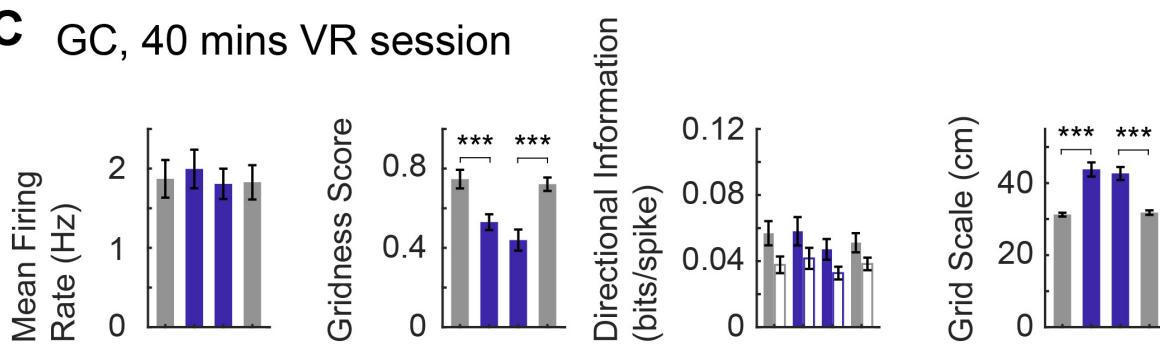
A PC, 40 mins VR session



B PC, first 20 mins in VR



C GC, 40 mins VR session



D GC, first 20 mins in VR

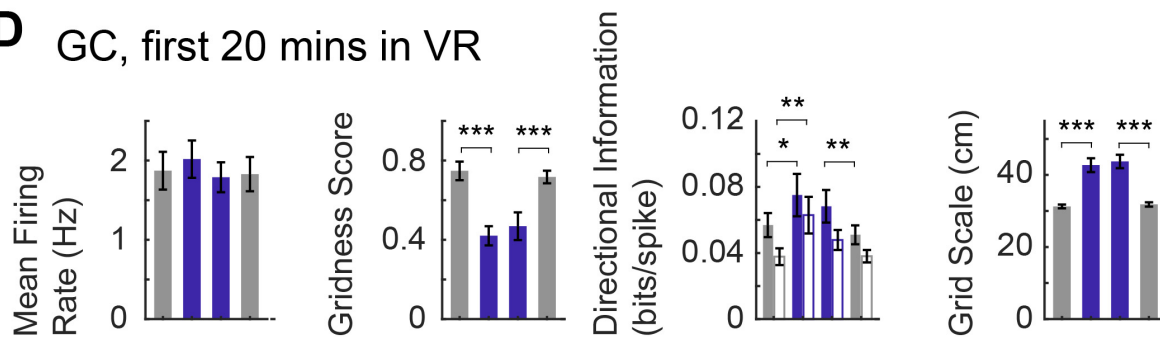
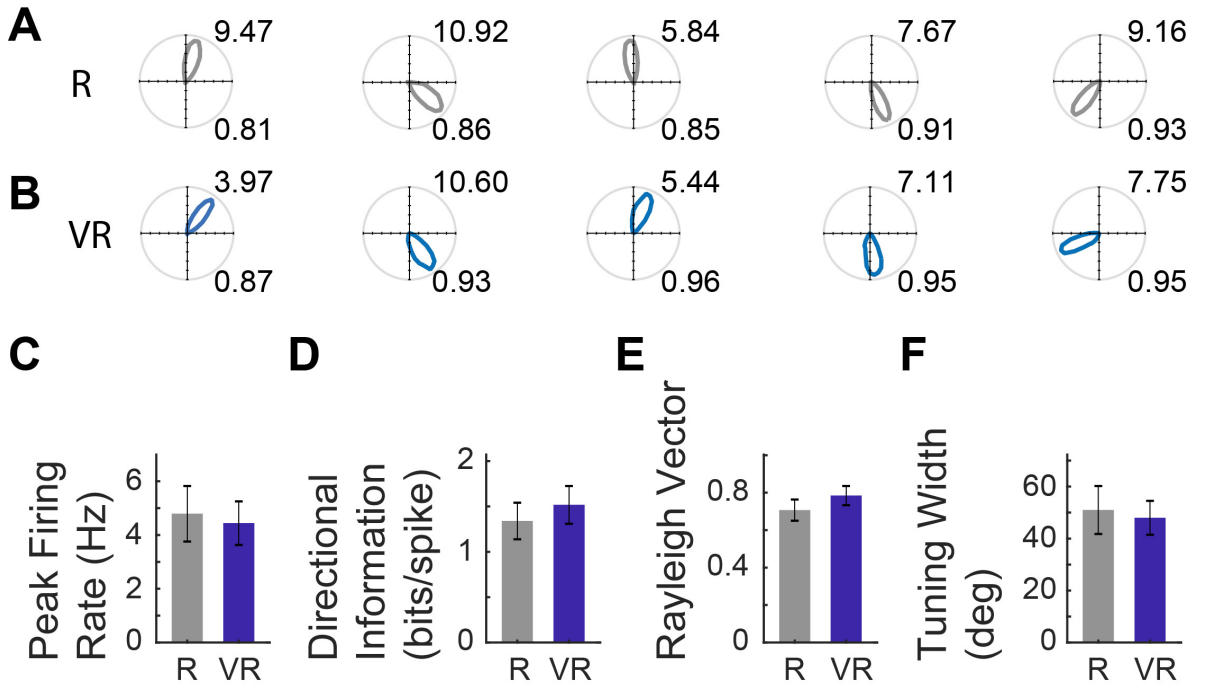


Figure 3.10: **Trial order and trial length effects on comparing cell firing properties in real and virtual environments in additional data from 4 mice.** (A-B) Place cell firing properties comparing 20min R trials with 40min VR trials (A) and the first 20 minutes of the VR trials (B). (C-D) Grid cell firing properties comparing 20min R trials with 40min VR trials (C) and the first 20 minutes of the VR trials (D). Solid bars stand for standard binning and open bars stand for 'pxd' binning)

We also recorded head-direction cells in the dMEC, as previously reported in rats (Sargolini et al., 2006) and mice (Fyhn et al., 2008). These cells showed similar firing rates in VR and R, with similar tuning widths. See Figure 3.11. The relative differences in the tuning directions of simultaneously recorded directional cells was maintained between R and VR, even though the absolute tuning direction was not (see Figure 3.12).



3.3. RESULTS

Figure 3.11: **Head direction cell firing in real and virtual environments.** (A-B) Polar plots of the same five HD cells in dMEC simultaneously recorded in R (A) and VR (B, one cell per column). Maximum firing rates are shown top right, Rayleigh vector length bottom right. (C-F) Comparisons of basic properties of HD cells in dMEC between R and VR.

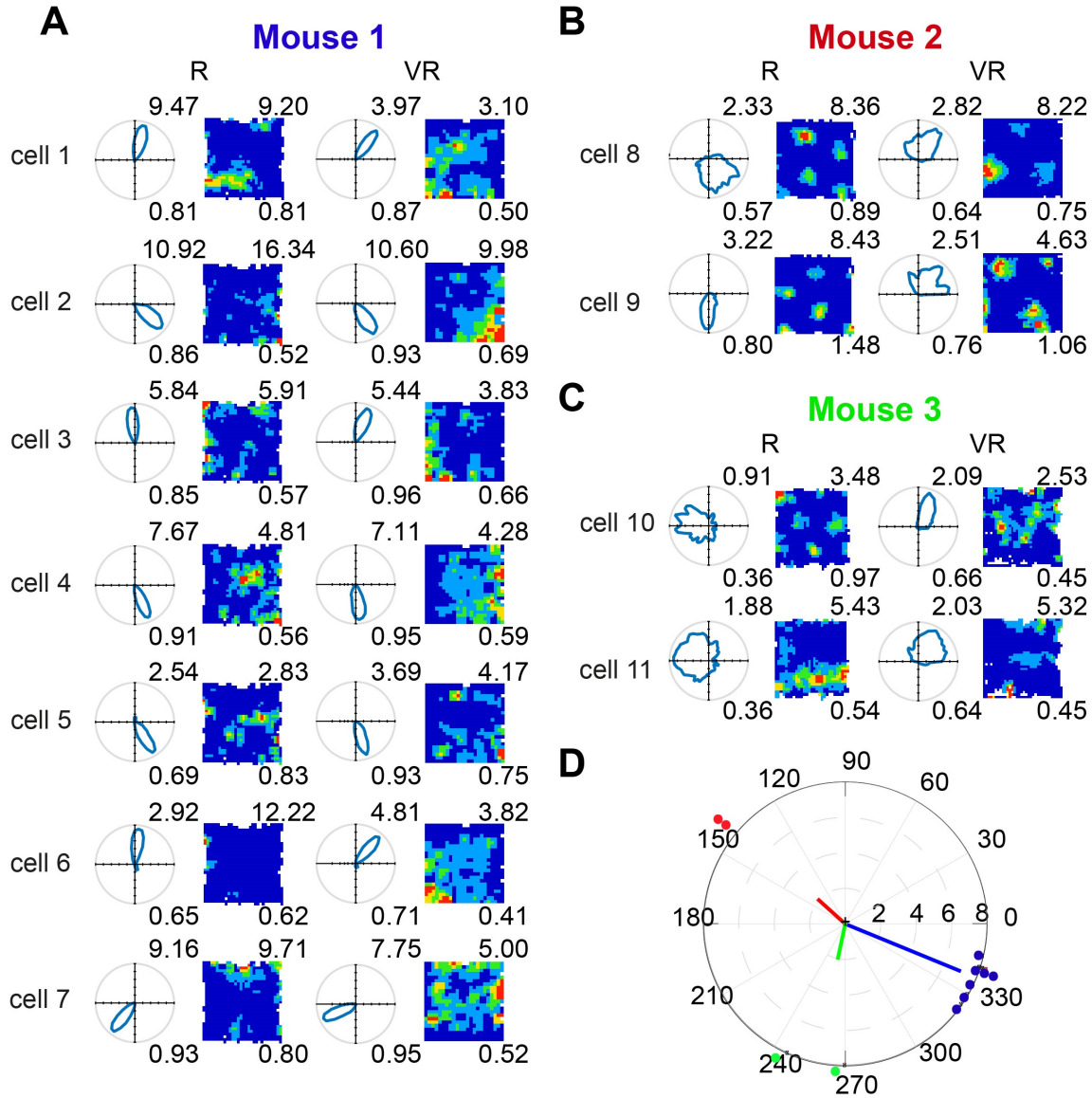


Figure 3.12: **Eleven directional cells recorded in dMEC.** (A) Polar plots (left column) and firing rate maps (right column) of seven cells found in mouse 1. (B) Two conjunctive grid cells found in mouse 2. (C) Two cells found in mouse 3. Numbers on the top right show maximum firing rates, and on the bottom show Rayleigh vector length (left columns) and spatial information (right columns). (D) The relative directional tuning difference of simultaneously recorded head-direction cells between VR and R: Mouse 1 (blue), 337.71 ± 8.28 ; Mouse 2 (red), 138.0 ± 0.00 ; Mouse 3 (green), 258.00 ± 16.97 . The dots represent the relative directional tuning difference of individual cells between VR and R. The lines represent the mean tuning difference within the animals. Each dot represents one cell, and each colour represents one animal.

The translational movement defining location within the virtual environment purely reflects feedback (visual, motoric and proprioceptive) from the virtual reality system, as location within the real world does not change. However, the animal’s sense of orientation might reflect both virtual and real-world inputs, as the animal rotates in both the real and virtual world. To check for the primacy of the controlled virtual inputs versus potentially uncontrolled real-world inputs (e.g. auditory or olfactory), we performed a 180° rotation of the virtual environment and the mouse’s entry to it between trials. Note that the geometry of the apparatus itself (square configuration of screens, overhead projectors on either side) would conflict with rotations other than 180° . In separate trials, we observed a corresponding rotation of the virtual firing patterns of place, grid and head-direction cells, indicating the primacy of the virtual environment over non-controlled real world cues. See Figure 3.13. While all the grid and head direction cells followed the rotation of VR cues (and entry point), a small percentage of place cells (7/141; 5%) did not. These place cells show much lower spatial information scores in both the R and VR conditions (see Figure 3.14), indicating that their lack of rotation might be the result of their weaker or less stable spatial tuning to the proximal

3.3. RESULTS

environmental cues that were rotated.

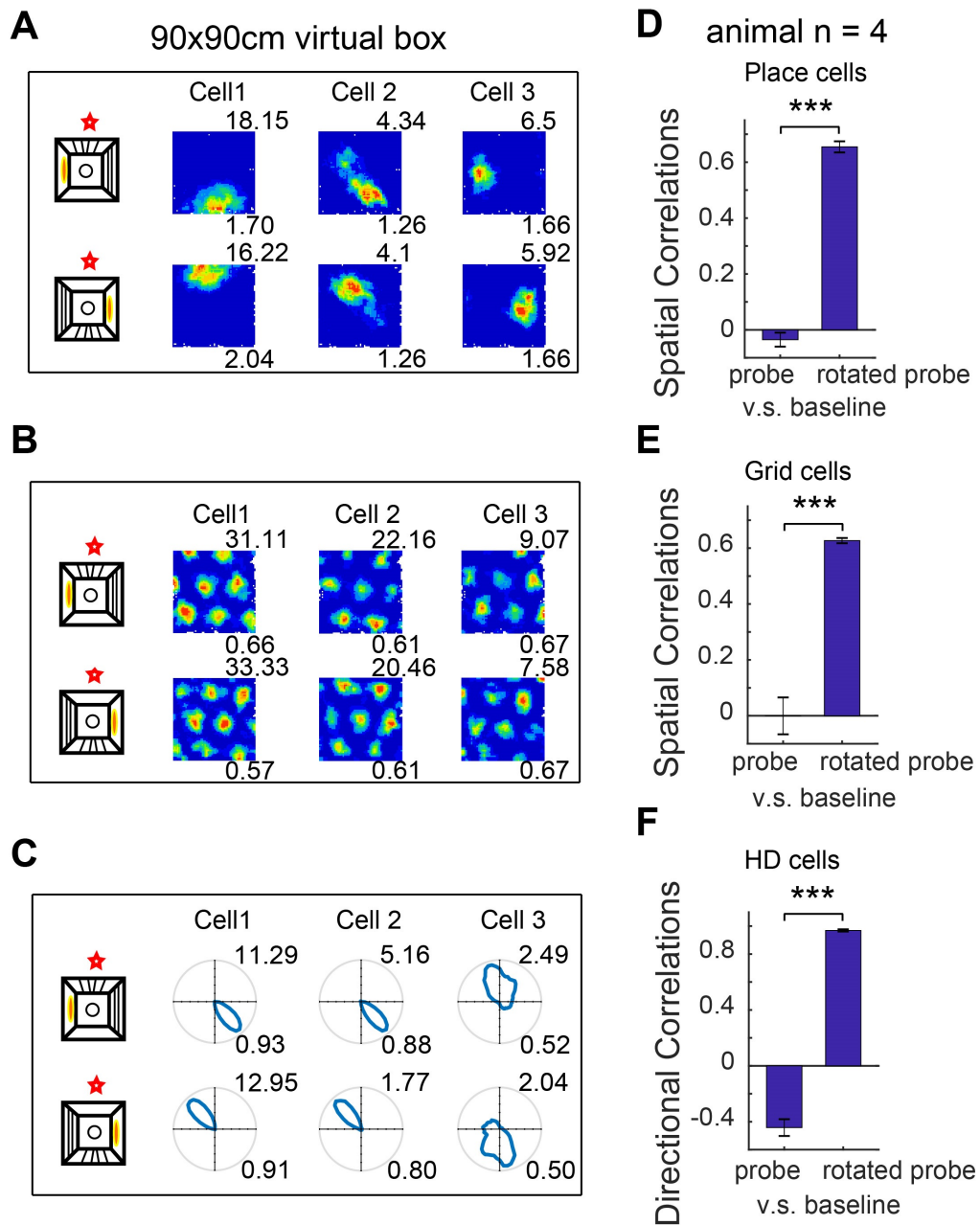


Figure 3.13: **Effect of rotating the virtual environment on spatial firing patterns.** (A-C) Three simultaneously recorded CA1 place cells (A), dmEC grid cells (B) and dmEC head-direction cells (C). Upper rows show firing patterns in baseline trials, lower rows show the rotated probe trials. Schematic (far left) shows the manipulation: virtual cues and entry point were rotated 180° relative to the real environment (marked by a red star). Maximum firing rates are shown top right, spatial information (A), gridness (B) or Rayleigh vector length (C) bottom right. (D-E) Comparison of correlations between cells' spatial rate maps in probe and baseline trials and correlations between 180° -rotated rate maps in probe trials and baseline trials in place cells (D) and grid cells (E). (F) Comparison of correlations between cells' directional rate vectors in probe and baseline trials and correlations between 180° -rotated rate vectors in probe trials and baseline trials in head direction cells.

The animal's running speed is known to correlate with the firing rates of cells, including place cells, grid cells and (by definition) speed cells (Sargolini et al., 2006; McNaughton et al., 1983; Kropff et al., 2015), and with the frequency of the local field potential theta rhythm (McFarland et al., 1975; Rivas et al., 1996; Ślawińska & Kasicki, 1998). So these experimental measures can give us an independent insight into perceived running speed. We found that the slope of the relationship between theta frequency and running speed was reduced within the VR compared to R, while this was not the case for the firing rates of place, grid and speed cells. See Figure 3.15. However, the changes in grid scale and theta frequency in virtual versus real environments did not correlate with each other significantly across animals. There was an effect of running speed on the sizes of place and grid fields that was similar in R and VR, but was not the monotonic relationship that would be predicted by an effect of (speed-related) theta frequency on field size (see Figure 3.16).

Finally, an important aspect of place and grid cell firing is the temporal coding seen

in the theta phase precession of firing in 1-d (O’Keefe & Recce, 1993; Hafting et al., 2008) and 2-d (Climer et al., 2015; Jeewajee et al., 2014) environments. We calculated the theta-band frequency modulation of firing of theta-modulated cells (see Section 2.4.2) and compared it to the LFP theta frequency in R and VR. This analysis shows that, despite the lower overall frequencies in VR, theta modulated firing frequency is slightly higher than the LFP frequency in both R and VR, consistent with theta phase precession (See Figure 3.17A). In addition, we directly analysed phase precession in place and grid cells with clear theta-modulation, finding normal 2-d phase precession in both VR and in R (as in 1-d VR reported by Harvey et al. (2009)). The phase precession slope is lower in VR, consistent with larger firing fields overall in VR environments, but correlations between slope and field size only reached significance for place cells in R ($n = 38$, $r = 0.46$, $p < .01$; all other $p > .3$, See Figure 3.17). These results indicate that theta phase precession in place and grid cells is independent of linear vestibular acceleration signals and the absolute value of theta frequency.

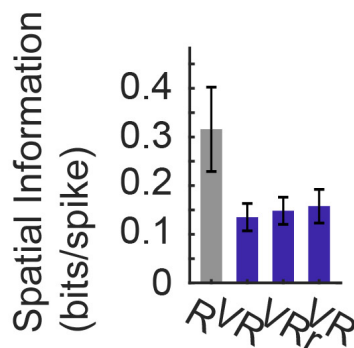


Figure 3.14: **Spatial information of place cells that did not follow the 180°-rotation of VR environment.** $n = 7$, spatial information were 0.32 ± 0.23 , 0.14 ± 0.07 , 0.15 ± 0.07 and 0.16 ± 0.09 in R, VR control, VR rotated and VR control trials respectively.

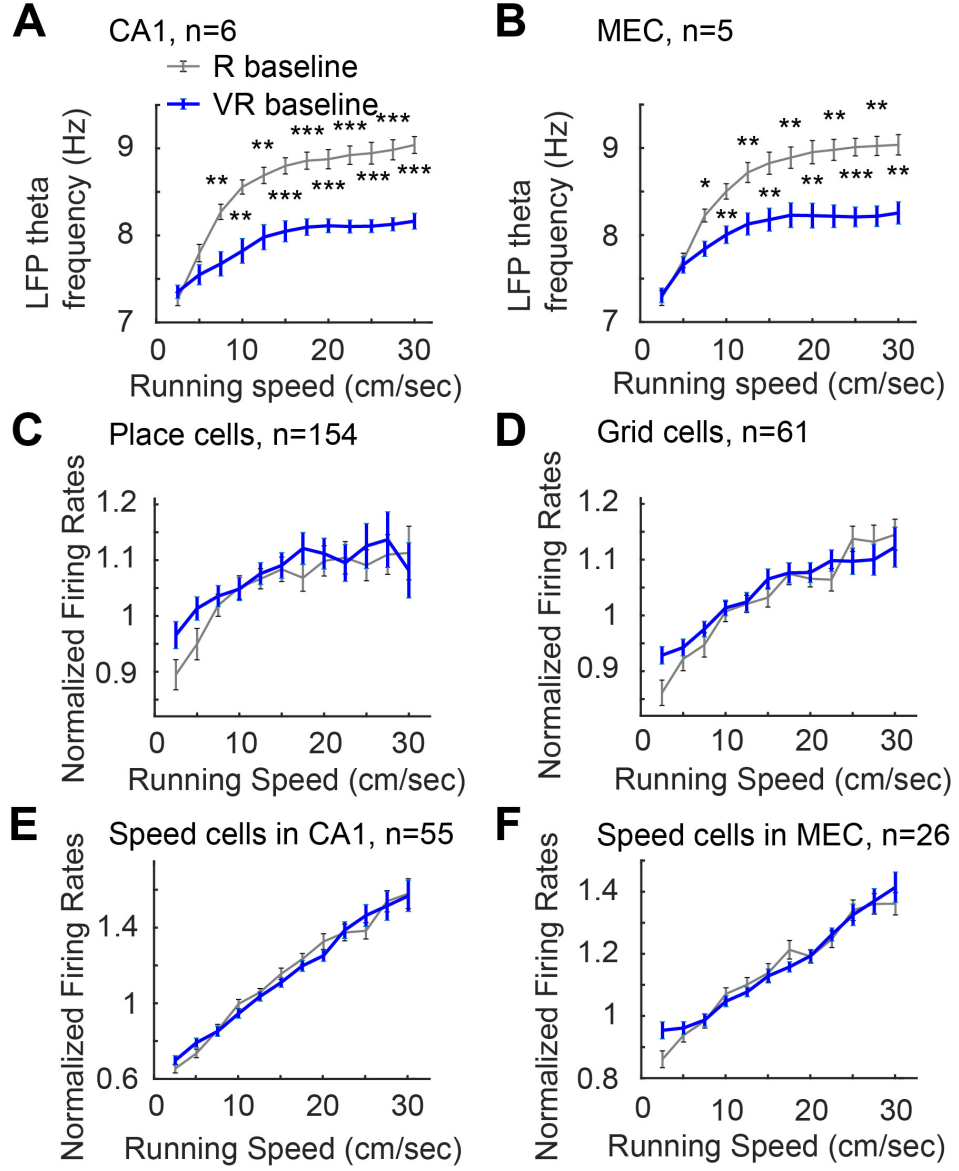


Figure 3.15: **Effect of running speed on theta frequency and firing rates in real and virtual environments.** Relationship between running speed in VR (blue) and R (black) on instantaneous LFP theta frequency in CA1 (A, $n = 6$), instantaneous LFP theta frequency in dMEC (B, $n = 5$), firing rates of place cells in CA1 (C, $n = 154$), firing rates of grid cells in dMEC (D, $n = 61$), speed-modulated cells in CA1 (E, $n = 55$), firing rates of speed-modulated cells in dMEC (F, $n = 26$). Lines show the mean (\pm s.e.m) in each speed bin (2.5cm/s to 30cm/s).

3.3. RESULTS

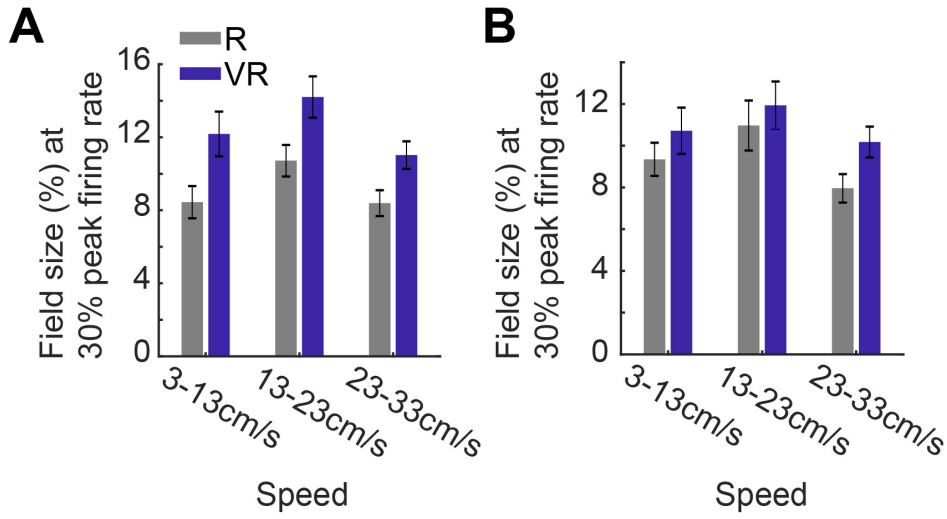


Figure 3.16: **Spatial cell field size was modulated by running speed in a similar way in real and virtual environments.** Comparison of grid cell field size (A) and place cell field size (B) when sampled in different speed ranges.

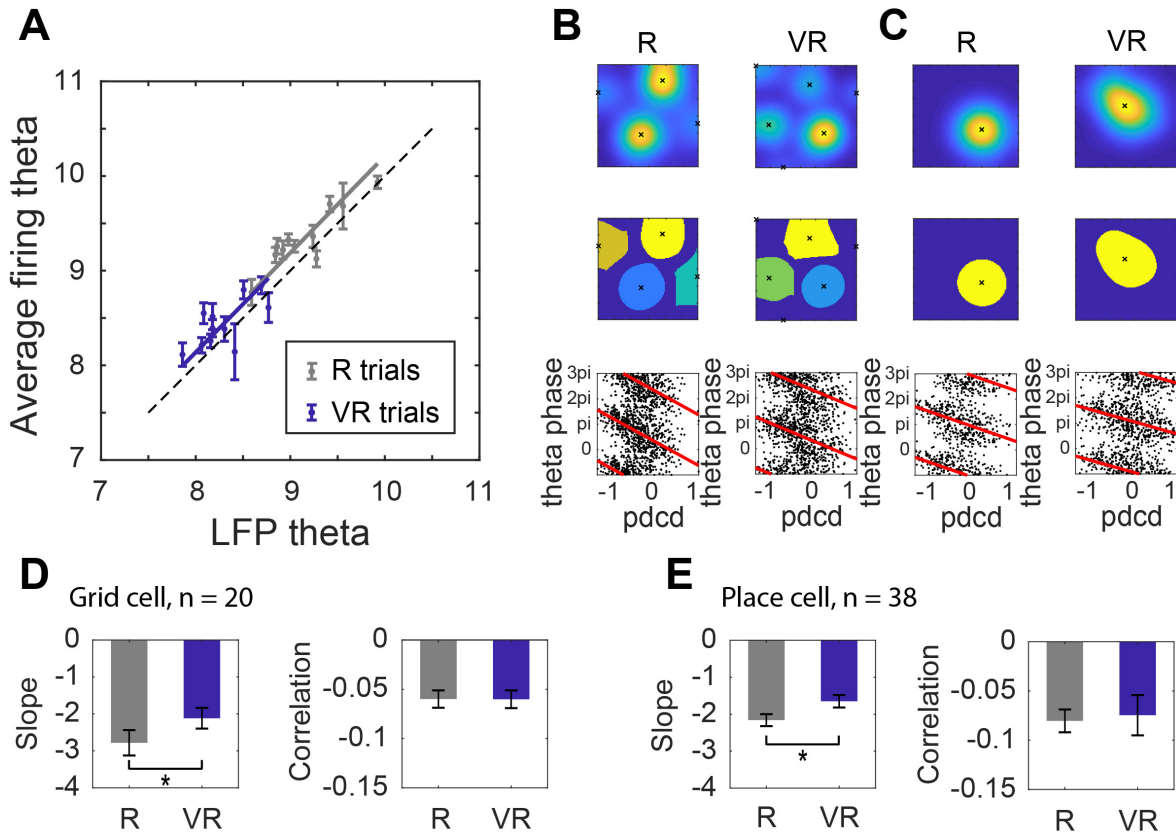


Figure 3.17: **Theta phase precession.** (A) Theta frequency modulation of firing rate versus LFP theta frequency (175 theta modulated cells recorded from EC and CA1, including 20 grid cells and 38 place cells). (B) Example of a grid cell’s theta phase precession in real (left) and virtual environments (right), showing the detection of peaks in the smoothed firing rate map (above), division of data into separate firing fields (middle) and firing phase with respect to LFP theta plotted against distance through field along the current direction of motion (pdcd). (C) Example of a place cell’s theta phase precession in real (left) and virtual environments (right), shown as in B). (D-E) Comparison of grid cell (D) and place cell (E) theta phase precession in R and in VR. Precession slope (left) and hase-pdcd correlation strengths (right) were statistically tested between R and VR trials.

3.4 Discussion

Mice could be trained to navigate smoothly and perform a spatial memory task in our 2-d VR system. Their average running speeds were no different to that observed in the real-world environment, and they displayed natural behaviours such as stop or turn when a visual wall approached, indicating their good understanding and acceptance of the virtual environment. In the meantime, their average angular velocity was significantly lower in VR. In (Aronov & Tank, 2014), he found that body-tethered rats run in much more straight paths and make sharp turns at the onset of trials. He further suggested this behaviour pattern was induced by a distal landmark anchored navigation strategy. In our case, since there is also no informative local cues, and with mice head-restraint possibly making it harder to make angular movements, it could be a combined influence of both. Further research was needed to tell how exactly navigation strategy changed behaviour and possibly further affected spatial representation.

About 80% of CA1 active units were classified as place cells in VR during free foraging (77% in R), which is higher than previously reported ($\sim 12\%$) when mice were to navigate in a 2D virtual open field but with the head fixed to prevent angular rotation (Acharya et al., 2016). Assuming the only difference between the two VR systems was angular motion, it suggests that angular vestibular input was very important for hippocampal position coding in 2D open field. In contrast, the lack of linear vestibular signal was possibly compensated by motor efference copy or proprioception. For example, a study showed that mice had coupled stride pace and whisking frequency during navigating in tactile virtual reality, thus providing registration of self-motion signal and sensory input (Sofroniew et al., 2014).

Similar to results from Acharya et al. (2016), we also observed increased directional tuning in place cells when mice were foraging in 2D VR versus R. Acharya et al. (2016) attributed such directionality to distal visual landmarks and the lack of proximal cues that could be repetitively paired with distal landmark cues through plasticity. The theory may partially explain the elevated directional tuning in spatial cells between VR and R environment since the lack of proximal cues and attention on visual landmarks were the most prominent contrast between the two conditions. However, it does not explain the increased directionality in linear tracks or zigzag mazes versus open fields, where both proximal cues and visual landmarks are present (McNaughton et al., 1983; Derdikman et al., 2009). Enlightened by the fact that omnidirectional spatial representation was difficult in environments that only allows sharp spot turns, coordinated smooth angular and translational motion may be needed for non-directional spatial representation. Future modelling and experimental works are needed.

We also recorded a dozen head direction cells in the medial entorhinal cortex, their selectivity for head direction tuning had no difference between VR and R environments.

CHAPTER 3. SPATIAL CELL FIRING DURING VIRTUAL NAVIGATION OF OPEN ARENAS BY HEAD-RESTRAINED MICE

In our VR system animals make physical head rotation which brings rotated views of both real-world and visual scenes naturally, so the conflict between sensory and self-motion input in the angular domain was minimal, which could be the reason why head direction information was well preserved. Also because both the physical cues and virtual cues were informative of subjects' head direction, we rotated the virtual presentation by 180 degrees, while also introducing the animal from a correspondingly rotated position and angle, to check individual influences of the two sources by putting them into conflict. Results showed a consistent reorientation in the majority of place cells, head direction cells and grid cells firing fields which indicated that combined with rotated the starting orientation, our virtual visual cues dominate and stabilise head direction tuning in the hippocampal formation over external real-world cues.

Interestingly, we did not find the same directionality in grid cell firing. Neither their whole-map spiking activity nor spiking within individual grid fields expressed higher directional tuning in VR than R environments. Two implications could be made in the case of this dissociation between grid cells and place cells. One is that the formation of grid cell firing patterns was under less influence of individual visual cues. Another is that in this particular case of 2D virtual navigation, it is more likely that the information flow was from place cells to grid cells rather than the other way around.

In VR both place cells and grid cells had bigger field sizes, for grid cells bigger grid scales too. One possible reason was that in VR, neither translational vestibular signals nor local cues were informative of the subject's virtual location and thus were in conflict with the virtual environmental cues. Such absent or conflicted inputs increased ambiguity of spatial coding which then could lead to increased field sizes and grid scale (Barry et al., 2012; Towse et al., 2014). The increased ambiguity theory was also supported by the decreased spatial information that we observed in VR place cells.

Speed modulation of LFP theta frequency, but not the firing rate of spatial cells and speed cells, also dropped during navigating in VR. The reduction likely reflected the effects of lacking linear vestibular signal in mice running with head restrained, which on the other hand did not seem to affect the speed modulation of cell firing rates. Previous researches and computational models suggested that speed modulation in the intrinsic firing frequency is linked to spatial scales of hippocampal cells' firing patterns (Maurer et al., 2005; Burgess et al., 2007; Burgess, 2008; Jeewajee et al., 2008; Giocomo et al., 2011). Though both expected trend of changes were observed in VR, we found no linear relationship between the degree of reduction in speed modulation and the increase in place field sizes or grid scales across subjects.

Phase precession for both place cells and grid cells was intact in VR, shown by higher frequency in cell firing theta modulation than local field potential theta frequency, as well as a comparable phase to position-in-field correlation coefficients in VR and R environments. This result was consistent with previous research (Aghajani et al., 2015). Moreover, we found that the phase precession slope was shallower in VR with place field sizes normalised to unit distance. Possibly due to decreased excitatory dendritic input, in our case the self-motion inputs from the medial entorhinal cortex, the phase precession would be slower according to the soma-dendritic interference model (Kamondi et al., 1998; Magee, 2001; Harris et al., 2002). Or it could also be an artefact of low signal-to-noise ratio in spatial selectivity which resulted in higher spiking rate threshold for field definition in VR. Further confirmation is needed.

In conclusion, our experiment established that we now had a functioning 2D virtual reality system that allowed freedom of 2D navigation and generated virtual environments that whose spatial layout was perceived by mice. Our virtual 2D system also engaged the 2D spatial representations found in the hippocampal formation. Place

cell, head direction cells and grid cells all displayed comparable spatial tuning properties in VR and R environments. Last but not least, our VR setup could be adapted for fine control and manipulation of the sensory feedback, and potentially compatible with recording techniques such as intracellular recording, two-photo imaging and so on.

Chapter 4

Differential influences of environment and self-motion on place and grid cell firing

4.1 Introduction

Recent studies have pointed out the importance of visual input in spatial coding, especially in linear path integration (Raudies & Hasselmo, 2015; Saleem et al., 2013; Chen et al., 2013). Place field locations were decided by a combination of self-motion and visual cues when the two were dissociated from each other (Chen et al., 2013). Firing rates of speed modulated V1 neurons are best predicted by weighed summation of in-conflict locomotion and visual velocity (Saleem et al., 2013). Also, hippocampal place cells encode linear track position in high consistency with position coding in v1 neurons (Saleem et al., 2018). Grid cells, on the other hand, are considered to be the path integrator in the brain that updates current location from self-motion tracking,

for which external inputs seem to be dispensable (Hafting et al., 2005; McNaughton et al., 2006). Since studies also show that their activity is in close link to that of place cells (Solstad et al., 2006; Fyhn et al., 2007; Brun et al., 2008a; Bonnevie et al., 2013; Ólafsdóttir et al., 2016), it would be interesting to examine whether grid cells would respond to the manipulation of external and self-motion inputs in coherence with place cells.

By stretching or compressing walls along one or both axes of a familiar environment, previous studies were able to show that both place fields and grid spacing deformed accordingly (O’Keefe & Burgess, 1996; Barry et al., 2007; Stensola et al., 2012). Although such deformation is experience-dependent for grid cells (Barry et al., 2007), i.e. a regular field spacing was recovered after exposure to the new configuration for a few days, it was surprising to many to observe a clear external-anchored grid pattern deformation. Environmental boundaries are considered to be important to ‘anchor’ grid fields location, like for place cells. In a real-world environment, boundaries can provide many distinct sensory cues, including local ones like tactile and olfactory cues, and distal ones such as static visual landmark and optic flow. It is interesting to check in a virtual environment where the boundaries are only indicated visually, would it be potent to drive grid cells to fire.

Virtual reality techniques allow us to better dissociate environmental cues from self-motion cues without confounding factors such as uncontrolled local cues. Previous studies that dissociated environmental cues from self-motion using virtual reality technique was all conducted in linear track (Chen et al., 2013; Saleem et al., 2013). Hippocampal tuning property has been shown different between linear track navigation and open field exploration (O’Keefe & Nadel, 1978; McNaughton et al., 1983; Hafting et al., 2005; Brun et al., 2008b; Derdikman et al., 2009). Head-fixation limits

any angular movement as well as the proprioceptive sense of linear acceleration which disables normal vestibular function and possibly causing unnormnal hippocampal representation (Aghajan et al., 2015; Acharya et al., 2016). Thus it is important to probe the integration of inputs under 2D open-field navigation with the underline 2D spatial representation intact and to draw a more general implication on the hippocampal spatial system.

In this experiment, we exploited the 2-d virtual reality system we established in a previous experiment (Chen et al., 2018) and manipulated the gain factor (G) between self-motion and virtual (visual) translation on one axis of the environment while recording from both hippocampal CA1 and dorsomedial entorhinal cortex (dMEC) at the same time. In the baseline condition ($G = 1$), mice travel 60cm on the air-cushioned styrofoam ball to get from side to side in the virtual environment. In the gain increase condition ($G > 1$), the virtual unit distance was kept constant and animals needed to cover less on the ball surface to traverse the virtual environment. In this case, the motor size of the environment on the manipulated axis is less than 60cm while the visual size is the same. On the contrary, in the gain decreased condition ($G < 1$), the motor size of the manipulated axis is bigger than 60 cm and visual size remained the same.

By dissociate the environmental input and self-motion signal, we were able to show that simultaneously recorded grid cells and place cells were affected by gain manipulations differently. Place cells fired under dominant influence of the VR visual input, while grid cell firing continued to be largely driven by self-motion input. Consequently, place cells and grid cells diverge in their spatial representations and together they might be complementary to form a flexible hippocampal representaion that reflect the influence of both the environmental and self-motion inputs.

4.2 Methods

4.2.1 Animal

Nine male C57Bl/6 mice were used in this experiment. One were implanted with 8 tetrodes in hippocampal CA1, Two with 8 tetrodes in the dorsomedial entorhinal cortex, and six mice received a dual implant with one microdrive in right CA1 and one in left dMEC (each microdrive carried 4 tetrodes).

4.2.2 Manipulating the gain of visual motion vs physical motion

After the animals had been trained in the ‘fading beacon’ task in VR, they ran in a 60x60cm VR square as their baseline environment. A probe session consisted of a 40-min random-foraging baseline trial followed by a 40-min random-foraging probe trial and a final 20-min real world (R) trial. In the probe trial, the ball-movement to visual-movement gain setting on one of the axes was either double for the gain increase manipulation ($\text{Gain} = 2$; i.e. animals only run half of the distance on the ball to move the same distance in the visual VR on the manipulated axis compared to the baseline trial) or $2/3$ for the gain decrease manipulation ($\text{Gain} = 2/3$; i.e. animals had to run 1.5x the distance on the ball to cover the same distance in the visual VR on the manipulated axis compared to the baseline trial).

4.2. METHODS

Table 4.1: Trial information

Mouse id	Implant type ^a	Number of grid firing patterns recorded ^b	Number of place firing patterns recorded ^b	Gain increase (G=2) ^c Baseline: 60x60cm Probe: 30x60cm	Gain decrease (G=2/3) ^c Baseline: 60x60cm Probe: 90x60cm	Number of grid patterns per session ^d	Number of place patterns per session ^d
864	E	2(2)	0	1	0	2.0	0.0
984	C	0	21(12)	1	1	0.0	6.0 \pm 0.0
986	E	17(17)	0	1	0	17.0	0.0
987	CE	29(29)	83(48)	2(1) ^e	1	9.7 \pm 2.8	24.0 \pm 3.0
1014	CE	7(7)	0	1	1	2.5 \pm 0.5	0.0
1015	CE	3(3)	53(27)	1	1	1.5 \pm 0.5	13.5 \pm 3.5
1060	CE	6(6)	38(30)	2	1	2.0 \pm 0	10.0 \pm 0.6
1061	CE	43(42)	178(105)	3	2	8.4 \pm 1.6	21.0 \pm 2.5
1176	CE	15(12)	124(53)	2	2	3.0 \pm 0.7	13.3 \pm 0.6

^aE: implant in left mEC; C: implant in left CA1; CE: implant in right CA1 and left mEC

^bNumbers in brackets indicate compact non-remapping firing patterns

^cNumber of whole-day recording sessions for each type of manipulation, environment size given in motor coordinates. Multiple recording sessions were included for the same animal when sessions are conducted at least one month apart and animals were regularly trained in the baseline gain condition.

Brackets indicate one session without compact non-remapping place firing patterns

^dMean \pm s.e.m of number of compact non-remapping place and grid firing patterns analysed per session per animal

^e Tetrapods advanced between of the two recording sessions.

The location in virtual environments can be plotted in motor coordinates or visual coordinates. In baseline trials (where Gain = 1) these locations and the size of

the virtual environment is the same in both coordinates. In probe trials, where the ball-to-vision gain changed ($\text{Gain} = 2$ or $2/3$), environment size is different to the 60x60cm baseline when measured in motor coordinates (i.e. 30 x 60cm or 90 x 60cm) but is the same in visual coordinates. We did not use $\text{Gain} = 1/2$ probe trials, as large environments - 120cm or more across in motor coordinates - become impractical in terms of getting good coverage and also produce less stable grid cell firing patterns near to the centre, presumably reflecting the absence of local cues and large distance and low parallax of visual cues to location.

4.2.3 Data analysis

Rate map construction

In VR probe trials, relative virtual visual positions were different from relative physical positions on the ball due to the changing gain between visual movement and physical movement. Rate maps in a visual coordinate were constructed by binning animal's virtual (visual) locations. Then rate maps in a motor coordinate were reconstructed by linear interpolation of the existing rate maps according to the applying gain ratio.

Cell and firing field classification

Place cell, grid cell and head direction cell were classified with the standard protocol (for threshold distribution see Figure 4.1). To check that grid-like responses were not generated by visual input from the hexagonal floor tiles we plotted the scales and phases of grid cell firing patterns relative to the floor pattern – finding no correspondence (see Figure 4.2).

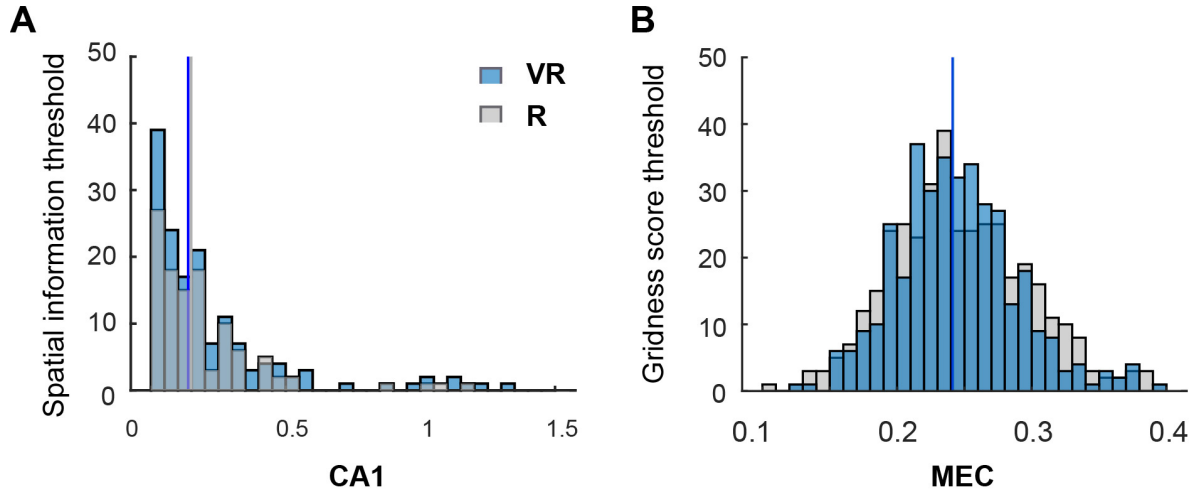


Figure 4.1: **Spatial cell classification.** Distribution of thresholds (99th percentile of the shuffled distribution in each cell) of spatial information for CA1 units (A) and gridness score for MEC units (B). Vertical line indicates the group median.

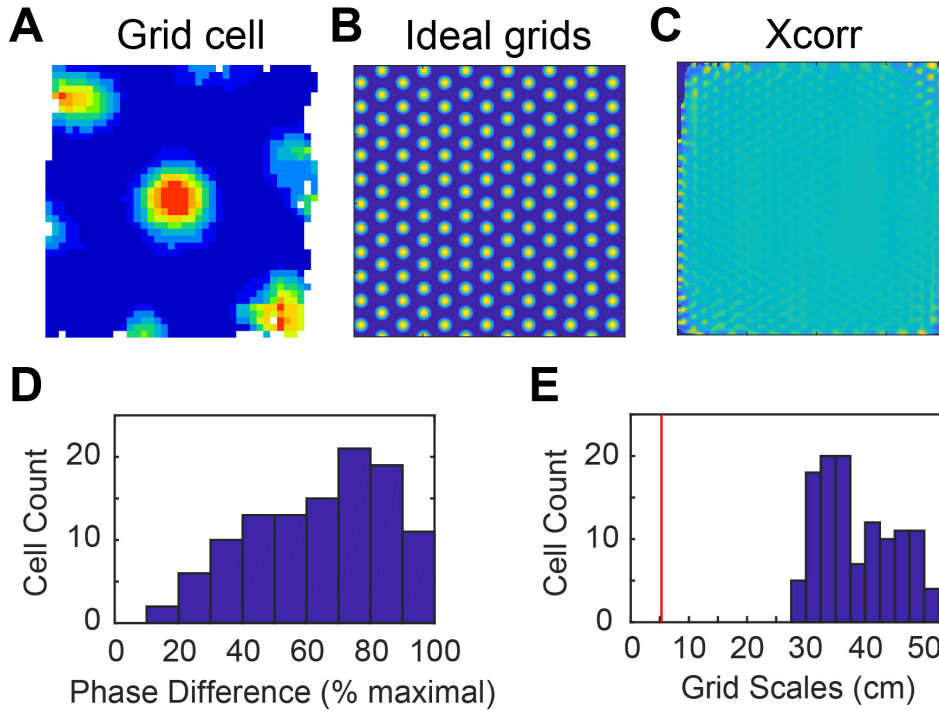


Figure 4.2: **Comparison of grid firing patterns with hexagonal virtual floor tiling pattern.** (A) A rate map of an example grid cell. (B) A rate map of an ideal grid cell whose pattern matched the floor pattern. (C) Cross-correlation of the rate maps between (A) and (B). (D) The distribution of phase differences. (E) The distribution of grid scales. The red line indicates the grid scale of the floor pattern.

Cells in MEC were defined as spatial non-grid cells, using similar criteria to place cells, if their spatial information in the baseline trial exceeded the 99th percentile of the shuffled distribution of spatial information and their gridness scores in the baseline trial did not exceed the 99th percentile of the shuffled gridness score distribution.

Remapping of firing patterns

We calculated the spatial correlation between a baseline firing rate map and the best-matching (stretched and offset) probe rate map (described above). We defined a remapped cell as having a spatial correlation between the two maps below 0.3. Only non-remapped place cells and grid cells were included in further analysis, leaving 425 out of 497 place cells and 118 out of 122 grid cells that were quantified as non-remapping cells. The proportions of place cells remapping between baseline and probe conditions did not differ between gain increase and gain decrease sessions (Figure 4.3).

For place cells, we then identified firing fields at 30% peak firing rates, and considered those cells whose fields covered more than 50% of either probe or baseline environments as too diffuse for analyses, leaving 275 out of 497 compact non-remapping place cells for further analysis.

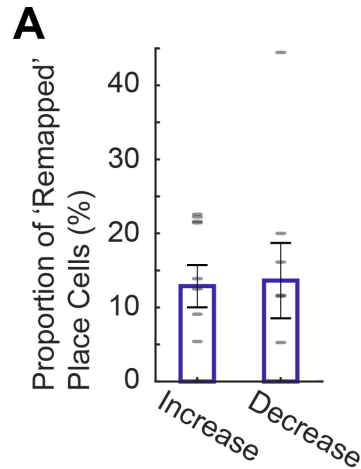


Figure 4.3: **Proportion of ‘remapped’ place cells.** There is no difference in the proportion of place cells remapping between baseline and probe trials when comparing gain increase and gain decrease sessions.

Grid scales along different axes

To compare scale changes along different axes, we fit an ellipse circumscribing the six peaks nearest to the centre on the autocorrelogram of a cell. The grid was not included in the analysis if the number of nearest peaks was less than six. We then measured the diameters of the ellipse along manipulated and un-manipulated axes. The ratios of the diameters in probe trials to those in baseline trials were calculated based on the autocorrelograms generated in visual coordinates and motor coordinates.

Motor influence score for firing patterns

A set of 20 transformed probe trial firing rate maps were generated via linearly interpolating firing rate maps plotted in a visual coordinate by stretch factors ranging from 1 to the applied gain ratio in 20 steps. Correlations between the transformed probe maps and baseline rate maps were then calculated with offsets of 1.5cm intervals

along the manipulated axis between the smaller to the larger map, keeping the largest (O’Keefe & Burgess, 1996). A stretch factor (F) was defined as the factor that produced the largest spatial correlation. The visual gain G is the ratio distance moved by the viewpoint in VR divided by the distance moved by the mouse on the ball surface. The ‘motor influence’ score was defined as $MI = (F-1)/(G-1)$ for the probe trials, so that $MI = 1$ if the stretch factor is equal to the visual gain (i.e. $F = G$) and $MI = 0$ if the stretch factor is unity despite non unity visual gain ($F = 1, G \neq 1$).

Motor influence score for population vectors

For each session containing more than one cell, we compute one population vector. First, we combined all simultaneously recorded place cells / grid cells in a vector. For each cell, we calculated the spatial correlation values between the baseline rate map and the transformed probe map with stretch factors ranging from 1 to the applied gain ratio in 20 steps. Then we calculated the average spatial correlation values over all cells for each stretch factor, with offsets of 1.5cm intervals along the manipulated axis between the smaller to the larger map. The offset and stretch factor for the population vector (Op, Fp) was defined as the pair with the highest average correlation over cells. The motor influence score for the population vector was defined as $MIp = (Fp-1)/(G-1)$.

Firing field sizes along different axes

To compare field size changes along different axes, we defined firing fields based on the rate maps of the cells. For each rate map, we first excluded the bins with firing rates lower than 30% of peak rates. Then firing fields were found by fitting ellipses around sets of contiguous bins containing firing. Fields which were smaller than 5% or bigger than 50% of the total area were excluded in further analysis.

To find matching fields in the probe trial, we calculated the centroid position $C(x,y)$ for each field in the baseline trial. We then calculated the matching centroid in a probe trial by shifting the x position of the baseline centroid by the best fitting stretch factor F . A matching field was defined as a field which included the matching centroid.

We excluded grid fields near the edge of the environment as they appear to be occluded by the edges – causing significant changes in field shape between baseline and probe trials (e.g. circular to semi-circular). Perhaps because they are largely motor driven, environmental edges simply prevents further sampling of grid field. By contrast, place fields near to the edge seem to retain their location and shape (albeit potentially stretched), perhaps because they are largely driven by vision (and, indeed, the distance to the boundary (O’Keefe & Burgess, 2005)). Place fields were processed similarly to grid fields for ease of comparison (i.e. setting the rate map outside of the field to zero and excluding place fields near to the edge).

Motor influence score for individual firing fields

For each field that we identified with the method described above, we constructed a new rate map including the field and zero spikes for the remaining position bins. Then we computed the motor influence score from the rate map constructed for that field.

4.2.4 Statistical analysis

Wilcoxon rank sum test (non-parametric test) was conducted for comparisons of MI scores in different conditions. Parametric statistical tests including student’s t -test and ANOVA were used on other behavioral and neuronal measures. In all figures * = significant at the 0.05 level, ** = significant at the 0.01 level, *** = significant at the

CHAPTER 4. DIFFERENTIAL INFLUENCES OF ENVIRONMENT AND SELF-MOTION ON PLACE AND GRID CELL FIRING

0.001 level. For all the statistical test results see Table 4.2.

Table 4.2: Statistical test results

Comparison	Test	Results	Fig.
proportion of 'remapped' cell	independent t test, $G_{in}-G_{de}^a$	$t(16)=-0.14$, $p=0.89$	Fig.4.3
PC, peak firing rates	paired t test,	$t(274)=3.68$, $p<.001$	Fig.4.6A
GC, peak firing rates	$VR_{baseline} -$	$t(117)=2.42$, $p<.05$	Fig.4.6B
GC, gridness score	VR_{probe}	$t(117)=8.09$, $p<.001$	Fig.4.6C
PC, G_{in} , visual coord., all field size	paired t test,	$t(172)=-14.35$, $p<.001$	Fig.4.7E
PC, G_{in} , visual coord., distal field size	X-Y axis ^b	$t(111)=-12.22$, $p<.001$	Fig.4.7E
PC, G_{in} , motor coord., all field size		$t(172)=0.29$, $p=0.77$	Fig.4.7F
PC, G_{in} , motor coord., distal field size		$t(111)=-0.03$, $p=0.98$	Fig.4.7F
PC, G_{de} , visual coord., all field size		$t(121)=1.07$, $p=0.29$	Fig.4.8E
PC, G_{de} , visual coord., distal field size		$t(83)=-0.45$, $p=0.65$	Fig.4.8E
PC, G_{de} , motor coord., all field size		$t(121)=9.77$, $p<.001$	Fig.4.8F
PC, G_{de} , motor coord., distal field size		$t(83)=7.71$, $p<.001$	Fig.4.8F
PC, G_{in} , rate map corr.	paired t test,	$t(165)=-1.05$, $p=0.30$	Fig.4.9D
GC, G_{in} , rate map corr.	$VR_{baseline} -$	$t(78)=0.63$, $p=0.53$	Fig.4.9D
PC, G_{de} , rate map corr.	$VR_{probe, stretched}$	$t(108)=2.06$, $p<.05$	Fig.4.9H
GC, G_{de} , rate map corr.		$t(38)=4.37$, $p<.001$	Fig.4.9H
GC, G_{in} , visual coord., grid scale	paired t test,	$t(71)=9.68$, $p<.001$	Fig.4.12E
GC, G_{in} , motor coord., grid scale	X-Y axis	$t(71)=-5.61$, $p<.001$	Fig.4.12F
GC, G_{in} , visual coord., all field size		$t(116)=2.90$, $p<.01$	Fig.4.12G
GC, G_{in} , visual coord., distal field size		$t(82)=6.27$, $p<.001$	Fig.4.12G
GC, G_{in} , motor coord., all field size		$t(116)=-8.09$, $p<.001$	Fig.4.12H
GC, G_{de} , motor coord., distal field size		$t(82)=-12.14$, $p<.001$	Fig.4.13H
GC, G_{de} , visual coord., grid scale		$t(34)=-6.31$, $p<.001$	Fig.4.13E
GC, G_{de} , motor coord., grid scale		$t(34)=3.00$, $p<.05$	Fig.4.13F

Continued on next page

4.2. METHODS

Table 4.2 – continued from previous page

Comparison	Test	Results	Fig.
GC, G_{de} , visual coord., all field size		$t(49)=3.96, p<.001$	Fig.4.13G
GC, G_{de} , visual coord., distal field size		$t(31)=2.11, p<.05$	Fig.4.13G
GC, G_{de} , motor coord., all field size		$t(49)=9.49, p<.001$	Fig.4.13H
GC, G_{de} , motor coord., distal field size		$t(31)=6.42, p<.001$	Fig.4.13H
MI score per cell	Wilcoxon rank	$z=-7.83, p<.001$	Fig.4.13K
Median MI score per session	sum test,	$t(15)=-5.66, p<.001$	Fig.4.13L
Population vector MI score per session	PC-GC	$z=-5.17, p<.001$	Fig.4.13M
GC, G_{de} , directional offset	paired t test,	$t(38)=6.34, p<.001$	Fig.4.14E
GC, G_{de} , directional offset	X-Y axis	$t(78)=3.08, p<.05$	Fig.4.14F
GC, directional offset	paired t test, x axis G_{de} -baseline	$t(38)=4.59, p<.001$	Fig.4.14G
GC, directional offset	independent t test, x axis G_{de} - G_{in}	$t(116)=5.11, p<.001$	Fig.4.14H
GC, G_d , visual coord., all field size (directional)	paired t test, X-Y axis	$t(64)=0.71, p=0.48$	Fig.4.14I
GC, G_i , visual coord., all field size (directional)		$t(64)=7.72, p<.001$	Fig.4.14J
GC, directional info.	paired t test,	$t(117)=1.12, p=0.27$	Fig.4.14K
PC, directional info.	VR-R	$t(274)=-10.20, p<.001$	Fig.4.14L
PC, G_{in} , MI score by wall distance	Pearson	$r=-0.62, p=0.18$	Fig.4.15A
PC, G_{de} , MI score by wall distance	corrcoef.,	$r=-0.38, p=0.45$	Fig.4.15B
GC, G_{in} , MI score by wall distance	one-sample t	$r=-0.01, p=0.97$	Fig.4.15C
GC, G_{de} , MI score by wall distance	test	$r=0.55, p=0.25$	Fig.4.15D
G_{in} , MI score per field, PC vs GC	Wilcoxon rank	$z=-5.01, p<.001$	Fig.4.15E
	sum test	Continued on next page	

CHAPTER 4. DIFFERENTIAL INFLUENCES OF ENVIRONMENT AND
SELF-MOTION ON PLACE AND GRID CELL FIRING

Table 4.2 – continued from previous page

Comparison	Test	Results	Fig.
G_{de} , MI score per field, PC vs GC		$z=-3.23$, $p<.05$	Fig.4.15F
G_{in} , MI score per cell, MEC non-grid spatial cells vs grid cells		$z=1.59$, $p=0.11$	Fig.4.16A
G_i , MI score per cell, MEC non-grid spatial cells vs place cells		$z=-4.33$, $p<.001$	Fig.4.16A
G_d , MI score per cell, MEC non-grid spatial cells vs grid cells		$z=2.74$, $p<.01$	Fig.4.16B
G_d , MI score per cell, MEC non-grid spatial cells vs place cells		$z=-5.79$, $p<.001$	Fig.4.16B
slope difference (X-Y axis) of LFP theta speed modulation	repeated measure ANOVA: gain(3)	$F(2,43)=5.47$, $p<.01$	Fig.4.17A
slope difference (X-Y axis) of speed cell speed modulation	independent ANOVA: gain(3)	$F(2,381)=1.10$, $p=0.33$	Fig.4.17B
^a G_{in} means the gain increased condition, G_{de} means the gain decreased condition			
^b X axis is the gain manipulated axis, Y axis is the un-manipulated axis			

Animal# 987

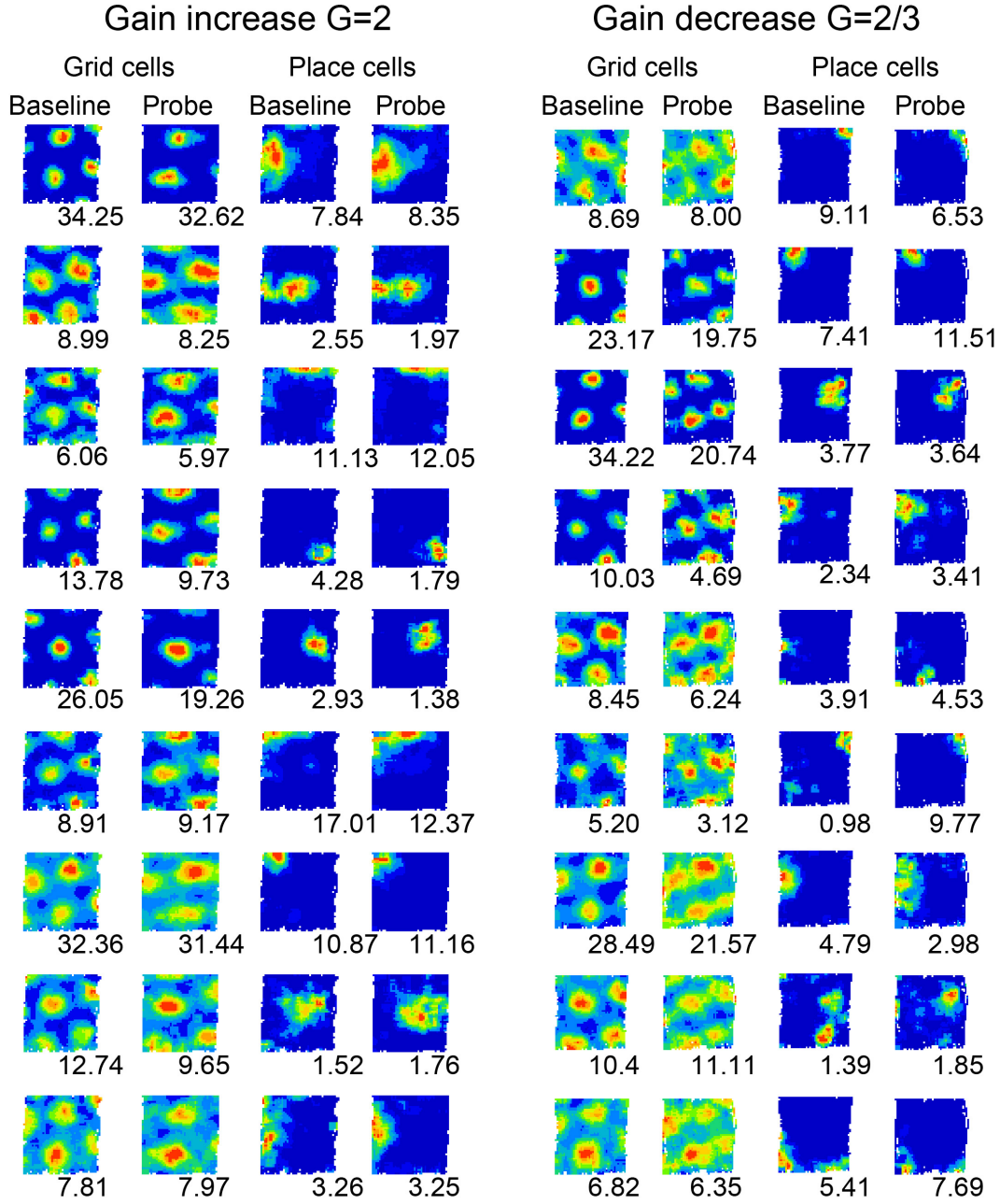


Figure 4.4: **Simultaneously recorded place and grid cells in mouse #987.** Firing rate maps from baseline and probe trials on a gain increase day and on a gain decrease day, with peak rate in Hz below.

Animal# 1061

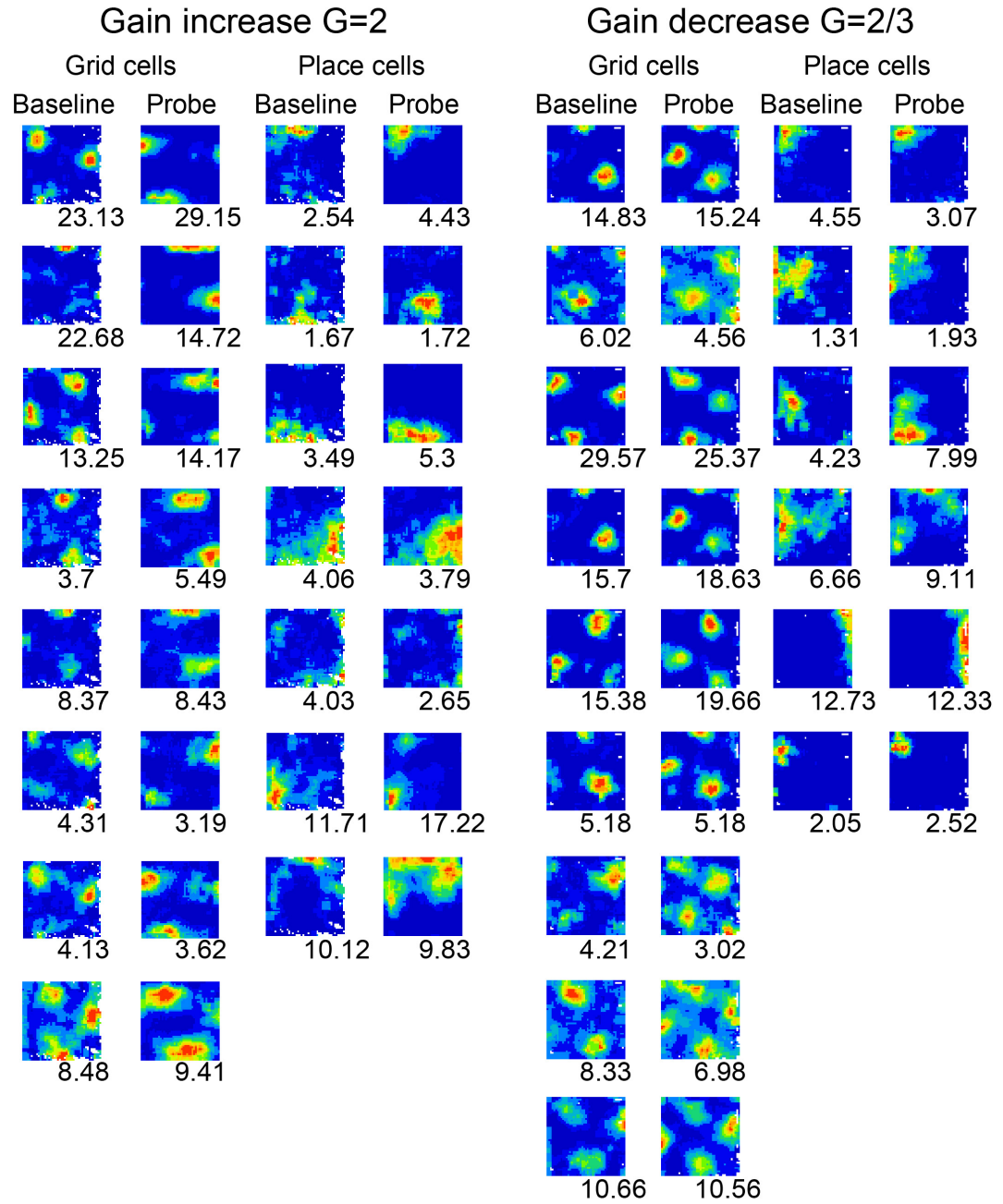


Figure 4.5: Simultaneously recorded place and grid cells in mouse #1061. As in Figure 4.4

4.3 Results

4.3.1 Place cells under gain manipulation

We examined the spatial firing patterns of place cells from hippocampal region CA1 and grid cells from medial Entorhinal Cortex (mEC) in 2-d VR, focusing on probe trials in which the visual ‘gain’ (G) applied to one axis of virtual movement was both increased ($G = 2$) and decreased ($G = 2/3$) compared to the baseline condition ($G = 1$). An experimental day comprised a baseline ($G = 1$) VR trial, a probe ($G \neq 1$) trial and a real-world trial. Under non-unity gain, firing rates can be plotted against the animal’s location according to vision (in visual coordinates) or physical movement (in motor coordinates). These plots are identical for baseline trials. See Methods for details and Figures 4.4 and 4.5 for examples of simultaneously recorded place and grid cell firing patterns. Overall, we found that there were no significant differences in mean firing rates and spatial information between the baseline and probe conditions, although decreases in peak firing rates and gridness scores were observed in the probe conditions (Figure 4.6).

We first compared place cell firing patterns between probe and baseline trials. Figures 4.7 and 4.8 show firing patterns for place cells plotted against visual or motor location under increases ($G = 2$) and decreases ($G = 2/3$) in visual gain, respectively. Firing fields had similar sizes along the manipulated dimension in probe trials compared to baseline trials when plotted in visual coordinates (Figures 4.7E and 4.8E), but different sizes when plotted in motor coordinates (Figures 4.7F and 4.8F), indicating predominantly visual coding. Field sizes along the un-manipulated dimension did not change between probe and baseline trials (paired t tests, $t(111) = 1.04$, $p = 0.30$ for gain increase; $t(83) = 1.55$, $p = 0.13$ for gain decrease).

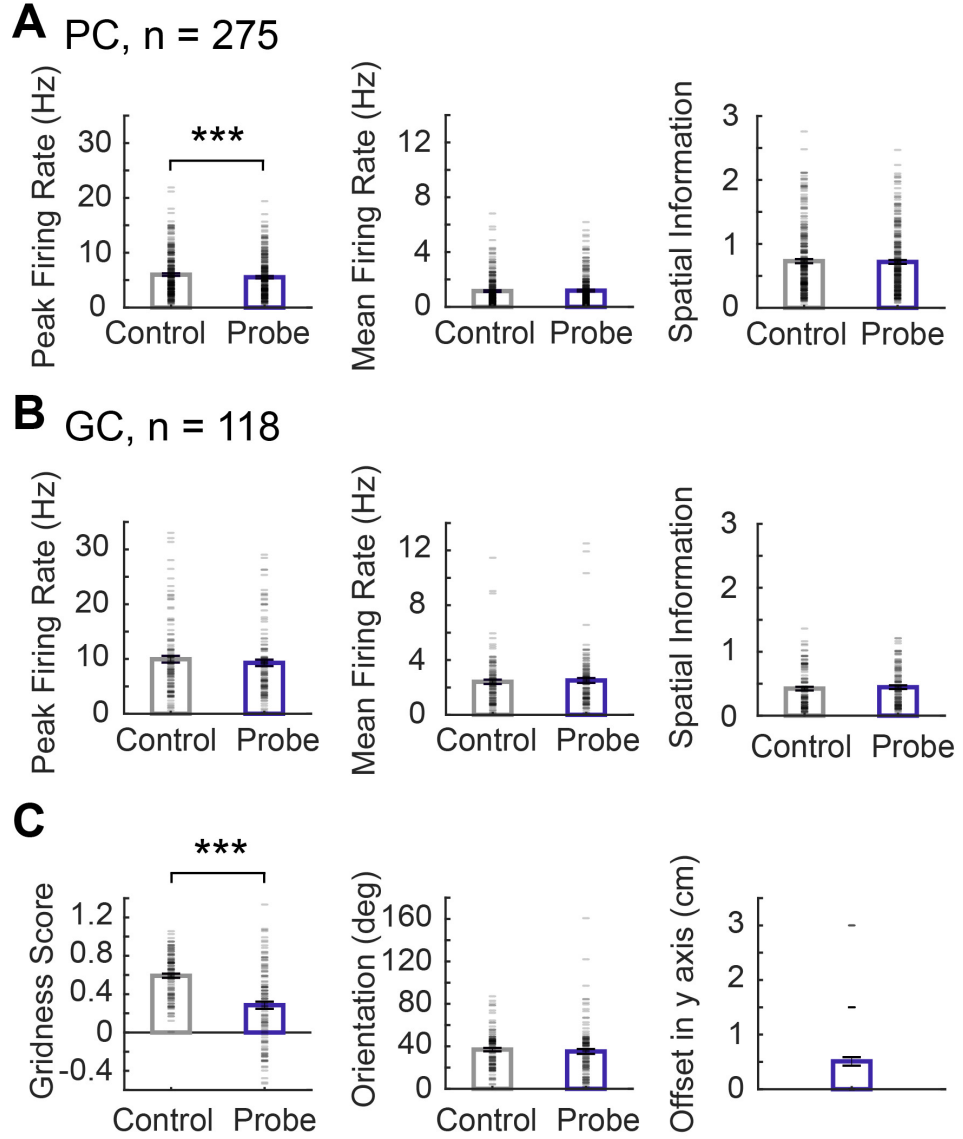


Figure 4.6: **Place and grid cell firing properties in VR baseline and gain manipulated trials.** (A) Comparison of place cell peak firing rate, mean firing rate and spatial information between VR baseline and probe trials. (B) Comparison of grid cell peak firing rate, mean firing rate and spatial information between VR baseline and probe trials. (C) Comparison of grid cell gridness score, grid orientation and grid pattern offset in y axis between VR baseline and probe trials. Probe trial analyses are performed with the best-fitting stretched rate maps.

4.3. RESULTS

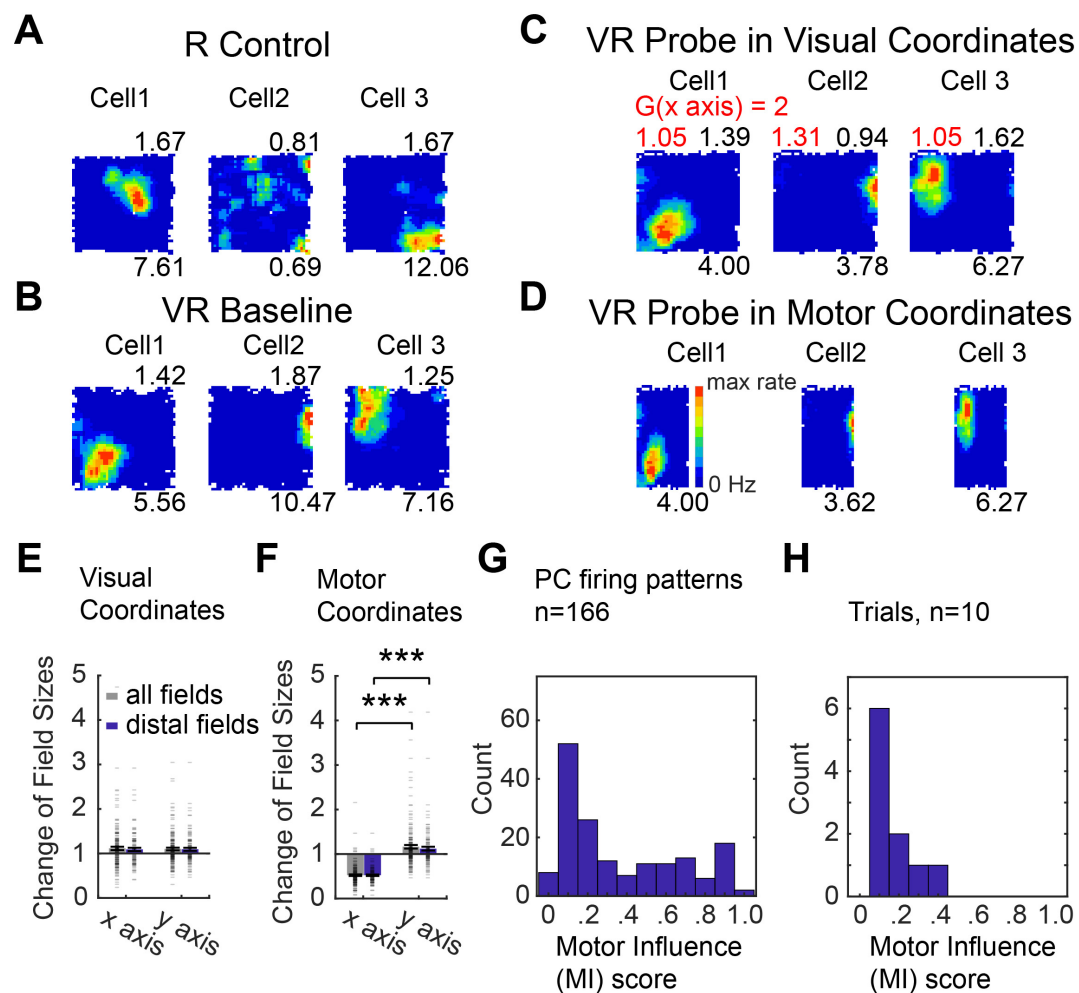


Figure 4.7: **Place cell firing patterns under visual gain increase.** (A-D) Three place cells simultaneously-recorded in a 60x60cm square box (A), a 60x60cm virtual square environment (B), and a probe trial where visual gain was increased along the x axis ($G = 2$) plotted in visual coordinates (C) and motor coordinates (D). Firing rate maps shown with max rate below (Hz) and spatial information above (bits/spike), stretch factor F mapping visual plots to baseline shown in red, all three trials recorded on the same day. (E-F) Change of place field size (ratio relative to baseline) was significantly larger on the manipulated than un-manipulated axis when plotted in motor coordinates (F; $n = 173$ for all fields and $n = 112$ for fields distal to boundaries), but not when plotted in visual coordinates (E), reflecting strong visual influence. (G-H) Distribution of motor influence scores ‘MI’ based on firing rate maps (G) or on population vectors (H).

We can quantify the relative influence of physical motion versus visual input on a cell’s spatial firing pattern (i.e. the firing rate map, plotted in visual coordinates) by comparing it to a stretched version of the baseline firing rate map, and finding the stretch factor (F) giving the best fit (allowing for all offsets of the smaller to the larger map; see Methods). For probe trials (i.e., $G \neq 1$), the ‘motor influence’ score $MI = (F-1)/(G-1)$ varies from 0 for firing patterns that resemble baseline patterns (i.e. $F = 1$; no effect of having to run more or less than expected from vision), to 1 for firing patterns that show stretching corresponding to the gain manipulation (i.e. $F = G$; the pattern in visual coordinates appears to stretch according to the gain relating vision to movement).

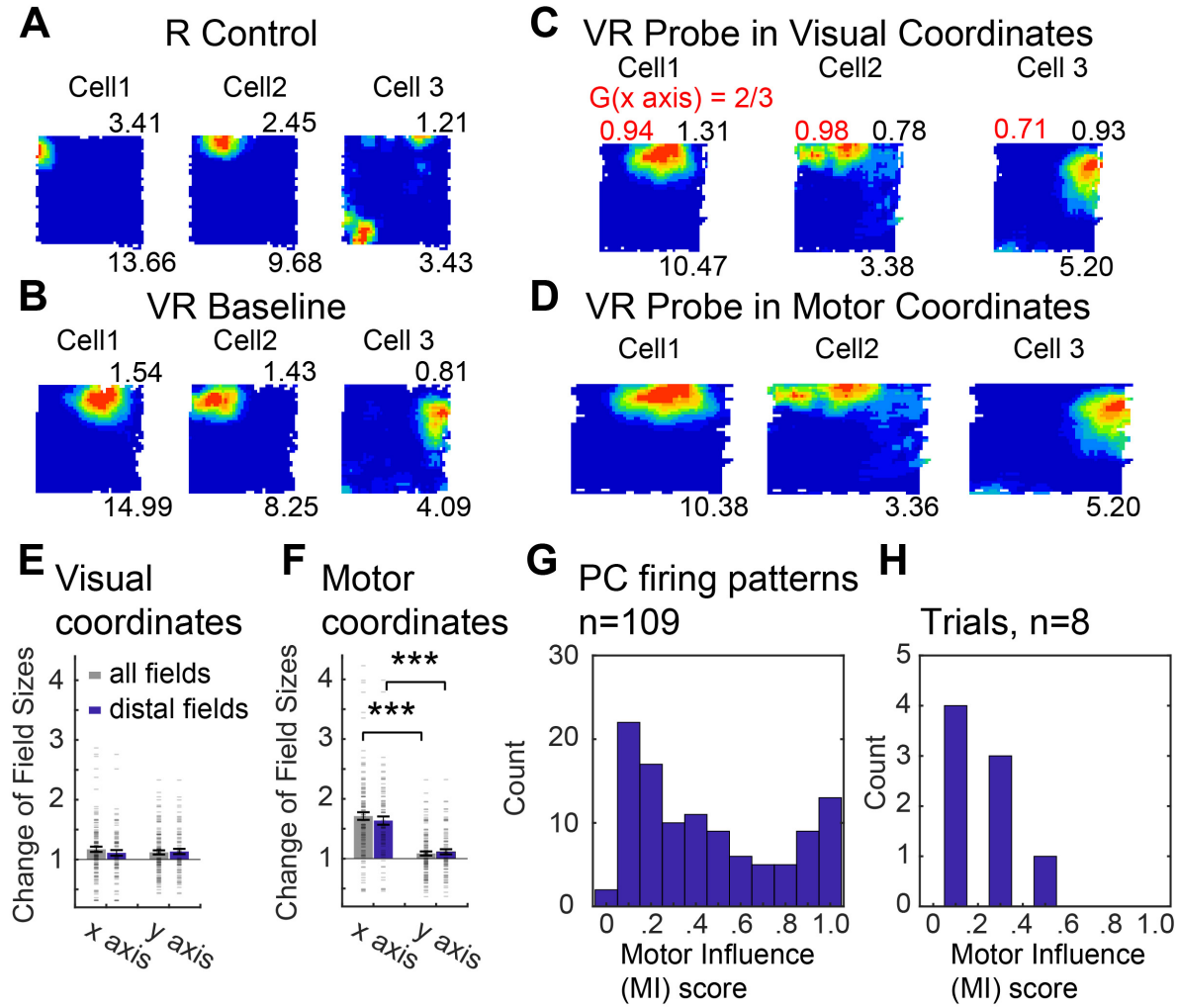


Figure 4.8: **Place cell firing patterns under visual gain decrease.** (A-B) Three place cells simultaneously-recorded in a 60x60cm square box (A), a 60 x 60cm virtual square (B), and a probe trial where visual gain was reduced along the x axis ($G = 2/3$) plotted in motor coordinates (C) and visual coordinates (D). Layout as Figure 1C-F, stretch factor F mapping visual plots to baseline shown in red. (E-F) Change of place field size was significantly larger on the manipulated than un-manipulated axis when plotted in motor coordinates (F; $n = 122$ for all fields and $n=84$ for fields distal to boundaries), but not when plotted in visual coordinates (E), reflecting strong visual influence. (G-H) Distribution of motor influence scores ‘MI’ based on firing rate maps (G) or population vectors (H; see Methods and Figure 4.7).

CHAPTER 4. DIFFERENTIAL INFLUENCES OF ENVIRONMENT AND SELF-MOTION ON PLACE AND GRID CELL FIRING

Place cell firing patterns can ‘remap’ (Muller & Kubie, 1987) or become diffuse, making comparisons difficult (e.g. if a cell fires over most of the arena, the field shape largely reflects the shape of the arena). Accordingly, we confined our analyses to compact firing patterns that did not remap between baseline and probe (occupying less than 50% of the arena and having a spatial correlation higher than 0.3 between baseline and the best fitting probe firing rate map, i.e. taking account of any gain-related offset and stretch), leaving 275/497 firing patterns (166/282 for gain increase, 109/215 for gain decrease, see Methods and Figure 4.9). The percentage of remapping varies across sessions (median: 12%, inter-quartile range: 16%) but did not differ between gain increase and decrease sessions (Figure 4.3). The results from both types of gain manipulation show an overall greater visual than motor influence on place cell firing (Median = 0.21, inter-quartile range (IQR) = 0.53 for MI scores in the gain increase, and Median = 0.37, IQR = 0.59 in the gain decrease, see Figures 4.7G, 4.8G and 4.10).

We also analysed the population vector responses of all simultaneously recorded place cells, finding the best single offset and stretch factor for each population (in 18 trials with multiple place and grid cells), again finding greater visual than motor influence on place cell populations (MI score in gain increase: Median=0.08, IQR=0.11; in gain decrease: Median=0.21, IQR=0.21, see Figures 4.7H, 4.8H and 4.11).

4.3. RESULTS

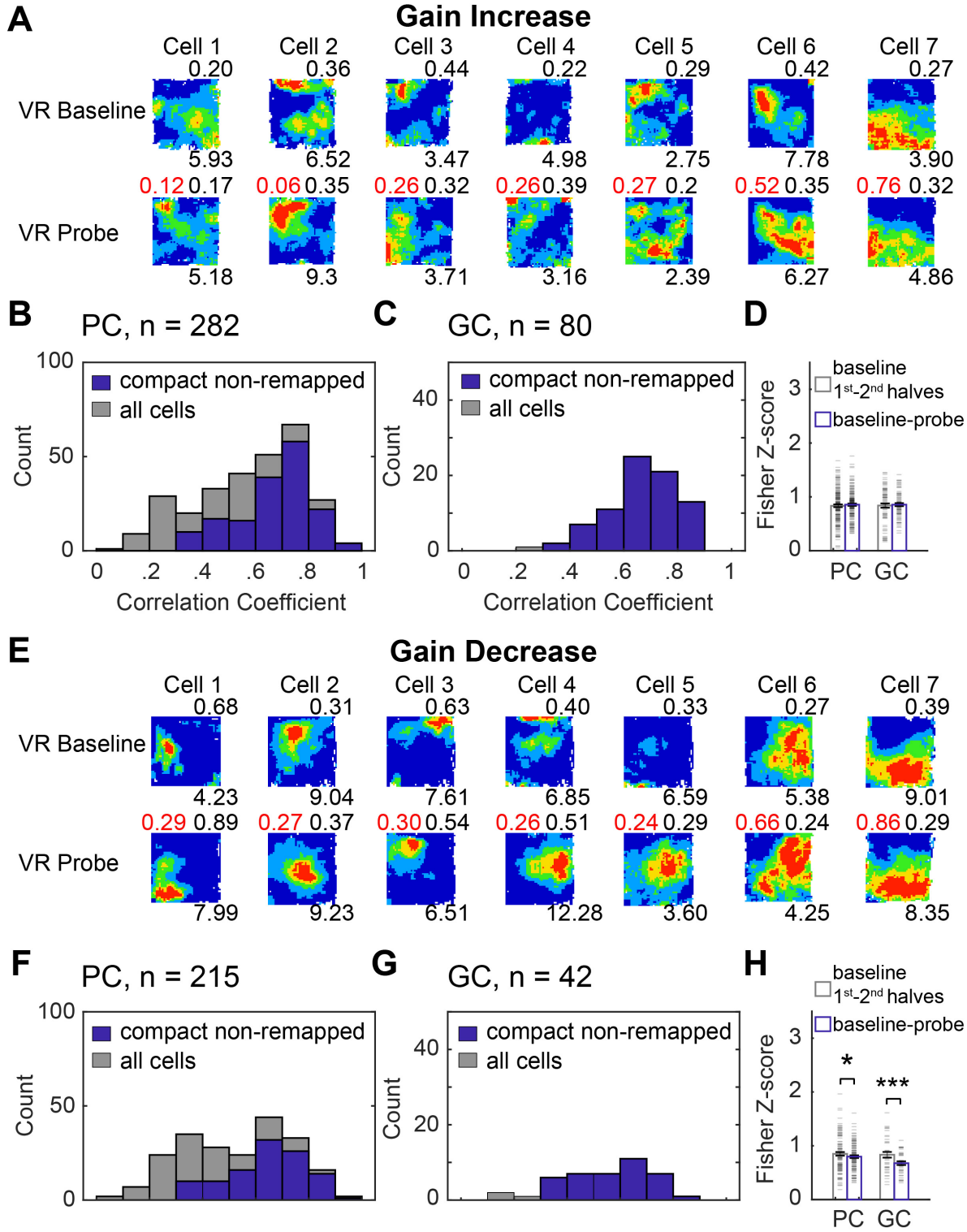


Figure 4.9: **Place cells and grid cells with compact non-remapping firing patterns.** To enter the main analyses, spatial correlations between probe and baseline firing rate maps (taking account of the effect of the gain manipulation) had to exceed 0.3, and place firing patterns had to cover less than 50% of baseline and probe environments, here we illustrate the properties of the excluded cells relative to the compact non-remapping cells. (A) Five place cells which remapped in the gain increase probe trial (bottom row, in visual coordinates) compared to the baseline trial (top row) and two place cells which had diffuse fields. Firing rate maps shown with spatial information (bits/spike) in black, correlation coefficients between baseline and best-fitting probe in red (above), and max rates (Hz, below). (B-C) Distribution of correlation coefficients between baseline and best-fitting (stretched and offset) probe rate maps in gain increase trials for place (B) and grid cells (C). (D) Fisher's Z scores of the correlation coefficients between baseline and best-fitting gain increase rate maps were similar to those between 1st and 2nd halves of baseline trials for both place and grid firing patterns. (E) Five place cells which remapped in the gain decrease probe trial (bottom row, in visual coordinates) compared to the baseline trial (top row) and two place cells which had diffuse fields. (F-G) Distribution of correlation coefficients between baseline and best-fitting probe rate maps in gain decrease trials for place (F) and grid cells (G). (H) Fisher's Z scores of the correlation coefficients between baseline and best-fitting gain decrease rate maps were lower than those between 1st and 2nd halves of the baseline trials, for both place and grid firing patterns. NB Fisher's Z-transformation of correlation coefficient r , to increase Normality, was: $Z = \frac{1}{2} \ln((1+r)/(1-r))$.

4.3. RESULTS

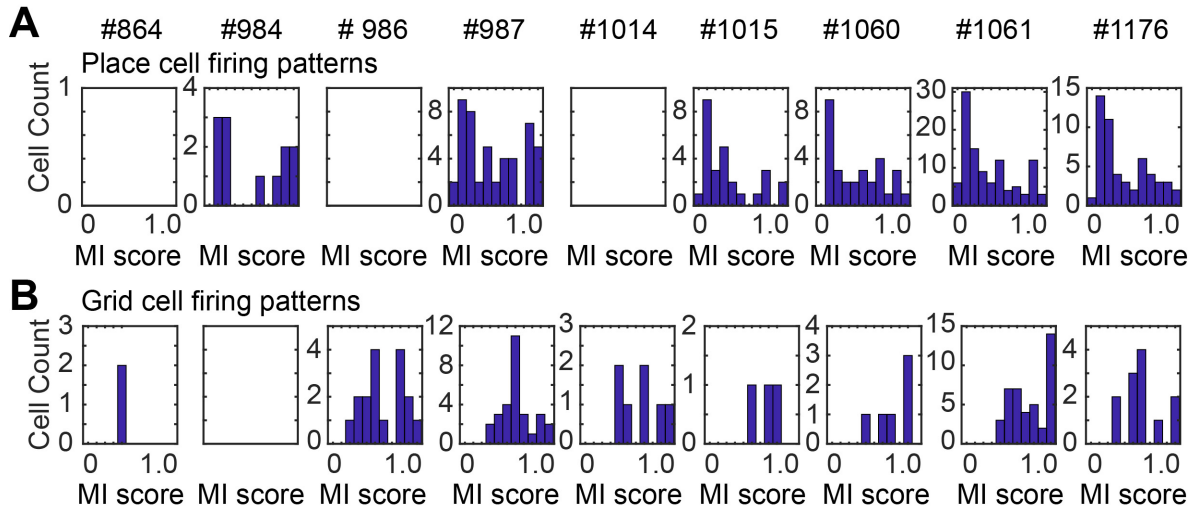


Figure 4.10: **Distribution of motor influence (MI) score per animal.** Note the overall weighting towards visual influence for place cell firing patterns (Figures 4.7G, 4.8G) and to intermediate or motor influence for grid cell firing patterns (Figures 4.12I, 4.13I).

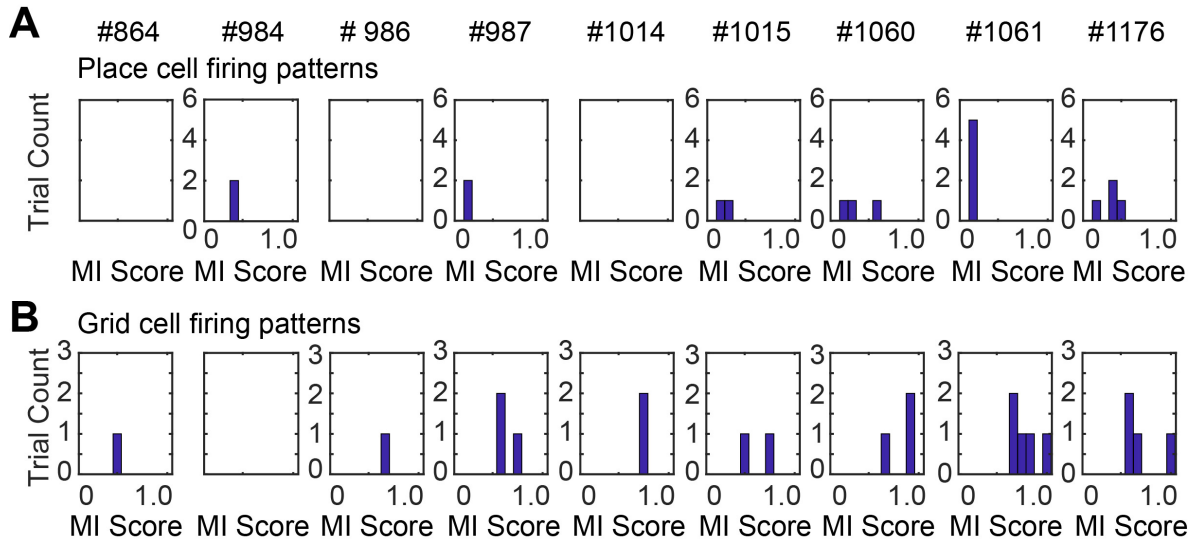


Figure 4.11: **Distribution of MI score for population vector per animal.** Note the overall weighting towards visual influence for place cell population vectors (Figures 4.7H and 4.8H) and to intermediate or motor influence for grid cell population vectors (Figures 4.12J and 4.13J).

4.3.2 Grid cells under gain manipulation

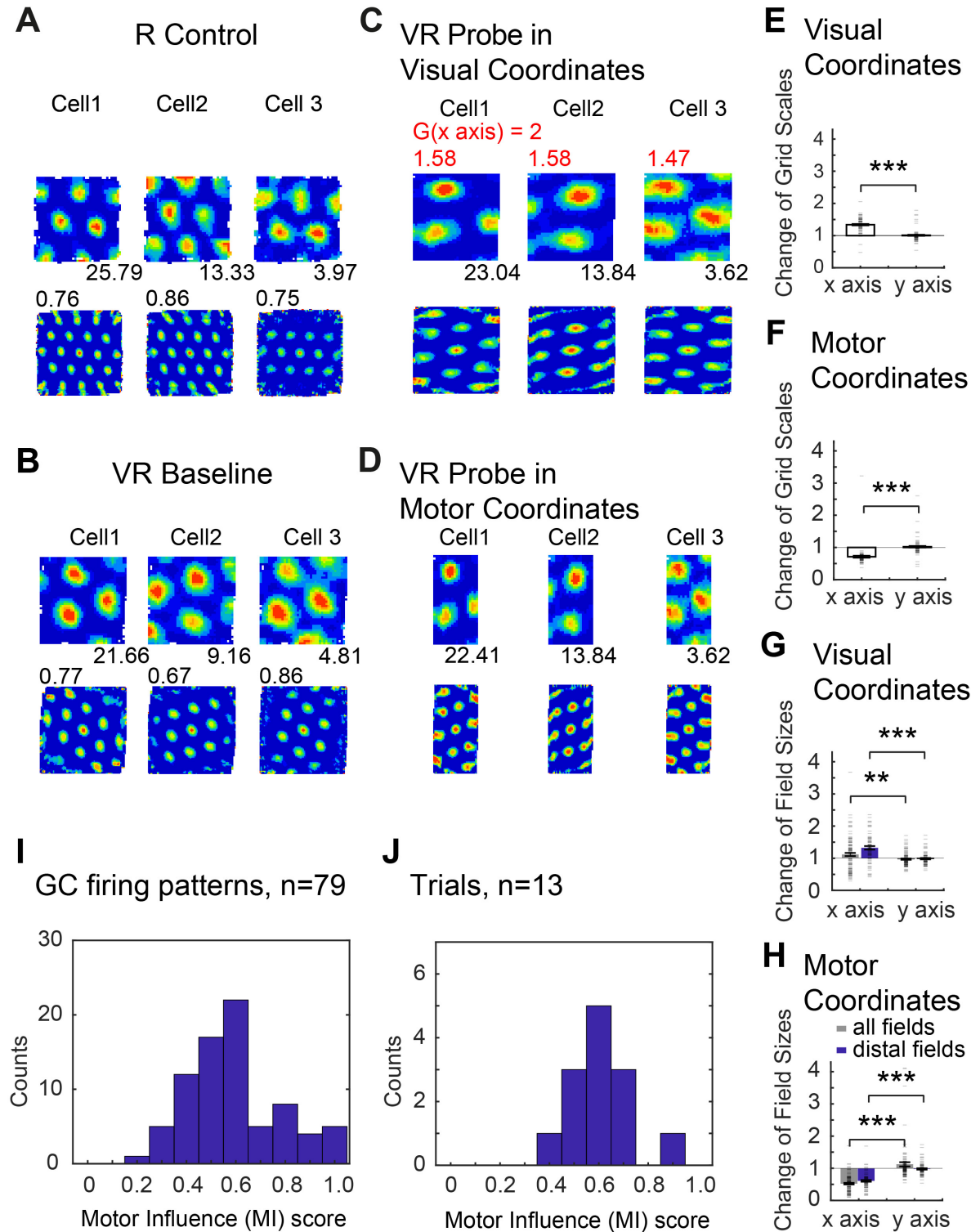


Figure 4.12: **Grid cell firing patterns under visual gain increase.** (A-D) Three grid cells simultaneously-recorded in the baseline 60x60cm square box (A), a 60x60cm virtual square environment (B) and a virtual probe trial where the gain of visual motion compared to physical motion on the ball was increased along the x axis (gain $G = 2$), plotted in visual coordinates (C) and motor coordinates (D). Firing rate maps (and max rates) shown above, spatial autocorrelograms (and gridness scores) below, one cell per column, stretch factor F mapping visual plots to baseline shown in red, all three trials recorded on the same day. (E-F) Change of grid scales was significantly larger on the manipulated than un-manipulated axis when plotted in visual coordinates (E; $n = 72$) or motor coordinates (F). (G-H) Change of firing field size was significantly larger on the manipulated than un-manipulated axis when plotted in both visual coordinates (G; $n = 117$ for all fields and $n = 83$ for distal fields) and in motor coordinates (H). (I-J) Distribution of motor influence scores ‘MI’ based on firing rate maps (I) or population vectors (J; see Methods or Figure 4.7).

Figure 4.12 shows firing patterns for grid cells plotted against visual or motor location under increases in visual gain ($G = 2$). Again we restricted analyses to grid patterns that remained similar between baseline and probe, giving 79/80 cells in gain increase days and 39/42 in gain decrease days. Firing patterns appear elliptical in probe trials when plotted in visual coordinates (increased in scale along the manipulated axis, as movement in visual space requires less physical movement) and in motor coordinates (decreased in scale, as physical movement produces greater visual movement), as shown by the changes in grid scale (Figure 4.12E-F). Equally the motor influence scores for firing rate maps and population vectors (Median = 0.58, IQR = 0.21, Figure 4.12I, and Median = 0.63, IQR = 0.25, Figure 4.12J) indicate a balance between motor and visual influence, weighted towards motor.

We also analysed the shapes of pairs of individual firing fields that remained similar

between probe and baseline trials (showing spatial correlation higher than 0.3 after accounting for gain-related offsets and stretches and setting the rest of the map to zero) and that were sufficiently centrally placed to avoid occlusion by the edge of the environment (115/167 grid fields). The changes in sizes of individual fields showed a similar pattern of both visual and motor influence to the overall grid patterns (see Figures 4.12G-H, and Methods for details).

Figure 4.13 shows grid cell firing patterns under visual gain decrease ($G = 2/3$). Grid scale and firing patterns show an even stronger weighting towards motor influence than for gain increase trials (Median MI score = 0.89, IQR = 0.30 for firing rate maps, Figure 4.13I, and Median = 0.71, IQR = 0.26 for population vectors, Figure 4.13J), with grid scale along the manipulated axis unchanged when plotted in motor coordinates and decreased when plotted in visual coordinates (because a given visual distance reflects greater physical distance, Figures 4.13E-F). It is possible that increasing visual gain increases the salience of (now increased) optic flow, and vice versa when decreasing gain, explaining the greater visual influence during gain increase (Figure 4.12), discussed below.

4.3. RESULTS

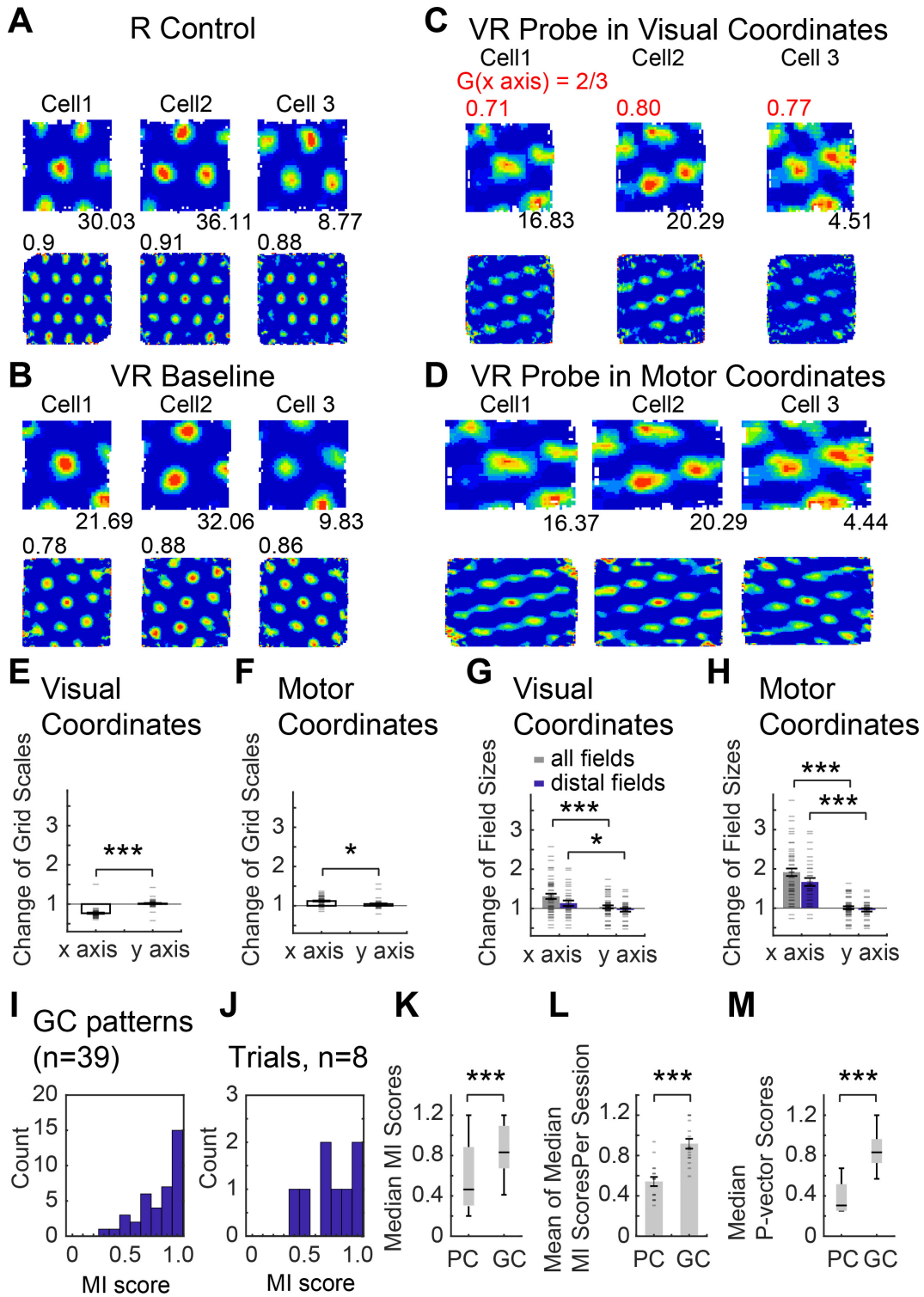


Figure 4.13: **Grid cell firing patterns under visual gain decrease.** (A-D) Three grid cells simultaneously-recorded in a 60x60 cm square box (A), a 60x60 cm virtual square (B) and a probe trial where visual gain was reduced along the x axis ($G = 2/3$) plotted in visual coordinates (C) and motor coordinates (D), on the same day, layout as Figure 4.12A-D, stretch factor F mapping visual plots to baseline shown in red. (E-F) Change of grid scales was significantly larger on the manipulated than un-manipulated axis when plotted in visual coordinates (E; $n = 35$), with a smaller effect when plotted in motor coordinates (F). (G-H) Change of firing field size was significantly larger on the manipulated than un-manipulated axis when plotted in visual coordinates (G; $n = 50$ for all fields and $n = 32$ for distal fields) and even more strongly when plotted in motor coordinates (H). (I-J) Distribution of motor influence score (MI) based on firing rate maps (I) or population vectors (J; see Methods or Figure 4.7). (K) Median MI scores of non-remapped place and grid cell firing patterns (Median (red line)=0.26, interquartile range (IQR, q_1 - q_3 , blue box) = 0.58 for place cells, Median = 0.63, IQR = 0.42 for grid cells). (L) Mean of the median MI scores of simultaneously recorded place cell and grid cells per trial (0.34 ± 0.05 for place cells, 0.72 ± 0.05 for grid cells, average difference of medians: 0.38 ± 0.07). (M) Median population vector MI scores between place cell and grid cell firing patterns (Median = 0.11, IQR = 0.26 for place cells, Median = 0.63, IQR = 0.24 for grid cells; dashed lines cover $q_1 - 1.5 \times \text{IQR}$ to $q_3 + 1.5 \times \text{IQR}$ including all data points).

4.3. RESULTS

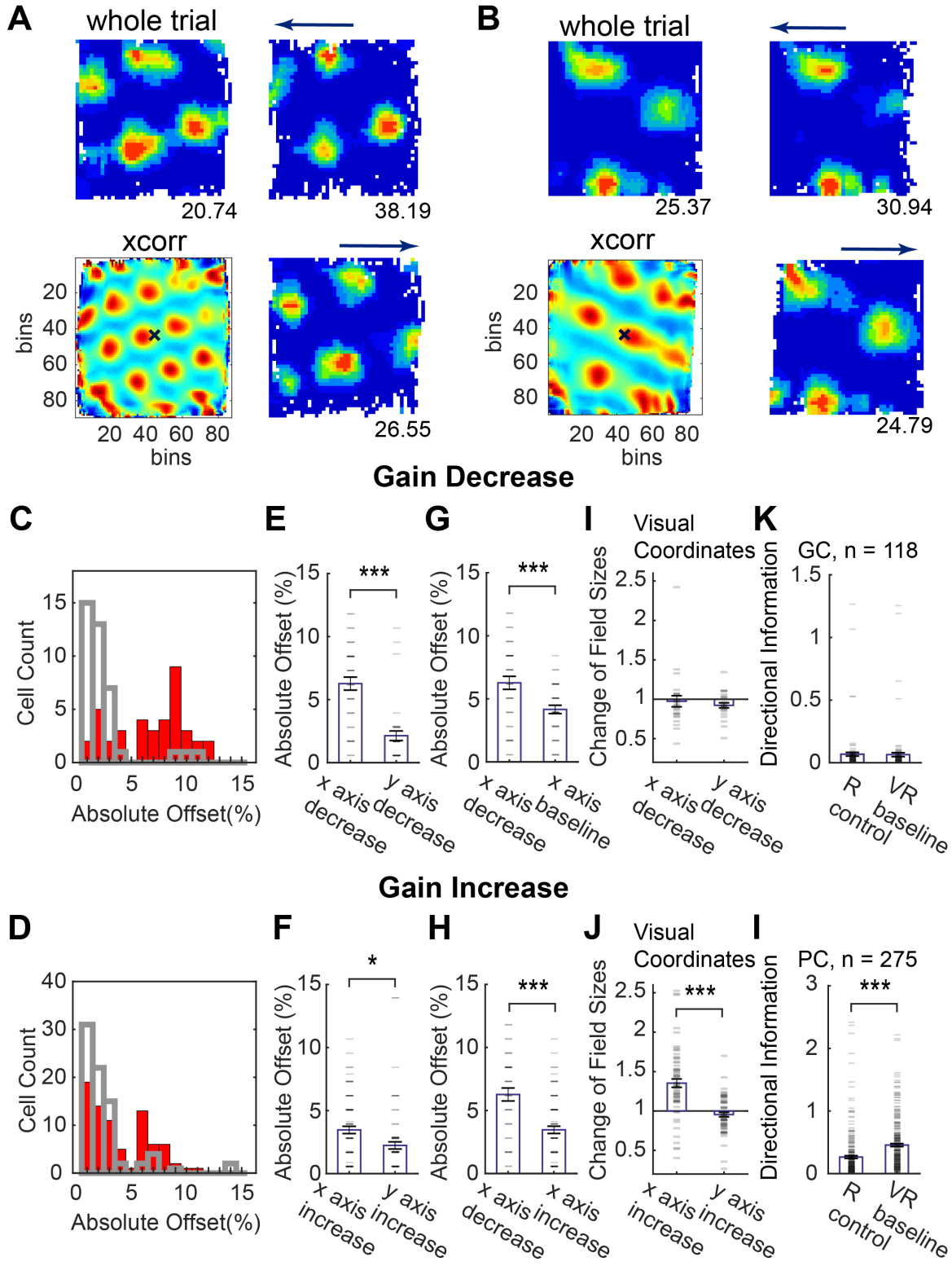


Figure 4.14: **Direction dependent offsets of grid patterns.** (A) Example grid cell showing grid fields shifting forwards in running direction along the manipulated axis of a gain decrease trial. (B) Example grid cell showing grid fields moving backwards against the running direction along the manipulated axis of a gain decrease trial. Rate maps are shown in visual coordinates for the whole trial (top left); filtered by running direction (arrow above plot, right column, westwards above and eastwards below). Max firing rates shown below the rate maps. The spatial cross-correlogram of the two direction-filtered rate maps (bottom left) shows the offset from the centre (x). (C-D) Distribution of absolute offsets in gain decrease (C) and gain increase (D) trials (red) and their baselines (grey). (E-F) Directional-offsets in probe trials along the manipulated (x) axis were greater than along the non-manipulated (y) axis in gain decrease (E) and gain increase trials (F). (G-H) The offset along the x axis in gain decrease trials was greater than baseline trials (G) and gain increase trials (H). (I) Change of grid field sizes, found separately for eastward and westward runs and then averaged, was similar on the manipulated (x) and un-manipulated (y) axes in gain decrease trials, unlike Figure 4.13G. (J) Change of grid field sizes, found separately for eastward and westward runs and then averaged, was greater along the x than y axes in gain increase trials as in Figure 4.12G. (K) The directionality of grid cell firing was similar in R and VR. (L) Place cell firing was more direction modulated in VR than R, precluding directional offset analyses.

However, changes in the shapes of individual grid firing fields shows the opposite effect to the scale of grid patterns (field size increased along the manipulated axis when plotted in visual coordinates, Figure 4.13G, while grid scale decreased, Figure 4.13E), giving broader firing fields in probe trials plotted in visual coordinates (Figures 4.13C, 4.4 and 4.5). If grid cell firing locations are reset by environmental inputs (Hardcastle et al., 2015) in disparate locations, but otherwise strongly driven by motor inputs, changes to gain will cause offsets between firing locations when running in opposing directions

along the manipulated axis. This directional-offset effect was present in grid cell firing during visual gain decrease, explaining the broader firing fields in whole-trial firing rate maps, and more so than in gain increase trials perhaps because of the greater visual influence during gain increase (Figure 4.14). The directional modulation of firing of place cells (but not grid cells) in VR precluded a similar directional-offset analysis of place fields, see Figure 4.14 and (Chen et al., 2018).

The analysis of individual fields also allowed us to assess the dependence of motor influence score on distance to the nearest environmental boundary, but we found no significant effect in place or grid fields (Figure 4.15). However, virtual boundaries are entirely visual and proximity to physical boundaries in real environments may have greater influence on firing (Hardcastle et al., 2015).

We also recorded cells in mEC with spatially modulated firing that was not grid-like, see Methods. These spatial cells showed motor influence scores similar to grid cells, but with lower scores in gain decrease conditions (a little more like place cells, see Figure 4.16).

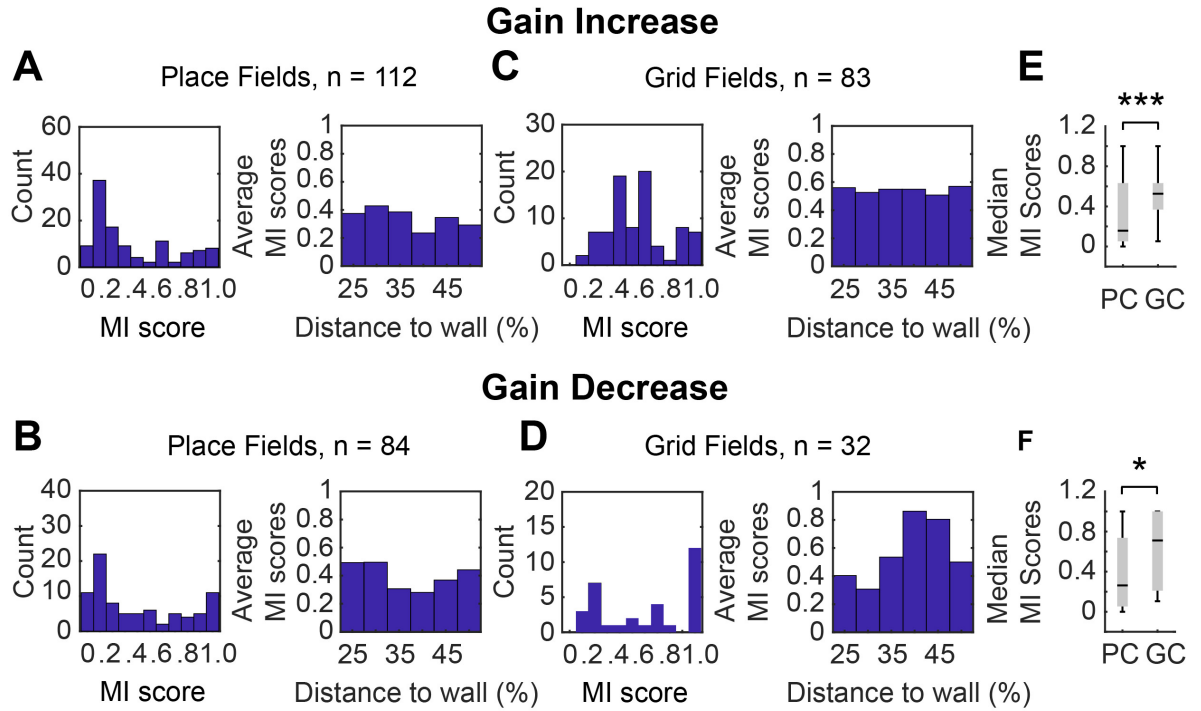


Figure 4.15: **Analysis of individual firing fields and distance to the nearest boundary.** (A-B) Motor influence (MI) distributions for place fields distal to boundaries under gain increase and decrease separately (note similarity to the MI for firing rate maps in Figs 4.7 and 4.8, but here the rate map outside the field is set to zero and only distal fields used, to match the grid field analysis). Distance to nearest boundary had no clear effect on the motor influence in place fields. (C-D) Motor influence (MI) distributions for grid fields distal to boundaries under gain increase and decrease separately (note similarity to MI Figures 4.12 and 4.13). Distance to nearest boundary had no significant effect on motor influence in grid fields. (E-F) Median motor influence scores of these place fields were lower from those of grid fields in both gain increase and gain decrease trials.

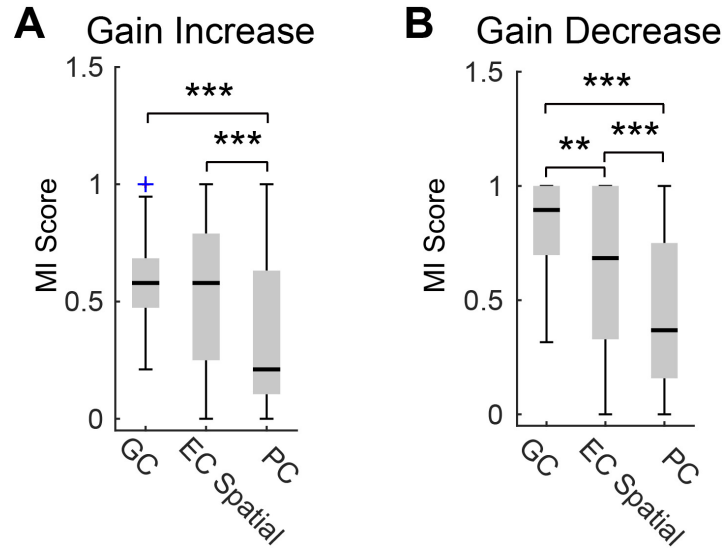


Figure 4.16: **MI score for spatial cells in MEC.** (A) Median MI scores of grid cells, entorhinal spatial cells and place cells in gain increase trials. Median (red line) = 0.58, interquartile range (IQR, blue box) = 0.21 for grid cells, median = 0.58, IQR = 0.54 for spatial cells, median = 0.21, IQR = 0.53 for place cells. (B) Median MI scores of grid cells, entorhinal spatial cells and place cells in gain decreased trials. Median = 0.89, IQR = 0.30 for grid cells, median = 0.68, IQR = 0.67 for EC spatial cells, median = 0.37, IQR = 0.59 for place cells.

During natural foraging, the animal's running speed is reflected in increases in the frequency of theta rhythmicity in the local field potential (Sławińska & Kasicki, 1998), and in increases in the firing rates of spatial cells (McNaughton et al., 1983; Sargolini et al., 2006) - most clearly seen in speed cells, by definition (Kropff et al., 2015). When running along the manipulated axis, there were effects of increasing or decreasing the visual gain on the speed dependence of LFP theta frequency and firing rates compared to the un-manipulated axis (which controls for non-specific changes in theta frequency). The effects on LFP theta frequency speed dependence (i.e. the slope of the plots in Figure 4.17) are as expected from the animal's perception of speed reflecting visual input in addition to physical motion, while effects on firing rate were qualitatively

CHAPTER 4. DIFFERENTIAL INFLUENCES OF ENVIRONMENT AND SELF-MOTION ON PLACE AND GRID CELL FIRING

similar but noisier and not significant.

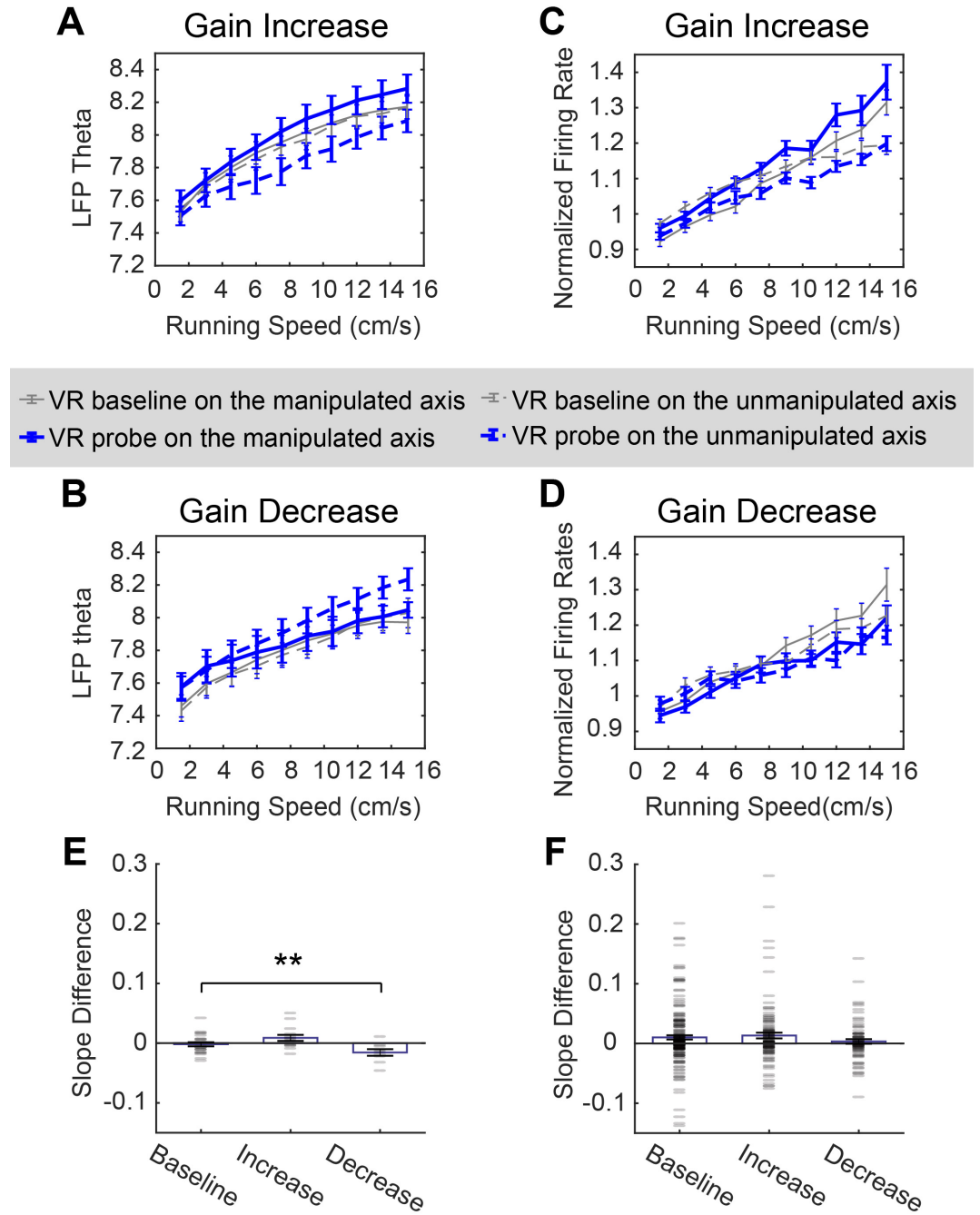


Figure 4.17: **Speed modulation of LFP theta frequency and speed cell firing rates.** (A-D) Lines show mean (\pm s.e.m) theta frequency (A-B) or speed cell firing rate (C-D; normalised by each cell's overall firing rate) in each running speed bin (1.5cm/s to 15cm/s). (E) The slope difference of the LFP theta frequency versus running speed relationship between manipulated and un-manipulated axes in baseline, gain increase and gain decrease trials. (F) The slope difference of speed cell firing rate versus running speed relationships in between manipulated and un-manipulated axes in baseline, gain increase and gain decrease trials. Slope was calculated as the gradient of the regression line fitted to the frequency-speed and the firing rate-speed data points.

4.4 Discussion

By decoupling the animal's physical motion and feedback from the virtual environmental input, we were able to show that spatial coding in place cells and grid cells are under influence of both self-motion and environmental inputs. However, place cell firing patterns are more similar to those if they were to use only visual cues for localization (Figure 4.7C-F, Figure 4.8A-D), while grid cells fired more in register with a self-motion updated spatial representation (Figure 4.12A-D, Figure 4.13A-D). It was further established by the motor influence (MI) score, which quantified self-motion influence, grid cells were under a greater influence of self-motion input (less of environmental inputs) than place cells (Figure 4.13k). There was no significant change in spatial firing patterns on the un-manipulated axis thus precluding any uncontrolled task effects such as novelty, attention and so on.

MI scores in place cells had a wide distribution even within animal (Figure 4.11). This is consistent with a previous study that found dispersed weights to combine self-motion versus visual inputs that best described the response of place cells to

gain decrease on a virtual linear track (Chen et al., 2013). Together our results fit the prediction of the predominant view that emphasizes the role of place cells being anchoring towards different sets of environmental cues while grid cells being updating location from self-motion signal. Note that the non-grid spatial cells in dMEC also showed higher MI scores, suggesting the difference may be anatomically rather than functionally originated.

We also found that visual input seems to exert a bigger influence on grid patterns under gain increase manipulation than under gain decrease manipulation. If we consider visual influence in the static visual landmark, increased visual gain means smaller environmental size thus bigger confliction between distance estimated from the last anchoring point and future landmark, as (Gothard et al., 2001) demonstrated in their linear track task. A shortened track caused place fields to rapidly switch from aligning with start location to aligning with distal visual landmarks. Another possibility is that in the gain increase condition, visual velocity perceived from the optic flow is higher than in gain decrease condition, which may lead to more potent visual control over the speed signal. We found the slope of LFP theta speed modulation changed in the same trend with changes in place fields size when mice ran in the direction of the manipulated axis, while speed cells did not show any effects on gain manipulation. However we did not observed higher visual influence in speed modulation under gain increase than under gain decrease.

Last, we found grid patterns to show directional offsets along the manipulated axis under gain decrease condition, which also caused grid fields to expand, giving rise to the opposite effect of field size change in grid cells under gain decrease. The offset was like to be caused by the visual boundary in VR resetting the grid patterns when accessible, as demonstrated by Hardcastle et al. (2015). In the meantime, no boundary

effect in MI score was observed, which predicted higher self-motion influence as the animal moves away from the walls. It could be due to the lack of local cues, such as tactile inputs, in our VR environment.

In conclusion, in this study, we found that when self-motion and environmental cues were put into conflict, place cells and grid cells received both inputs while combining them with a different bias. Place cell representation was weighted towards environmental visual cues and grid cells towards self-motion inputs. These results suggested that instead of one being derived from the other, place cells and grid cells may each serve different roles and together supporting a dynamic hippocampal spatial representation.

Chapter 5

Absence of Visual Input Affects Place and Grid Cell Activity

5.1 Introduction

Animals rely on external sensory cues to navigate in a familiar environment. Despite the dominance of visual landmarks in controlling firing fields orientation of place cells, grid cells and head direction cells (O'Keefe & Nadel, 1978; Taube et al., 1990a; Hafting et al., 2005), removal of visual input only slightly reduced spatial selectivity in spatial cells whilst their characteristic spatial tuning patterns were largely preserved (O'Keefe & Recce, 1993; Hafting et al., 2005). When vision is intact but motor related self-movement cues are eliminated by having rats passively transported by a clear cart, although head direction cells' characteristic tuning are spared, both grid cell firing patterns and the speed modulation in LFP theta are disrupted (Winter et al., 2015). Those results call into question how much visual input contributes to spatial navigation, specifically to translational path integration.

Recent studies showed that grid cell spatial firing in the mouse was heavily disrupted while head direction tuning remained stable when visual cues were not available (Chen et al., 2016; Perez-Escobar et al., 2016). Velocity signals including the speed modulation of local field potential theta oscillation and speed modulation of speed cells firing rate were both reduced in darkness (Chen et al., 2016; Perez-Escobar et al., 2016). In contrary to previous views, these results suggest that visual input may play an important role in velocity coding and path integration (Chen et al., 2016; Perez-Escobar et al., 2016). However, it is not known from the previous studies whether the disruption of grid cells in darkness is due (wholly or in part) to disruption in place cell firing (Bonnevie et al., 2013).

Environmental boundaries are also important external cues for spatial representations (O’Keefe & Burgess, 1996; Hartley et al., 2000; Barry et al., 2006; Lever et al., 2009). Stretching or compressing a familiar rectangular environment causes both place and grid cells’ firing patterns to deform accordingly (O’Keefe & Burgess, 1996; Barry et al., 2007; Hartley et al., 2000; Stensola et al., 2012). It was proposed that boundary input serves as a reset mechanism whenever animals run into contact with them (Hardcastle et al. (2015); reviewed by Evans et al. (2016)). However, when tested in normal lighting, reset potentially happened at any point via visual input such as distal landmarks (Taube et al., 1990a,b) and optic flow (Saleem et al., 2013) not necessarily depending on boundary input (Hardcastle et al., 2015). Thus we predict that, in the absence of visual input and minimized local olfactory cues, the boundary reset effect would be more salient.

In the current research we co-recorded place cells and grid cells while mice navigated in complete darkness. The floor was cleaned after every trial to mix up any residual odours. We found that, consistently with previous studies in the mouse (Chen et al., 2016;

Perez-Escobar et al., 2016), both place and grid cells show decreased spatial information. Grid cells show heavily disrupted fields' regularity. Place fields proximal to the walls are less expanded and shift less compared to those recorded under light condition. On average both place cells and grid cells show a higher similarity in responses between the dark and light trials when the animal is closer to walls than when it is further from them.

5.2 Methods

5.2.1 Animals

Fifteen male C57Bl/6 mice were used in this experiment. One was implanted with 8 tetrodes in CA1, and fourteen received a dual implant with one microdrive aimed at the right CA1 and one in the left dmEC (each microdrive carried 4 tetrodes).

5.2.2 Behavioural training

Cells were screened and recorded whilst animals locomoted in the same square environment (eight mice in a 60 X 60cm sized box, and seven in a 80 X 80cm sized box). Two trials were recorded on each day with half an hour break, each trial lasted for 20 minutes. Once cells displayed stable spatial firing patterns across trials (after 16.6 ± 8.3 days), dark probe trials started. For dark trials, recordings were performed in the same environment but x minutes before mice were introduced in the environment and until mice were taken out of the environment all room lights were turned off. A dark probe session consisted of one dark trial followed by one light trial in the same environment as control. To track the evolution of spatial representations in darkness, dark sessions were

recorded for each animal (for 5.1 ± 3.3 days depending on anatomical and functional stability of the recorded cell populations). The floor was carefully wiped with 70% ethanol before every trial to mix up and minimise any local olfactory traces. Mice were always introduced to the environment from the southeast corner facing towards the north.

5.2.3 Data analysis

Definition of 'boundary' and 'centre' regions

In order to assess whether boundary contact helped self-localizing in darkness, the environment was divided into a boundary region and a centre region according to the accessibility to boundary input (Hardcastle et al., 2015). The boundary region includes locations within 12 cm distance from the nearest wall (criteria close to that used in Hardcastle et al. (2015)). The centre region is the inner square area co-centred with the environment, and its perimeter is decided so that it has comparable area size with the boundary region.

Place cell firing fields definition

In the rate map any bins with firing rate smaller than 30% of peak firing were set to zero. Bins that have local maximum firing rates were detected. Fields were defined as the area made up of contiguous bins that surrounded local peak firing rate bins. Fields with less than eight bins were removed. Field sizes were calculated by multiply fields bin counts and unit bin size. Field locations were defined as the coordinates of peak firing rate bins in each field. To match place fields between the two trials on the same day, distance between a field location in one trial and a field location in another

trial was calculated for all possible field pairs. The field pair with the smallest distance was defined as a match across trials.

Statistical tests

For repeated measure data set, repeated-measure ANOVA (rmANOVA) was done to estimate null hypothesis probability in main effects and interactions. If main effects were tested significant, for factors with more than two levels, post-hoc paired t-tests were done. If interactions were tested significant, post-hoc paired t-tests were done. P-values for the post-hoc paired t-test were corrected for multiple comparisons with Bonferroni-Holm correction (Holm, 1979). For between subject comparison, mixed ANOVA was done instead of rmANOVA and independent t-test was used instead of paired t-test. Specifically, significance between the dark and light trials were confirmed by 1) significant interaction between two days and two trials in a two-way ANOVA; 2) significant difference of group means in t-test between the dark and light trial on day two, and non-significant difference (or smaller difference) of group means between two light trials on day one. Correlation coefficient scores were normalized following Fisher's z-transformation (Fisher, 1915).

5.3 Results

5.3.1 Navigation in the dark

On average, the animals' running speeds in the dark trials were not different from the speeds in the light trials (interaction, $F(1, 14) = 0.01$, $p = 0.92$, see Figure 5.1A). However, the histogram of instant running speeds showed different probability

5.3. RESULTS

distribution between the dark and light trials. Mice in the dark are less likely to either stay still (0 - 5cm/s; $t(14) = -3.50$, $p < .01$, corrected $p < .05$) or reach some high speed range (30 - 35cm/s; $t(14) = -2.54$, $p < .05$, corrected $p = 0.14$) compared to the light trials recorded on the same day. Instead they spend significantly more time running at medium speed ranges in the dark (5 - 10cm/s, $t(14) = 5.33$, $p < .001$, corrected $p < .01$; 10 - 15cm/s, $t(14) = 5.09$, $p < .001$, corrected $p < .01$; 15 - 20cm/s, $t(14) = 3.78$, $p < .01$, corrected $p < .05$).

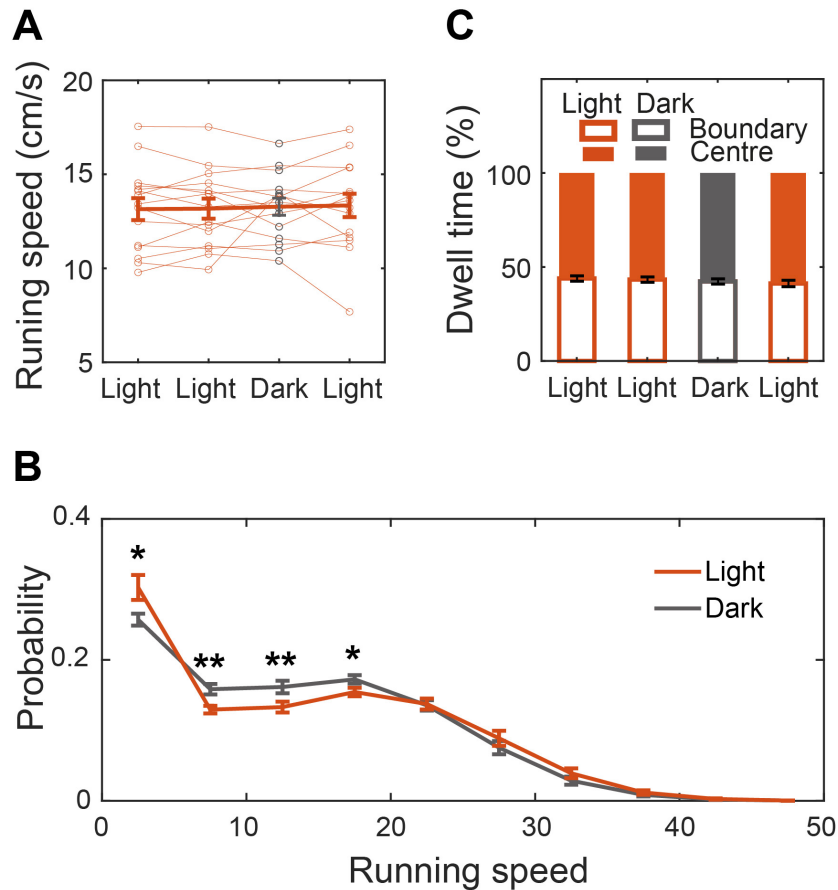


Figure 5.1: **Running speed and occupancy in boundary and centre region.** (A) Average running speed of animals in dark and in light trials. Each thin line represented one individual animal, the thick line represented the average speed, mean \pm sem. (B) Histogram of instant running speed, binned from 0 to 50 cm/s with 5 cm/s stepwise. (C) Stacked bar plotted for animals dwell time in percentage in either boundary or centre region. *** denotes significance at $p < 0.001$, ** at $p < 0.01$, * at $p < 0.05$, same notation applies to all the figures.

To compare the dwelling time in the boundary region and the center region in proportion (see Methods) between dark and light trials. We found that in general animals visit the center region more than the boundary region both in dark and light trials (main effect, $F(1, 14) = 46.82$, $p < .001$). There was no significant difference in such center preference between dark and light trials (interaction, $F(1, 14) = 0.28$, $p = 0.61$). Paired-t tests again confirmed that the proportional dwelling time in boundary/center regions was comparable between dark and light trials ($t(14) = 0.52$, $p = 0.61$). Together the dwelling pattern suggest no sampling bias would contribute to spatial representational difference between boundary and center regions.

5.3.2 Electrophysiology

A total of 372 units were isolated in 13 mice with tetrodes implanted in the medial entorhinal cortex (MEC); of these, 83 units were qualified as grid cells (for threshold distribution see Figure 5.2). Four trials per animal were included in the analysis, two trials on day one (D1) with room lights on and another two on day two (D2) with lights off for first trial and lights on for the second trial.

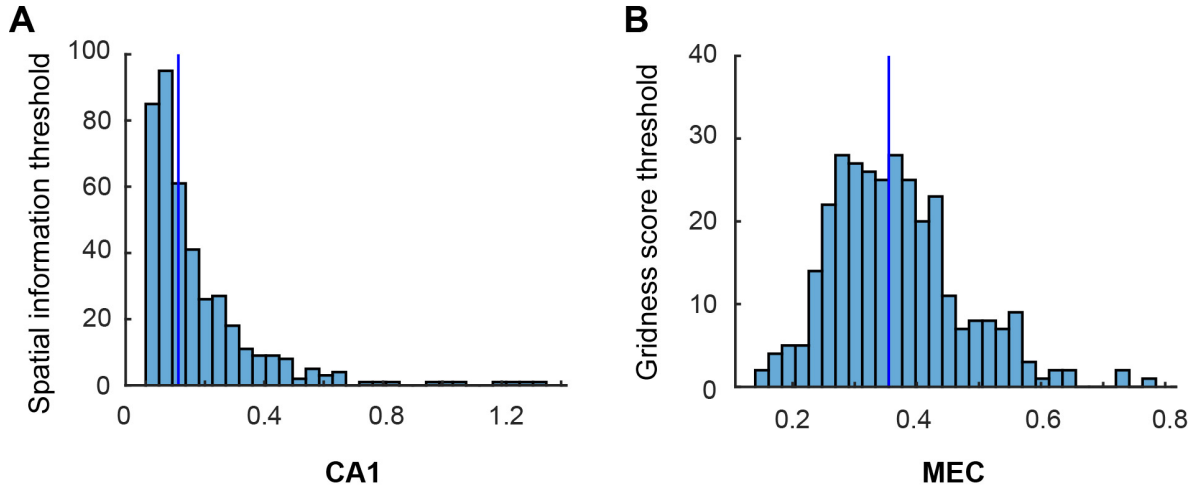


Figure 5.2: **Spatial cell classification.** Distribution of thresholds of spatial information for CA1 units A) and gridness score for MEC units B). Vertical line indicates the group median.

We first measured whether grid cells' spatial properties were disrupted in the absence of visual input. Results showed that both spatial information indices (interaction, $F(1,82) = 69.29$, $p < .001$; dark vs light, $t(82) = -8.79$, $p < .001$, corrected $p < .001$; light vs light $t(82) = 0.78$, $p = 0.44$) and gridness score (interaction, $F(1,82) = 61.76$, $p < .001$; dark vs light, $t(82) = -8.28$, $p < .001$, corrected $p < .001$; light vs light $t(82) = 0.10$, $p = 0.92$) were significantly reduced in the dark trials compared to the light trials (see Figure 5.3BC). These results suggest that grid cell firing patterns became less predictive of the animals location in the dark, and that their characteristic hexagonal firing patterns were disrupted.

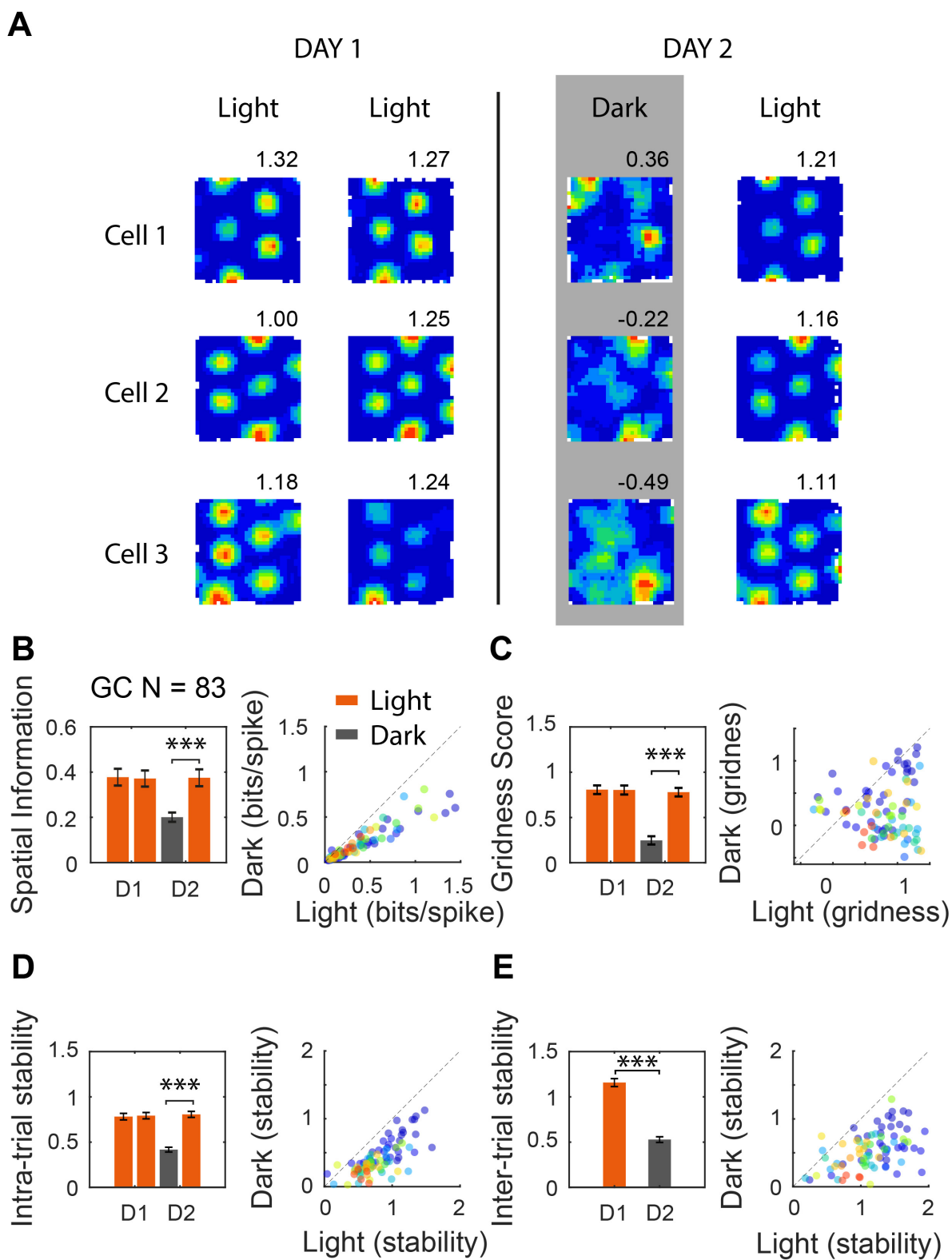


Figure 5.3: **Comparison of grid cell firing patterns between dark and light trials.** (A) Three example grid cells recorded over two days, two light trials on day one (D1) and one dark trial followed by one light trial on day two (D2). The number on the top right side of each rate map stands for gridness score. (B-E) Bar graph and individual scatter plot for dark-light comparison of cell spatial information (B), gridness score (C), intra-trial stability (D) and inter-trial stability. different colours of dots in scatter plot stand for different animals the cells were recorded from.

Next, I tested the stability of grid cell firing by computing the correlation coefficients between the first and second halves of a whole trial (intra-trial stability). Statistical testing revealed that within a trial the stability of grid cell firing was significantly lower in darkness (interaction, $F(1,82) = 205.67$, $p < .001$; dark vs light, $t(82) = -17.06$, $p < .001$, corrected $p < .001$; light vs light $t(82) = -0.67$, $p = 0.51$, see Figure 5.3D). Inter-trial stability of firing patterns were calculated by correlate rate maps between trials on the same day, e.g. on D1 calculate the correlation coefficient between the two light trials and on D2 between the dark trial and the light trial. Decrease in stability was observed from D1 to D2 (main effect, $F(1, 82) = 254.55$, $p < .001$, see Figure 5.3E).

250 out of 681 cells recorded from CA1 implants in 15 mice were classified as place cells. Similarly to grid cells, a decrease in spatial information (interaction, $F(1,249) = 71.90$, $p < .001$; dark vs light, $t(249) = -9.82$, $p < .001$, corrected $p < .001$; light vs light $t(249) = -0.98$, $p = 0.33$), intra-trial stability (interaction, $F(1,249) = 60.20$, $p < .001$; dark vs light, $t(249) = -11.57$, $p < .001$, corrected $p < .001$; light vs light $t(249) = -3.28$, $p < .01$, corrected $p < .01$) and inter-trial stability (main effect, $F(1,249) = 256.24$, $p < .001$) were observed in the average of place cell populations between dark and light trials (see Figure 5.4BDE). However, the average ratio of spatial information decrease was significantly smaller in place cells than in grid cells (PC, 0.18 ± 0.02 ; GC, 0.44 ± 0.02 ; $t(331) = -6.30$, $p < .001$). The cumulative density distribution also

confirmed that there were more grid cells than place cells whose spatial information, intra-trial stability and inter-trial stability were lower in the dark trial than in the light trial (see Figure 5.6). There was no correlation in such proportional spatial information reduction between place cells and grid cells across individual animal ($n = 13$, $r = 0.34$, $p = 0.25$). In place cells, removal of visual input also resulted in higher directional information (interaction, $F(1,249) = 9.86$, $p < .01$; dark vs light, $t(249) = -5.96$, $p < .001$, corrected $p < .001$; light vs light $t(249) = -0.92$, $p = 0.36$; see Figure 5.4C).

We then set out to check whether it is degradation in head directional tuning that lead to disrupted spatial representation in place cells and grid cells. We detected 33 head direction cells in recordings from the medial entorhinal cortex. There was mild disruption in their directional tuning properties as shown by decreased directional information between the dark and light trial (interaction, $F(1,32) = 9.28$, $p < .001$; dark vs light, $t(32) = -3.77$, $p < .001$, corrected $p < .01$; light vs light $t(32) = -0.64$, $p = 0.52$, see Figure 5.5B), but preserved vector lengths (interaction, $F(1,32) = 0.10$, $p = 0.75$, see Figure 5.5C). Similarly for firing stability, intra-trial stability were comparable between dark and light trials (interaction, $F(1,32) = 1.93$, $p = 0.17$, see Figure 5.5D) while inter-trial stability (main effect, $F(1,32) = 9.95$, $p < .01$, see Figure 5.5E) decreased.

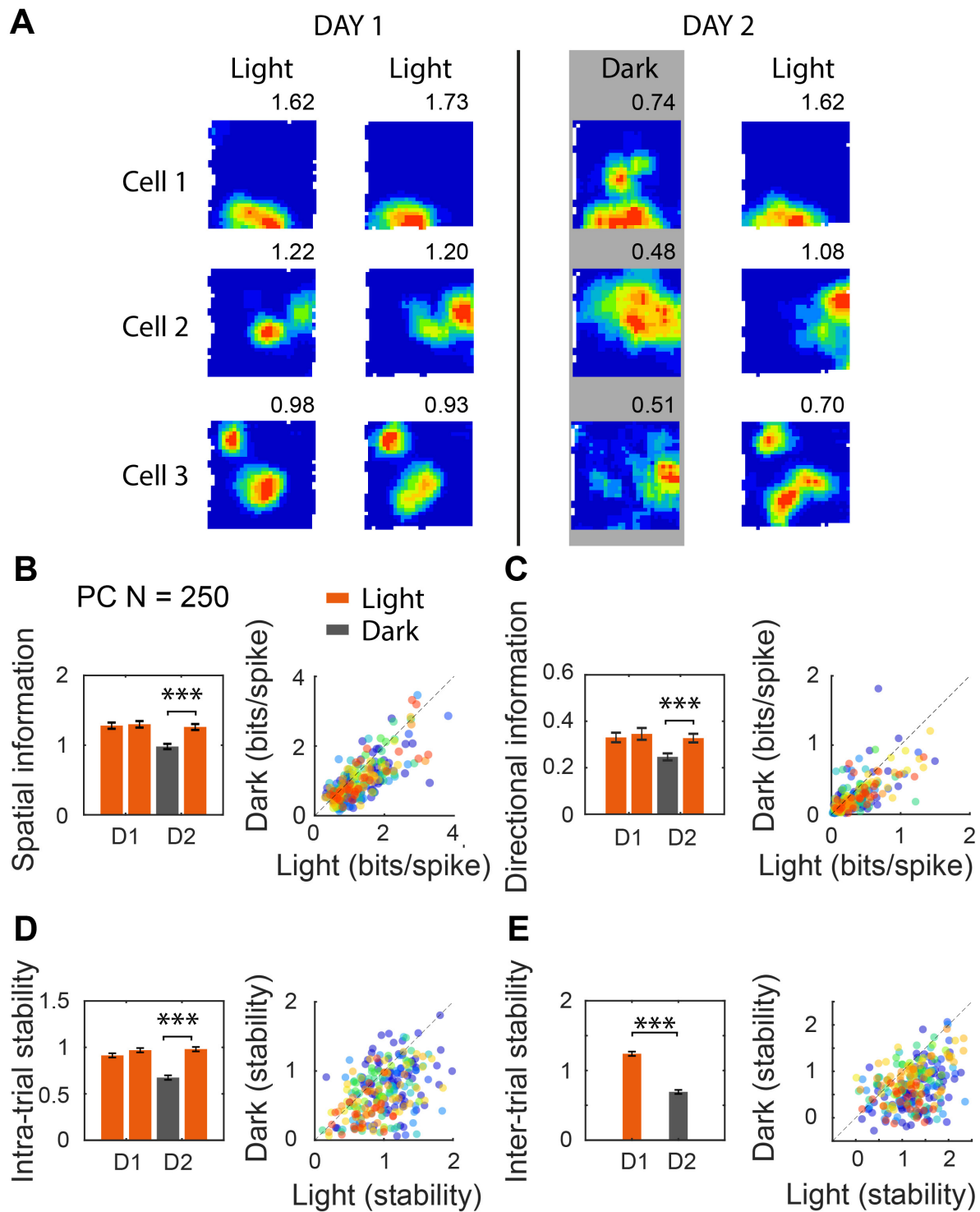


Figure 5.4: **Comparison of place cell firing patterns between dark and light trials.** (A) Three example place cells recorded over two days, two light trials on D1 and one dark trial followed by one light trial on D2. The number on the top right side of each rate map stood for spatial information. (B-E) Bar graphs and individual scatter plots for dark-light comparison of cells' spatial information (B), directional information (C), intra-trial stability (D) and inter-trial stability. Different colours of dots in scatter plots refer to different animals.

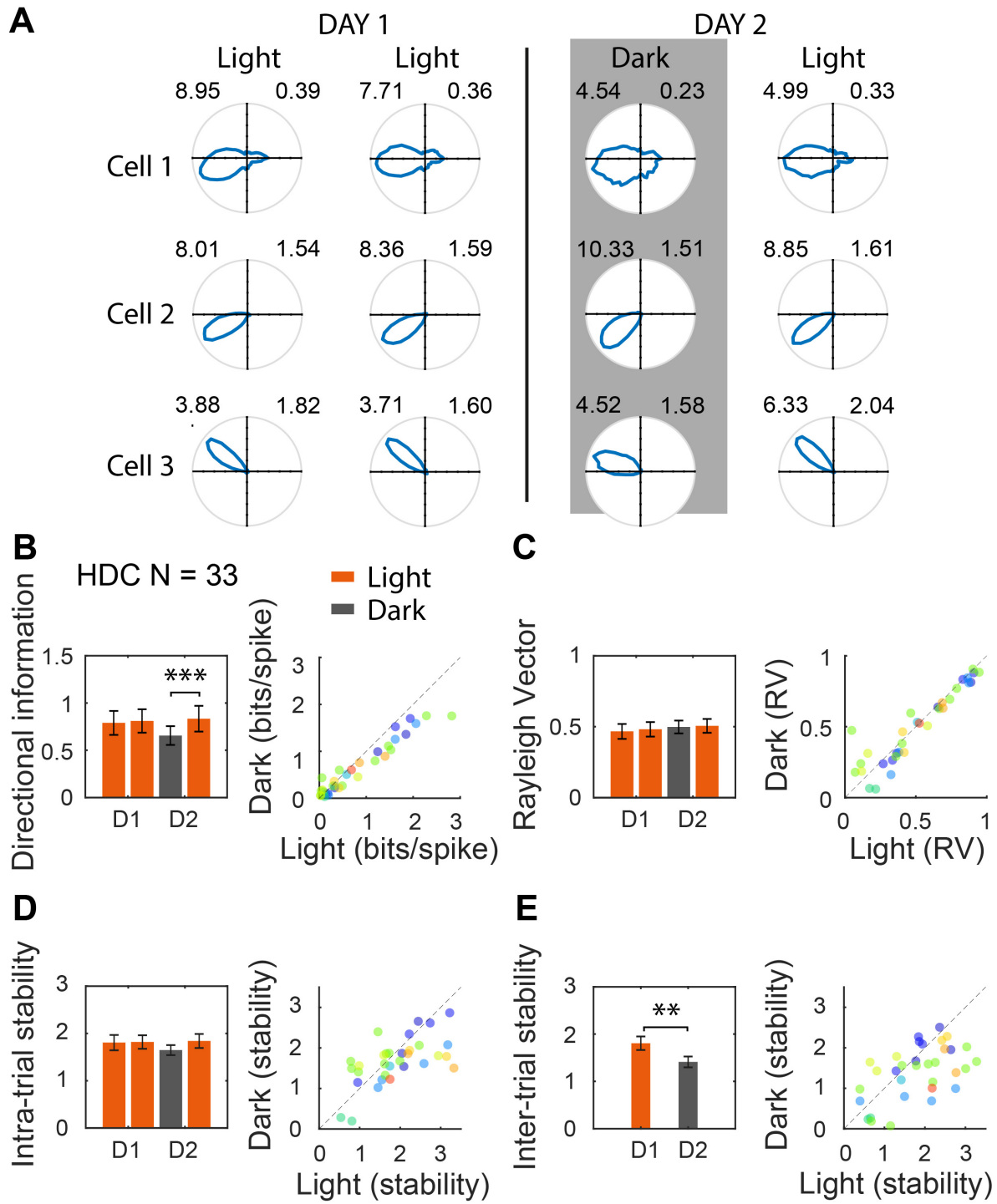


Figure 5.5: **Comparison of head direction cell firing patterns between dark and light trials.** (A) Three example head direction cells recorded over two days, two light trials on D1 and one dark trial followed by one light trial on D2. The numbers on the top left and right side of each polar plot stood for peak firing rate and spatial information, respectively. (B-E) Bar graphs and individual scatter plots for dark and light trial comparison of head direction cell directional information (B), Rayleigh vector length (C), intra-trial stability (D) and inter-trial stability. Different colours of dots in scatter plots refer to different animals.

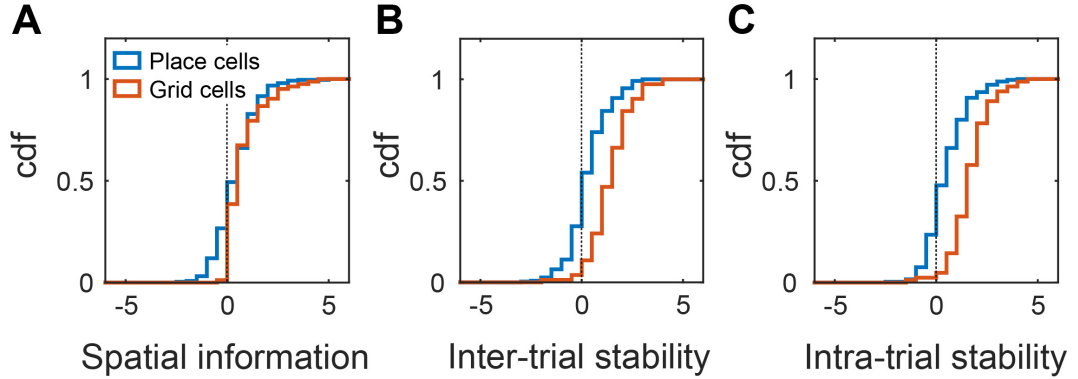


Figure 5.6: **Cumulative density function of spatial tuning reduction in place cells and grid cells from the light to dark trials.** Probability distributions (with normalized standard deviation) of difference between the light and dark trial (light trial minus dark trial) for spatial information A), Inter-trial stability B) and Intra-trial stability c). Note how a smaller proportion of grid cells had negative values compared to place cells.

During the dark trial mice still have access to boundary inputs when they were near walls. We performed a set of analyses aimed at understanding whether wall proximity helps spatial localization in place cells and grid cells. For place cells, we first defined place fields for each cell in each trial and calculated field sizes and peak firing locations (see Methods). Place fields were split into three categories according to their distances towards the nearest wall. Mixed ANOVA was done for comparison across fields. Field

5.3. RESULTS

size increased significantly in dark trials compare to light trials ($F(1,443) = 21.09$, $p < .001$), but no main effect was found for field-wall distances ($F(2,443) = 0.27$, $p = 0.76$) nor was significant interaction ($F(2,443) = 2.17$, $p = 0.11$) observed (see Figure 5.7B). Shift distances of place fields between the dark and light trial were significantly longer than between the two light trials ($F(1,443) = 32.29$, $p < .001$). Moreover, interaction between visual inputs and field-wall distance was also significant ($F(2,443) = 4.33$, $p < .05$). Simple F-test revealed that only field shift distances between the dark and light trial varied with field-wall distance ($F(2,221) = 4.06$, $p < .05$, corrected $p < .05$), and those between the two light trials were not affected by field-wall distance ($F(2,222) = 1.35$, $p = 0.26$).

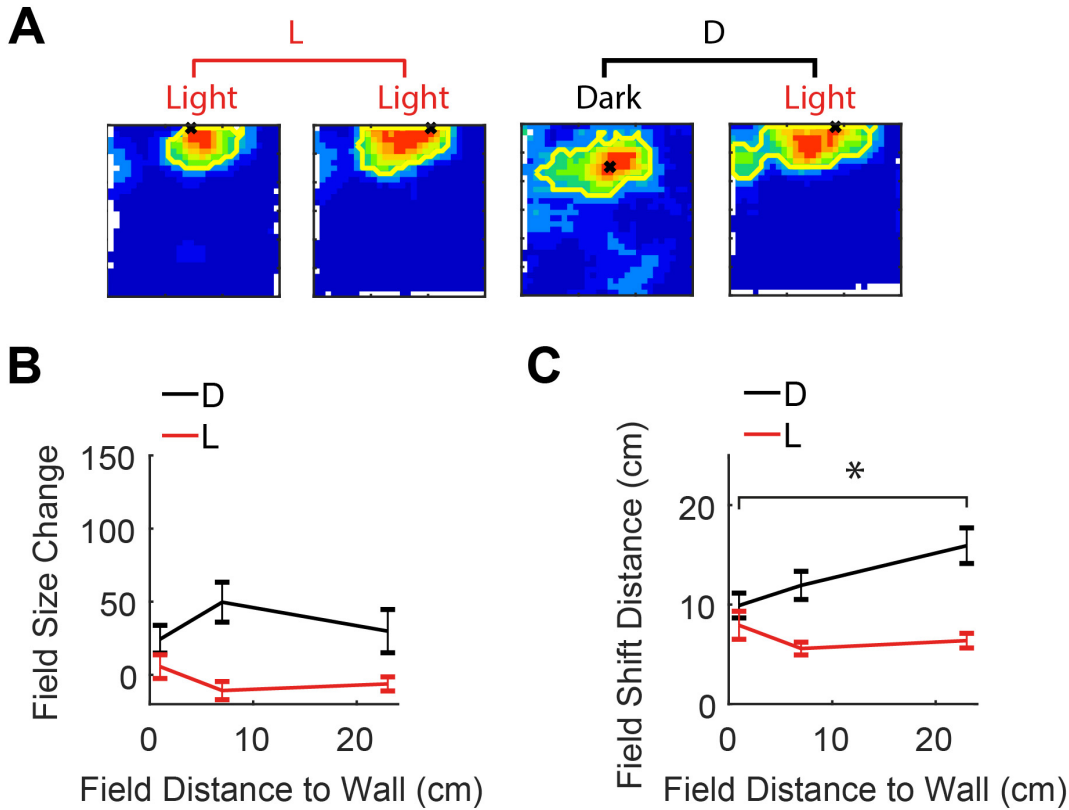


Figure 5.7: **Place cell field size and stability are modulated by its distance towards the nearest wall.** (A) Rate maps of one place cell recorded in four trials, trial conditions were specified on top of the rate map ('Light' vs 'Dark'), yellow line indicates the edges of detected place fields, black cross indicate the field location. Field size changes and field location drift were compared between two light trials ('L') and between a dark and a light trial ('D') recorded on the same day. Average field size changes (B) and field location shift distances (C) were plotted as a function of fields' distance towards the nearest wall.

Having established that distance to the nearest wall affected place field shifts in the dark trial relative to the light trial, we now proceeded to separate every rate maps into a 'boundary' rate map and a 'centre' rate map and characterized their stability across trials separately. For place cells, we found that firing similarity was much higher for boundary rate maps than for centre rate maps across the dark and light trials (interaction $F(1, 249) = 25.08$, $p < .001$; Dark-light (DL) inter-trial stability, $t(249) = 5.57$, $p < .001$, corrected $p < .001$; Light-light (LL) inter-trial stability, $t(249) = 0.48$, $p = 0.63$; see Figure 5.8AB). On the other hand, grid cell firing patterns displayed double dissociation between boundary-vs-centre and DL-vs-LL stability. The interaction was significant ($F(1,82) = 27.95$, $p < .001$), as well as boundary rate maps showed higher stability in DL comparison ($t(82) = 2.38$, $p < .05$, corrected $p < .05$) and centre rate maps were more similar in LL comparison ($t(82) = -4.25$, $p < .001$, corrected $p < .001$).

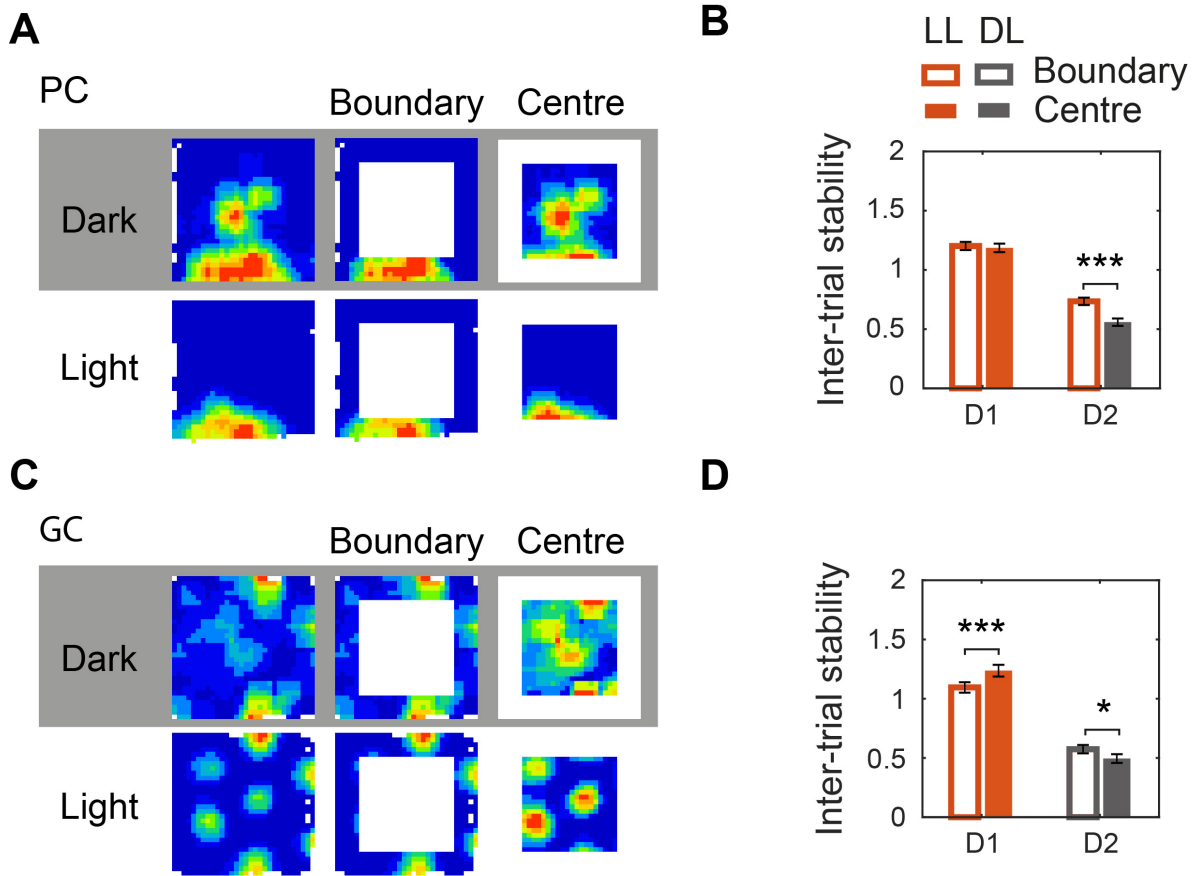


Figure 5.8: **Place cell and grid cell firing in the boundary and centre region.** Rate maps of a place cell (A) and a grid cell (C) were shown, trial conditions were labeled on the left side of rate maps ('Dark' vs 'Light'), from left to right were the whole rate maps, the boundary rate maps and the centre rate maps, respectively. Boundary rate map inter-trial stability and centre rate map inter-trial stability in place cells (B) and grid cells (D) between dark trial and light trial ('DL') and between two light trials ('LL') are shown.

5.4 Discussion

5.4.1 Speed distribution in darkness

No systematic change in animals' average running speed between the dark and light trial was found. Similarly, there was no difference in the animals' dwelling pattern between the light and dark conditions in terms of preference to boundary or centre regions. However, distinct speed distributions were observed: when locomoting in the dark, animals displayed significantly less quiescent or extremely high speed moments. In a previous study with 'tilted' mice whose otolith function was disrupted, shorter duration of stops during their outbound exploration journey was observed (Yoder et al., 2015). This suggests that the observed speed change in darkness in our wild type mice may be a reflection of altered linear speed computation in the dark.

5.4.2 Spatial cell properties in the dark

Mouse head direction cells were only mildly affected by the removal of visual input, as evinced by slightly decreased directional information but intact Rayleigh vector length. Place and grid cells, on the other hand, displayed significant deficits in spatial selectivity. Specifically, they both displayed lower spatial information and spatial firing stability within and across trials in the dark condition. Comparison between place cells and grid cells found that overall the ratio of spatial information decrease was higher in the latter. Also, about 20% ~ 30% of place cells showed no decrease (light trial measures minus dark trial measures equal or higher than zero) in spatial properties (including spatial information, intra-trial and inter-trial stability), whilst less than 4% of grid cells had equal or higher spatial selectivity in the dark. The characteristic six-fold symmetry of

grid cells' firing patterns was severely reduced. It thus seems that grid cells suffered most in their spatial representation in the dark while head direction cells were the best preserved, and the impact of visual deprivation fell in the middle range and with large variation for place cells.

By comparing changes in spatial information between light and dark trials across animals, we found no significant correlation between place cells and grid cells across individual mouse. This results is at odds with the proposal that grid cell may play a more important role in supporting place cells firing and hippocampal spatial representation in general in darkness (?). Grid cells are considered to be the neural substrates of path integration, and their firings are thought to be more dependent on directional and speed signals. While place cells are widely accepted to be integrating from a large variety of inputs which includes both external sensory inputs and self-motion inputs. The fact that grid cells were affected more than place cells suggested that visual inputs were important for velocity estimation, at least in mice. The observed heterogeneous responses under visual deprivation in place cells are in line with the proposed flexible cue integration function. However, no obvious bimodal distribution was observed in their responses. worth noticing that insufficient sampling (especially for place cells) in some of the animals may reduce the power of this analysis and its related conclusions.

5.4.3 Boundary effects in the dark

Influence from boundary inputs were obvious in the dark. Place cell firing fields close to boundaries drifted less and remained more compact in the dark trials. This was also true for grid cells. When we analysed separately each cell's boundary and centre maps, both place and grid cells' boundary maps displayed higher stability compared to centre

maps. This boundary over centre advantage was positively correlated across different animals in the dark trials but not in the light trials for both place and grid cells . This suggests that boundary input helps to stabilize local place fields and grid cell fields and this effect likely originates in either place or grid cells and is then projected to the other cell class. Considering that the effect size was bigger in the former it is more likely that place cells relayed boundary input to the grid cell population in darkness rather than vice versa.

In summary, spatial selectivity in place and grid cells firing was largely reduced in the absence of visual input, while head direction cells remained robust in their directional tuning. Overall firing of grid cells suffered worse disruption than place cells despite its proposed function of path integration. Proximity to walls increased spatial firing similarity between the dark and light trials confirmed the influence of boundary input.

Chapter 6

General discussion

6.1 Difference between place cells and grid cells in combining external and self-motion inputs

We consistently observed the difference in responses between place cells and grid cells in our experiments. When mice navigated in our 2D virtual reality systems, place cells had increased directionality while grid cell did not (Chapter3). Changing the gain that maps an animal's physical movement into the visual translation of a virtual environment leads to higher weight towards visual input in place cells and higher self-motion influence in grid cells (Chapter4). Last, visual input deprivation compromised the spatial tuning property in grid cells more than that observed in place cells (Chapter5).

While the increased directional tuning in place cells (Acharya et al., 2016), the combined influence of visual input and self-motion input in place cells (Chen et al., 2013), and in grid cells (Campbell et al., 2018) were separately discovered in other studies. Our experiments are the first to establish a direct and quantitative comparison between

place cells and grid cells, leading to the conclusion of partial independence between place cells and grid cells in establishing spatial representation based on visual inputs and self-motion inputs.

Highly integrated relationships between grid cells and place cells have been proposed, such as place cells being generated from a linear summation of grid cells (Solstad et al., 2006), and grid cells' firing pattern arising from the non-negative principal component analysis of place cell inputs (Dordek et al., 2016). However, it is unlikely that linear summation of non-directional grid fields would result in highly directional place fields or that eigendecomposition of place cell population vector that has strong environmental bounding characteristics in our gain manipulation experiment (Chapter 4) and our dark trial (Chapter 5) would generate grid cell firing as we observed (future simulation work needed). Our results seem to contradict those model predictions and suggest (at least when the environment is novel) place cells and grid cells are supported by external inputs and self-motion inputs in different ways. It would be interesting to see, in future works, how navigation behaviours are shaped by these discrepant spatial representations in the hippocampal-entorhinal system. By combining spatial memory task, such as the Morris water maze task, we could examine during gain manipulation and dark trials whether population vectors of place cells' or grid cells' firing rates reflect the animals' reward searching/expectation behaviours better.

We showed that, in our gain manipulation experiment, place cells are more weighed towards visual inputs than grid cells. However, in the dark experiment when the visual input was eliminated, place cells seemed less disrupted in their spatial tuning than grid cells. These seemingly contradictory results could be due to some experimental factors. First, uncontrolled local cues (e.g. tactile, olfactory) could help to stabilize place fields in the dark. Second, the stability measure in the dark trial is more sensitive to changes

6.2. POSSIBLE CAUSES OF DISCREPANCY BETWEEN PLACE CELLS AND GRID CELLS

in the field location, while the MI score in gain manipulation experiment is to capture changes in the field size. Alternatively, it could be that a constant relationship between velocity signals from self-motion inputs and optic flow, albeit scaled, is sufficient to stabilize the path integrator. Future experiments to check the firing of place cells and grid cells with the visual projection turned off in the VR setup would be better to decide the visual influence in hippocampal spatial representation.

6.2 Possible causes of discrepancy between place cells and grid cells

6.2.1 Velocity versus static cues

There are two ways that the external cues could act on spatial representation in our VR gain manipulation paradigm (and others' as well). One is through velocity coding and another is through anchoring towards static visual landmarks. When the gain between animal's locomotion and visual projection was changed, both the perceived visual landmark location and speed of optic flow were changed to disagree with those derived from self-motion signals. There is a wealth of velocity signals in MEC including theta field potential oscillation (Jeewajee et al., 2008), speed cells (Kropff et al., 2015) and conjunctive cells (Sargolini et al., 2006), as well as in hippocampus (McNaughton et al., 1983; O'Keefe & Recce, 1993), which could be used to drive grid cell activity (Mcnaughton et al., 1996; McNaughton et al., 2006; Burgess & O'Keefe, 2011). Both static landmarks and optic flow has been established to be effective in affecting spatial cells' firing and velocity coding in rodents (see reviews in section XX).

In our experiment, we checked the slope of speed modulation in theta-band local field

oscillations and the firing rate of speed cells in CA1 and MEC under gain manipulations. Our results showed that LFP theta frequency, but not the firing rates of speed cells, seemed to be a more sensitive measure of speed signals that reflected the changes in spatial scales represented in place cells' and grid cells' firing patterns, which is consistent with results found in rats travelling in a circular track (Jacob et al., 2019). But no significant quantitative correlations between the speed measures and the spatial representation was detected when compared across animals. In Campbell et al. (2018), they tested the effect of gain manipulation on mice grid cells' activity on a virtual linear track and found grid cell firing patterns to offset and stretch under the combined influence of both visual inputs and self-motion inputs. They also reported a coherent change in the firing rate modulation of MEC speed cells that showed a general bias towards self-motion inputs but with higher visual influence under gain increase than gain decrease conditions.

In our experiments, we found clear offsets when animals are travelling in the opposite direction in the gain decreased axis, showing possibly boundary driven reset of grid firing patterns. While stretching and offsetting of the grid cells firing patterns were reported under gain decrease manipulations and gain increase manipulations respectively. Such results could be caused by task difference, for example, we know that place cells respond to distance rather than allocentric locations on the linear track (Gothard et al., 1996a). Nevertheless, both studies showed the combined effects of landmark anchoring and speed signal modulation.

Future experiments could try to isolate the influence of optic flow from visual landmarks by constructing a virtual environment that emphasises the visual motion yet with little spatial specificity in the visual scenes at any 'pose' state (a combination of position and orientation, Heinze et al. (2018)) in the environment, similar to that in Saleem et al.

(2013).

6.2.2 Distal versus proximal cues

Within the domain of static visual cues, the distinction between its proximal and distal influence is also important. By definition, distal cues radiate influence over a long distance while proximal cues have restricted effects around its vicinity. For example, tactile patterns are only available when they are within the touch of the animal, while visual cues are accessible both distally and proximally. While distal visual cues were long-established to have a strong influence in controlling the orientation of hippocampal spatial representation (Muller1987; Shapiro1997), it is only recently that VR techniques could finally remove all non-visual local influences and found that the presence of proximal visual cues (3D visual objects) increased the proportion of active place cells and sharpened their spatial tuning around them (Bourboulou et al., 2019).

First, it is important to understand the influential radius of different cues and sensory modalities to validate any navigation models that are based upon those inputs, as well as to estimate to what degree those models could be transferred to natural navigation. Animals in the wild often navigate over thousands of miles with high accuracy. And some studies stressed the importance of vision, such as optic flow and storage of panoramic landscape at home location, e.g. in helping bees to navigate between home and feeder (Wehner, 1981; Esch & Burns, 1996). It is rather a multi-scaled spatial representation than a single-scale one that is more plausible to support natural navigation. Indeed both place cells and grid cells along the dorsoventral axis of CA1 and MEC have different field/spacing sizes (Jung et al., 1994; Maurer et al., 2005; Kjelstrup et al., 2008; Barry et al., 2007; Stensola et al., 2012). Considering that different grid scales are incommensurable and they often respond to experimental

manipulations differently (Barry et al., 2007; Stensola et al., 2012), it is likely they receive environmental influence independently. For example, distal visual cues may not be informative in distance anchoring to grid cells and place cells with smaller fields, but they could be vital to cells with wider tuning.

We observed similar MI scores in our gain manipulation experiment no matter the spatial fields are further away or close to the boundaries, suggesting both distal and proximal influence of visual inputs in place cells and grid cells. Future experiments could add a comparison of manipulating VR gain factor in environments of larger sizes, as well as recording from cells tuned to different spatial scales. Parametric estimation of the effect of sensory input with different acuity on spatial representation at different scales could potentially help us to build a more comprehensive model of multi-scale spatial representation in hippocampus.

Secondly, in the physical world, distal cues are often sensory only, while proximal cues are likely to affect behaviour. An object or a boundary, when approached, not only gives you a rich sensory experience but also signals a change in behaviour (‘policy’) such as to turn away or manoeuvre around. It has been observed that changing the environmental configuration (O’Keefe & Burgess, 1996; Barry et al., 2007; Krupic et al., 2015), allowing to travel between the otherwise divided portions of the environment (Carpenter et al., 2015; Wernle et al., 2018) and the presence of a fixed-location reward (Boccarda et al., 2019) shifted grid cells fields. All those changes were both sensory and behavioural and could be explained by behavioural changes only within something like a successor representation model (Stachenfeld et al., 2017). The effect observed with the 3D objects in the VR linear track could also be triggered by the behavioural policy change that is often associated with a normal object (Bourboulou et al., 2019). In our virtual reality, movement of mice would not be stopped by the wall because

6.2. POSSIBLE CAUSES OF DISCREPANCY BETWEEN PLACE CELLS AND GRID CELLS

sudden stops of the ball from rotating would startle the animal and affect behaviour in general. At the end of the training, mice learned not to run into walls too much yet the movement impedance aspect of the boundary could be compromised. Future experiments could pair tactile VR (Ayaz et al., 2019) with visual VR to test the effects of boundary and object configurations on hippocampal representation.

6.2.3 Novel versus familiar environments

Experience also plays an important role in hippocampal representation, as well as in plasticity and memory functions that have been attributed to the hippocampus. It was found that when the boundaries of a physical square enclosure were stretched or compressed, grid cells first respond by changing their field spacings in proportion to the manipulation, but gradually relaxed towards their original spacings after familiarizing with it over a few sessions (Barry et al., 2007). It would be interesting to record long-term follow-up of the firing patterns of place cells and grid cells when the animal gets repeated exposure to the same gain manipulation. There are many questions to ask for such a followup recording. Do place cells and grid cells firing patterns become more visual driven or more self-motion driven? Do they form one stable and coherent representation or they settle to different representations that are biased towards either visual input or self-motion inputs? If place cells and grid cells converge in their representation, is there one party leading the other, and is that replay/ sharp-wave ripple dependent?

6.3 Future direction

Our results strengthened the idea that the activity of place cells and grid cells, albeit both tuned to subjects' allocentric location, are governed by different inputs and computations. It is important thus to understand the dynamics within the hippocampal-entorhinal circuit. It has been proposed since the discovery of place cells that they might form a cognitive map representation to support further experience organized and retrieved based on the map structure (O'Keefe & Nadel, 1978). Sequential (Wilson & McNaughton, 1994) and low dimensional attractor manifold (Chaudhuri et al., 2019) organization were discovered in place cell population activity vectors, but it is not yet understood what is the cause of such activity structure, and what roles the inputs from grid cells and MEC play.

Place cells were shown to rapidly detect changes in the environment and form orthogonal representations of multiple 'maps' (Muller & Kubie, 1987). Grid cells, on the other hand, maintain coherence among firing fields of individual cells and across different cells that are functionally connected. The ability to rapidly obtain and associate a large amount of input ('one-shot' learning), as well as the stability and continuity of our cognitive experience possibly supported by the internal-driven network structure, are both essential to human cognition. How they strike a balance and how they interact and shape information structure at the population vector level needs future experimental and computational effort.

Taken together, our experiments established that 1) Our VR system possesses a good potential for accessing neuronal spatial representations under highly controlled external cue manipulations, such as changing the speed of visual motion without altered self-motion cues; 2) Place cells and grid cells integrate visual input and self-motion cues differently. Place cells resolve the discrepancy between visual input and self-motion

input by leaning towards visual motion while grid cell weigh self-motion cues more strongly. In the absence of visual input, place cell displayed better preserved spatial tuning in a portion of cells; And 3) Boundary inputs stabilize the local firing fields of both place cells and grid cells in the absence of visual input. Our results shed new light on how we should consider maybe a more complementary role between hippocampal and parahippocampal area.

Bibliography

- Acharya, L., Aghajan, Z. M., Vuong, C., Moore, J. J., & Mehta, M. R. (2016). Causal Influence of Visual Cues on Hippocampal Directional Selectivity. *Cell*, *164*(1-2), 197–207.
- Aggleton, J. P. (2000). Differential cognitive effects of colloid cysts in the third ventricle that spare or compromise the fornix. *Brain*, *123*(4), 800–815.
- Aghajan, Z. M., Acharya, L., Moore, J. J., Cushman, J. D., Vuong, C., & Mehta, M. R. (2015). Impaired spatial selectivity and intact phase precession in two-dimensional virtual reality. *Nature Neuroscience*, *18*(1), 121–128.
- Alonso, A., & García-Austt, E. (1987a). Neuronal sources of theta rhythm in the entorhinal cortex of the rat - I. Laminar distribution of theta field potentials. *Experimental Brain Research*, *67*(3), 493–501.
- Alonso, A., & García-Austt, E. (1987b). Neuronal sources of theta rhythm in the entorhinal cortex of the rat - II. Phase relations between unit discharges and theta field potentials. *Experimental Brain Research*, *67*(3), 502–509.
- Anagnostaras, S. G., Maren, S., & Fanselow, M. S. (1999). Temporally graded retrograde amnesia of contextual fear after hippocampal damage in rats: Within-subjects examination. *Journal of Neuroscience*, *19*(3), 1106–1114.

BIBLIOGRAPHY

- Andersen, P., Bliss, T. V., & Skrede, K. K. (1971). Lamellar organization of hippocampal excitatory pathways. *Experimental Brain Research*, 13(2), 222–238.
- Andersen, P., Morris, R., Amaral, D., Bliss, T., & O’keefe, J. (2007). The Hippocampus Book. Tech. rep.
- Andersen, R. A., Essick, G. K., & Siegel, R. M. (1985). Encoding of Spatial Location by Posterior Parietal Neuro. *Science*, 230, 456–458.
- Angeli, S. J., Murray, E. A., & Mishkin, M. (1993). Hippocampectomized monkeys can remember one place but not two. *Neuropsychologia*, 31(10), 1021–1030.
- Aronov, D., Nevers, R., & Tank, D. W. (2017). Mapping of a non-spatial dimension by the hippocampal-entorhinal circuit. *Nature*, 543(7647), 719–722.
- Aronov, D., & Tank, D. W. W. (2014). Engagement of Neural Circuits Underlying 2D Spatial Navigation in a Rodent Virtual Reality System. *Neuron*, 84(2), 442–456.
- Ayaz, A., Stauble, A., Hamada, M., Wulf, M.-A., Saleem, A. B., & Helmchen, F. (2019). Layer-specific integration of locomotion and sensory information in mouse barrel cortex. *Nature Communications*, 10(1), 2585.
- Barry, C., Ginzberg, L. L., O’Keefe, J., & Burgess, N. (2012). Grid cell firing patterns signal environmental novelty by expansion. *Proc. Nati. Acad. Sci. USA*, 109(43), 17687–17692.
- Barry, C., Hayman, R., Burgess, N., & Jeffery, K. J. (2007). Experience-dependent rescaling of entorhinal grids. *Nature Neuroscience*, 10(6), 682–684.
- Barry, C., Lever, C., Hayman, R., Hartley, T., Burton, S., O’Keefe, J., Jeffery, K., & Burgess, N. (2006). The boundary vector cell model of place cell firing and spatial memory. *Reviews in the Neurosciences*, 17(1-2), 71–97.

BIBLIOGRAPHY

- Bassett, J. P., & Taube, J. S. (2001). Neural Correlates for Angular Head Velocity in the Rat Dorsal Tegmental Nucleus. *Journal of Neuroscience*, *21*(15), 5740–5751.
- Bassett, J. P., Tullman, M. L., & Taube, J. S. (2007). Lesions of the tegmentomammillary circuit in the head direction system disrupt the head direction signal in the anterior thalamus. *Journal of Neuroscience*, *27*(28), 7564–7577.
- Battaglia, F. P., Sutherland, G. R., & McNaughton, B. L. (2004). Local sensory cues and place cell directionality: Additional evidence of prospective coding in the hippocampus. *Journal of Neuroscience*, *24*(19), 4541–4550.
- Beraneck, M., & Cullen, K. E. (2007). Activity of vestibular nuclei neurons during vestibular and optokinetic stimulation in the alert mouse. *Journal of Neurophysiology*, *98*(3), 1549–1565.
- Bjerknes, T. L., Dagslott, N. C., Moser, E. I., & Moser, M. B. (2018). Path integration in place cells of developing rats. *Proceedings of the National Academy of Sciences of the United States of America*, *115*(7), E1637–E1646.
- Bjerknes, T. L., Langston, R. F., Kruge, I. U., Moser, E. I., & Moser, M. B. (2015). Coherence among head direction cells before eye opening in rat pups. *Current Biology*, *25*(1), 103–108.
- Blackstad, T. W. (1956). Commissural connections of the hippocampal region in the rat, with special reference to their mode of termination. *Journal of Comparative Neurology*, *105*(3), 417–537.
- Blackstad, T. W., Brink, K., Hem, J., & June, B. (1970). Distribution of hippocampal mossy fibers in the rat. An experimental study with silver impregnation methods. *Journal of Comparative Neurology*, *138*(4), 433–449.

BIBLIOGRAPHY

- Blair, H. T., Cho, J., & Sharp, P. E. (1998). Role of the lateral mammillary nucleus in the rat head direction circuit: A combined single unit recording and lesion study. *Neuron*, 21(6), 1387–1397.
- Boccaro, C. N., Nardin, M., Stella, F., O’Neill, J., & Csicsvari, J. (2019). The entorhinal cognitive map is Attracted To Goals. *Science*, 1447(March), 1443–1447.
- Bolhuis, J. J., Stewart, C. A., & Forrest, E. M. (1994). Retrograde amnesia and memory reactivation in rats with ibotenate lesions to the hippocampus or subiculum. *The Quarterly journal of experimental psychology. B, Comparative and physiological psychology*, 47(2), 129–50.
- Bonnevie, T., Dunn, B., Fyhn, M., Hafting, T., Derdikman, D., Kubie, J. L., Roudi, Y., Moser, E. I., & Moser, M.-B. (2013). Grid cells require excitatory drive from the hippocampus. *Nature Neuroscience*, 16(3), 309–317.
- Bostock, E., Muller, R. U., & Kubie, J. L. (1991). Experience[U+2010]dependent modifications of hippocampal place cell firing. *Hippocampus*, 1(2), 193–205.
- Bourboulou, R., Marti, G., Michon, F.-X., El Feghaly, E., Nougui r, M., Robbe, D., Koenig, J., & Epsztein, J. (2019). Dynamic control of hippocampal spatial coding resolution by local visual cues. *eLife*, 8.
- Bragin, A., Jando, G., Nadasdy, Z., Hetke, J., Wise, K., & Buzsaki, G. (1995). Gamma (40-100 Hz) oscillation in the hippocampus of the behaving rat. *Journal of Neuroscience*, 15(1 I), 47–60.
- Brandon, M. P., Koenig, J., Leutgeb, J. K., & Leutgeb, S. (2014). New and Distinct Hippocampal Place Codes Are Generated in a New Environment during Septal Inactivation. *Neuron*, 82(4), 789–796.

- Broadbent, N. J., & Clark, R. E. (2013). Remote context fear conditioning remains hippocampus-dependent irrespective of training protocol, training-surgery interval, lesion size, and lesion method. *Neurobiology of Learning and Memory*, 106, 300–308.
- Brodmann, K. (1909). Vergleichende Lokalisationslehre der Grosshirnrinde in ihren Prinzipien dargestellt auf Grund des. *Leipzig : Barth*.
- Brooks, D. N., & Baddeley, A. D. (1976). What can amnesic patients learn? *Neuropsychologia*, 14(1), 111–122.
- Brun, V. H., Leutgeb, S., Wu, H. Q., Schwarcz, R., Witter, M. P., Moser, E. I., & Moser, M. B. (2008a). Impaired Spatial Representation in CA1 after Lesion of Direct Input from Entorhinal Cortex. *Neuron*, 57(2), 290–302.
- Brun, V. H., Solstad, T., Kjelstrup, K. B., Fyhn, M., Witter, M. P., Moser, E. I., & Moser, M.-B. (2008b). Progressive increase in grid scale from dorsal to ventral medial entorhinal cortex. *Hippocampus*, 18(12), 1200–1212.
- Burak, Y., & Fiete, I. R. (2009). Accurate path integration in continuous attractor network models of grid cells. *PLoS Computational Biology*, 5(2).
- Burgess, N. (2008). Grid cells and theta as oscillatory interference: Theory and predictions. *Hippocampus*, 18(12), 1157–1174.
- Burgess, N., Barry, C., & O’Keefe, J. (2007). An oscillatory interference model of grid cell firing. *Hippocampus*, 17(9), 801–812.
- Burgess, N., & Hitch, G. (2005). Computational models of working memory: Putting long-term memory into context. *Trends in Cognitive Sciences*, 9(11), 535–541.
- Burgess, N., & O’Keefe, J. (2011). Models of place and grid cell firing and theta rhythmicity. *Current Opinion in Neurobiology*, 21(5), 734–744.

BIBLIOGRAPHY

- Burwell, R. D. (2001). Borders and cytoarchitecture of the perirhinal and postrhinal cortices in the rat. *Journal of Comparative Neurology*, 437(1), 17–41.
- Burwell, R. D., & Amaral, D. G. (1998). Cortical efferents of the perirhinal, postrhinal, and entorhinal cortices of the rat. *Journal of Comparative Neurology*, 398, 179–205.
- Bush, D., Barry, C., Manson, D., & Burgess, N. (2015). Using Grid Cells for Navigation. *Neuron*, 87(3), 507–520.
- Bush, D., & Burgess, N. (2014). A Hybrid Oscillatory Interference/Continuous Attractor Network Model of Grid Cell Firing. *Journal of Neuroscience*, 34(14), 5065–5079.
- Buzsáki, G., & Moser, E. I. (2013). Memory, navigation and theta rhythm in the hippocampal-entorhinal system. *Nature Neuroscience*, 16(2), 130–138.
- Calton, J. L., Stackman, R. W., Goodridge, J. P., Archey, W. B., Dudchenko, P. A., & Taube, J. S. (2003). Hippocampal Place Cell Instability after Lesions of the Head Direction Cell Network. *Journal of Neuroscience*, 23(30), 9719–9731.
- Campbell, M. G., Ocko, S. A., Mallory, C. S., Low, I. I., Ganguli, S., & Giocomo, L. M. (2018). Principles governing the integration of landmark and self-motion cues in entorhinal cortical codes for navigation. *Nature Neuroscience*, 21(8), 1096–1106.
- Canto, C. B., & Witter, M. P. (2012a). Cellular properties of principal neurons in the rat entorhinal cortex. I. The lateral entorhinal cortex. *Hippocampus*, 22(6), 1256–1276.
- Canto, C. B., & Witter, M. P. (2012b). Cellular properties of principal neurons in the rat entorhinal cortex. II. The medial entorhinal cortex. *Hippocampus*, 22(6), 1277–1299.

BIBLIOGRAPHY

- Canto, C. B., Wouterlood, F. G., & Witter, M. P. (2008). What does the anatomical organization of the entorhinal cortex tell us? *Neural Plasticity*, 2008.
- Carpenter, F., Manson, D., Jeffery, K., Burgess, N., & Barry, C. (2015). Grid cells form a global representation of connected environments. *Current Biology*, 25(9), 1176–1182.
- Carrel, J. S. (1972). An improved treading device for tethered insects. *Science*, 175(4027), 1279.
- Chaudhuri, R., Gerçek, B., Pandey, B., Peyrache, A., & Fiete, I. (2019). The intrinsic attractor manifold and population dynamics of a canonical cognitive circuit across waking and sleep. *Nature Neuroscience*, 22(9), 1512–1520.
- Chen, G., King, J. A., Burgess, N., & O’Keefe, J. (2013). How vision and movement combine in the hippocampal place code. *Proc. Natl. Acad. Sci. USA*, 110(1), 378–383.
- Chen, G., King, J. A., Lu, Y., Cacucci, F., & Burgess, N. (2018). Spatial cell firing during virtual navigation of open arenas by head-restrained mice. *eLife*.
- Chen, G., Manson, D., Cacucci, F., & Wills, T. J. (2016). Absence of Visual Input Results in the Disruption of Grid Cell Firing in the Mouse. *Current Biology*, 26(17), 2335–2342.
- Chen, L. L., Lin, L. H., Green, E. J., Barnes, C. A., & McNaughton, B. L. (1994). Head-direction cells in the rat posterior cortex - I. anatomical distribution and behavioral modulation. *Experimental Brain Research*, 101(1), 8–23.
- Cheng, K., Shettleworth, S. J., Huttenlocher, J., & Rieser, J. J. (2007). Bayesian Integration of Spatial Information. *Psychological Bulletin*, 133(4), 625–637.

BIBLIOGRAPHY

- Clark, B. J., & Taube, J. S. (2011). Intact landmark control and angular path integration by head direction cells in the anterodorsal thalamus after lesions of the medial entorhinal cortex. *Hippocampus*, *21*(7), 767–782.
- Clark, B. J., & Taube, J. S. (2012). Vestibular and attractor network basis of the head direction cell signal in subcortical circuits. *Frontiers in Neural Circuits*, *6*(FEBRUARY), 1–12.
- Clark, R. E., Broadbent, N. J., & Squire, L. R. (2005). Hippocampus and remote spatial memory in rats. *Hippocampus*, *15*(2), 260–272.
- Climer, J. R., DiTullio, R., Newman, E. L., Hasselmo, M. E., & Eden, U. T. (2015). Examination of rhythmicity of extracellularly recorded neurons in the entorhinal cortex. *Hippocampus*, *25*(4), 460–473.
- Cohen, N. J., & Squire, L. R. (1980). Preserved learning and retention of pattern-analyzing skill in amnesia: dissociation of knowing how and knowing that.
- Cohen, S. J., & Stackman, R. W. (2015). Assessing rodent hippocampal involvement in the novel object recognition task. A review. *Behavioural Brain Research*, *285*, 105–117.
- Collett, M., & Collett, T. S. (2000). How do insects use path integration for their navigation. *Biological Cybernetics*, *83*, 245–259.
- Colom, L. V., & Bland, B. H. (1987). State-dependent spike train dynamics of hippocampal formation neurons: evidence for theta-on and theta-off cells. *Brain Research*, *422*(2), 277–286.
- Constantinescu, A. O., O'Reilly, J. X., & Behrens, T. E. (2016). Organizing conceptual knowledge in humans with a gridlike code. *Science*, *352*(6292), 1464–1468.

- Corkin, S. (2002). What's new with the amnesic patient H.M.? *Nature Reviews Neuroscience*, 3(2), 153–160.
- Csicsvari, J., Hirase, H., Czurkó, A., Mamiya, A., & Buzsáki, G. (1999). Oscillatory coupling of hippocampal pyramidal cells and interneurons in the behaving rat. *Journal of Neuroscience*, 19(1), 274–287.
- Dahmen, H. J. (1980). A simple apparatus to investigate the orientation of walking insects. *Experientia*, 36(6), 685–687.
- Darwin, C. (1873). Origin of certain instincts. *Nature*, 7(179), 417–418.
- Deneve, S., Latham, P. E., & Pouget, A. (2001). Efficient computation and cue integration with noisy population codes. *Nature Neuroscience*, 4(8), 826–831.
- Deneve, S., & Pouget, A. (2004). Bayesian multisensory integration and cross-modal spatial links. *Journal of Physiology Paris*, 98(1-3 SPEC. ISS.), 249–258.
- Derdikman, D., Whitlock, J. R., Tsao, A., Fyhn, M., Hafting, T., Moser, M.-B. B., & Moser, E. I. (2009). Fragmentation of grid cell maps in a multicompartiment environment. *Nature Neuroscience*, 12(10), 1325–1332.
- Deshmukh, S. S., & Knierim, J. J. (2013). Influence of local objects on hippocampal representations: Landmark vectors and memory. *Hippocampus*, 23(4), 253–267.
- Diba, K., & Buzsáki, G. (2008). Hippocampal network dynamics constrain the time lag between pyramidal cells across modified environments. *Journal of Neuroscience*, 28(50), 13448–13456.
- Dickson, C. T., Magistretti, J., Shalinsky, M. H., Fransén, E., Hasselmo, M. E., & Alonso, A. (2000). Properties and Role of I_h in the Pacing of Subthreshold

BIBLIOGRAPHY

- Oscillations in Entorhinal Cortex Layer II Neurons. *Journal of Neurophysiology*, 83(5), 2562–2579.
- Dombeck, D. A., Harvey, C. D., Tian, L., Looger, L. L., & Tank, D. W. (2010). Functional imaging of hippocampal place cells at cellular resolution during virtual navigation. *Nature Neuroscience*, 13(11), 1433–1440.
- Domnisoru, C., Kinkhabwala, A. A., & Tank, D. W. (2013). Membrane potential dynamics of grid cells. *Nature*, 495(7440), 199–204.
- Dordek, Y., Soudry, D., Meir, R., & Derdikman, D. (2016). Extracting grid cell characteristics from place cell inputs using non-negative principal component analysis. *eLife*, 5.
- Dudai, Y. (2004). The Neurobiology of Consolidations, Or, How Stable is the Engram? *Annual Review of Psychology*, 55(1), 51–86.
- Dupret, D., O’Neill, J., Pleydell-Bouverie, B., & Csicsvari, J. (2010). The reorganization and reactivation of hippocampal maps predict spatial memory performance. *Nature Neuroscience*, 13(8), 995–1002.
- Egorov, A. V., Hamam, B. N., Fransén, E., Hasselmo, M. E., & Alonso, A. A. (2002). Graded persistent activity in entorhinal cortex neurons. *Nature*, 420(6912), 173–178.
- Eichenbaum, H. (2017). Memory: Organization and Control. *Annual Review of Psychology*, 68(1), 19–45.
- Eichenbaum, H., & Cohen, N. J. (2014). Can We Reconcile the Declarative Memory and Spatial Navigation Views on Hippocampal Function? *Neuron*, 83(4), 764–770.
- Eichenbaum, H., Dudchenko, P., Wood, E., Shapiro, M., & Tanila, H. (1999). The

- Hippocampus, Memory, and Place Cells: Is It Spatial Memory or a Memory Space? *Neuron*, 23(2), 209–226.
- Ekstrom, A. D., Caplan, J. B., Ho, E., Shattuck, K., Fried, I., & Kahana, M. J. (2005). Human hippocampal theta activity during virtual navigation. *Hippocampus*, 15(7), 881–889.
- Elazar, Z., & Adey, W. R. (1967). Spectral analysis of low frequency components in the electrical activity of the hippocampus during learning. *Electroencephalography and Clinical Neurophysiology*, 23(3), 225–240.
- Eliav, T., Geva-Sagiv, M., Yartsev, M. M., Finkelstein, A., Rubin, A., Las, L., & Ulanovsky, N. (2018). Nonoscillatory Phase Coding and Synchronization in the Bat Hippocampal Formation. *Cell*, 175(4), 1119–1130.e15.
- Ernst, M. O., & Banks, M. S. (2002). Humans integrate visual and haptic information in a statistically optimal fashion. *Nature*, 415(6870), 429–433.
- Esch, H. E., & Burns, J. E. (1996). Distance estimation by foraging honeybees. *Journal of Experimental Biology*, 199(1), 155–162.
- Etienne, A. S., Maurer, R., & Saucy, F. (1988). Limitations in the Assessment of Path Dependent Information. *Behaviour*, 106(1), 81–111.
- Etienne, A. S., Maurer, R., Saucy, F., & Teroni, E. (1986). Short-distance homing in the golden hamster after a passive outward journey. *Animal Behaviour*, 34(3), 696–715.
- Etienne, A. S., Teroni, E., Hurni, C., & Portenier, V. (1990). The effect of a single light cue on homing behaviour of the golden hamster. *Animal Behaviour*, 39(1), 17–41.

BIBLIOGRAPHY

- Evans, T., Bicanski, A., Bush, D., & Burgess, N. (2016). How environment and self-motion combine in neural representations of space. *Journal of Physiology*, *594*(22), 6535–6546.
- Fenton, A. A., Csizmadia, G., & Muller, R. U. (2000). Conjoint control of hippocampal place cell firing by two visual stimuli: II. A vector-field theory that predicts modifications of the representation of the environment. *Journal of General Physiology*, *116*(2), 211–221.
- Ferbinteanu, J., & Shapiro, M. L. (2003). Prospective and retrospective memory coding in the hippocampus. *Neuron*, *40*(6), 1227–1239.
- Fiete, I. R., Burak, Y., & Brookings, T. (2008). What Grid Cells Convey about Rat Location. *Journal of Neuroscience*, *28*(27), 6858–6871.
- Fisher, R. A. (1915). Frequency distribution of the values of the correlation coefficient in samples from an indefinitely large population. *Biometrika*, *10*(4), 507–521.
- Foster, D. J., & Wilson, M. A. (2006). Reverse replay of behavioural sequences in hippocampal place cells during the awake state. *Nature*, *440*(7084), 680–683.
- Frank, L. M., Brown, E. N., & Wilson, M. A. (2001). A comparison of the firing properties of putative excitatory and inhibitory neurons from CA1 and the entorhinal cortex. *Journal of Neurophysiology*, *86*(4), 2029–2040.
- Fraser, D., & MacVicar, B. (1991). Low-threshold transient calcium current in rat hippocampal lacunosum- molecular interneurons: kinetics and modulation by neurotransmitters. *Journal of Neuroscience*, *11*(9), 2812–2820.
- Fuhrmann, F., Justus, D., Sosulina, L., Kaneko, H., Beutel, T., Friedrichs, D., Schoch, S., Schwarz, M. K., Fuhrmann, M., & Remy, S. (2015). Locomotion,

- Theta Oscillations, and the Speed-Related Firing of Hippocampal Neurons Are Controlled by a Medial Septal Glutamatergic Circuit. *Neuron*, 86(5), 1253–1264.
- Fyhn, M., Hafting, T., Treves, A., Moser, M.-B. B., & Moser, E. I. (2007). Hippocampal remapping and grid realignment in entorhinal cortex. *Nature*, 446(7132), 190–4.
- Fyhn, M., Hafting, T., Witter, M. P., Moser, E. I., & Moser, M.-B. (2008). Grid cells in mice. *Hippocampus*, 18(12), 1230–1238.
- Fyhn, M., Molden, S., Witter, M. P., Moser, E. I., & Moser, M. B. (2004). Spatial representation in the entorhinal cortex. *Science*, 305(5688), 1258–1264.
- Gaffan, D. (1998). Idiothetic input into object-place configuration as the contribution to memory of the monkey and human hippocampus: A review. *Experimental Brain Research*, 123(1-2), 201–209.
- Garden, D. L. F., Dodson, P. D., O'Donnell, C., White, M. D., & Nolan, M. F. (2008). Tuning of synaptic integration in the medial entorhinal cortex to the organization of grid cell firing fields. *Neuron*, 60(5), 875–889.
- Gil, M., Ancau, M., Schlesiger, M. I., Neitz, A., Allen, K., De Marco, R. J., & Monyer, H. (2018). Impaired path integration in mice with disrupted grid cell firing. *Nature Neuroscience*, 21(1), 81–93.
- Giocomo, L. M., Hussaini, S. A., Zheng, F., Kandel, E. R., Moser, M.-B., & Moser, E. I. (2011). Grid cells use HCN1 channels for spatial scaling. *Cell*, 147(5), 1159–1170.
- Giocomo, L. M., Zilli, E. A., Fransen, E., & Hasselmo, M. E. (2007). Temporal frequency of subthreshold oscillations scales with entorhinal grid cell field spacing. *Science*, 315(5819), 1719–1722.

BIBLIOGRAPHY

- Golding, N. L., Staff, N. P., & Spruston, N. (2002). Dendritic spikes as a mechanism for cooperative long-term potentiation. *Nature*, *418*(6895), 326–331.
- Goodridge, J. P., Dudchenko, P. A., Worboys, K. A., Golob, E. J., & Taube, J. S. (1998). Cue control and head direction cells. *Behavioral Neuroscience*, *112*(4), 749–761.
- Goodridge, J. P., & Taube, J. S. (1997). Interaction between the postsubiculum and anterior thalamus in the generation of head direction cell activity. *Journal of Neuroscience*, *17*(23), 9315–9330.
- Gothard, K. M., Hoffman, K. L., Battaglia, F. P., & McNaughton, B. L. (2001). Dentate Gyrus and CA1 Ensemble Activity during Spatial Reference Frame Shifts in the Presence and Absence of Visual Input. *Journal of Neuroscience*, *21*(18), 7284–7292.
- Gothard, K. M., Skaggs, W. E., & McNaughton, B. L. (1996a). Dynamics of mismatch correction in the hippocampal ensemble code for space: Interaction between path integration and environmental cues. *Journal of Neuroscience*, *16*(24), 8027–8640.
- Gothard, K. M., Skaggs, W. E., Moore, K. M., & McNaughton, B. L. (1996b). Binding of hippocampal CA1 neural activity to multiple reference frames in a landmark-based navigation task. *Journal of Neuroscience*, *16*(2), 823–835.
- Gray, J. R., Pawlowski, V., & Willis, M. A. (2002). A method for recording behavior and multineuronal CNS activity from tethered insects flying in virtual space. *Journal of Neuroscience Methods*, *120*(2), 211–223.
- Gu, Y., Lewallen, S., Kinkhabwala, A. A., Domnisoru, C., Yoon, K., Gauthier, J. L., Fiete, I. R., & Tank, D. W. (2018). A Map-like Micro-Organization of Grid Cells in the Medial Entorhinal Cortex. *Cell*, *175*(3), 736–750.e30.

- Gulyás, A. I., Hájos, N., & Freund, T. F. (1996). Interneurons containing calretinin are specialized to control other interneurons in the rat hippocampus. *Journal of Neuroscience*, *16*(10), 3397–3411.
- Hafting, T., Fyhn, M., Bonnevie, T., Moser, M.-B., & Moser, E. I. (2008). Hippocampus-independent phase precession in entorhinal grid cells. *Nature*, *453*(7199), 1248–1252.
- Hafting, T., Fyhn, M., Molden, S., Moser, M.-B. B., & Moser, E. I. (2005). Microstructure of a spatial map in the entorhinal cortex. *Nature*, *436*(7052), 801–806.
- Hamam, B. N., Amaral, D. G., & Alonso, A. A. (2002). Morphological and electrophysiological characteristics of layer V neurons of the rat lateral entorhinal cortex. *Journal of Comparative Neurology*, *451*(1), 45–61.
- Hamam, B. N., Kennedy, T. E., Alonso, A., & Amaral, D. G. (2000). Morphological and electrophysiological characteristics of layer V neurons of the rat medial entorhinal cortex. *The Journal of comparative neurology*, *418*(4), 457–72.
- Hardcastle, K., Ganguli, S., & Giocomo, L. M. (2015). Environmental Boundaries as an Error Correction Mechanism for Grid Cells. *Neuron*, *86*(3), 827–839.
- Hargreaves, E. L., Rao, G., Lee, I., & Knierim, J. J. (2005). Neuroscience: Major dissociation between medial and lateral entorhinal input to dorsal hippocampus. *Science*, *308*(5729), 1792–1794.
- Harris, K. D., Henze, D. A., Hirase, H., Leinekugel, X., Dragoi, G., Czurkó, A., & Buzsáki, G. (2002). Spike train dynamics predicts theta-related phase precession in hippocampal pyramidal cells. *Nature*, *417*(6890), 738–741.

BIBLIOGRAPHY

- Hartley, T., Burgess, N., Lever, C., Cacucci, F., & O'Keefe, J. (2000). Modeling place fields in terms of the cortical inputs to the hippocampus. *Hippocampus*, *10*(4), 369–379.
- Harvey, C. D., Collman, F., Dombeck, D. A., & Tank, D. W. (2009). Intracellular dynamics of hippocampal place cells during virtual navigation. *Nature*, *461*(7266), 941–6.
- Heinze, S., Narendra, A., & Cheung, A. (2018). Principles of Insect Path Integration.
- Herkenham, M. (1978). The connections of the nucleus reuniens thalami: Evidence for a direct thalamo[U+2010]hippocampal pathway in the rat. *Journal of Comparative Neurology*, *177*(4), 589–609.
- Heys, J. G., Rangarajan, K. V., & Dombeck, D. A. (2014). The functional micro-organization of grid cells revealed by cellular-resolution imaging. *Neuron*, *84*(5), 1079–1090.
- Hjorth-Simonsen, A., & Jeune, B. (1972). Origin and termination of the hippocampal perforant path in the rat studied by silver impregnation. *The Journal of Comparative Neurology*, *144*(2), 215–231.
- Holm, S. (1979). A simple sequentially rejective multiple test procedure. *Scandinavian Journal of Statistics*, (pp. 65–70).
- Hölscher, C., Jacob, W., & Mallot, H. A. (2003). Reward modulates neuronal activity in the hippocampus of the rat. *Behavioural Brain Research*, *142*(1-2), 181–191.
- Hölscher, C., Schnee, A., Dahmen, H., Setia, L., Mallot, H. A., & Holscher, C. (2005). Rats are able to navigate in virtual environments. *Journal of Experimental Biology*, *208*(3), 561–569.

- Hopfield, J. J. (1982). Neural networks and physical systems with emergent collective computational abilities. *Proceedings of the National Academy of Sciences*, 79(8), 2554–2558.
- Høydal, Ø. A., Skytøen, E. R., Andersson, S. O., Moser, M. B., & Moser, E. I. (2019). Object-vector coding in the medial entorhinal cortex. *Nature*, 568(7752), 400–404.
- Hunsaker, M. R., Thorup, J. A., Welch, T., & Kesner, R. P. (2006). The role of CA3 and CA1 in the acquisition of an object-trace-place paired-associate task. *Behavioral Neuroscience*, 120(6), 1252–1256.
- Huxter, J., Burgess, N., & O’Keefe, J. (2003). Independent rate and temporal coding in hippocampal pyramidal cells. *Nature*, 425(6960), 828–832.
- Hyman, B., Hoesen, G. W. V., Damasio, A. R., & Barnes, C. L. (1984). Alzheimer’s Disease : Cell-Specific Pathology Isolates the Hippocampal Formation. *Science*, 225, 1168–1170.
- Ishizuka, N., Cowan, W. M., & Amaral, D. G. (1995). A quantitative analysis of the dendritic organization of pyramidal cells in the rat hippocampus. *Journal of Comparative Neurology*, 362(1), 17–45.
- Jacob, P. Y., Capitano, F., Poucet, B., Save, E., & Sargolini, F. (2019). Path integration maintains spatial periodicity of grid cell firing in a 1D circular track. *Nature Communications*, 10(1), 1–13.
- Jacob, P. Y., Poucet, B., Liberge, M., Save, E., & Sargolini, F. (2014). Vestibular control of entorhinal cortex activity in spatial navigation. *Frontiers in Integrative Neuroscience*, 8(JUNE), 1–9.

BIBLIOGRAPHY

- Jarsky, T., Roxin, A., Kath, W. L., & Spruston, N. (2005). Conditional dendritic spike propagation following distal synaptic activation of hippocampal CA1 pyramidal neurons. *Nature Neuroscience*, 8(12), 1667–1676.
- Jeewajee, A., Barry, C., Douchamps, V., Manson, D., Lever, C., & Burgess, N. (2014). Theta phase precession of grid and place cell firing in open environments. *Philosophical Transactions of the Royal Society B*, 369(1635).
- Jeewajee, A., Barry, C., O’Keefe, J., & Burgess, N. (2008). Grid cells and theta as oscillatory interference: Electrophysiological data from freely moving rats. *Hippocampus*, 18(12), 1175–1185.
- Jung, M. W., Wiener, S. I., & McNaughton, B. L. (1994). Comparison of spatial firing characteristics of units in dorsal and ventral hippocampus of the rat. *Journal of Neuroscience*, 14(12), 7347–7356.
- Kaada, B. R., Jarisen, J., & Andersen, P. (1953). Stimulation of the Hippocampus and Medial Cortical Areas in Unanesthetized Cats. *Neurology*, 3(11), 844–844.
- Kadir, S. N., Goodman, D. F., & Harris, K. D. (2014). High-dimensional cluster analysis with the masked EM algorithm. *Neural Computation*, 26(11), 2379–2394.
- Kamondi, A., Acsády, L., Wang, X.-J., & Buzsáki, G. (1998). Theta Oscillations in Somata and Dendrites of Hippocampal Pyramidal Cells in vivo. *Hippocampus*, 261(March), 244–261.
- Kapur, N., & Brooks, D. J. (1999). Temporally-specific retrograde amnesia in two cases of discrete bilateral hippocampal pathology. *Hippocampus*, 9(3), 247–254.
- Kerr, K. M., Agster, K. L., Furtak, S. C., & Burwell, R. D. (2007). Functional

- neuroanatomy of the parahippocampal region: The lateral and medial entorhinal areas. *Hippocampus*, 17(9), 697–708.
- Kesner, R. P. (1993). Paired associate learning in the rat: Role of hippocampus, medial prefrontal cortex, and parietal cortex. *Psychobiology*, 21(3), 183–192.
- Kim, J. J., & Fanselow, M. S. (1992). Modality-specific retrograde amnesia of fear. *Science*, 256(5057), 675–677.
- Kim, S. S., Rouault, H., Druckmann, S., & Jayaraman, V. (2017). Ring attractor dynamics in the *Drosophila* central brain. *Science*, 356(6340), 849–853.
- Kjelstrup, K. B., Solstad, T., Brun, V. H., Hafting, T., Leutgeb, S., Witter, M. P., Moser, E. I., & Moser, M. B. (2008). Finite scale of spatial representation in the hippocampus. *Science*, 321(5885), 140–143.
- Knierim, J., Kudrimoti, S., & McNaughton, L. (1995). Place Cells, Head Direction Stability. *Journal of Neuroscience*, 15(March), 1648–1659.
- Knierim, J. J. (2002). Dynamic Interactions between Local Surface Cues, Distal Landmarks, and Intrinsic Circuitry in Hippocampal Place Cells. *Journal of Neuroscience*, 22(14), 6254–6264.
- Koenig, J., Linder, A. N., Leutgeb, J. K., & Leutgeb, S. (2011). The Spatial Periodicity of Grid Cells Is Not Sustained During Reduced Theta Oscillations. *Science*, 332(6029), 592–595.
- Köhler, C. (1985). Intrinsic projections of the retrohippocampal region in the rat brain. I. The subicular complex. *Journal of Comparative Neurology*, 236(4), 504–522.
- Kramis, R., Vanderwolf, C. H., & Bland, B. H. (1975). Two types of hippocampal rhythmical slow activity in both the rabbit and the rat: Relations to behavior

BIBLIOGRAPHY

- and effects of atropine, diethyl ether, urethane, and pentobarbital. *Experimental Neurology*, 49(1), 58–85.
- Kraus, B. J., Robinson, R. J., White, J. A., Eichenbaum, H., & Hasselmo, M. E. (2013). Hippocampal "Time Cells": Time versus Path Integration. *Neuron*, 78(6), 1090–1101.
- Kropff, E., Carmichael, J. E., Moser, M.-B., & Moser, E. I. (2015). Speed cells in the medial entorhinal cortex. *Nature*, 523(7561), 419–424.
- Krupic, J., Bauza, M., Burton, S., Barry, C., & O'Keefe, J. (2015). Grid cell symmetry is shaped by environmental geometry. *Nature*, 518(7538), 232–235.
- Krupic, J., Bauza, M., Burton, S., & O'Keefe, J. (2018). Local transformations of the hippocampal cognitive map. *Science*, 359(6380), 1143–1146.
- Landau, B., Spelke, E., & Gleitman, H. (1984). Spatial knowledge in a young blind child. *Cognition*, 16(3), 225–260.
- Langston, R. F., Ainge, J. A., Couey, J. J., Canto, C. B., Bjerknes, T. L., Witter, M. P., Moser, E. I., & Moser, M.-B. (2010). Development of the Spatial Representation System in the Rat. *Science*, 328(5985), 1576–1580.
- Lawson, V. H., & Bland, B. H. (1993). The Role of the Septohippocampal Pathway in the Regulation of Hippocampal Field Activity and Behavior: Analysis by the Intraseptal Microinfusion of Carbachol, Atropine, and Procaine. *Experimental Neurology*, 120(1), 132–144.
- Lee, A. K., & Wilson, M. A. (2002). Memory of sequential experience in the hippocampus during slow wave sleep. *Neuron*, 36(6), 1183–1194.

- Lee, H. Y., Kuo, M. D., Chang, T. C., Ou-Yang, Y. S., & Chen, J. J. J. (2007). Development of virtual reality environment for tracking rat behavior. *Journal of Medical and Biological Engineering*, 27(2), 71–78.
- Lehmann, H., Lacanilao, S., & Sutherland, R. J. (2007). Complete or partial hippocampal damage produces equivalent retrograde amnesia for remote contextual fear memories. *European Journal of Neuroscience*, 25(5), 1278–1286.
- Lenck-Santini, P. P., Save, E., & Poucet, B. (2001). Place-cell firing does not depend on the direction of turn in a Y-maze alternation task. *European Journal of Neuroscience*, 13(5), 1055–1058.
- Leutgeb, S., Leutgeb, J. K., Barnes, C. A., Moser, E. I., McNaughton, B. L., & Moser, M. B. (2005). Neuroscience: Independent codes for spatial and episodic memory in hippocampal neuronal ensembles. *Science*, 309(5734), 619–623.
- Lever, C., & Burgess, N. (2012). The virtues of youth and maturity (in Dentate Granule Cells). *Cell*, 149(1), 18–20.
- Lever, C., Burton, S., Jeewajee, A., O’Keefe, J., & Burgess, N. (2009). Boundary Vector Cells in the Subiculum of the Hippocampal Formation. *Journal of Neuroscience*, 29(31), 9771–9777.
- Lever, C., Wills, T., Cacucci, F., Burgess, N., & Keefe, J. O. (2002). Long-term plasticity in hippocampal place-cell representation of environmental geometry. *Nature*, 416(March), 90–94.
- Loomis, J. M., Klatzky, R. L., Golledge, R. G., Cicinelli, J. G., Pellegrino, J. W., & Fry, P. A. (1993). Nonvisual Navigation by Blind and Sighted: Assessment of Path Integration Ability. *Journal of Experimental Psychology: General*, 122(1), 73–91.

BIBLIOGRAPHY

- Lorente De Nó, R. (1934). Studies on the structure of the cerebral cortex. II. Continuation of the study of the ammonic system. *Journal für Psychologie und Neurologie*.
- Louie, K., & Wilson, M. A. (2001). Temporally structured replay of awake hippocampal ensemble activity during rapid eye movement sleep. *Neuron*, 29(1), 145–156.
- MacDonald, C. J., Carrow, S., Place, R., & Eichenbaum, H. (2013). Distinct hippocampal time cell sequences represent odor memories in immobilized rats. *Journal of Neuroscience*, 33(36), 14607–14616.
- MacDonald, C. J., Lepage, K. Q., Eden, U. T., & Eichenbaum, H. (2011). Hippocampal "time cells" bridge the gap in memory for discontinuous events. *Neuron*, 71(4), 737–749.
- Magee, J. C. (2001). Dendritic mechanisms of phase precession in hippocampal CA1 pyramidal neurons. *Journal of Neurophysiology*, 86(1), 528–532.
- Manns, J. R., & Eichenbaum, H. (2009). A cognitive map for object memory in the hippocampus. *Learning and Memory*, 16(10), 616–624.
- Manns, J. R., Hopkins, R. O., & Squire, L. R. (2003). Semantic memory and the human hippocampus. *Neuron*, 38(1), 127–133.
- Maren, S., Aharonov, G., & Fanselow, M. S. (1997). Neurotoxic lesions of the dorsal hippocampus and Pavlovian fear conditioning in rats. *Behavioural Brain Research*, 88(2), 261–274.
- Markus, E. J., Barnes, C. A., McNaughton, B. L., Gladden, V. L., & Skaggs, W. E. (1994). Spatial information content and reliability of hippocampal CA1 neurons: Effects of visual input. *Hippocampus*, 4(4), 410–421.

- Martina, M., & Jonas, P. (1997). Functional differences in Na⁺ channel gating between fast-spiking interneurons and principal neurons of rat hippocampus. *Journal of Physiology*, 505(3), 593–603.
- Maurer, A. P., VanRhoads, S. R., Sutherland, G. R., Lipa, P., & McNaughton, B. L. (2005). Self-motion and the origin of differential spatial scaling along the septo-temporal axis of the hippocampus. *Hippocampus*, 15(7), 841–852.
- McClelland, J. L., McNaughton, B. L., & O'Reilly, R. C. (1995). Why there are complementary learning systems in the hippocampus and neocortex: Insights from the successes and failures of connectionist models of learning and memory. *Psychological Review*, 102(3), 419–457.
- McFarland, W. L., Teitelbaum, H., & Hedges, E. K. (1975). Relationship between hippocampal theta activity and running speed in the rat. *Journal of Comparative and Physiological Psychology*, 88(1), 324–328.
- Mcnaughton, B. L., Barnes, C. A., Gerrard, J. L., Gothard, K., Jung, M. W., Knierim, J. J., Kudrimoti, H., Qin, Y., Skaggs, W. E., Suster, M., & Weaver, K. L. (1996). Deciphering the hippocampal polyglot: The hippocampus as a path integration system. *Journal of Experimental Biology*, 199(1), 173–185.
- McNaughton, B. L., Barnes, C. A., & O'Keefe, J. (1983). The contributions of position, direction, and velocity to single unit activity in the hippocampus of freely-moving rats. *Experimental Brain Research*, 52(1), 41–49.
- McNaughton, B. L., Battaglia, F. P., Jensen, O., Moser, E. I., & Moser, M.-B. (2006). Path integration and the neural basis of the 'cognitive map'. *Nature Reviews Neuroscience*.

BIBLIOGRAPHY

- Menzel, R., Brandt, R., Gumbert, A., Komischke, B., & Kunze, J. (2000). Two spatial memories for honeybee navigation. *Proceedings of the Royal Society B*, 267(1447), 961–968.
- Mitchell, S. J., & Ranck, J. B. (1980). Generation of theta rhythm in medial entorhinal cortex of freely moving rats. *Brain Research*, 189(1), 49–66.
- Mittelstaedt, H. (1999). The role of the otoliths in perception of the vertical and in path integration. In *Annals of the New York Academy of Sciences*, vol. 871, (pp. 334–344). New York Academy of Sciences.
- Mittelstaedt, H., & Mittelstaedt, M.-L. (1982). Homing by Path Integration. In *Avian Navigation*, (pp. 290–297).
- Mittelstaedt, M. L., & Mittelstaedt, H. (1980). Homing by path integration in a mammal. *Naturwissenschaften*, 67(11), 566–567.
- Mizumori, S., & Williams, J. (1993). Directionally selective mnemonic properties of neurons in the lateral dorsal nucleus of the thalamus of rats. *Journal of Neuroscience*, 13(9), 4015–4028.
- Morris, R. G., Anderson, E., Lynch, G. S., & Baudry, M. (1986). Selective impairment of learning and blockade of long-term potentiation by an N-methyl-D-aspartate receptor antagonist, AP5. *Nature*, (319), 774–776.
- Morris, R. G., Garrud, P., Rawlins, J. N., & O’Keefe, J. (1982). Place navigation impaired in rats with hippocampal lesions. *Nature*, 297, 681–683.
- Morris, R. G., Schenk, F., Tweedie, F., & Jarrard, L. E. (1990). Ibotenate Lesions of Hippocampus and/or Subiculum: Dissociating Components of Allocentric Spatial Learning. *European Journal of Neuroscience*, 2(12), 1016–1028.

BIBLIOGRAPHY

- Mosko, S., Lynch, G., & Cotman, C. W. (1973). The distribution of septal projections to the hippocampus of the rat. *Journal of Comparative Neurology*, 152(2), 163–174.
- Muessig, L., Hauser, J., Wills, T. J., & Cacucci, F. (2015). A Developmental Switch in Place Cell Accuracy Coincides with Grid Cell Maturation. *Neuron*, 86(5), 1167–1173.
- Muir, G. M., Brown, J. E., Carey, J. P., Hirvonen, T. P., Della Santina, C. C., Minor, L. B., & Taube, J. S. (2009). Disruption of the head direction cell signal after occlusion of the semicircular canals in the freely moving chinchilla. *Journal of Neuroscience*, 29(46), 14521–14533.
- Muller, M., & Wehner, R. (1988). Path integration in desert ants, *Cataglyphis fortis*. *Proc. Natl. Acad. Sci. USA*, 85, 5287–5290.
- Müller, M., & Wehner, R. (2010). Path integration provides a scaffold for landmark learning in desert ants. *Current Biology*, 20(15), 1368–1371.
- Muller, R. U., & Kubie, J. L. (1987). The effects of changes in the environment on the spatial firing of hippocampal complex-spike cells. *Journal of Neuroscience*, 7(7), 1951–68.
- Muller, U., Kubie, J. L., Ranck, B., & Biology, C. (1987). Spatial firing patterns of hippocampal complex-spike cells in a fixed environment. *Cell*, 7(July).
- Mumby, D. G., Astur, R. S., Weisend, M. P., & Sutherland, R. J. (1999). Retrograde amnesia and selective damage to the hippocampal formation: Memory for places and object discriminations. *Behavioural Brain Research*, 106(1-2), 97–107.
- Murray, E. A., Davidson, M., Gaffan, D., Olton, D. S., & Suomi, S. (1989). Effects of fornix transection and cingulate cortical ablation on spatial memory in rhesus monkeys. *Experimental Brain Research*, 74(1), 173–186.

BIBLIOGRAPHY

- Murray, E. A., Gaffan, D., & Mishkin, M. (1993). Neural substrates of visual stimulus-stimulus association in rhesus monkeys. *Journal of Neuroscience*, *13*(10), 4549–4561.
- Murray, E. A., & Mishkin, M. (1985). Amygdalectomy Impairs Crossmodal Association in Monkeys. *Science*, *228*(May), 604–606.
- Naber, P. A., Lopes Da Silva, F. H., & Witter, M. P. (2001). Reciprocal connections between the entorhinal cortex and hippocampal fields CA1 and the subiculum are in register with the projections from CA1 to the subiculum. *Hippocampus*, *11*(2), 99–104.
- Navratilova, Z., Hoang, L. T., Daniela Schwindel, C., Tatsuno, M., & McNaughton, B. L. (2012). Experience-dependent firing rate remapping generates directional selectivity in hippocampal place cells. *Frontiers in Neural Circuits*, *6*(FEBRUARY), 1–14.
- Ocampo, A. C., Squire, L. R., & Clark, R. E. (2017). Insufficient Sleep Is a Public Health Problem Sleep-Related Unhealthy Behaviors. *Centers for Disease Control and Prevention*, (pp. 563–569).
- O'Keefe, J. (1976). Place units in the hippocampus of the freely moving rat. *Experimental Neurology*, *51*(1), 78–109.
- O'Keefe, J., & Burgess, N. (1996). Geometric Determinants Of Place Cell Firing. *Nature*, *381*(May), 435–428.
- O'Keefe, J., & Burgess, N. (2005). Dual phase and rate coding in hippocampal place cells: Theoretical significance and relationship to entorhinal grid cells.

- O'Keefe, J., Dostrovsky, J., & J. O'Keefe, J. D. (1971). Short Communications The hippocampus as a spatial map . Preliminary evidence from unit activity in the freely-moving rat. *Brain Research*, *34*(1), 171–175.
- O'Keefe, J., & Nadel, L. (1978). *The Hippocampus as a Cognitive Map*.
- O'Keefe, J., & Recce, M. L. (1993). Phase relationship between hippocampal place units and the EEG theta rhythm. *Hippocampus*, *3*(3), 317–330.
- Ólafsdóttir, H. F., Carpenter, F., & Barry, C. (2016). Coordinated grid and place cell replay during rest. *Nature Neuroscience*, *19*(6), 792–794.
- Olton, D. S., Becker, J. T., & Handemann, G. E. (1979). Hippocampus , space , and memory. *The Behavioral and Brain Sciences*, *2*(1979), 313–365.
- Olton, D. S., Walker, J. A., & Gage, F. H. (1978). Hippocampal connections and spatial discrimination. *Brain Research*, *139*(2), 295–308.
- Papez, J. W. (1937). A proposed mechanism of emotion. *Archives of Neurology And Psychiatry*, *38*(4), 725–743.
- Parkinson, J. K., Murray, E. A., & Mishkin, M. (1988). A selective mnemonic role for the hippocampus in monkeys: Memory for the location of objects. *Journal of Neuroscience*, *8*(11), 4159–4167.
- Pastalkova, E., Itskov, V., Amarasingham, A., & Buzsaki, G. (2008). Internally Generated Cell Assembly Sequences in the Rat Hippocampus. *Science*, *321*(5894), 1322–1327.
- Perez-Escobar, J. A., Kornienko, O., Latuske, P., Kohler, L., & Allen, K. (2016). Visual landmarks sharpen grid cell metric and confer context specificity to neurons of the medial entorhinal cortex. *eLife*, *5*(e16937).

BIBLIOGRAPHY

- Pyapali, G., Sik, A., Penttonen, M., Buzsaki, G., & Turner, D. (1998). Dendritic properties of hippocampal CA1 pyramidal neurons in the rat: Intracellular staining in vivo and in vitro. *The Journal of Comparative Neurology*, 391(3), 335–352.
- Quirk, G. J., Muller, R. U., Kubie, J. L., & Ranck, J. B. (1992). The positional firing properties of medial entorhinal neurons: Description and comparison with hippocampal place cells. *Journal of Neuroscience*, 12(5), 1945–1963.
- Quirk, Gregory, J., Muller, R. U., & Kubie, J. L. (1990). The Firing of Hippocampal Rat ' s Recent Experience Place Cells in the Dark Depends on the Rat's Recent Experience. *Journal of Neuroscience*, 10(6), 2008–2017.
- Ramon y Cajal, S. (1911). Histologie du système nerveux de l'homme et des vertébrés. *Maloine, Paris*, 2, 153–173.
- Ranck, J. B. (1973). Studies on single neurons in dorsal hippocampal formation and septum in unrestrained rats. Part I. Behavioral correlates and firing repertoires. *Experimental Neurology*, 41(2), 462–531.
- Raudies, F., & Hasselmo, M. E. (2015). Differences in Visual-Spatial Input May Underlie Different Compression Properties of Firing Fields for Grid Cell Modules in Medial Entorhinal Cortex. *PLoS Computational Biology*, 11(11), e1004596.
- Ravassard, P., Kees, A., Willers, B., Ho, D., Aharoni, D., Cushman, J., Aghajan, Z. M., & Mehta, M. R. (2013). Multisensory control of hippocampal spatiotemporal selectivity. *Science*, 340(6138), 1342–1346.
- Rawlins, J. N., & Olton, D. S. (1982). The septo-hippocampal system and cognitive mapping. *Behavioural Brain Research*, 5(4), 331–358.

BIBLIOGRAPHY

- Rawlins, J. N. P. (1985). Associations across time: The hippocampus as a temporary memory store. *Behavioral and Brain Sciences*, 8(3), 479–497.
- Rivas, J., Gaztelu, J. M., & García-Austt, E. (1996). Changes in hippocampal cell discharge patterns and theta rhythm spectral properties as a function of walking velocity in the guinea pig. *Experimental Brain Research*, 108(1), 113–118.
- Roth, T. C., & Pravosudov, V. V. (2009). Hippocampal volumes and neuron numbers increase along a gradient of environmental harshness: A large-scale comparison. *Proceedings of the Royal Society B*, 276(1656), 401–405.
- Saleem, A. B., Ayaz, A. I., Jeffery, K. J., Harris, K. D., & Carandini, M. (2013). Integration of visual motion and locomotion in mouse visual cortex. *Nature Neuroscience*, 16(12), 1864–1869.
- Saleem, A. B., Diamanti, E. M., Fournier, J., Harris, K. D., & Carandini, M. (2018). Visual Cortex and Hippocampus. *Nature*, 562(7725), 124–127.
- Samsonovich, A., & McNaughton, B. L. (1997). Path integration and cognitive mapping in a continuous attractor neural network model. *Journal of Neuroscience*, 17(15), 5900–5920.
- Sargolini, F., Fyhn, M., Hafting, T., McNaughton, B. L., Witter, M. P., Moser, M.-B. B., & Moser, E. I. (2006). Conjunctive representation of position, direction, and velocity in entorhinal cortex. *Science*, 312(5774), 758–762.
- Save, E., Cressant, A., Thinus-Blanc, C., & Poucet, B. (1998). Spatial firing of hippocampal place cells in blind rats. *Journal of Neuroscience*, 18(5), 1818–1826.
- Save, E., Nerad, L., & Poucet, B. (2000). Contribution of multiple sensory information to place field stability in hippocampal place cells. *Hippocampus*, 10(1), 64–76.

BIBLIOGRAPHY

- Savelli, F., & Knierim, J. J. (2019). Origin and role of path integration in the cognitive representations of the hippocampus: Computational insights into open questions. *Journal of Experimental Biology*, 222.
- Schmidt-Hieber, C., & Hausser, M. (2013). Cellular mechanisms of spatial navigation in the medial entorhinal cortex. *Nature Neuroscience*, 16(3), 325–331.
- Scoville, W. B., & Milner, B. (1957). Loss of recent memory after bilateral hippocampal lesions. *Journal of Neurology, Neurosurgery and Psychiatry*, 20(11), 11–22.
- Seelig, J. D., & Jayaraman, V. (2013). Feature detection and orientation tuning in the *Drosophila* central complex. *Nature*, 503(7475), 262–266.
- Seelig, J. D., & Jayaraman, V. (2015). Neural dynamics for landmark orientation and angular path integration. *Nature*, 521(7551), 186–191.
- Séguinot, V., Maurer, R., & Etienne, A. S. (1993). Dead reckoning in a small mammal: the evaluation of distance. *Journal of Comparative Physiology A*, 173(1), 103–113.
- Selden, N. R., Everitt, B. J., Jarrard, L. E., & Robbins, T. W. (1991). Complementary roles for the amygdala and hippocampus in aversive conditioning to explicit and contextual cues. *Neuroscience*, 42(2), 335–350.
- Shapiro, M. L., Tanila, H., & Eichenbaum, H. (1997). Cues that hippocampal place cells encode: Dynamic and hierarchical representation of local and distal stimuli. *Hippocampus*, 7(6), 624–642.
- Sharp, P. E., Blair, H. T., & Brown, M. (1996). Neural network modeling of the hippocampal formation spatial signals and their possible role in navigation: A modular approach. *Hippocampus*, 6(6), 720–734.

- Sharp, P. E., & Koester, K. (2008). Lesions of the mammillary body region severely disrupt the cortical head direction, but not place cell signal. *Hippocampus*, *18*(8), 766–784.
- Sharp, P. E., Tinkelman, A., & Cho, J. (2001). Angular velocity and head direction signals recorded from the dorsal tegmental nucleus of guinea in the rat: Implications for path integration in the head direction cell circuit. *Behavioral Neuroscience*, *115*(3), 571–588.
- Shipley, M. T. (1975). The topographical and laminar organization of the presubiculum's projection to the ipsi[U+2010] and contralateral entorhinal cortex in the guinea pig. *Journal of Comparative Neurology*, *160*(1), 127–145.
- Skaggs, W. E., Knierim, J. J., Kudrimoti, H. S., & McNaughton, B. L. (1995). A model of the neural basis of the rat's sense of direction. *Advances in Neural Information Processing Systems*, *7*(1984), 173–180.
- Skaggs, W. E., & McNaughton, B. L. (1998). Spatial firing properties of hippocampal CA1 populations in an environment containing two visually identical regions. *Journal of Neuroscience*, *18*(20), 8455–8466.
- Sławińska, U., & Kasicki, S. (1998). The frequency of rat's hippocampal theta rhythm is related to the speed of locomotion. *Brain Research*, *796*(1-2), 327–331.
- Sofroniew, N. J., Cohen, J. D., Lee, A. K., & Svoboda, K. (2014). Natural whisker-guided behavior by head-fixed mice in tactile virtual reality. *Journal of Neuroscience*, *34*(29), 9537–9550.
- Solstad, T., Boccara, C. N., Kropff, E., Moser, M.-B., & Moser, E. I. (2008). Representation of Geometric Borders in the Entorhinal Cortex. *Science*, *322*(5909), 1865–1868.

BIBLIOGRAPHY

- Solstad, T., Moser, E. I., & Einevoll, G. T. (2006). From grid cells to place cells: a mathematical model. *Hippocampus*, *16*(12), 1026–1031.
- Sparks, F. T., Lehmann, H., Hernandez, K., & Sutherland, R. J. (2011). Suppression of neurotoxic lesion-induced seizure activity: Evidence for a permanent role for the hippocampus in contextual memory. *PLoS ONE*, *6*(11).
- Spiers, H. J., Maguire, E. A., & Burgess, N. (2001). Hippocampal Amnesia. *Neurocase*, *7*(5), 357–382.
- Stachenfeld, K. L., Botvinick, M. M., & Gershman, S. J. (2017). The hippocampus as a predictive map. *Nature Neuroscience*, *20*(11), 1643–1653.
- Stackman, R. W., & Taube, J. S. (1998). Firing Properties of Rat Lateral Mammillary Single Units: Head Direction, Head Pitch, and Angular Head Velocity. *Journal of Neuroscience*, *18*(21), 9020–9037.
- Steele, R. J., & Morris, R. G. (1999). Delay-dependent impairment of a matching-to-place task with chronic and intrahippocampal infusion of the NMDA-antagonist D-AP5. *Hippocampus*, *9*(2), 118–136.
- Stensola, H., Stensola, T., Solstad, T., Frøland, K., Moser, M.-B. B., & Moser, E. I. (2012). The entorhinal grid map is discretized.
- Stensola, T., Stensola, H., Moser, M. B., & Moser, E. I. (2015). Shearing-induced asymmetry in entorhinal grid cells. *Nature*, *518*(7538), 207–212.
- Steward, O. (1976). Topographic organization of the projections from the entorhinal area to the hippocampal formation of the rat. *Journal of Comparative Neurology*.
- Steward, O., & Scoville, S. A. (1976). Cells of origin of entorhinal cortical afferents to

- the hippocampus and fascia dentata of the rat. *Journal of Comparative Neurology*, 169(3), 347–370.
- Sutherland, R. J., O'Brien, J., & Lehmann, H. (2008). Absence of systems consolidation of fear memories after dorsal, ventral, or complete hippocampal damage. *Hippocampus*, 18(7), 710–718.
- Sutherland, R. J., Weisend, M. P., Mumby, D., Astur, R. S., Hanlon, F. M., Koerner, A., Thomas, M. J., Wu, Y., Moses, S. N., Cole, C., Hamilton, D. A., & Hoesing, J. M. (2001). Retrograde amnesia after hippocampal damage: Recent vs. remote memories in two tasks. *Hippocampus*, 11(1), 27–42.
- Tamamaki, N., Abe, K., & Nojyo, Y. (1987). Columnar organization in the subiculum formed by axon branches originating from single CA1 pyramidal neurons in the rat hippocampus. *Brain Research*, 412(1), 156–160.
- Tanila, H., Shapiro, M. L., & Eichenbaum, H. (1997). Discordance of spatial representation in ensembles of hippocampal place cells. *Hippocampus*, 7(6), 613–623.
- Taube, J. S. (2007). The Head Direction Signal: Origins and Sensory-Motor Integration. *Annual Review of Neuroscience*, 30(1), 181–207.
- Taube, J. S., & Burton, H. L. (1995). Head direction cell activity monitored in a novel environment and during a cue conflict situation. *Journal of Neurophysiology*, 74(5), 1953–1971.
- Taube, J. S., Muller, R. U., & Ranck, J. B. (1990a). Head-direction cells recorded from the postsubiculum in freely moving rats. I. Description and quantitative analysis. *Journal of Neuroscience*, 10(2), 420–435.

BIBLIOGRAPHY

- Taube, J. S., Muller, R. U., & Ranck, J. B. (1990b). Head-direction cells recorded from the postsubiculum in freely moving rats. II. Effects of environmental manipulations. *Journal of Neuroscience*, *10*(2), 436–447.
- Tennant, S. A., Fischer, L., Garden, D. L., Gerlei, K. Z., Martinez-Gonzalez, C., McClure, C., Wood, E. R., & Nolan, M. F. (2018). Stellate Cells in the Medial Entorhinal Cortex Are Required for Spatial Learning. *Cell Reports*, *22*(5), 1313–1324.
- Terrazas, A., Krause, M., Lipa, P., Gothard, K. M., Barnes, C. A., & McNaughton, B. L. (2005). Self-motion and the hippocampal spatial metric. *Journal of Neuroscience*, *25*(35), 8085–8096.
- Thompson, L. T., & Best, P. J. (1989). Place Cells and Silent Cells in the Hippocampus Rats of. *Journal of Neuroscience*, *9*(7), 2382–2390.
- Thompson, L. T., & Best, P. J. (1990). Long-term stability of the place-field activity of single units recorded from the dorsal hippocampus of freely behaving rats. *Brain Research*, *509*(2), 299–308.
- Tolman, E. C. (1948). Cognitive maps in rats and men. *Psychological Review*, *55*(4), 189–208.
- Towse, B. W., Barry, C., Bush, D., & Burgess, N. (2014). Optimal configurations of spatial scale for grid cell firing under noise and uncertainty. *Philosophical Transactions of the Royal Society B*, *369*(1635).
- Tulving, E., & Markowitsch, H. J. (1998). Episodic and declarative memory: Role of the hippocampus. *Hippocampus*, *8*(3), 198–204.
- Ulanovsky, N., & Moss, C. F. (2007). Hippocampal cellular and network activity in freely moving echolocating bats. *Nature Neuroscience*, *10*(2), 224–233.

- van Groen, T., Miettinen, P., & Kadish, I. (2003). The entorhinal cortex of the mouse: Organization of the projection to the hippocampal formation. *Hippocampus*, 13(1), 133–149.
- Van Groen, T., & Wyss, J. M. (1990). Extrinsic projections from area CA1 of the rat hippocampus: Olfactory, cortical, subcortical, and bilateral hippocampal formation projections. *Journal of Comparative Neurology*, 302(3), 515–528.
- van Hoesen, G. W., Hyman, B. T., & Damasio, A. R. (1991). Entorhinal cortex pathology in Alzheimer’s disease.
- Vanderwolf, C. H. (1969). Hippocampal electrical activity and voluntary movement in the rat. *Electroencephalography and Clinical Neurophysiology*, 26, 407–418.
- Vargha-Khadem, F., Gadian, D. G., Watkins, K. E., Connelly, A., Van Paesschen, W., & Mishkin, M. (1997). Differential effects of early hippocampal pathology on episodic and semantic memory. *Science*, 277(5324), 376–380.
- Vida, I., Bartos, M., & Jonas, P. (2006). Shunting inhibition improves robustness of gamma oscillations in hippocampal interneuron networks by homogenizing firing rates. *Neuron*, 49(1), 107–117.
- Vinogradova, O. S. (1995). Expression, control, and probable functional significance of the neuronal theta-rhythm.
- Wehner, R. (1981). *Spatial vision in arthropods*.
- Wehner, R. (2003). Desert ant navigation: How miniature brains solve complex tasks. *Journal of Comparative Physiology A*, 189(8), 579–588.
- Wehner, R., & Wehner, S. (1986). Path Integration in desert ants — approaching

BIBLIOGRAPHY

- a long-standing puzzle in insect navigation. *Monitore Zoologico Italiano - Italian Journal of Zoology*, 20(3), 309–331.
- Welday, A. C., Shlifer, I. G., Bloom, M. L., Zhang, K., & Blair, H. T. (2011). Cosine directional tuning of theta cell burst frequencies: Evidence for spatial coding by oscillatory interference. *Journal of Neuroscience*, 31(45), 16157–16176.
- Wernle, T., Waaga, T., Mørreaunet, M., Treves, A., Moser, M. B., & Moser, E. I. (2018). Integration of grid maps in merged environments. *Nature Neuroscience*, 21(1), 92–105.
- Wills, T. J., Cacucci, F., Burgess, N., & O’Keefe, J. (2010). Development of the Hippocampal Cognitive Map in Prewanling Rats. *Science*, 328(5985), 1573–1576.
- Wills, T. J., Lever, C., Cacucci, F., Burgess, N., & O’Keefe, J. (2005). Attractor Dynamics in the Hippocampal Representation of the Local Environment. *Science*, 308(May), 873–876.
- Wilson, M., & McNaughton, B. (1993). Dynamics of the hippocampal ensemble code for space. *Science*, 261(5124), 1055–1058.
- Wilson, M. A., & McNaughton, B. L. (1994). Reactivation of Hippocampal Ensemble Memories During Sleep. *Science*, 265(5172), 676–679.
- Winocur, G., Frankland, P. W., Sekeres, M., Fogel, S., & Moscovitch, M. (2009). Changes in context-specificity during memory reconsolidation: Selective effects of hippocampal lesions. *Learning & Memory*, 16(11), 722–729.
- Winter, S. S., Mehlman, M. L., Clark, B. J., & Taube, J. S. (2015). Passive Transport Disrupts Grid Signals in the Parahippocampal Cortex. *Current Biology*, 25(19), 2493–2502.

- Witter, M. P. (1993). Organization of the entorhinal—hippocampal system: A review of current anatomical data. *Hippocampus*, 3(1 S), 33–44.
- Witter, M. P., Doan, T. P., Jacobsen, B., Nilssen, E. S., & Ohara, S. (2017). Architecture of the entorhinal cortex a review of entorhinal anatomy in rodents with some comparative notes. *Frontiers in Systems Neuroscience*, 11(June), 1–12.
- Witter, M. P., Groenewegen, H. J., Lopes da Silva, F. H., & Lohman, A. H. (1989). Functional organization of the extrinsic and intrinsic circuitry of the parahippocampal region.
- Wittlinger, M., Wehner, R., & Wolf, H. (2007). The desert ant odometer: A stride integrator that accounts for stride length and walking speed. *Journal of Experimental Biology*, 210(2), 198–207.
- Wood, E. R., Dudchenko, P. A., & Eichenbaum, H. (1999). The global record of memory in hippocampal neuronal activity. *Nature*, 397(6720), 613–616.
- Wyss, J. M., & Groen, T. V. (1992). Connections Between the Retrosplenial Cortex and the Hippocampal Formation in the Rat: A Review. *Hippocampus*, 2(1), 1–12.
- Xing, J., & Andersen, R. A. (2000). Models of the posterior parietal cortex which perform multimodal integration and represent space in several coordinate frames. *Journal of Cognitive Neuroscience*, 12(4), 601–614.
- Yartsev, M. M., Witter, M. P., & Ulanovsky, N. (2011). Grid cells without theta oscillations in the entorhinal cortex of bats. *Nature*, 479(7371), 103–107.
- Yoder, R. M., Clark, B. J., Brown, J. E., Lamia, M. V., Valerio, S., Shinder, M. E., & Taube, J. S. (2011). Both visual and idiothetic cues contribute to head direction

BIBLIOGRAPHY

- cell stability during navigation along complex routes. *Journal of Neurophysiology*, 105(6), 2989–3001.
- Yoder, R. M., Goebel, E. A., Köppen, J. R., Blankenship, P. A., Blackwell, A. A., & Wallace, D. G. (2015). Otolithic information is required for homing in the mouse. *Hippocampus*, 25(8), 890–899.
- Yoder, R. M., & Taube, J. S. (2009). Head direction cell activity in mice: Robust directional signal depends on intact otolith organs. *Journal of Neuroscience*, 29(4), 1061–1076.
- Yoon, K., Buice, M. A., Barry, C., Hayman, R., Burgess, N., & Fiete, I. R. (2013). Specific evidence of low-dimensional continuous attractor dynamics in grid cells. *Nature Neuroscience*, 16(8), 1077–1084.
- Zhang, K. (1996). Representation of spatial orientation by the intrinsic dynamics of the head-direction cell ensemble: A theory. *Journal of Neuroscience*, 16(6), 2112–2126.
- Zhang, K., Ginzburg, I., McNaughton, B. L., & Sejnowski, T. J. (1998). Interpreting Neuronal Population Activity by Reconstruction: Unified Framework With Application to Hippocampal Place Cells. *Journal of Neurophysiology*, 79(2), 1017–1044.
- Zhang, S., & Manahan-Vaughan, D. (2015). Spatial olfactory learning contributes to place field formation in the hippocampus. *Cerebral Cortex*, 25(2), 423–432.
- Ziv, Y., Burns, L. D., Cocker, E. D., Hamel, E. O., Ghosh, K. K., Kitch, L. J., Gamal, A. E., & Schnitzer, M. J. (2013). Long-term dynamics of CA1 hippocampal place codes. *Nature Neuroscience*, 16(3), 264–266.